STUDY FOR IRS RETRIEVALS AND APPLICATIONS AT HIGH SATELLITE ZENITH ANGLE

FINAL STUDY REPORT

For: EUMETSAT
Addressee: Tim Hultberg and Thomas August
Reference: IRS-TN-0016-TS
Date: 21.06.2020
Edition: 1
Revision: 1
Page: **i**/ 195

THALES Services SAS
290 allée du Lac
31670 Labège
France

Tel.: +33-562 88 86 00

Fax: +33-562 88 76 00

Web: http://www.thalesgroup.com

THALES

Division Secure Communications and Information Systems (SIX), 2020

Evolution sheet

Issue	Date	Evolution	Reason for evolution
1.1	21.06.2020	§2.2.1.2 The text regarding the Interpolation/extrapolation of the parameters profiles to the RTTOV pressure level has been improved. §2.3.2 Minor modifications in the text: terminology and typo corrections. §3.2 The text regarding the computation of the *a priori* error matrices w.r.t. the pressure levels has been improved. Additional section (§4.4.3) and corresponding annex to illustrate the impact of SZA on Averaging Kernels and DOFS. Minor adjustments and corrections (mainly typo) made throughout the report.	Modifications following EUMETSAT's comments and recommendations during the final meeting on 9 June 2020.
draft	06/05/2020	Creation	EUMETSAT Contract No. EUM/C0/19/4600002242/THH

Approval sheet

Function	Name	Date	Signature
Written by Project team	IRS study team	21.06.2020	
Verified by Quality Manager	Chantal TOUJAS	21.06.2020	
For application by Project Manager	Laure CHAUMAT	21.06.2020	

Summary

List of Figures

List of Tables

1 INTRODUCTION

1.1 PURPOSE OF THE DOCUMENT

This document constitutes the final report of the study *"Study for IRS Retrievals and Applications at high Satellite Zenith Angle"* and comprises a comprehensive description of the generation of the dataset as well as the characterisation of the impact of the sensing geometry on the retrievals.

Section 2 provides a comprehensive description of the generation of the dataset:

- Section 2.1 describes the method to select the atmospheric situations to be used for the simulations with RTTOV. These atmospheric situations constitute the dataset relevant for the study;
- Section 2.2 provides a comprehensive description of the generation of the dataset: both the file content and the file structure are described as well as the origin of the data and how they are manipulated;
- Section 2.3 is dedicated to the radiative transfer simulation: it describes the configuration of RTTOV and provides some examples of output of the simulation chain used to generate the dataset.

Section 3 describes the method used to estimate the averaging kernels and the retrieval errors for all Jacobians available in the generated dataset and how the initial dataset has been complemented by additional information required for the retrieval error analysis.

Section 4 presents the results of the analysis of the impact of the sensing geometry on the retrievals and provides conclusions which are discussed. This section gives also some potential and limitations of the geophysical products at high zenith angles.

Section 5 provides the results of studying the impact of high zenith angles on surface emissivity and some recommendations regarding the potential applicability of limb sounder retrieval algorithms to MTG-IRS instrument.

1.2 REFERENCES

ID	Reference	Document title
[RD-1]	https://www.eumetsat.int/website/home/Satellites/FutureSatellites/MeteosatThirdGeneration/MTGDesign/index.html	MTG Design - EUMETSAT
[RD-2]	Copernicus Climate Change Service (C3S), 2017 Copernicus Climate Change Service Climate Data Store (CDS), date of access. https://cds.climate.copernicus.eu/cdsapp#!/home	ERA5: Fifth generation of ECMWF atmospheric reanalyses of the global climate.

ID	Reference	Document title
[RD-3]	Saunders, R., Hocking, J., Turner, E., Rayer, P., Rundle, D., Brunel, P., Vidot, J., Roquet, P., Matricardi, M., Geer, A., Bormann, N., and Lupu, C., 2018 Geosci. Model Dev., 11, 2717-2737	An update on the RTTOV fast radiative transfer model (currently at version 12) https://www.nwpsaf.eu/site/software/rttov/rttov-v12/
[RD-4]	Borbas, E and Ruston B.C. 2010. *Report NWPSAF-MO-VS-042, 24pp.*	The RTTOV UWiremis IR land surface emissivity module

2 GENERATION OF THE DATASET

2.1 SELECTION OF THE ATMOSPHERIC SITUATIONS

To generate a large set of representative clear scenes of MTG-IRS observations [RD-1], we first perform a selection to obtain a number of atmospheric situations sufficiently representative of the atmospheric dynamics. To this end, we have chosen to analyse the K-index provided by ECMWF's ERA-5 database [RD-2]. We firstly recall the definition of the K-index. Subsequently, the method used to select the scenes that will be simulated by RTTOV [RD-3] is described. The method is based on the difference of the K-index value for the same Earth point between two different time stamps in the same day.

2.1.1 K-index

The K-index is a measure of air stability. It provides an indication of thunderstorm frequency in a given air mass and can be calculated from:

$$K = (T_{850} - T_{500}) + D_{850} - (T_{700} - D_{700}) \qquad (1)$$

where

- D_{850} : dew point at 850 hPa
- D_{850} : dew point at 850 hPa
- D_{700} : dew point at 700 hPa
- T_{850} : temperature at 850 hPa
- T_{500} : temperature at 500 hPa
- T_{700} : temperature at 700 hPa

The probability of the thunderstorm risk is given by:

$$P = 4 * (K - 15) \qquad (2)$$

The following table correlates the values of the K-index with the probability of thunderstorm occurrence.

Table 1: Relation of Thunderstorm probability to K-index

K-index	Stormy probability (%)
<15	closed to 0
15 - 20	20
21 - 25	20 to 40
26 - 30	40 to 60
31- 35	60 to 80
36-40	80 to 90
> 40	closed to 100

2.1.2 Selection of the situations using the K-index

As explained before, the idea is to extract the ERA-5 situations that are representative of the dynamics of the atmosphere for a given day. Before analysing the K-index, the values of K-index are forced to be in the range [15:40], that is, K-index values smaller than 15 are fixed to 15 while values larger than 40 are fixed to 40. An example of the diurnal variation of the K-index derived from ERA-5 data is given in Table 2.

Table 2: Diurnal variation of K-index values derived from ERA-5 for the scene at 27°S, 72°W on January 1, 2018. K-index is calculated every 3 hours

Times (UTC)	0:00	3:00	6:00	9:00	12:00	15:00	18:00	21:00
K-index	**15.00**	21.98	27.70	33.00	**35.02**	33.70	33.19	33.58

From these values, we determinate and select **the 2 times** that present the maximum difference of the K-indices. In the previous example, K indices at **0:00 UTC and 12:00 UTC are selected.**

Thus, for a given day and for each ERA-5 grid cell, the largest differences in K-index values are computed. Histograms of these largest differences are given in Figure 1.

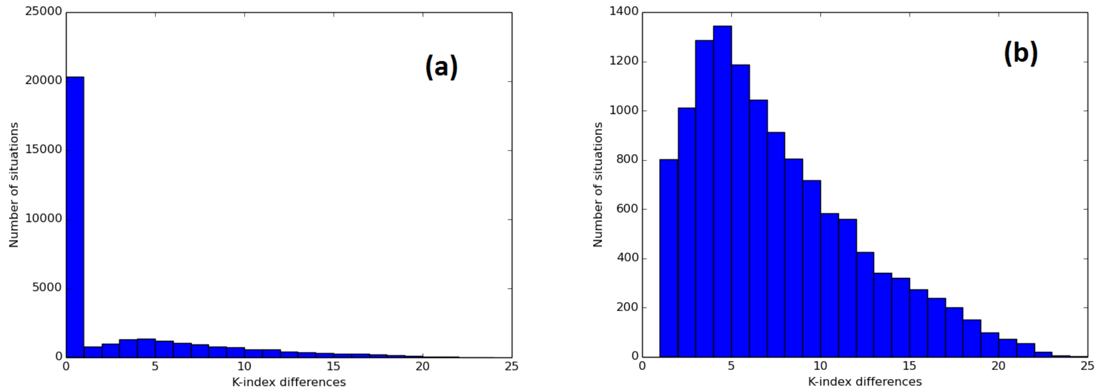

Figure 1: (a) Histogram of maximum difference of K-index. Maximum differences were calculated for all grid points on January 1, 2018. (b) As in (a) but maximum K-index differences smaller than 1 are excluded.

Finally, in order to select representative scenes, we have chosen to extract randomly 25 scenes where the K-index differences are between 0 and 1 (Figure 1 (a)). These situations present the same degree of stability during the day. In a next step, we extracted 225 scenes where the K-index differences are greater than 1 (Figure 1 (b)). At the end, we have 250 scenes; each scene contains 2 timestamps per day.

Figure 2 (a) shows all the selected scenes for January 1, 2018 between 90°W and 90°E (half disc centred to Europe). The colour represents the values of the K-index differences between two selected times.

Figure 2 (b) represents the stable scenes, i.e. K-indices are smaller than 20 during the day. These scenes are randomly distributed over the half-disc.

Figure 2 (c) represents the scenes with some thunderstorms during the day, i.e. K indices are > 20. As expected, these scenes are mainly located in the tropics.

Figure 2 (d) displays the scenes that present a low value K-index and a high value K-index during the day. These scenes provide situations that show the evolution of the atmosphere's stability over the day.

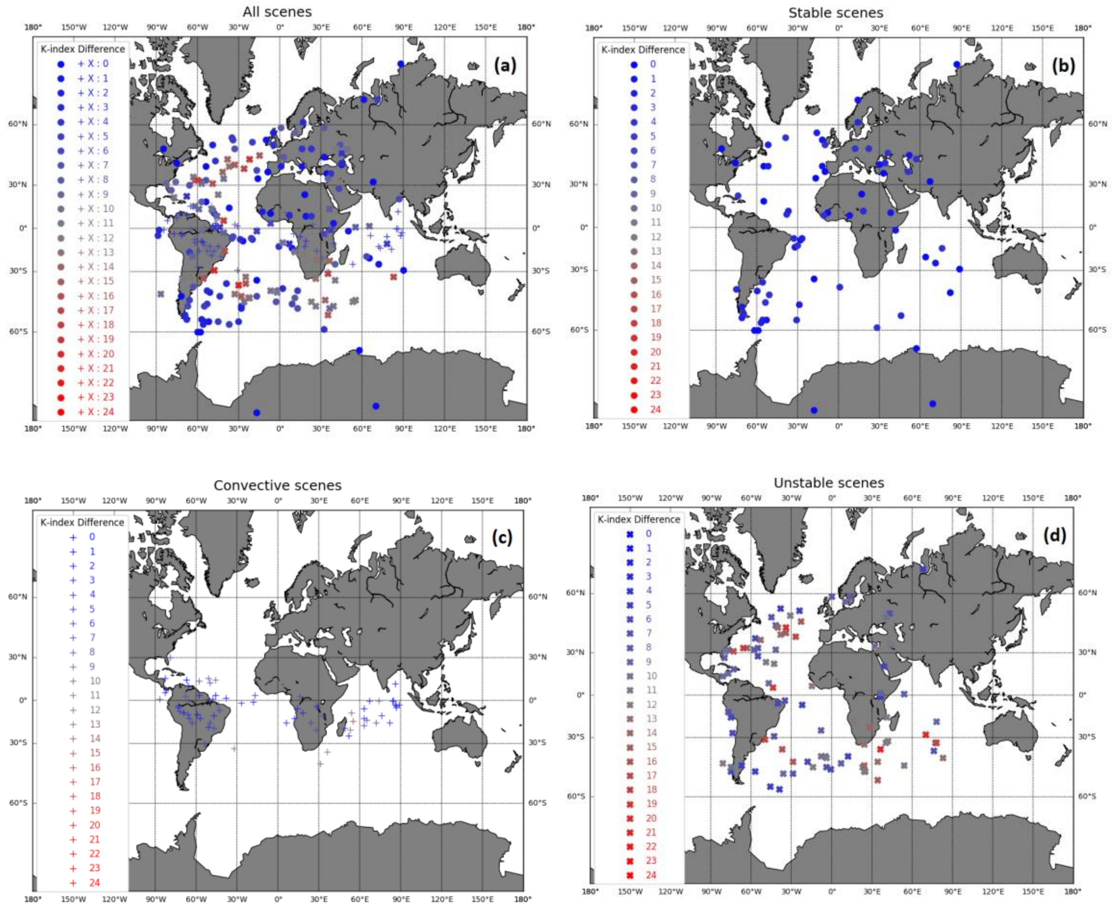

Figure 2: Distribution of K-indices on 1 January 2018. (a) All extracted situations (one-point represents 2 time steps) between [90°E;90°W]. The colour of the point represents the different values of the K-index between the 2 selected times. (b) Situations extracted with low K-index values (inferior to 20: non-stormy scenes). (c) Situations of high K-index values (superior to 20: stormy scenes). (d) Situations with one K-index value inferior to 20 and the other K-index value superior to 20 (unstable scenes during the day).

The method described in this section is applied to the ERA-5 database for extracting relevant scenes (2 time stamps per grid point), for January, April, July and October 2018; 15 days per month with a step of 2 days per month (odd days are selected).

2.2 COMPILATION OF THE DATASET

2.2.1 Pressure profiles and interpolation to the RTTOV pressure levels

In order to decrease the computation time, the profiles of temperature, water vapour and ozone are provided to RTTOV directly on the RTTOV internal pressure levels. To this end:

1. First, the pressure levels of the ERA-5 model are reconstructed for each scene using the surface pressure (section 2.2.1.1);
2. These profiles are then interpolated/extrapolated on the RTTOV internal pressure levels (section 2.2.1.2).

2.2.1.1 Computation of the pressure profiles of the ERA-5 model

For each selected scene, the full pressure levels are computed using the a(n) and b(n) coefficients defining the 137 ECMWF model levels (see ANNEXE A - coefficients defining the 137 model levels). The half-level pressures p_h^i are computed as follows:

$$p_h^i = a(i) + b(i)P_{surf} \tag{3}$$

We deduce the full-level pressures, associated with each model layer (i.e. the middle of the layer), from the half-level pressures (equation (3)):

$$p_f^i = \frac{p_h^{i+1} + p_h^i}{2} \tag{4}$$

2.2.1.2 Interpolation/extrapolation of the RTTOV pressure levels

The profiles for the water vapour, ozone and temperature profiles available at 137 levels are interpolated onto the 101 RTTOV pressure levels using a linear interpolation (linearly in logarithmic pressure). The RTTOV's lowermost pressure level is set to 1100 hPa while ECMWF denotes surface pressures which typically range from 850 to 1100 hPa. Consequently, in case the ECMWF surface pressure is smaller than 1100 hPa, it is necessary to fill the last levels of the profile.

Since these profiles will be used to compute the *a priori* variance-covariance matrices as part of the next step of this study, we applied a linearly extrapolation in logarithmic pressure to fill the missing levels. However, this extrapolation does not ensure that the *a priori* matrices remain invertible and distorts the *a priori* matrices at the levels next to the surface. That is the reason why those levels are not taken into account during the computation of the *a priori* variance-covariance matrices (see section 3.2).

2.2.2 Examples of means and standard deviations of the dataset

Mean and corresponding standard deviation of the ozone, water vapour and temperature profiles have been computed for the five geographic areas. These profiles, extracted from the ERA-5 data of ECMWF, are part of RTTOV inputs. Figure 3 and Figure 4 provide examples of such mean profiles.

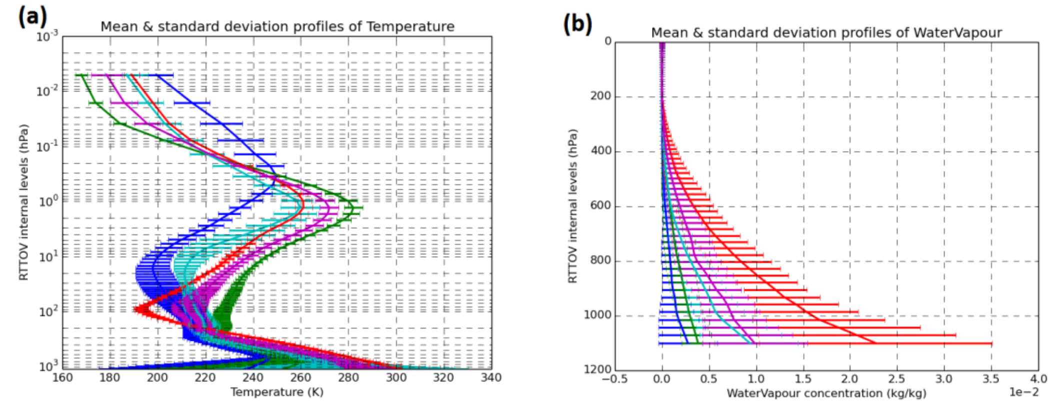

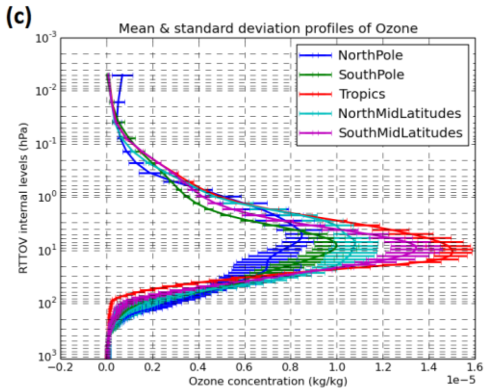

Figure 3: Mean and standard deviation of the profiles of (a) temperature; (b) water vapour and (c) ozone, averaged in January over Tropics (red), Northern Mid-latitudes (cyan), Southern Mid-latitudes (purple), North pole (blue) and South pole (green).

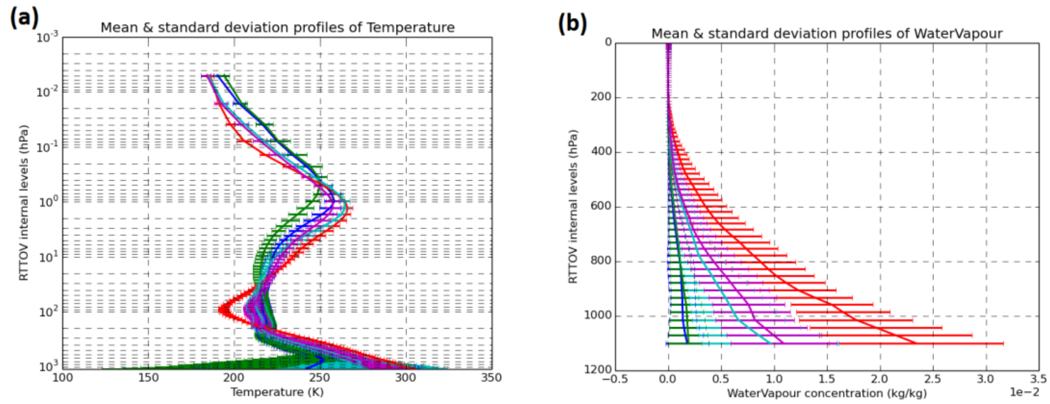

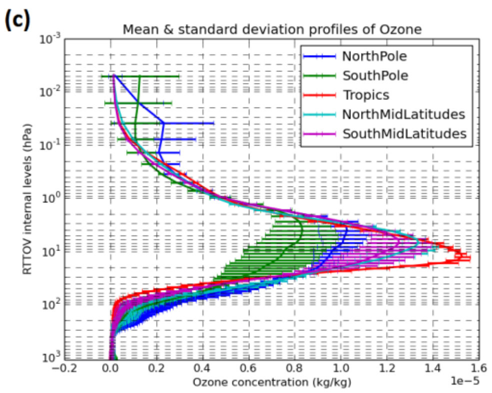

Figure 4: Mean and standard deviation of the profiles of (a) temperature; (b) water vapour and (c) ozone, averaged in April over Tropics (red), Northern Mid-latitudes (cyan), Southern Mid-latitudes (purple), North pole (blue) and South pole (green).

2.2.3 ERA-5 data used as input for RTTOV

In this section, we list the data of ERA-5 which are used as input for RTTOV:

- Localisation:
  - Latitude (mandatory RTTOV input)
  - Longitude,
  - Date (mandatory RTTOV input);
- Profile data, interpolated onto the 101 RTTOV level pressures:
  - Water vapour (mandatory RTTOV input),
  - Ozone,
  - Temperature (mandatory RTTOV input);
- Surface properties:
  - Surface pressure (mandatory RTTOV input),
  - Land sea mask (mandatory RTTOV input),
  - Sea-ice fraction (mandatory RTTOV input),
- Skin temperature (mandatory RTTOV input),
  - 2 meter temperature (mandatory RTTOV input),
  - 10m wind u, v components (required for sea surface type only to compute the surface emissivity).

In addition, the K-index variable is also extracted.

2.2.4 Description of the HDF5 file

In this section, we present the HDF5 file structure. This proposed structure can be discussed and adapted according to EUMETSAT comments.

The following screenshot (**Figure 5**) shows the HDF5 file structure:

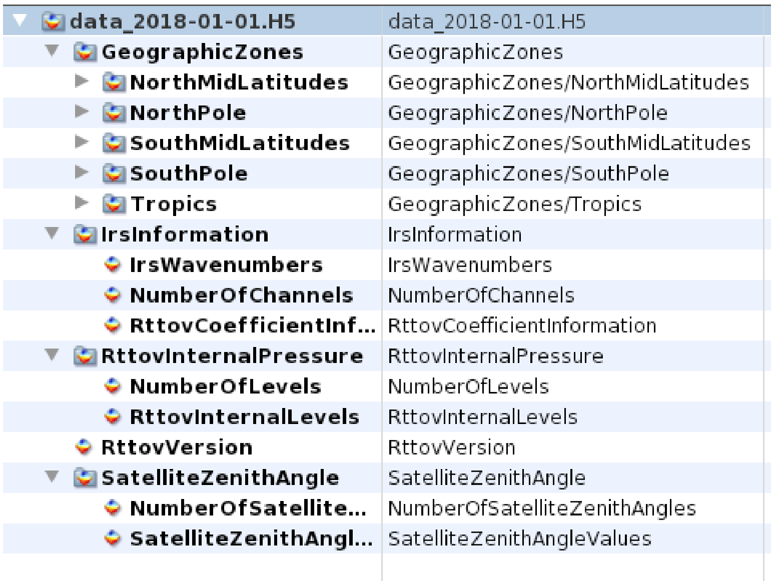

Figure 5: HDF5 file structure

The information of the extracted scenes is aggregated by region: North/South mid-latitude; North/South pole and tropics.

The IRS information like the wavenumbers of IRS channels, the number of channels and the name of the RTTOV coefficients are stored in the field “IRS information”.

The profiles in this file are provided on the RTTOV internal pressure levels. The number of pressure levels (101) and the values of these pressure levels are regrouped in the field “RTTOV internal levels”.

In each region, the scenes are separated between “Sea surface” and “Land surface”. In each of these two subfields, we find:

- **RTTOV input** (Figure 6): it contains the information needed by RTTOV to compute spectra and Jacobians for each scene;
- **Scene characterisation** (Figure 6): it contains the K-index, land-sea mask and sea ice area fraction for each scene in the region;
- **RTTOV output** (Figure 7): it contains all the Jacobians and the associated radiance spectrum for each satellite zenith angle in the range from 0° to 85° (by 5° step) and each scene :
    - The emissivity spectra used by RTTOV. The corresponding array has the following dimension: number of scenes, number of angles, and number of channels.
    - The Jacobians w. r. t. the temperature, the logarithm of the water vapour mixing ratio and the logarithm of the ozone-mixing ratio are written into on array. The corresponding Jacobian array has the following dimension: number of scenes, number of angles, number of channels and finally the number of levels multiplied by 3 (as there are profiles of the 3 variables).
    - The surface temperature and surface emissivity Jacobians are stored separately for each geographic area, with the following dimension: number of scenes, number of angles, and number of channels.
    - A quality flag is also stored in order to indicate if any inputs of RTTOV are out of range of the validity domain. The quality is provided by channels. If the value of the quality flag is:

- 0: For successful simulation without any warning;
- 1: the simulation presents at least one RTTOV warning (probably on gas concentration is out of RTTOV validity range);
- 2: RTTOV simulation failed;

data_2018-01-01.H5	data_2018-01-01.H5	Local File
GeographicZones	GeographicZones	—
NorthMidLatitudes	GeographicZones/NorthMidLatitudes	—
LandSurface	GeographicZones/NorthMidLatitude...	—
NumberOfSce...	NumberOfScenes	—
OEMOneState...	GeographicZones/NorthMidLatitude...	—
RttovInput	GeographicZones/NorthMidLatitude...	—
APrioriMatrix	GeographicZones/NorthMidLatitude...	—
DateTime	DateTime	—
Latitude	Latitude	1D
Longitude	Longitude	1D
Profiles	GeographicZones/NorthMidLatitude...	—
Ozone	Ozone	2D
Tempera...	Temperature	2D
WaterVa...	WaterVapour	2D
SurfacePro...	GeographicZones/NorthMidLatitude...	—
10MeterU...	10MeterUWindComponent	1D
10MeterV...	10MeterVWindComponent	1D
2MeterTe...	2MeterTemperature	1D
SkinTemp...	SkinTemperature	1D
SurfaceP...	SurfacePressure	1D
RttovOutput	GeographicZones/NorthMidLatitude...	—
SceneCharact...	GeographicZones/NorthMidLatitude...	—
KIndex	KIndex	1D
Land-seaMa...	Land-seaMask	1D
SeaSurface	GeographicZones/NorthMidLatitude...	—
NorthPole	GeographicZones/NorthPole	—
SouthMidLatitudes	GeographicZones/SouthMidLatitudes	—
SouthPole	GeographicZones/SouthPole	—
Tropics	GeographicZones/Tropics	—
IrsInformation	IrsInformation	—
RttovInternalPressure	RttovInternalPressure	—
RttovVersion	RttovVersion	—
SatelliteZenithAngle	SatelliteZenithAngle	—

Figure 6: HDF5 file: detailed input structure by geographical zone and by surface type

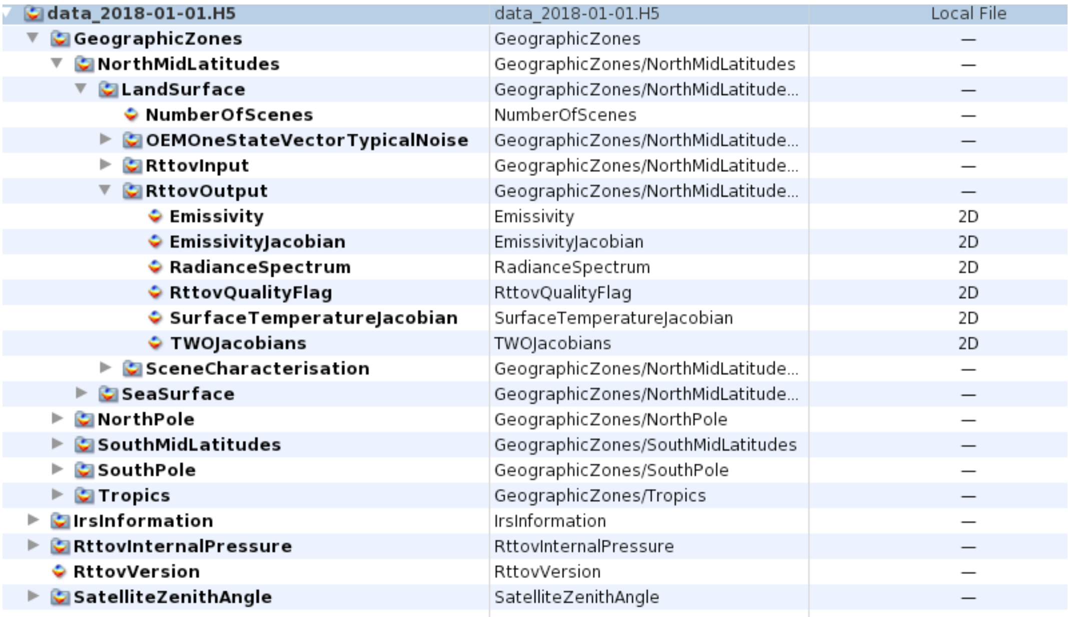

Figure 7: HDF5 file: detailed output structure by geographical zone and surface type

Furthermore, a description is associated to each variable of the HDF5 file. Here is an example on the Figure 8 :

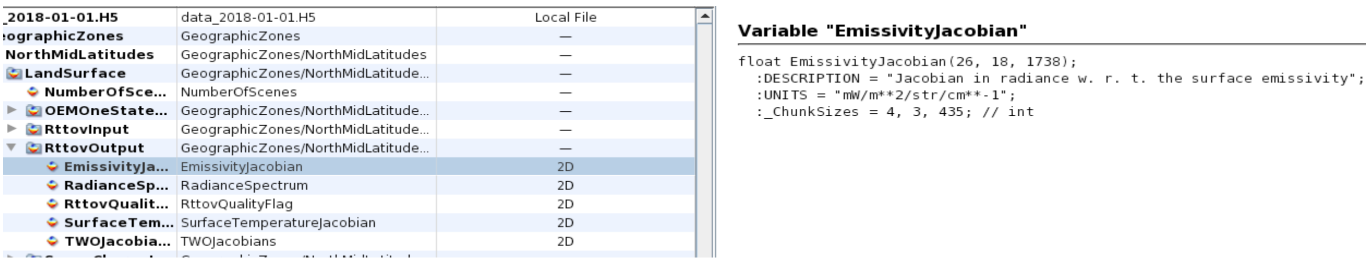

Figure 8: Description of a variable in the HDF5 file

On the right column of Figure 8, type, name and dimension of the variable are mentioned in the first line. In the second line, a short description provides the basic information on the variable. The third line indicates the unit of the variable. Finally, on the last line, the chunk size is given. It indicates how the data are stored in the file.

2.3 SIMULATIONS WITH RTTOV

2.3.1 RTTOV configuration

A configuration for RTTOV has been defined, containing the following information:

- The RTTOV version used for this study: RTTOV V12.2;
- Surface emissivity:
  - Over land: UW IREMIS atlases are used [RD-4],
  - Over sea: provided by the RTTOV internal sea surface emissivity model IREMIS (not UWIREMIS);
- The simulation are performed without cloud and aerosol, i.e. in clear sky situations only;
- The RTTOV Jacobians are provided by RTTOV in terms of radiance;
- The temperature is fixed to the 2 meter temperature for the pressure levels superior to the surface pressure;
- The solar radiation is not taken into account.

2.3.2 Examples of RTTOV outputs

2.3.2.1 Examples of radiances

The following Figure 9 shows the mean of IRS radiances over the scenes in Tropics (30°S:30°N), Northern Mid-latitudes (30°N:60°N), Southern Mid-latitudes (60°S:30°S), north pole (60°N:90°N) and south pole (90°S:60°S) and for two different satellite zenith angles: at nadir and for SZA=85°. These curves have been computed using the database and over the available period.

As expected:

- the values of the radiance are higher at nadir than for a 85° satellite zenith angle;
- The radiances are higher in the tropics, where the temperature values are the highest. In comparison, the radiances are lower at the poles.

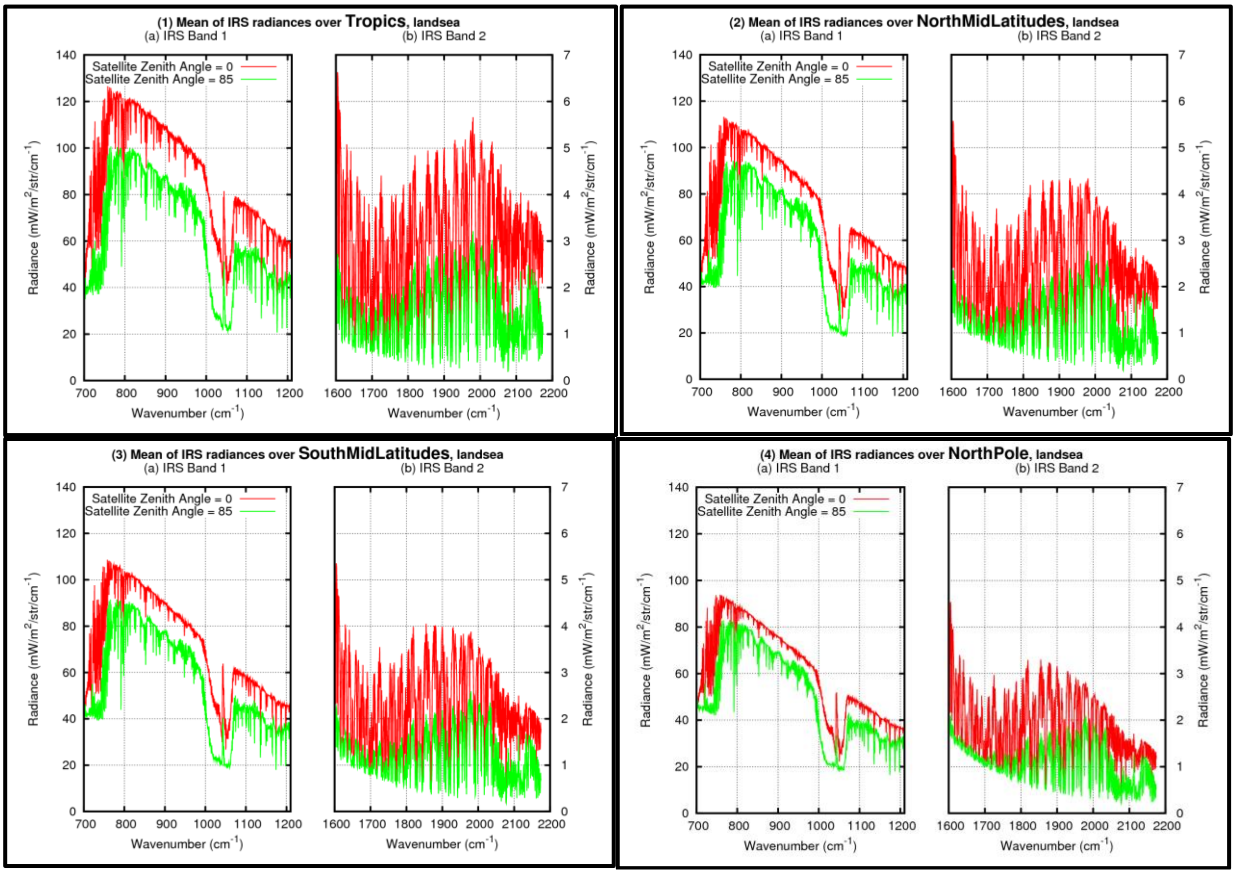

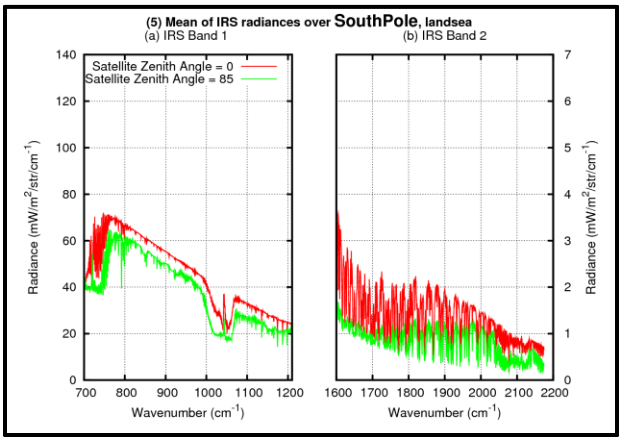

Figure 9: Mean of IRS *radiances* over (1) Tropics (30°S:30°N), (2) Northern Mid-latitudes (30°N:60°N), (3) Southern Mid-latitudes (60°S:30°S), (4) north pole (60°N:90°N) and (5) south pole (90°S:60°S) for a nadir viewing point (red) and for a 85° Satellite Zenith Angle (green). (a) Mean IRS radiances for the first IRS band. (b) Mean radiances for the second IRS bands.

2.3.2.2 Examples of radiance sensitivities (Jacobians)

Here, we present some radiance sensitivities computed using the Jacobians available in the database.

2.3.2.2.1 Temperature

Figure 10 shows the mean of the Jacobians w.r.t. the temperature per Kelvin per layer for all layers over the scenes in the Tropics (30°S:30°N), Northern Mid-latitudes (30°N:60°N), Southern Mid-latitudes (60°S:30°S), north pole (60°N:90°N) and south pole (90°S:60°S) and for two different satellite zenith angles (nadir and SZA=85°). These curves have been computed using the database and over the available period.

For the first IRS band (700 - 1210 cm^{-1}), the radiances are more sensitive to the temperature profile at a satellite zenith angle of 85° than at nadir. Conversely, for the second IRS band (1600 - 2175 cm^{-1}), the radiances are less sensitive to the temperature profile at a satellite zenith angle of 85° than at nadir.

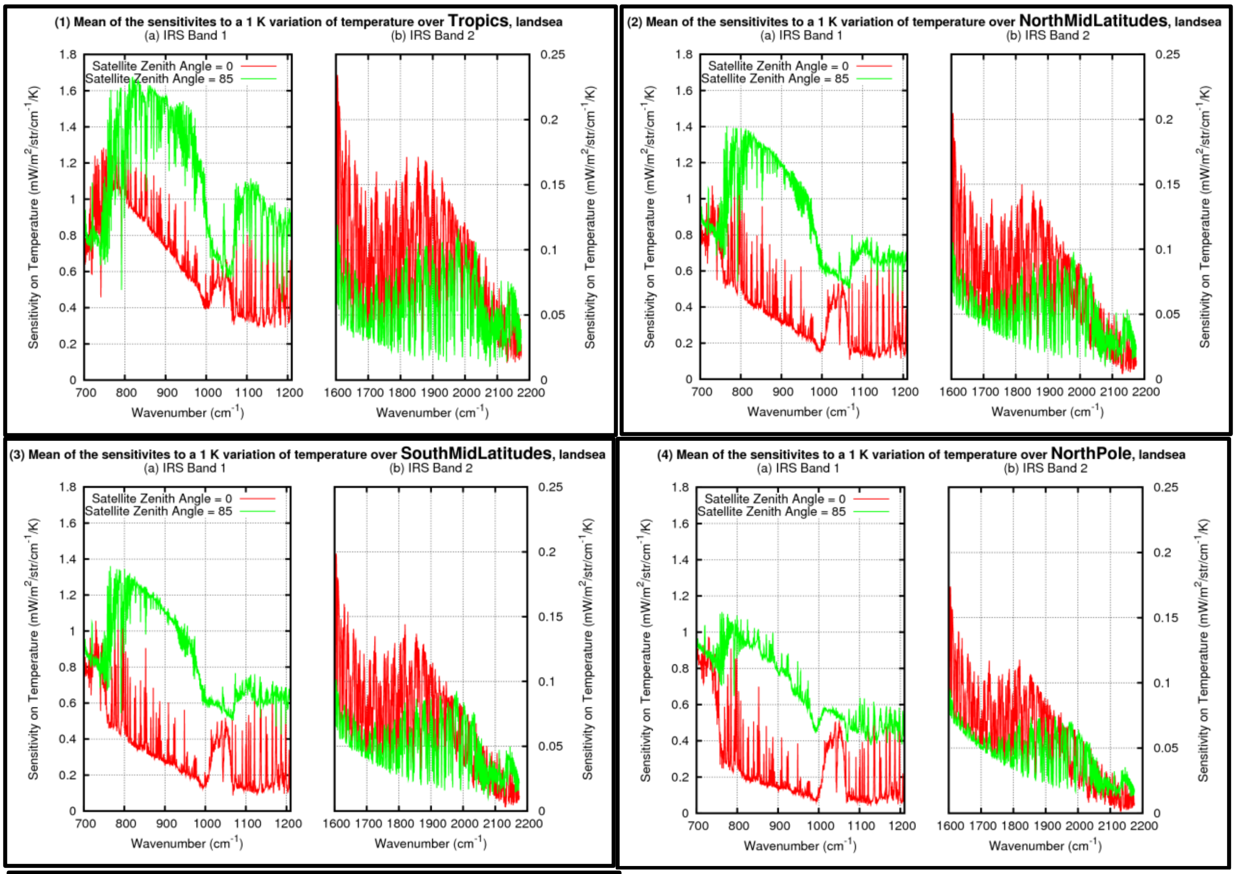

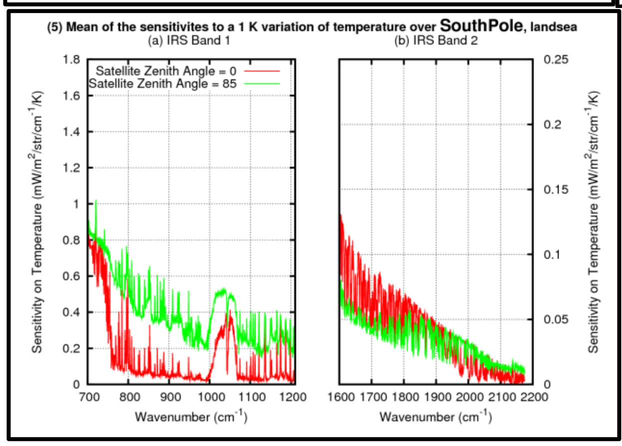

Figure 10: Mean of the Jacobians w.r.t. the temperature per Kelvin.layer for all layers over (1) Tropics (30°S:30°N), (2) Northern Mid-latitudes (30°N:60°N), (3) Southern Mid-latitudes (60°S:30°S), (4) north pole (60°N:90°N) and (5) south pole (90°S:60°S) for a nadir viewing point (red) and for a 85° Satellite Zenith Angle (green). (a) Mean Jacobian for the first IRS band. (b) Mean Jacobian for the second IRS bands.

2.3.2.2.2 Water vapour

Figure 11 shows the mean of the Jacobians w.r.t. the water vapour per layer for 20% variation of H_2O for all layers over the scenes in the Tropics (30°S:30°N), Northern Mid-latitudes (30°N:60°N), Southern Mid-latitudes (60°S:30°S), north pole (60°N:90°N) and south pole (90°S:60°S) and for two different satellite zenith angles (nadir and SZA=85°). These curves have been computed using the database and over the available period.

For the first IRS band (700-1210 cm^{-1}), the radiances are more sensitive to the water vapour profile for a satellite zenith angle of 85° than at nadir. Conversely, the second IRS band (1600 - 2175 cm^{-1}), the radiances are less sensitive to the water vapour profile for a satellite zenith angle of 85° than at nadir. The scenes over tropics are more sensitive to the water vapour as the water vapour mixing ratios become more important. Inversely, for the scenes over the poles, the radiances are a little sensitive to the water vapour because the H_2O mixing ratio is low.

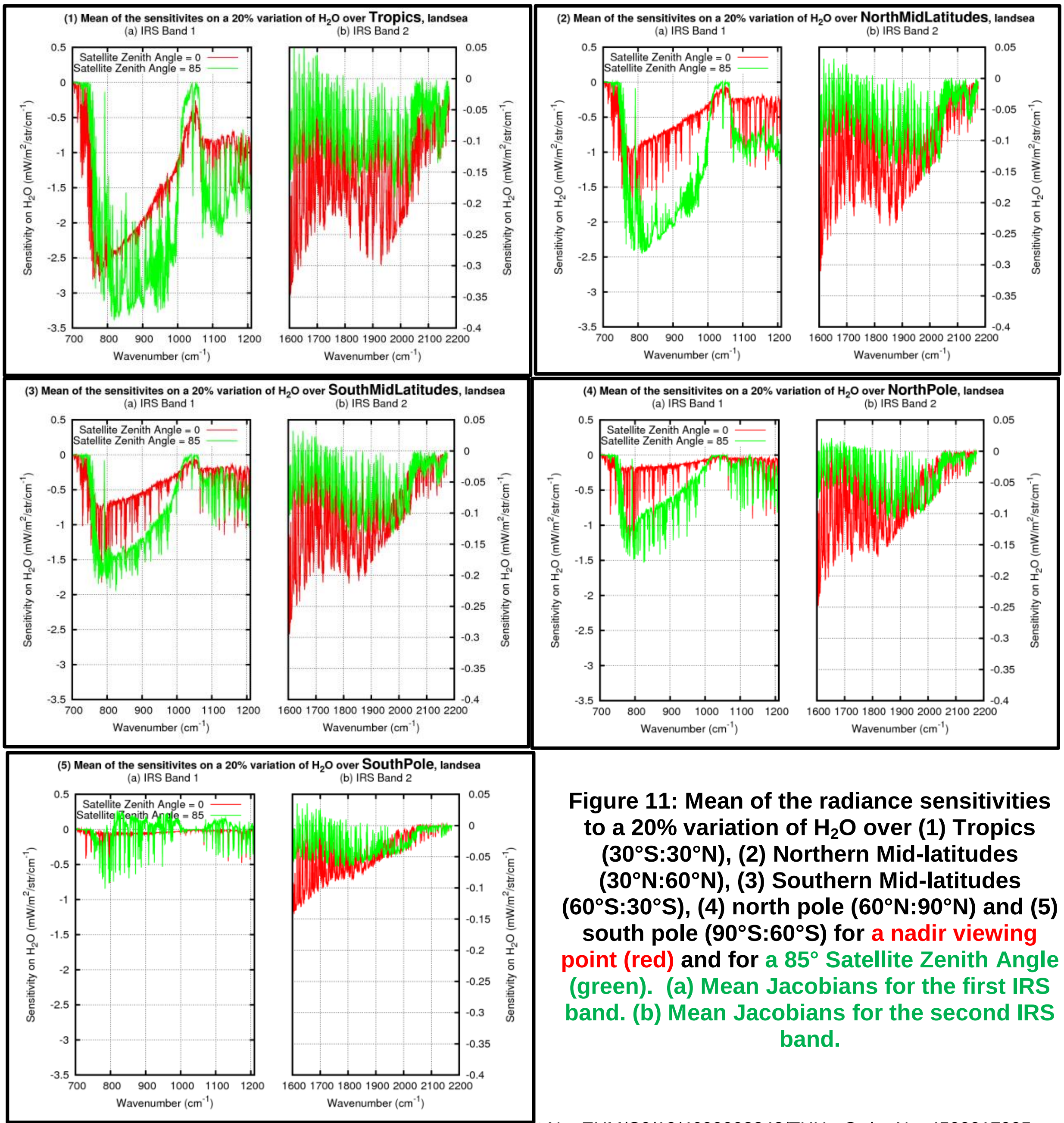

Figure 11: Mean of the radiance sensitivities to a 20% variation of H_2O over (1) Tropics (30°S:30°N), (2) Northern Mid-latitudes (30°N:60°N), (3) Southern Mid-latitudes (60°S:30°S), (4) north pole (60°N:90°N) and (5) south pole (90°S:60°S) for a nadir viewing point (red) and for a 85° Satellite Zenith Angle (green). (a) Mean Jacobians for the first IRS band. (b) Mean Jacobians for the second IRS band.

2.3.2.2.3 Ozone

The following Figure 12 shows the mean of Jacobians w.r.t. ozone for 10% variation of O_3 per layer for all layers over the scenes in the Tropics (30°S:30°N), Northern Mid-latitudes (30°N:60°N), Southern Mid-latitudes (60°S:30°S), north pole (60°N:90°N) and south pole (90°S:60°S) and for two different satellite zenith angles: at nadir and for SZA=85°. These curves have been computed using the database and over the available period.

In the first IRS band, the radiance sensitivities of ozone are located between 700 and 800 cm^{-1}, 960 and 1200 cm^{-1}. In the second IRS band, the IRS channels are a little sensitive to ozone between 2000 and 2200 cm^{-1}.

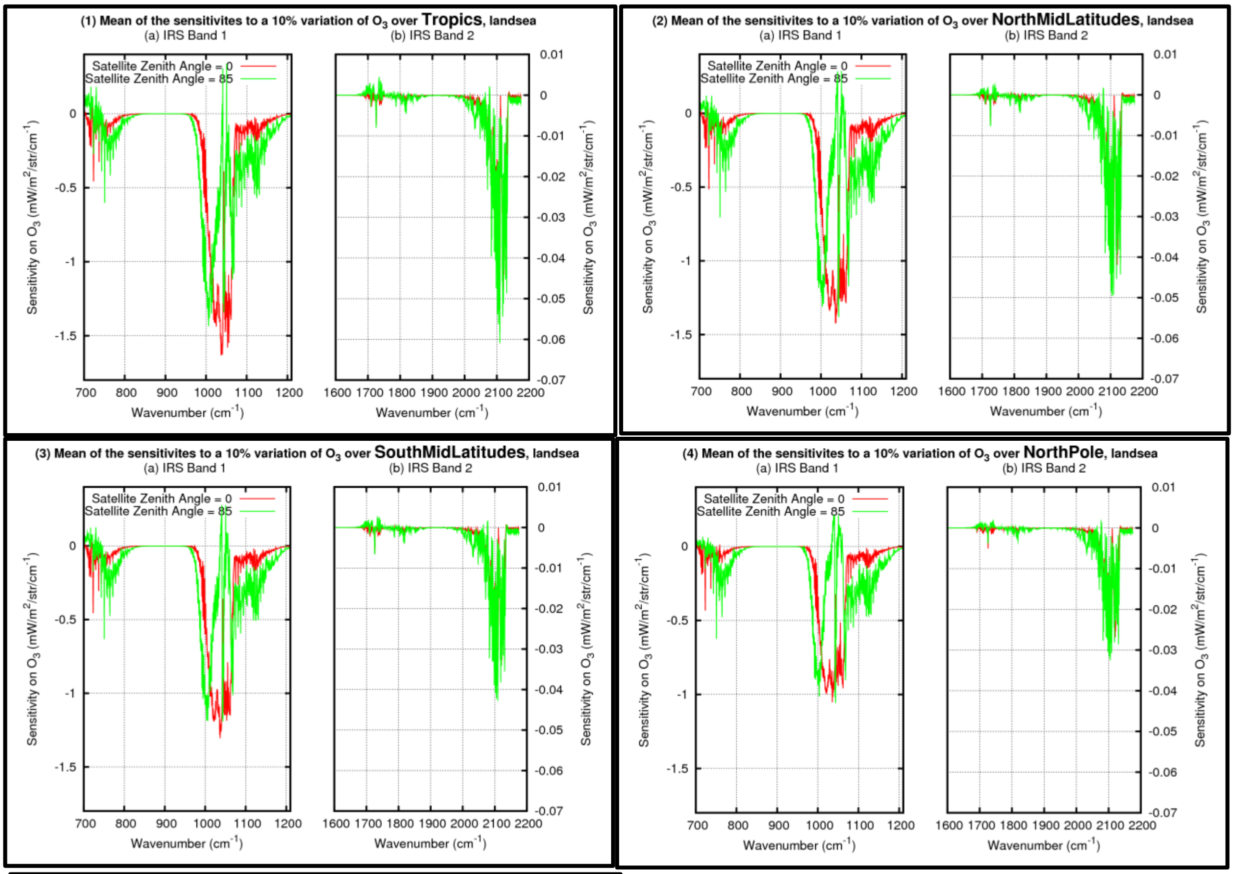

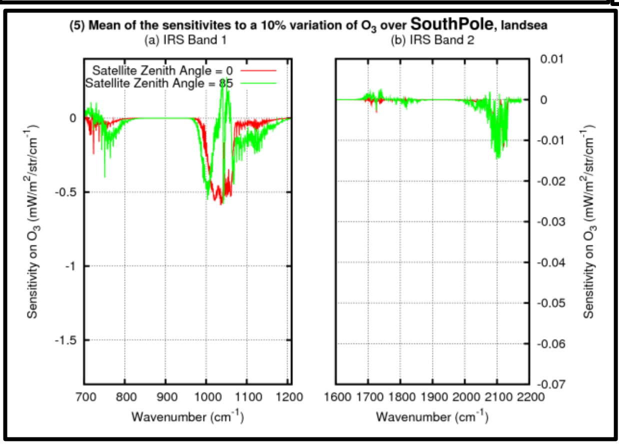

Figure 12: Mean of the radiance sensitivities to a 10% variation of O_3 over (1) Tropics (30°S:30°N), (2) Northern Mid-latitudes (30°N:60°N), (3) Southern Mid-latitudes (60°S:30°S), (4) north pole (60°N:90°N) and (5) south pole (90°S:60°S) for a nadir viewing point (red) and for a 85° Satellite Zenith Angle (green). (a) Mean Jacobians in the first IRS band. (b) Mean Jacobians in the second IRS band.

2.3.2.2.4 Emissivity

The following Figure 13 represents the mean of the radiance sensitivities to a 0.1 emissivity variation. These curves have been computed using the Jacobians w.r.t. the surface emissivity provided by the database.

As expected, the radiances are more sensitive to the emissivity at nadir than at a satellite zenith angle of 85°. The only exception appears for the South Pole scenes where the sensitivities are quite close.

<u>Note:</u> Over sea, the emissivity is provided by the internal RTTOV database IREMIS (not UWIREMIS). In these cases, the Jacobian w.r.t the surface emissivity is not computed by RTTOV as explained in the RTTOV user-guide. To solve this problem, RTTOV is called a second time with the emissivity as RTTOV input provided by the previous call. In this case, the Jacobian w.r.t the surface emissivity is computed by RTTOV and stored in the dataset.

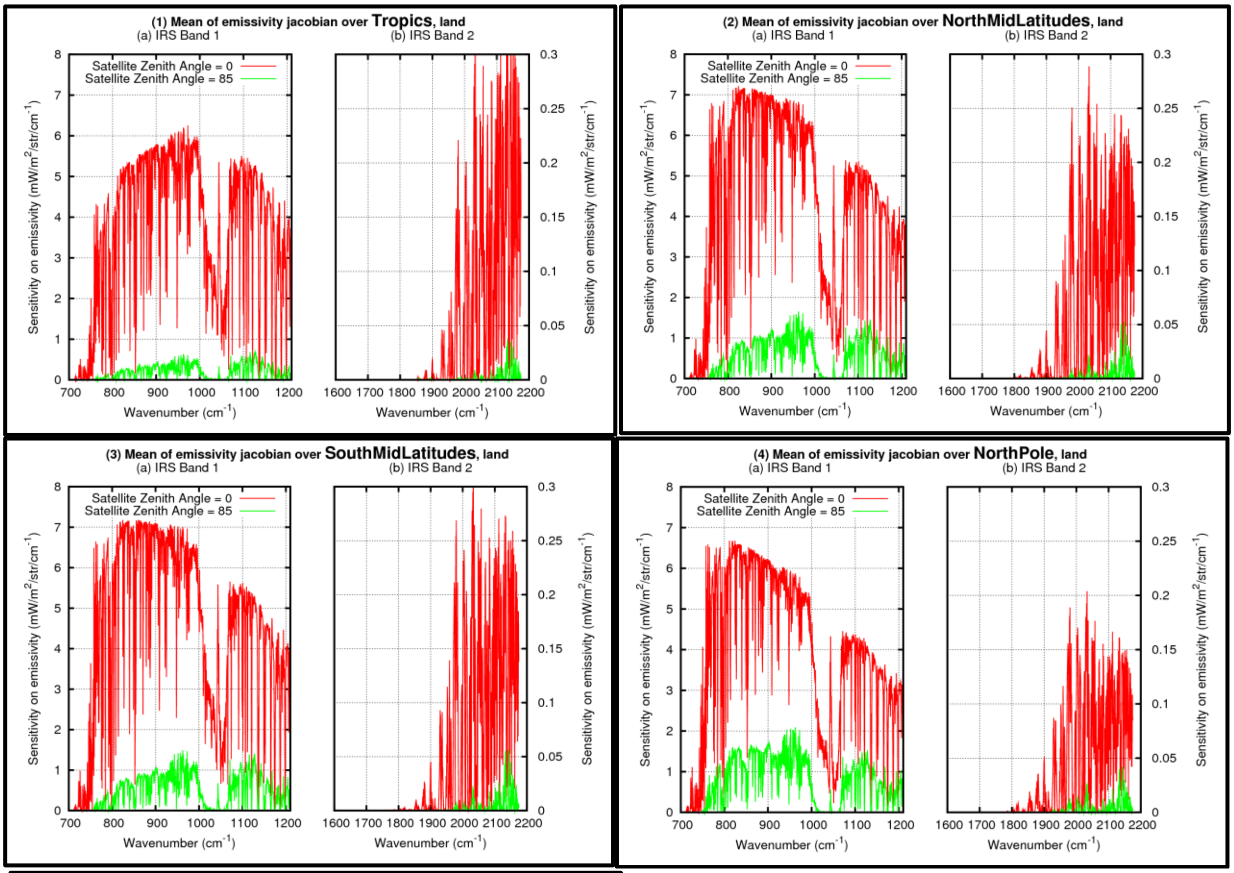

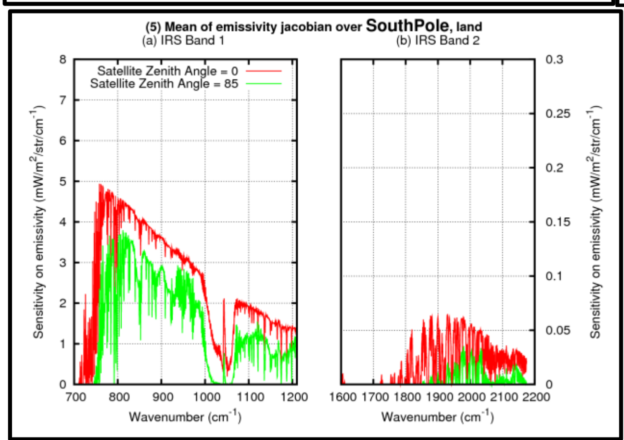

Figure 13: Mean of the Jacobians w.r.t the surface emissivity for 10% variation of the emissivity over (1) Tropics (30°S:30°N), (2) Northern Mid-latitudes (30°N:60°N), (3) Southern Mid-latitudes (60°S:30°S), (4) north pole (60°N:90°N) and (5) south pole (90°S:60°S) for a nadir viewing point (red) and for SZA=85° (green). (a) Sensitivities obtained for the first IRS band. (b) Sensitivities obtained for the second IRS band.

2.3.2.2.5 Surface temperature

The following Figure 14 shows the mean of the radiance sensitivities to 1 K variation of the surface temperature over the scenes in Tropics (30°S:30°N), Northern Mid-latitudes (30°N:60°N), Southern Mid-latitudes (60°S:30°S), north pole (60°N:90°N) and south pole (90°S:60°S) and for two different satellite zenith angles: at nadir and for SZA=85°. These curves have been computed using the database and over the available period.

The radiances for a satellite zenith angle of 85° are weakly sensitive to the surface temperature in comparison with the radiances at nadir. At SZA=85°, the IRS channels are less sensitive to the surface temperature in the tropics. Going poleward, the radiances become more and more sensitive to the surface temperature for a satellite zenith angle of 85°.

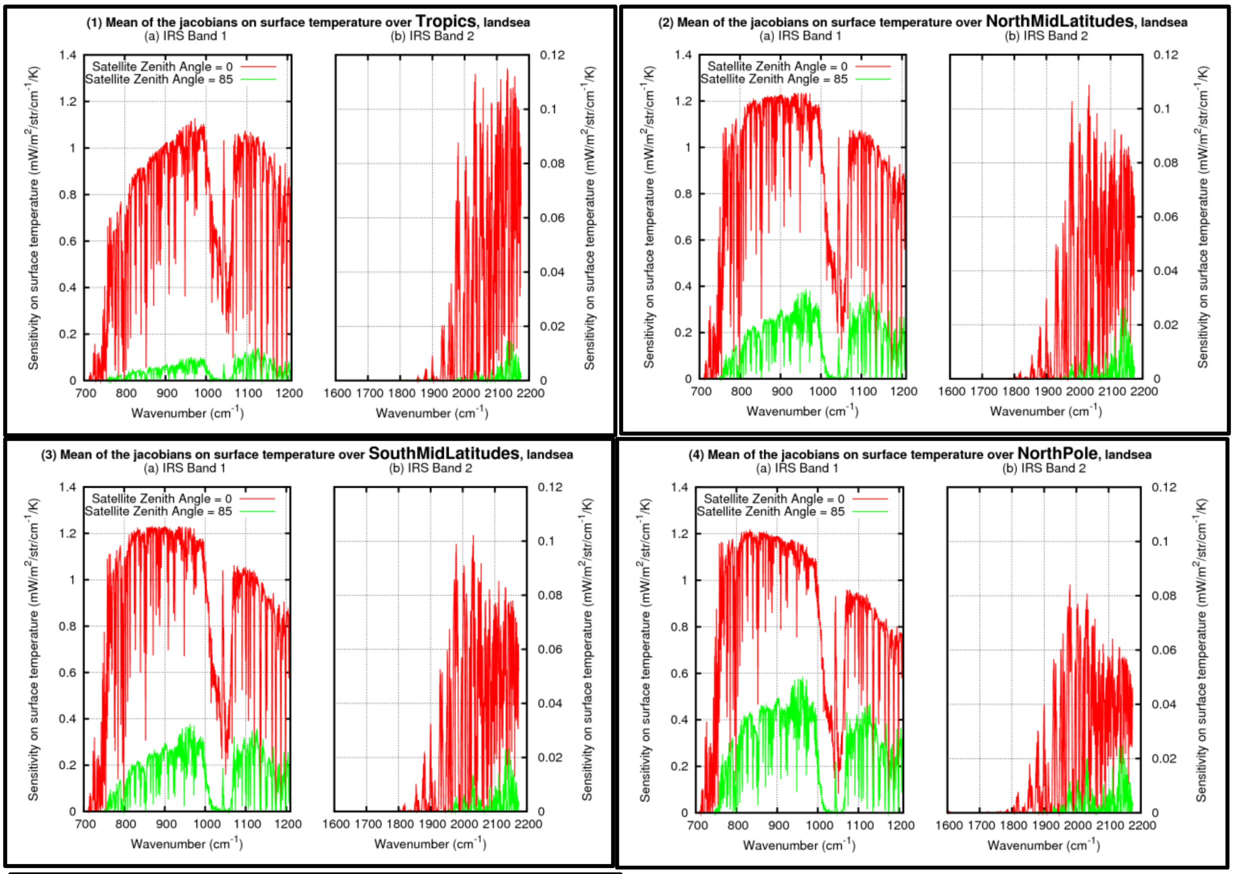

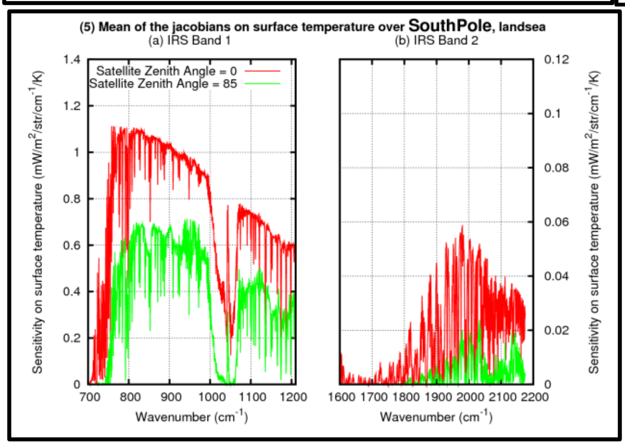

Figure 14: Mean of the Jacobians w.r.t the surface temperature for 1 K variation of the surface temperature over (1) Tropics (30°S:30°N), (2) Northern Mid-latitudes (30°N:60°N), (3) Southern Mid-latitudes (60°S:30°S), (4) north pole (60°N:90°N) and (5) south pole (90°S:60°S) for a nadir viewing point (red) and for a 85° Satellite Zenith Angle (green). (a) Sensitivities obtained for the first IRS band. (b) Sensitivities obtained for the second IRS band.

3 RETRIEVAL ERRORS ASSESSMENT

3.1 DESCRIPTION OF THE METHOD

The method used to assess the retrieval errors for all Jacobians described previously (Phase A) is the Optimal Estimation Method (OEM). OEM formulates the retrieval as a minimisation problem. It aims at retrieving a state vector from a single observation vector and *a priori* information used to constrain the inversion. The cost function to minimize is the following:

$$J = \left(y - F(x)\right)^T S_y^{-1}\left(y - F(x)\right) + (x_a - x)^T S_a^{-1}(x_a - x) \quad \textbf{(5)}$$

Where:

- x is the state vector to be retrieved
- x_a is the a priori state vector
- S_a is the error variance-covariance matrix of the a priori state vector
- y is the observation vector
- S_y the error covariance matrix of observation
- $F(x)$ is the forward model function

The minimisation of the cost function is performed following an iterative process that updates the state vector x using the Jacobians K of the forward model F. The corresponding *a posteriori* error variance-covariance matrix contains retrieval errors and correlations between the elements of the state vector; it is calculated as follows:

$$\hat{S} = \left(K^T S_y^{-1} K + S_a^{-1}\right)^{-1} \quad \textbf{(6)}$$

Matrix $\hat{S}$ represents the variance/covariance matrix of the *a posteriori* error of the elements of the state vector. The diagonal elements provide information on the estimated error of each element of the state vector, while the off-diagonal elements provide information on the error correlation between the elements. The retrieval variance-covariance matrix $\hat{S}$ can be decomposed into measurement error matrix and smoothing error matrix. The smoothing error matrix S_{smooth} is the error source associated with a priori information, which is in our case the a priori variance-covariance matrix. The measurement error matrix S_m is the error source associated with the observation error matrix. When the measurement error is large compared to the smoothing error, the retrieval error does not depend on the a priori information. These two error values are used to determine the impact of the a priori information on the retrieval error budget.

$$\hat{S} = S_m + S_{smooth} \quad \text{with} \quad S_m = G.S_\varepsilon.G^T \quad \text{and} \quad S_{smooth} = (A - I)\, S_a\, (A - I)^T \quad \textbf{(7)}$$

The performance of the inversion can be analysed through the following quantities:

- Averaging Kernels: Averaging kernels represent the sensitivity of the retrieval to the true state, allowing the evaluation of the vertical resolution;
- The number of degrees of freedom (or DOFS for Degree Of Freedom For Signal): DOFS are obtained by calculating the trace of Averaging Kernels and provide global information, in particular on how many useful independent quantities can be found in a measurement;
- *A priori/a posteriori* errors: These errors represent errors before (*a priori*) and after (*a posteriori*) the retrieval processing, respectively.

The Averaging Kernel matrix is by definition:

$$A = \frac{\partial \hat{x}}{\partial x} = \left(K^T S_y^{-1} K + S_a^{-1}\right)^{-1} \left(K^T S_y^{-1} K\right) \quad \textbf{(8)}$$

The elements $A(i,j)$ of the Averaging Kernel matrix provide the relative contribution of the elements $x(i)$ of the true state vector to each element $\hat{x}(j)$ of the retrieved state vector.

Considering a linear approach, the gain matrix G (or the contribution function matrix) can be defined as follows:

$$G = \left(K^T S_y^{-1} K + S_a^{-1}\right)^{-1} K^T S_y^{-1} = \hat{S}\, K^T S_y^{-1} = \frac{\partial \hat{x}}{\partial y} \quad \textbf{(9)}$$

The gain matrix can be readily computed from the Jacobians and the Averaging Kernel matrices. The gain is appropriate for studying the variations of the state vector elements according to the variation of the observation vector. For example, the gain matrix G can be used to determine the impact of the emissivity errors on the retrievals, knowing the emissivity Jacobian of the observation vector and whether emissivity is included in the state vector.

In case of having the emissivity not included in the state vector, the impact of an emissivity error on the retrieval can be computed using the emissivity Jacobian and the Gain matrix (Eq. 11). More generally, the systematic error of a parameter X, denoted ε_X , can be transported as an systematic error ε_{ret}, to the retrieval using the Jacobians w. r. t. X, denoted K_X, according to:

$$\varepsilon_{ret} = G.K_X.\varepsilon_X \quad \textbf{(10)}$$

If we assume that the error of the parameter X is Gaussian distributed and characterised by the variance-covariance matrix S_x, the associated retrieval error matrix S_{ret} can be calculated from:

$$S_{ret} = G.K_X.S_X.{K_X}^T.G^T \quad \textbf{(11)}$$

In conclusion, the impact of an error on the emissivity and the surface temperature can be studied and derived in terms of retrieval error using the previous equations

3.2 COMPUTATION OF THE *A PRIORI* VARIANCE-COVARIANCE ERROR MATRICES

3.2.1 General procedure

To perform the optimal estimation computations, we have calculated the *a priori* variance-covariance error matrices using the profiles of the generated dataset.

These matrices are computed:

- Per zone (same zone as in the generated dataset): Tropics, Northern Mid-latitudes, Southern Mid-latitudes, northern high-latitudes and southern high-latitudes;
- For water vapour and ozone, we calculated the correlations using the logarithm of the mixing ratio;

- Taking into account the surface pressure for each scene. Initially, the profiles used to compute the matrices were extrapolated linearly between the surface pressure level of the scene and the last level of the RTTOV internal pressure grid (see section 2.2.1.2). However, since further unrealistic information could be provided, this could generate unstable *a priori* variance-covariance matrices. So in the current version, the values for temperature, water vapour and ozone are set to NaN for levels between the surface level and the last level of RTTOV. An appropriate function of the Numpy library able to manage NaN values is used to calculate the *a priori* covariance matrix;
- The matrices are then recomputed in order to obtain a smaller condition number. Please see 3.2.2 for further information;
- The *a priori* error matrix for each zones is constructed as: $S_a = \begin{pmatrix} \boldsymbol{T} & 0 & 0 \\ 0 & \boldsymbol{W} & 0 \\ 0 & 0 & \boldsymbol{O} \end{pmatrix}$.
- **The cross correlations between temperature, water vapour and ozone are not taken into account.**

3.2.2 Conditioned *a priori* matrices and retrieved error

The condition number corresponds to the ratio between the maximal and the minimal eigenvalues. The condition number of the *a priori* matrix should not be too large; otherwise the matrix system of the Optimal Estimation Method (OEM) could not be well-conditioned and could lead to large numerical errors. To obtain the reconditioned matrices, all the negative eigenvalues are fixed to a small positive number and the highest eigenvalues are reduced.

In order to choose a relevant condition number, it is necessary to observe the impact of a reconditioned matrix on the retrieved error profile. To this end, the *a priori* matrices have been computed for several condition numbers: 6 000, 10 000 and 20 000. Then an analysis in terms of retrieval error profiles permits to evaluate the impact of the *a priori* matrices on the result. The computation of retrievals errors is described in 3.5.

To begin, here is a representation of the profile of the *a priori* matrices for temperature, ozone and water vapour above the Tropics (see Figure 15, Figure 16 and Figure 17 respectively). The different curves correspond to a specific conditioning:

- NONCOND: the a priori matrix is not conditioned;
- COND06 : the *a priori* matrix is conditioned with a condition number equal to 6 000;
- COND10: the *a priori* matrix is conditioned with a condition number equal to 10 000;
- COND20: the *a priori* matrix is conditioned with a condition number equal to 20 000.

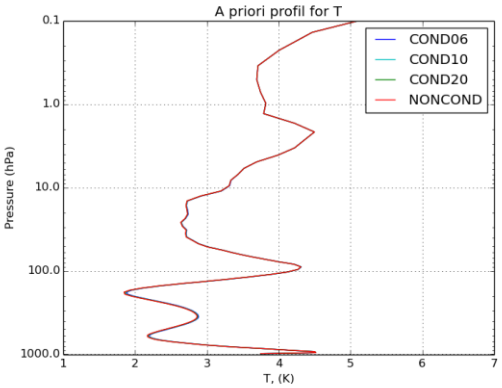

Figure 15: Profile (square root of the diagonal) of the temperature *a priori* variance-covariance error matrix for three different condition numbers (6000 in blue, 10000 in cyan and 20000 in green) compared to the profile of the non-conditioned error matrix (in red).

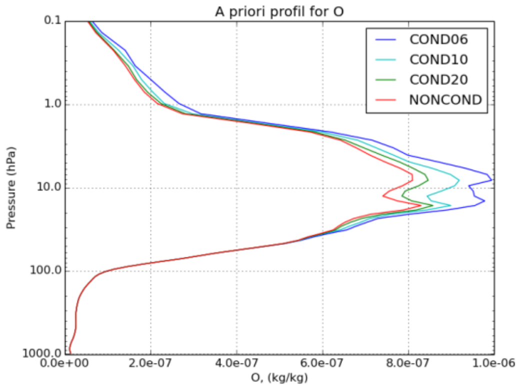

Figure 16: Same as Figure 15 for ozone.

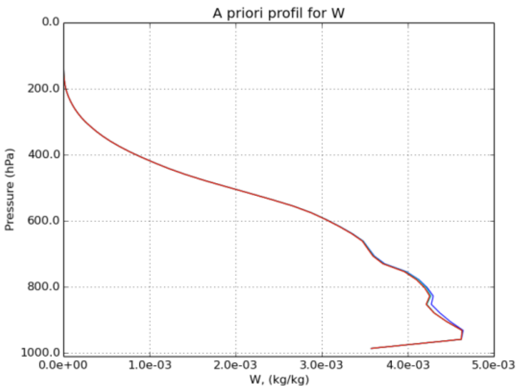

Figure 17: Same as Figure 15 for water vapour.

The differences in terms of Kelvin and kg/kg for temperature and water vapour respectively are small as shown by Figure 15 and Figure 17.

For ozone (Figure 16), the difference is more pronounced and the lower the condition number, the higher the *a priori* error on the profile.

These figures only represent the profile of the *a priori* error matrix, that is to say the diagonal of the *a priori* matrix. In order to better understand the impact of the conditioning on the entire matrix, the relative difference of the reconditioned matrix with respect to the initial matrix (not conditioned) of ozone is plotted for three condition numbers on Figure 18.

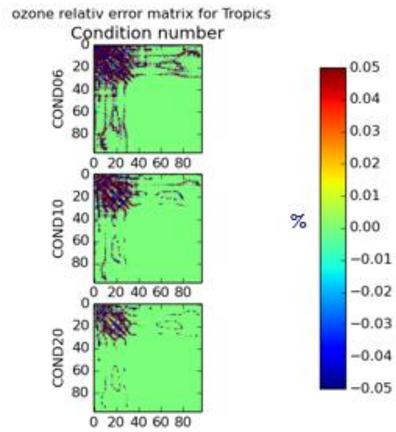

Figure 18: Relative difference of the reconditioned matrix with respect to the initial matrix (not conditioned) for ozone in the tropics.

The lower the condition number, the higher the number of coefficients changed in the matrix. The non-diagonal elements of the matrix are also impacted.

The effect of the condition number on the retrieved error profiles is also studied. The following figures represent the retrieved error profiles for temperature, ozone and water vapour and the associated *a priori* error profiles.

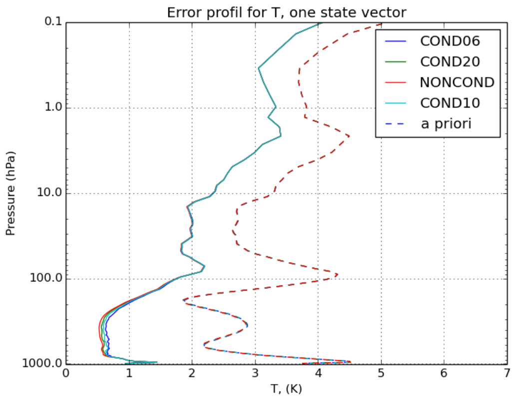

Figure 19: Retrieved error profiles (solid line) and *a priori* error profiles (dotted line) for temperature for three different condition numbers (6000 in blue, 10000 in cyan and 20000 in green) and without conditioning (in red).

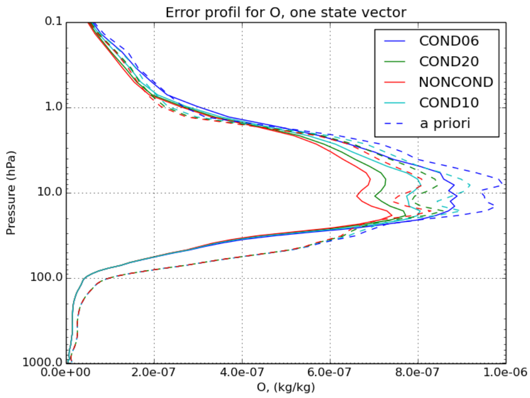

Figure 20: Same as Figure 19 for ozone.

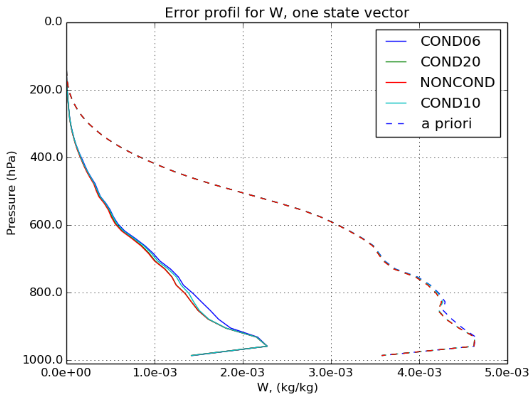

Figure 21: Same as Figure 19 for water vapour.

The maxima differences in terms of retrieved error profiles between the unconditioned *a priori* error matrix and the conditioned error matrix are for the condition number around 6 000 and as follows:

- For temperature: $\mathbf{0,26}$ K (at 300 hPa);
- For ozone: $\mathbf{2,3.10^{-7}}$ kg/kg (at 10 hPa);
- For water vapour: $\mathbf{1,3.10^{-4}}$ kg/kg (at 890 hPa).

In summary, there is a low impact of the condition number but we need to have to choose the most appropriate matrix, that is:

- a proper matrix without negative eigenvalues and allowing a well-conditioned system (and to avoid too large numerical errors);
- but a matrix which remains realistic enough to characterize the true variation of the atmosphere state (since we can see in Figure 20 for ozone that the error profile tends to deviate from its original shape for a condition number of 6000).

In conclusion, a condition number around 10 000 seems to be a good compromise.

3.3 IRS INSTRUMENT NOISE

EUMETSAT provided the noise in terms of NeΔT (Tref=280K) for a typical (nominal) case and worst-case scenario. These noises have been converted in terms of NeΔL (mW/m²/str/cm-1) as follows:

$$Ne\Delta L_\nu = Ne\Delta T_\nu(T_{ref} = \mathbf{280}K)\frac{\partial B_\nu}{\partial T}(T_{ref}) \qquad (12)$$

The Python code used to convert the noise in terms of NeΔL (mW/m²/str/cm^{-1}) has been provided to EUMETSAT.

The IRS wavenumbers in the noise files are not the same as those provided by RTTOV. These noises are therefore linearly interpolated/extrapolated to the RTTOV/IRS wavenumbers.

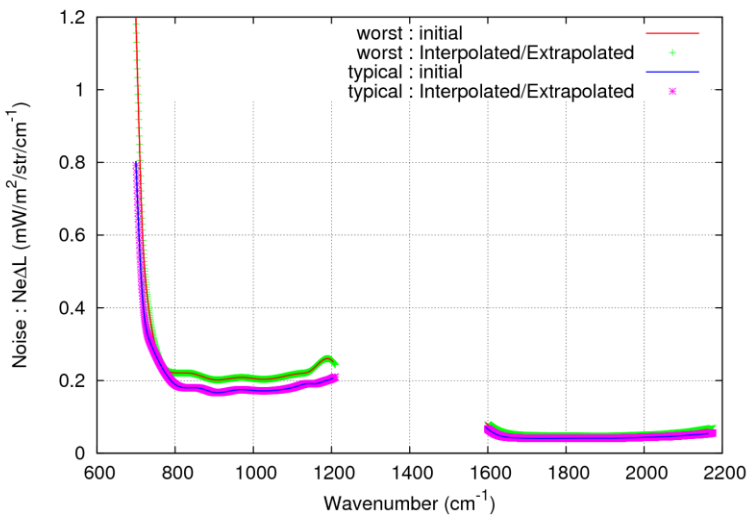

Figure 22: IRS noise according to the wavenumbers of the initial IRS channels for the typical (blue curve) and the noise of the worst case (red curve), respectively. (Purple dots) Interpolated/extrapolated noises according to the wavenumbers of the RTTOV/IRS channels for the typical noise. (Green dots) Interpolated/extrapolated noises according to the wavenumbers of the RTTOV/IRS channels for the worst case.

3.4 OBSERVATION ERROR MATRIX

The observation error matrix (denoted by S_y) has been provided by EUMETSAT: it contains both the typical instrument noise computed by Thales and additional errors, for instance errors introduced by the radiative transfer forward model. The elements of S_y are given in (mW/m²/str/cm-1)². Matrix S_y and its inverse are stored in the initial generated dataset completed with retrieval errors results (described in the next section 3.6).

This matrix is constructed as follows:

- The matrix, denoted “OmC”, is mainly computed from the differences between the observed and computed radiances at the top of the atmosphere, denoted “Obs” and “Calc” respectively: OmC = Obs minus Calc.
  - The observed radiances are L1b radiances simulated for MTG-IRS and come from the training set generated for the 15th of March 2016 at 12:00 UTC. The development of the L2 IRS Processing Prototype is based on them. The training set gathers the 280 dwells of the Earth’s disc as observed by MTG-IRS. Only the dwell 49 of LAC4 is considered to compute the error matrix,
  - The computed radiances are those computed according to the geophysical data retrieved by the Piece Wise Linear Regression algorithm (trained with the full training set);
- The covariance matrix OmC is computed by taking into consideration only the clear-sky pixels (9157 pixels among the 25600 pixels of the IRS dwell);
- The diagonal of the variances from the instrumental noise matrix for a “typical” noise is added to this covariance matrix representing the errors of the forward model. The instrumental noise matrix is expressed in terms of radiance/luminance (NoiseEquivalentΔL) and computed as described above (see equation (12) in section 3.3): from the instrument noise matrix in brightness temperature (NoiseEquivalentΔT) and interpolated according to the nominal spectral range of IRS (1738 channels: 817 in the low infrared band and 921 in the middle infrared one).

3.5 RETRIEVALS ERRORS COMPUTATION

The following figure (Figure 23) shows the processing chain for the generation of the retrieval errors dataset:

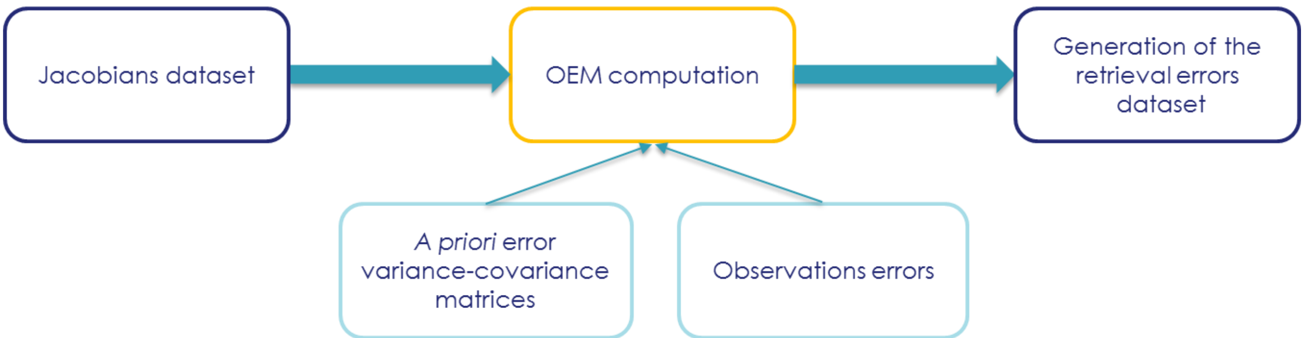

Figure 23: Design of the processing chain for the generation of the retrieval errors dataset

The *a posteriori* error variance-covariance matrices are computed as follows:

- the Jacobians computed from RTTOV as per section 2 (denoted by K);
- The *a priori* error matrices (denoted by S_a) and the observation error matrix (noted S_y) are used and stored in the dataset.

The following Table 3 lists the different results of the OEM calculations which are stored in the dataset.

Table 3: Retrieval error matrices and averaging kernels stored in the retrieval errors dataset

Retrieval error matrices	$\hat{S} = \left(K^T S_y^{-1} K + S_a^{-1}\right)^{-1}$
Gain (not stored in the dataset)	$G = \hat{S}\ K^T S_y^{-1}$
Averaging kernels	$A = G\ K$
Smoothing error matrices	$S_{smooth} = (A - I)\ S_a\ (A - I)^T$
Measurement error matrices	$S_m = G\ S_y\ G^T$
Retrieval error matrices induced by a emissivity error	$\hat{S}_{ret,\ emis} = G\ K_{emis}\ S_{emis}\ K_{emis}{}^T\ G^T$
Retrieval error matrices induced by a surface temperature error	$\hat{S}_{ret,Tsurf} = G\ K_{Tsurf}\ S_{Tsurf}\ K_{Tsurf}{}^T\ G^T$

<u>Special case for the retrieval error matrices induced by an emissivity error:</u>

The emissivity value of the IRS channels number “n” (denoted by ε_n) only affects the RTTOV computation of the radiance of IRS channel number “n” (Rad_n). In other words, the Jacobian of the IRS radiance for the channel number “n” w. r. t. the emissivity for the channel “p” is equal to zero if n≠p:

$$\frac{\partial Rad_n}{\partial \varepsilon_p} = 0\ if\ n\ \neq p \tag{13}$$

In this case, the emissivity Jacobian matrix,K_{emis} is filled with zero values except on the diagonal that contains the values of the Jacobian w. r. t. the emissivity:

$$K_{emis} = \begin{pmatrix} \frac{\partial Rad_1}{\partial \varepsilon_1} & 0 & 0 \\ 0 & \ddots & 0 \\ 0 & 0 & \frac{\partial Rad_{1738}}{\partial \varepsilon_{1738}} \end{pmatrix} \tag{14}$$

3.6 DESCRIPTION OF THE HDF5 FILE

As show on Figure 24Figure 24:

- The *a priori* matrices per zone have been introduced in the dataset;
- The noise matrix (typical noise) has been stored in the "IrsInformation" group;

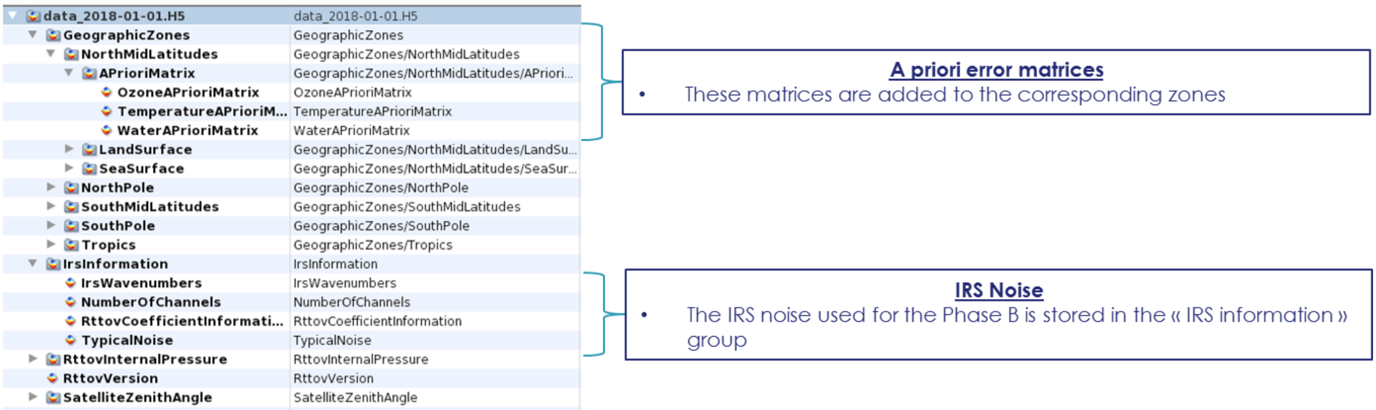

Figure 24: description of the HDF5 file: a priori matrix and noise matrix

The different retrieval error matrices and averaging kernels (described in the Table 3) have been grouped into two subgroups:

- ***OEMOneStateVector:*** This group contains the retrievals error matrices and the averaging kernel using **only one state vector for all the parameters**, e.g. all parameters: temperature profile, ozone profile and water vapour profile are assembled into the same state vector. In this case the retrievals matrices contains the cross retrieval correlation between these parameters;
- ***ThreeStateVector:*** This group contains three subgroups: "Temperature", "WaterVapour" and "Ozone". Each subgroup corresponds to the results that use **one state vector that contains only one profile (Temperature or Water vapour or Ozone)**.

A snapshot of an HDF5 file containing these groups and subgroups is provided in Figure 25.

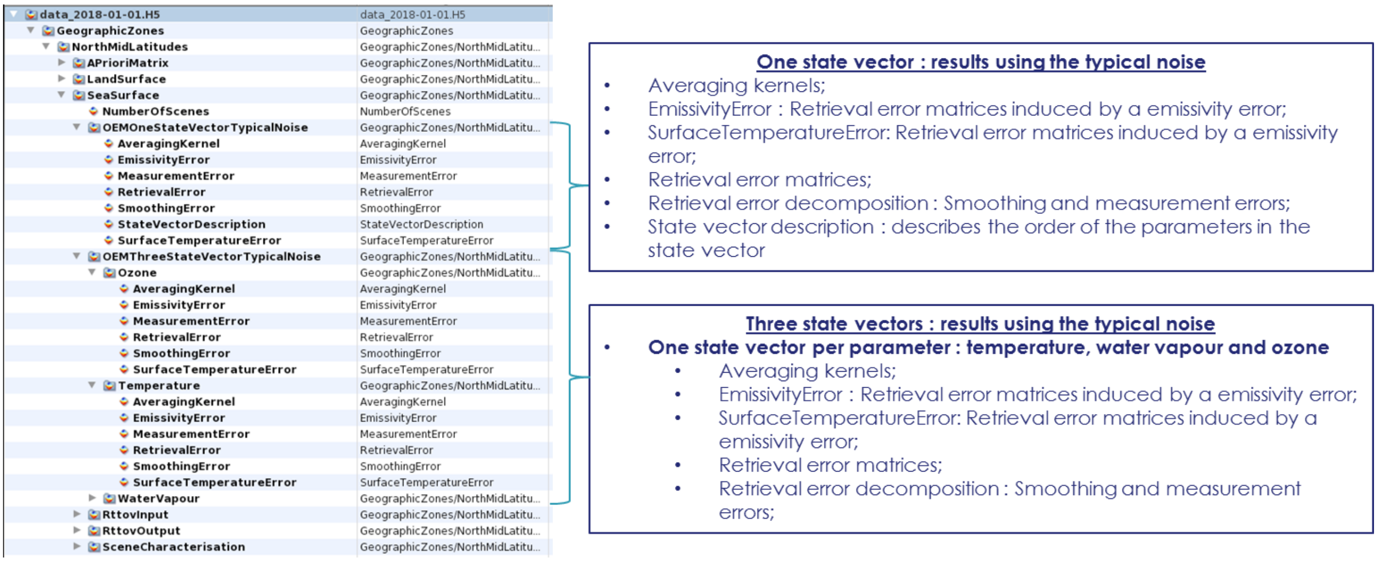

Figure 25: Description of the HDF5 file: one state vector or three state vectors

The observation error matrix that contains the typical noise and other sources of errors, was provided by EUMETSAT, and has been introduced in the dataset. Its inverse has been computed offline and introduced in the dataset. A snapshot of an HDF5 file containing these matrices is provided in Figure 26.

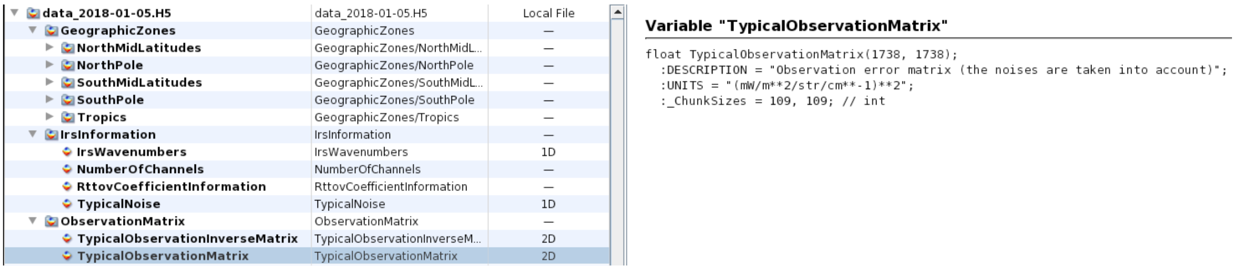

Figure 26: Description of the HDF5 file: the observation error matrix and its inverse

3.7 EXAMPLES OF OEM OUTPUTS

Figure 27 to Figure 29 show examples of the averaging kernels averaged over tropics, for temperature, water vapour and ozone respectively.

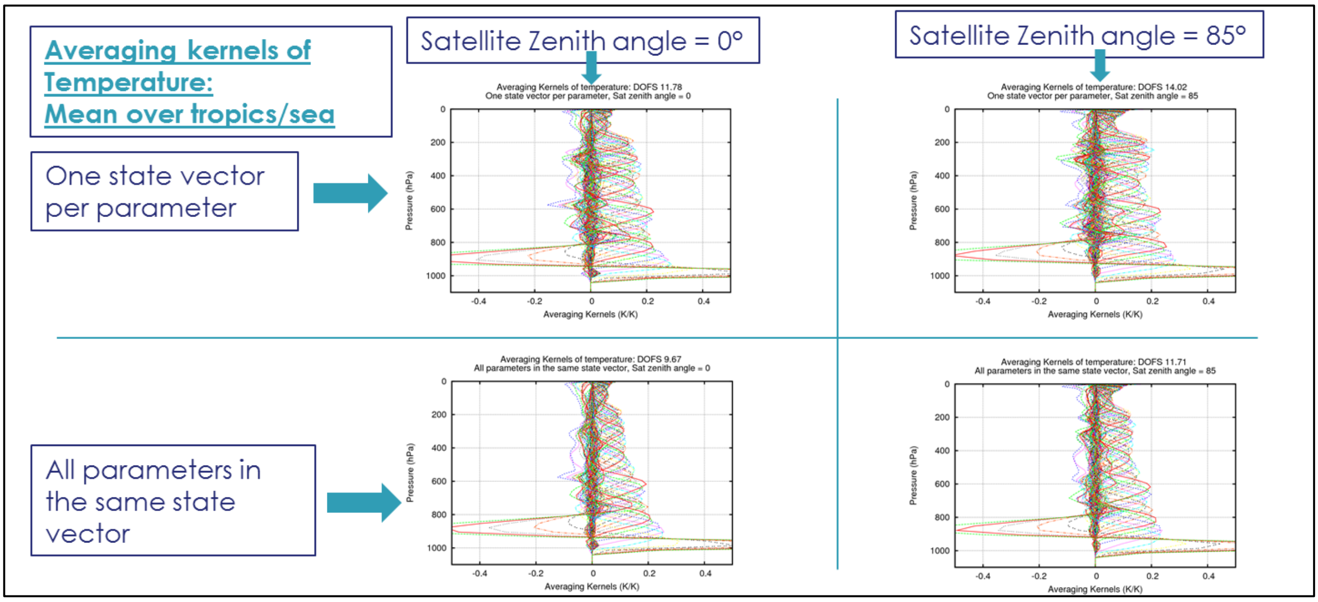

Figure 27: Examples of mean averaging kernels for the temperature profile over tropical sea. Results are shown for a satellite zenith angle equal to 0° (nadir) and 85°.

Retrieved profiles of temperature are sensitive to all levels (the impact of the satellite zenith angle is not clearly perceptible on Figure 27).

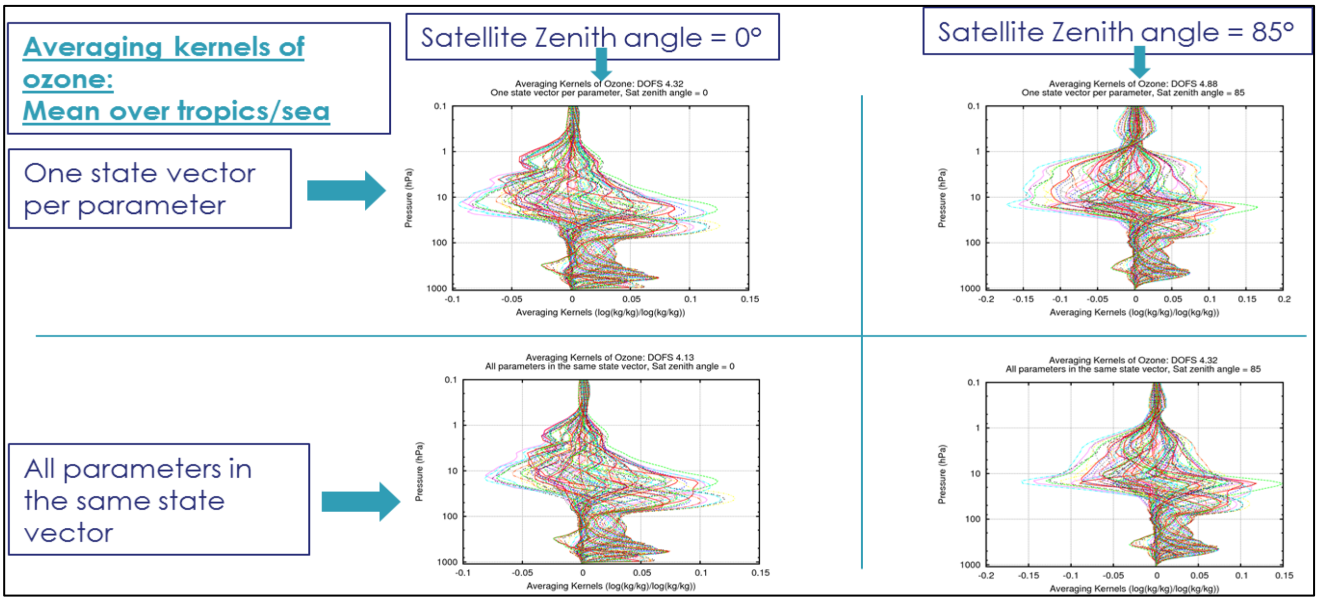

Figure 28: Examples of mean averaging kernels for the ozone profile over tropical sea. Results are shown for a satellite zenith angle equal to 0° (nadir) and 85°.

Retrieved ozone profiles are mainly sensitive at altitudes where the ozone mixing ratios are the most important, i.e., between 100 hPa and 1 hPa. It can be noted that the retrieved profiles are also sensitive to ozone mixing ratios in the troposphere. Results further indicate the sensitivities of the retrieved ozone profiles are more important for a satellite zenith angle equal to 85° than for nadir at pressures 100 to 1 hPa.

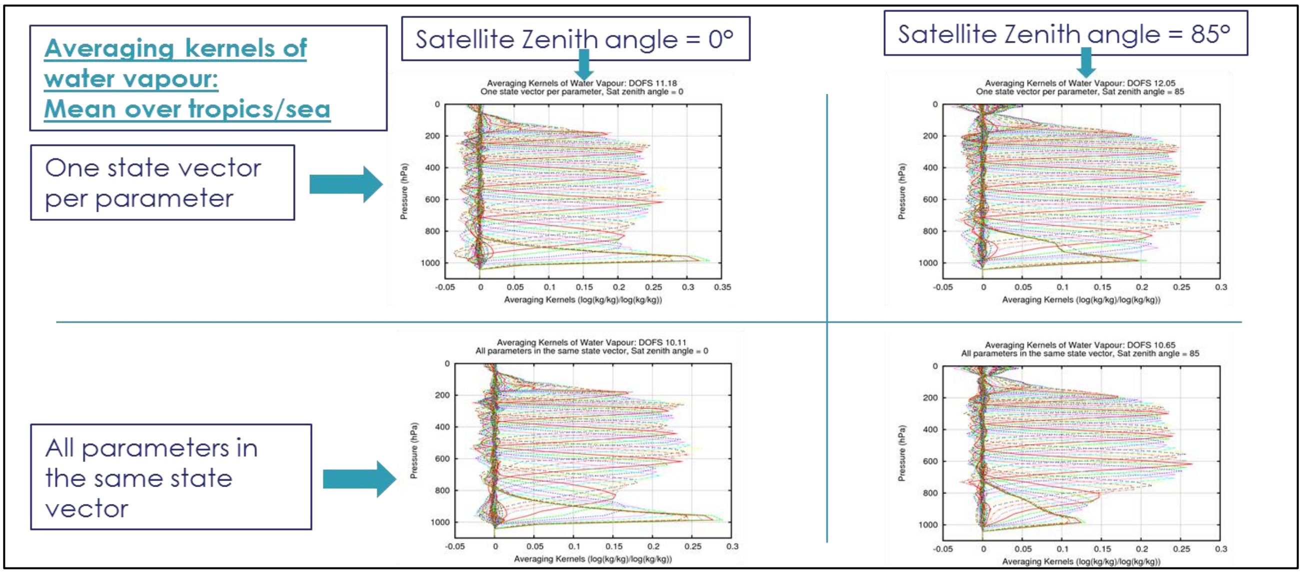

Figure 29: Examples of means of averaging kernels for the water vapour profile over tropics and sea, at nadir, and for a satellite zenith angle equal to 85

Retrieved water vapour profiles are mainly sensitive in the troposphere (between surface and 100 hPa) where the water vapour mixing ratios are the most pronounced (Figure 29). Results further indicate that, around 600 hPa, the sensitivities of the retrieved profiles of water vapour are more important for a satellite zenith angle equal to 85° than at nadir. Conversely, for the levels close to surface, the sensitivities of the retrieval profiles decrease when the satellite zenith angle is 85°.

4 PRESENTATION OF THE RESULTS AND DISCUSSION: ANALYSIS OF THE RETRIEVAL ERRORS

The following analysis has been performed using the retrieval error matrix and one state vector, i.e., the three parameters, temperature, water vapour and ozone, are assembled into the same state vector. The used observation error matrix contains the typical noise.

4.1 DERIVATION OF THE RETRIEVAL ERRORS IN TERMS OF MIXING RATIO AND COMPUTATIONS OF THE ERRORS IN TERMS OF COLUMN

Water vapour and ozone errors are defined in terms of the logarithm of the mixing ratio ($log(X_i)$). In the following analyses, the error matrices of water vapour and ozone are derived in terms of mixing ratio errors (denoted $\boldsymbol{X_i}$) using the following assumption:

$$Cov\left(log(X_i), log(X_j)\right) \approx \frac{\boldsymbol{Cov(X_i,X_j)}}{X_i^{\boldsymbol{a\,priori}} X_j^{\boldsymbol{a\,priori}}} \text{for X} = \text{W or O} \tag{15}$$

To compute the retrieval column errors, we use the following equations:

$$Var[col] = \boldsymbol{h^T}.\,\boldsymbol{\widehat{S}^{layer}}\,\boldsymbol{h}.\text{ with } h_i = \frac{\Delta p_i}{P_{surf}} \tag{16}$$

To compute the retrieval sub-column errors, we use the following equations:

$$Var[col] = \boldsymbol{h^T}.\,\boldsymbol{\widehat{S}^{layer}}\,\boldsymbol{h}.\text{ with } h_i = \frac{\Delta p_i}{\sum_i \Delta p_i}\ \textit{with i the levels of the considered sub-column} \tag{17}$$

$$\hat{S}^{layer}{}_{i,j} = Cov\left(X_i^{layer}, X_j^{layer}\right) = \frac{1}{4}\left(\sum_{k=0}^{k=1}\sum_{l=0}^{l=1} Cov\left(X_{i+k}, X_{j+l}\right)\right) \tag{18}$$

4.2 DIFFERENT EMISSIVITY BEHAVIOR OF THE EMISSIVITY ACCORDING TO THE SURFACE TYPE: SEA OR LAND

We recall here the important difference in the behaviours of the emissivity between land and sea surfaces according to satellite zenith angle. Over sea, the values of the emissivity depend on the satellite zenith angle and the IRS channels (Figure 30(a)). Over land, the emissivity spectra used by RTTOV do not depend on the satellite zenith angle (Figure 30(b))

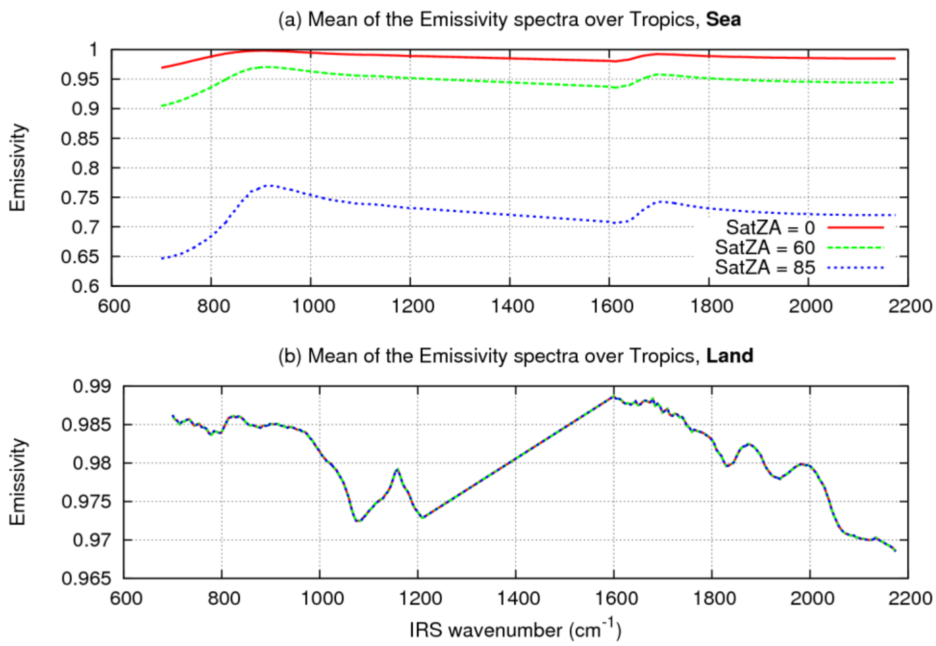

Figure 30: Average values of the emissivity per IRS channels over sea (a) and over land (b) using the scenes in tropics

4.3 USING THE ANOMALIES BETWEEN THE NADIR AND SATZA = 85° TO EXTRACT THE EXTREME SITUATIONS

To extract the extreme scenes, we compute the relative difference of the retrieval error between the nadir and a SatZA (Satellite Zenith Angle) of 85°.

$$R_a = \frac{Error[SatZA = 85°] - Error[SatZA = 0°]}{Error[SatZA = 0°]}$$

For each temperature, water vapour and ozone profile, two extreme situations (i.e. min and max of R_a) are extracted per day, geographic zone and surface type.

4.4 RESULTS ANALYSIS

All the figures are regrouped in annex B. We regroup here the principal conclusions and plots of the results analysis.

We first study the impact of SatZA on retrieval sub-column errors (see section 4.1). The aim of this study is not to study specifically this kind of retrieval errors. Rather, we aim to observe remarkable behaviours. Following this first analysis, an analysis in terms of retrieval error profiles will be presented (see section 4.4.2).

4.4.1 Impact of SatZA on retrieval sub-column errors

In order to have a relevant analysis on the errors of the products, the retrieval errors are observed within specific sub-columns. The division in sub-columns were proposed by EUMETSAT and depends on the product:

- Temperature: [surface-700] ; [700-300] ; [300-100] ; [100-10] hPa;
- Water vapour: [surface-800] ; [800-500] ; [500; 300] hPa;
- Ozone: [100-1] hPa.

First, specific sub-columns are selected to analyse in the best way the different errors. Then, for these specific sub-columns, the averaged sub-columns over the whole year are plotted in order to study the mean and the error budget of the retrieval errors for each latitude zones.

Here are all the sub-columns for each product over the tropics and sea for the first day of April:

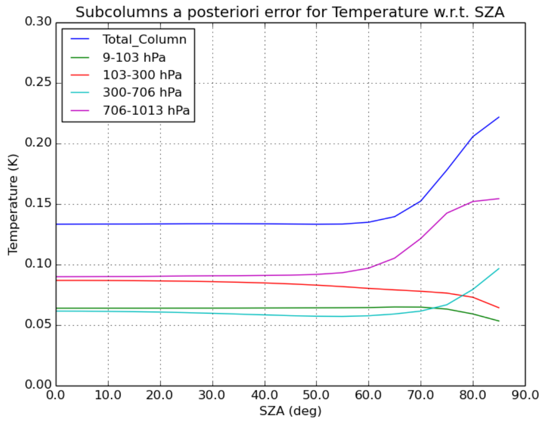

Figure 31: Mean retrieval error for temperature w.r.t SatZA for each sub-column. (Blue) Total column. (Green) 9-103 hPa. (Red) 103-300 hPa. (Cyan) 300-706 hPa. (Purple) 706-1013 hPa.

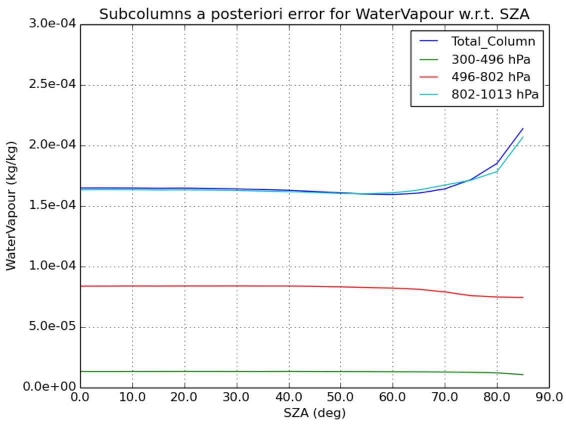

Figure 32: Mean retrieval error for water vapour w.r.t SatZA for each sub-column. (Blue) Total column. (Green) 300-496 hPa. (Red) 496-802 hPa. (Cyan) 802-1013 hPa.

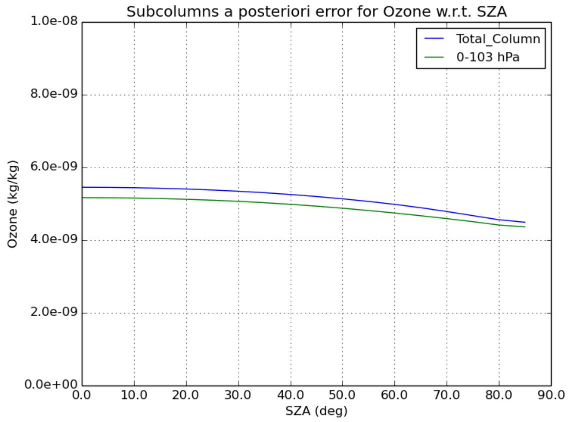

Figure 33: Mean retrieval error for ozone w.r.t SatZA for each sub-column. (Blue) Total column. (Green) 0-103 hPa.

In order to analyse in the best way the mean and the error budget according to the SatZA, we choose some specific sub-columns for each product:

- Temperature: the three sub-columns corresponding to the lower, middle and upper troposphere are kept ([surface-700], [700-300], [300-100] hPa). Thus, we have two distinct behaviours of the mean retrieval error according to the SatZA;
- Water vapour: the two sub-columns closest to the surface ([surface-800], [800-500] hPa) are kept. Indeed, the amount of water vapour in these sub-columns is preponderant and the error for those sub-columns dominates the error of the total column;
- Ozone: the only sub-column is kept ([100-1] hPa).

All the figures are available in ANNEXE B – All figures/§2.1.

In the following sub-sections, we choose the sub-columns closest to the surface for temperature and water vapour.

4.4.1.1 Temperature

The analysis is made on **the sub-column 700 hPa–surface** in this section.

The mean of the retrieval errors is stable **until SatZA reaches 60°** for each latitude zones (Figure 34):

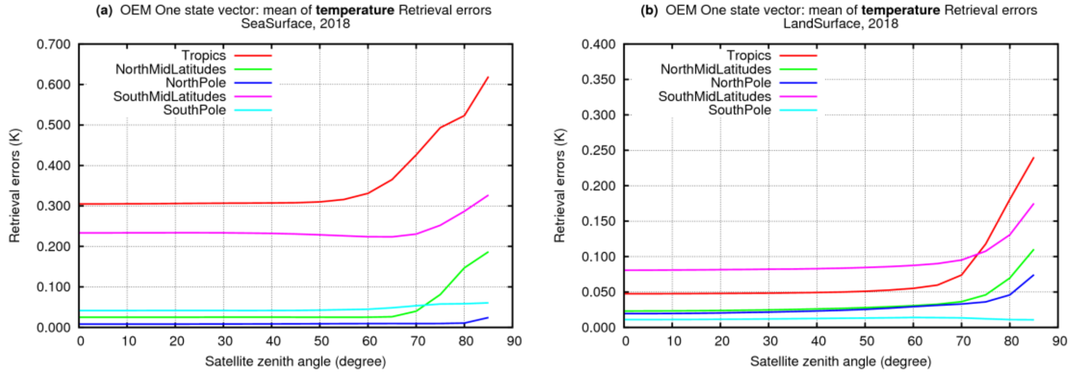

Figure 34: Mean retrieval errors of temperature in the averaging sub-column 700 hPa–surface as a function of the satellite zenith angle value over sea (a) and over land (b). (Red) results for the tropics are given as red line. (Green) Results for Northern mid-latitudes. (Purple) Results for Southern mid-latitudes (purple curve). (Cyan) Results for South Pole. (Blue) Results for North Pole (blue curve). Results are averaged over all situations available in 2018.

The mean of the retrieval errors increases strongly with increasing SatZA in the tropics (Figure 34, red curves) and mid-latitudes (Figure 34, green and purple curves). In contrast, mean retrieval errors are stable with increasing SatZA at higher latitudes. In summary, **the main impact of large SatZA is found in the tropics and at mid-latitudes.** Similar retrieval errors are found for sea and land situations (Figure 34).

However, in the upper troposphere (sub-column 103-300 hPa), the mean of the retrieval errors decreases with an increasing SatZA (see Temperature in ANNEXE B – All figures/§2.1.).

The error budget of the retrieval error is dominated by the measurement error (Figure 35, red curves; (a) in the tropics and (b) over South Pole). The smoothing error (Figure 35, green curves; (a) in the tropics and (b) over South Pole) is by approximately a factor 2 smaller than the measurement error. **Therefore, we conclude that the retrieval error is dominated by the observation error matrix.** More specifically, we found:

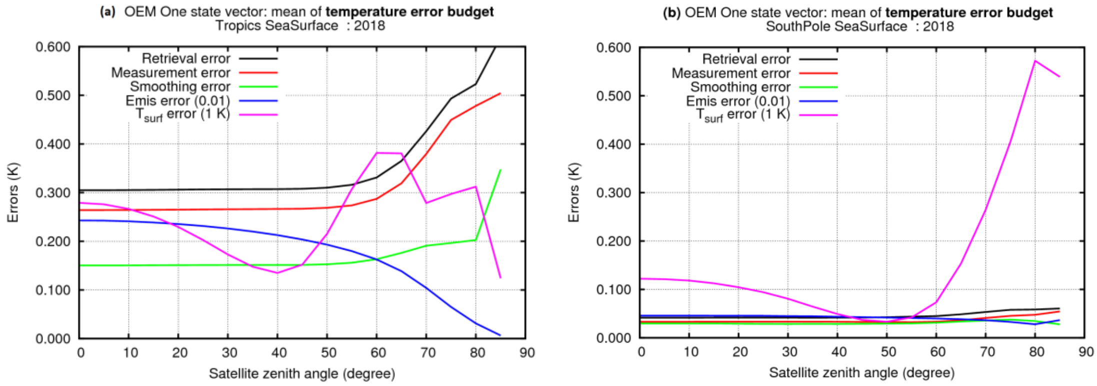

Figure 35: Retrieval error budget of the temperature in sub-column 700 hPa–surface against the satellite zenith angle. (Black) Mean error in temperature column retrieval. (Red) Measurement error. (Green) Smoothing error. (Blue) Retrieval error induced by a 0.01 emissivity incertitude. (Purple) Retrieval error induced by a 1 K surface temperature incertitude. Errors are averaged over all situations in (a) the tropics and (b) South Pole over sea during 2018.

- (Figure 35, blue curves; (a) over tropics and (b) over South Pole) A 0.01 random error in the emissivity (for each IRS channel) induced a mean retrieval error smaller or close to 0.25 K. These errors typically decrease with increasing SatZA. These mean errors are stable for SatZA between nadir and 40° in tropics, between nadir and 70° in Mid-latitudes and between nadir and 75° over both poles. We conclude **that the retrieval error induced by a 0.01 random error on the emissivity seems to stable for low SatZA and decreases for SatZA > 40° in tropics and for SatZA > 80° over both Poles;**
- (Figure 35, purple curves; (a) over tropics and (b) over South Pole) A 1 K random error on the surface temperature:
  - induces **a large error for the situations over the tropics** at nadir (about 0.27 K in the tropics and 0.12 K in South Pole). This mean error decreases to 0.15 K until SatZA = 40° and then increases in the tropics,
  - At nadir, this mean error decreases poleward,
  - At the higher SatZA values:
    - the error value increases and becomes important poleward,
    - this error is more important over sea than over land, probably because the emissivity decreases with SatZA;

- Per zone, the mean retrieval errors do not seem to depend strongly on month (Figure 36), except for the North Pole where the mean retrieval error in January is greater than for the other months.

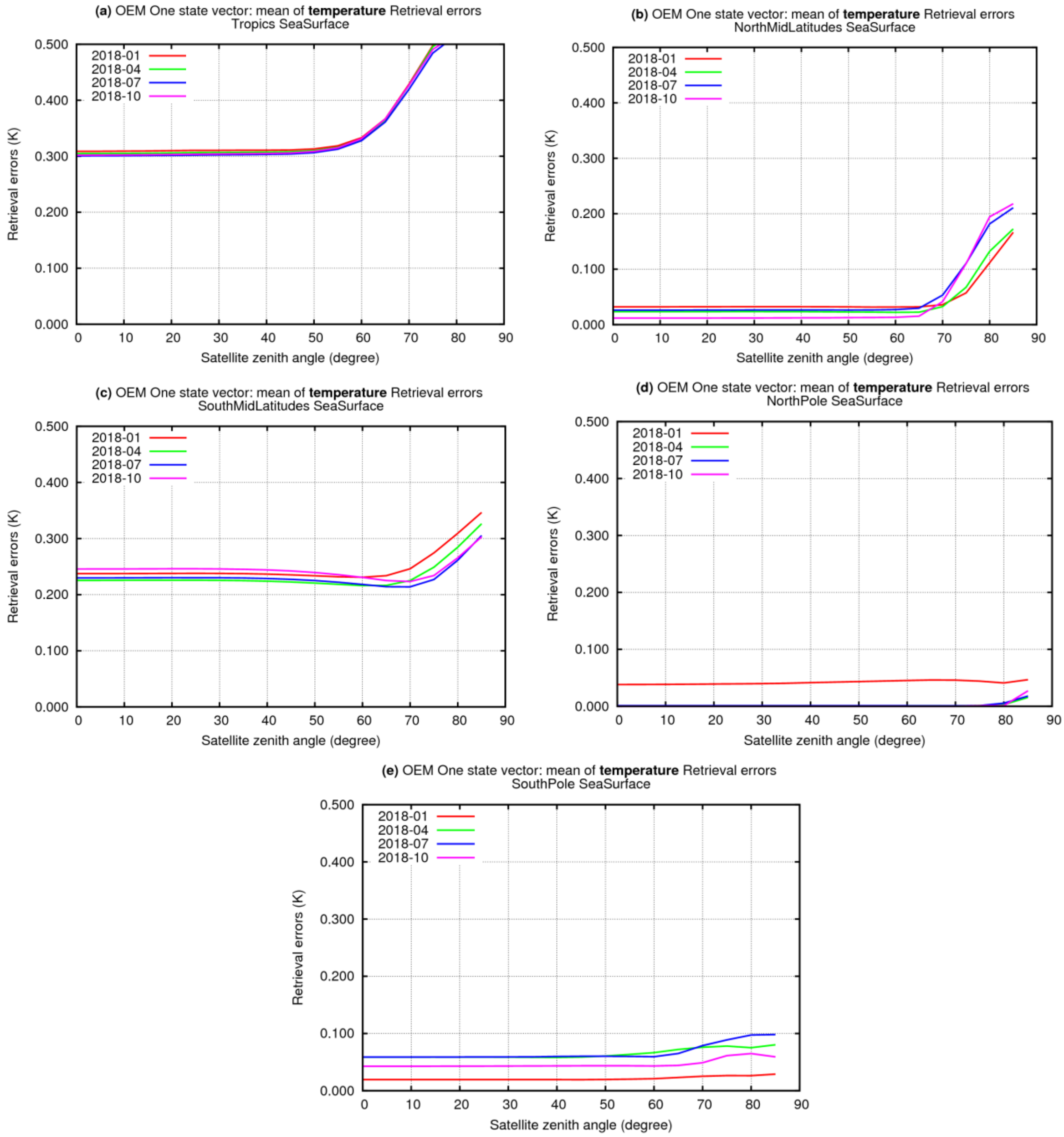

Figure 36: Retrieval errors for temperature sub-column 700 hPa–surface according to the satellite zenith angles, averaged over January (red line), April (green curve), July (blue line) and October (purple line) and, over tropics (a), northern (b) and southern mid-latitudes, North (d) and South (e) Poles.

- Extreme situations exhibiting highest and lowest anomalies (see section 4.3 for the definition of anomalies), i.e. the situations that are most impacted by the high SatZA, were extracted per day and per zone. Figure 37 regroups all the situations extracted during 2018.

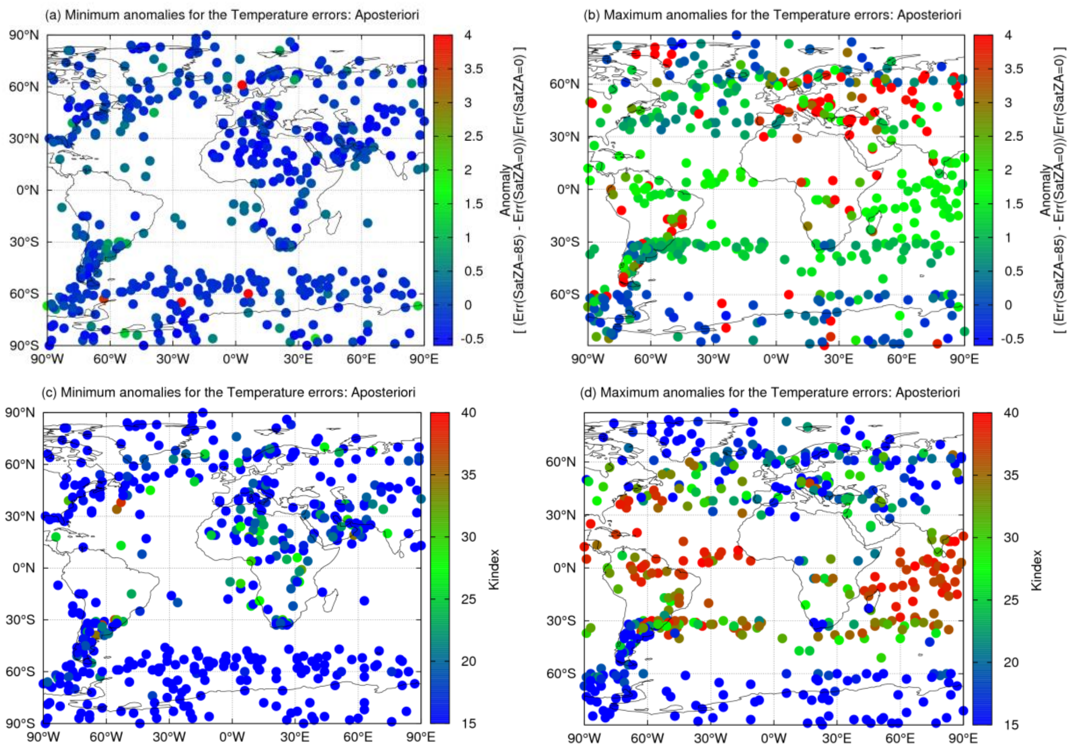

Figure 37: Maps of the extracted situations from the retrieval errors dataset with the minimum (a) and maximum (b) anomalies values. Associated K index values for these situations are given for minimum anomaly dataset (c) and the maximum anomaly dataset (d).

- **The situations with anomalies values close or greater than 2 exhibit a K index greater than 25 if they are located in tropics and mid-latitudes (**Figure 37 **(b) and (d)). An important anomaly value could also be found in high latitudes with a low value of K index. Conversely, the situations with negative anomalies values close to or smaller than -0.5 exhibit a K index smaller than 20 (**Figure 37 **(a) and (c))**.

4.4.1.2 Water vapour

The analysis is made on **the sub-column 800 hPa–surface** in this section (all the figures are available in ANNEXE B – All figures/§2.1.).

The main impacts of SatZA on retrieval column errors of water vapour are summarized below:

- Over sea (Figure 38 (a)), the mean retrieval errors are relatively stable for SatZA < 30°. For SatZA > 30°, **the mean retrieval error decreases until SatZA reaches 75° and increases strongly in the tropics. This increase is reduced poleward;**
- Over land (Figure 38 (b)), the mean retrieval errors are relatively stable for SatZA < 70°. **In the tropics, this mean error increases strongly with for SatZA > 70°. In the other areas, this error is stable or increases weakly with an increasing SatZA;**
- The difference between the behaviour of the mean retrieval errors for the sea surface and that for the land surface (Figure 38 (a) and (b)) is probably induced by the different behaviour of the surface emissivity according to the SatZA between both types of surface: in the RTTOV simulations, the surface emissivity depends on SatZA over sea while there is no angular dependence over land (see section 4.2).

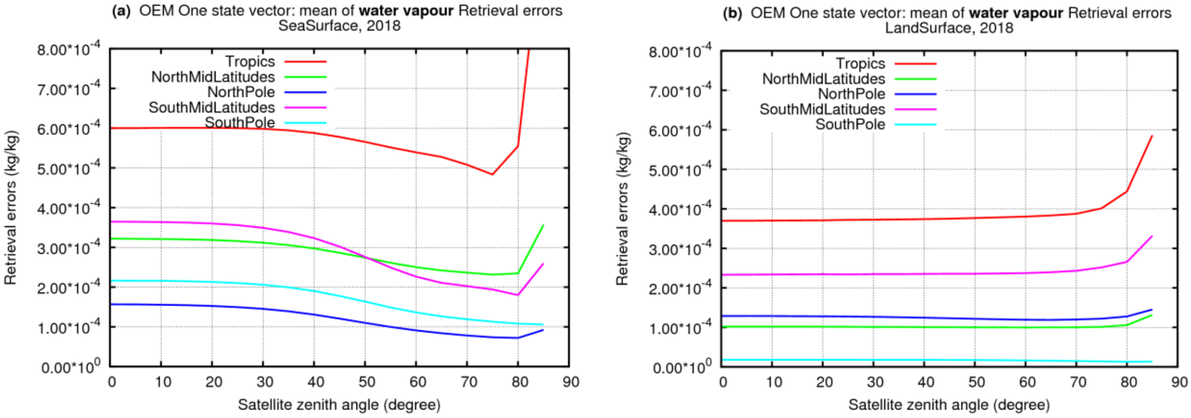

Figure 38: Mean retrieval errors of water vapour in sub-column 800 hPa–surface as a function of the satellite zenith angle value over sea (a) and over land (b) in the tropics (red curve), northern mid-latitudes (green curve), southern mid-latitudes (purple curve), South Pole (cyan curve) and North Pole (blue curve). Results are averaged over all situations available during 2018

- The error budget of the retrieval error (Figure 39) is dominated by the measurement error for all SatZA < 80°. For SatZA > 80°, the smoothing error overcomes the measurement error in some regions such as the tropics (a). Poleward (b), the smoothing error becomes small in comparison with the measurement error. **Therefore, the observation error matrix affects mainly the retrieval error in the tropics. The influence of the *a priori* matrix (smoothing error) decreases towards high latitudes but increases at high zenith angles;**

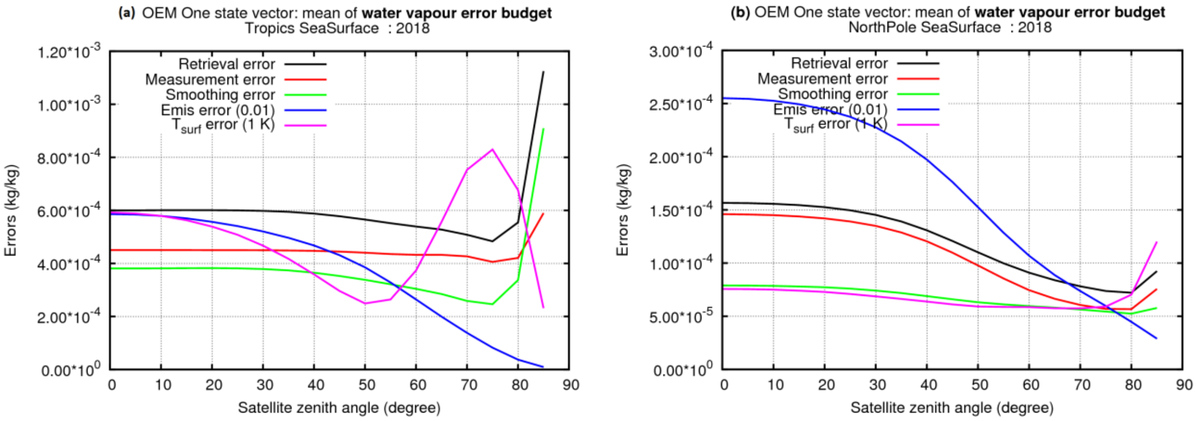

Figure 39: Retrieval error budget of water vapour in sub-column 800 hPa–surface against the satellite zenith angle. (Black) Mean error in water vapour column retrieval error. (Red) Measurement error. (Green) Smoothing error. (Blue) Retrieval error induced by 0.01 emissivity incertitude. (Purple) Retrieval error inducted by 1 K surface temperature incertitude. Results are averaged over all situations in (a) the tropics and (b) North Pole over sea and during 2018.

- A 0.01 random error on the emissivity (for each IRS channel) induces a mean retrieval error in the surface layers (800 hPa–surface) smaller or close to 6 10^{-4} kg/kg (close to the retrieval error value) in the tropics (Figure 39 (a)) and a mean retrieval error of 2.5 10^{-4} kg/kg in the North Pole region (Figure 39 (b)). These errors begin to decrease to 0 for SatZA > 20° (Figure 39 (a) and (b));
- A 1 K random error on the surface temperature:
  - induces an error close to the retrieval error value for the situations over the tropics at nadir (about 6 10^{-4} kg/kg) and an important error at SatZA around 70° (Figure 39 (a)),
  - At nadir, this mean error is about 7,5 10^{-5} kg/kg poleward,
  - At high SatZA values, the error value decreases poleward;
- Per zone and season, the mean retrieval errors (Figure 40):
  - do not seem to depend strongly on the month (Figure 40 (a)),
  - appear more important during July (summer) and less important during January (winter) in the northern hemisphere (Figure 40 (b) and (d)),
  - appear less important during July (winter) and more important during January (summer) and April (autumn) in the southern hemisphere (Figure 40 (c) and (e))
  - decrease with increasing SatZA until 80° and increase for SatZA>80° specially over the tropics and Northern Mid-latitudes;

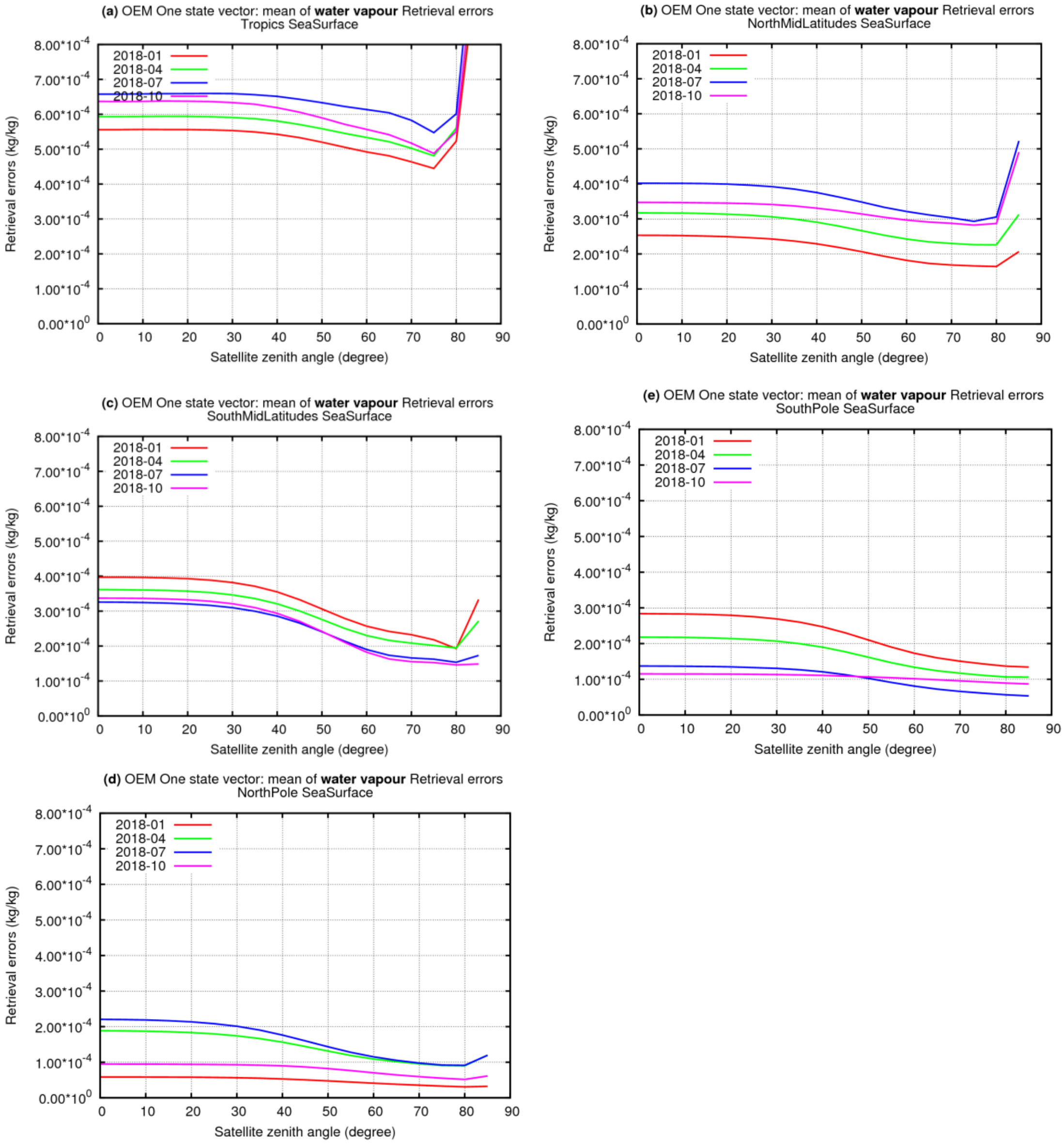

Figure 40: Retrieval errors for water vapour sub-column 800 hPa–surface according to the satellite zenith angles, averaged over January (red line), April (green curve), July (blue line) and October (purple line), over tropics (a), northern (b) and southern mid-latitudes, North (d) and South (e) Poles.

- Extreme situations exhibiting highest and lowest anomalies (see section 4.3 for the definition of anomalies), i.e. the situations that are most affected by the high SatZA, were extracted per day and per zone. Figure 41 regroups all the situations extracted during 2018.

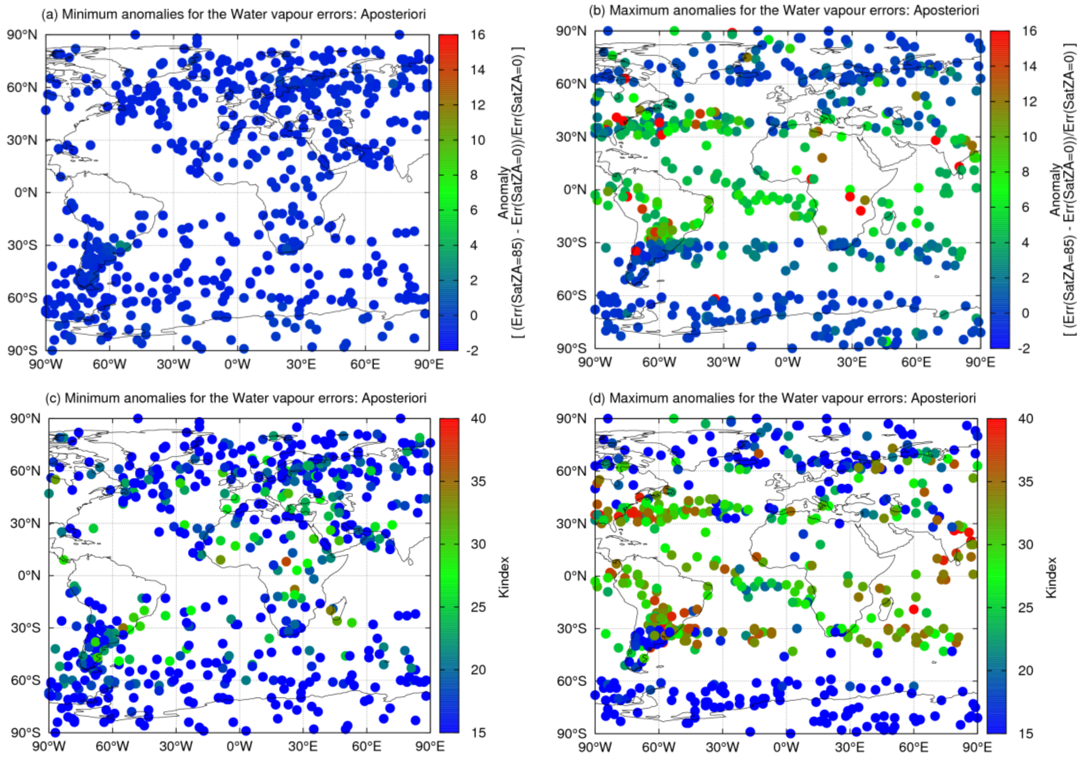

Figure 41: Maps of the extracted situations from the retrieval error dataset with minimum (a) and maximum (b) anomaly values Associated K index values for these situations are given for minimum anomaly dataset (c) and the maximum anomaly dataset (d).

- **The situations with anomalies values close to 6 exhibit a K index above 25 and are found in the tropics and mid-latitudes. Conversely, the situations with negative anomalies values close to or smaller than -2 exhibit a K index below 20 and are mainly found in the high latitudes bands.**

4.4.1.3 Ozone

The analysis is made on **the sub-column 0-103 hPa** in this section (all the figures are available in ANNEXE B – All figures/§2.1.).

The main impact of SatZA on retrieval column errors of ozone are deduced from Figure 42 and summarized below:

- The mean of the retrieval error depends on the geographical zone and the surface type;
- Figure 42 (a) over sea,
    - Over the tropics, the mean error seems stable for SatZA < 70° and decreases beyond,
    - Over South Pole and Southern Mid-latitudes, the error decreases until SatZA = 60° and then increases weakly,
    - Over the North Pole and Northern Mid-latitudes, the error drops slowly until SatZA = 80°;
- Figure 42 (b) over land:
    - The mean of the retrieval error depends on the zone: the error is about 1.8 10^{-8} kg/kg over the tropics and increases poleward,
    - At mid-latitudes, the mean error remains quite stable until SatZA = 70° and increases weakly beyond,
    - Poleward, the mean error decreases with an increasing SatZA;

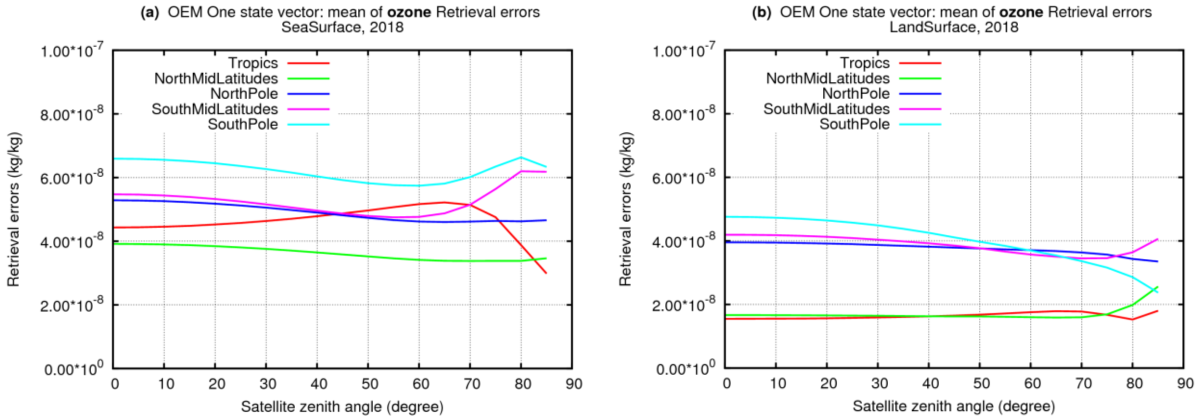

Figure 42: Mean retrieval errors of ozone in sub-column 0-103 hPa as a function of the satellite zenith angle over (a) sea and over (b) land. (Red) Mean retrieval errors in the tropics. (Green) Mean retrieval errors over northern mid-latitudes. (Purple) Mean retrieval errors over southern mid-latitudes. (Cyan) Mean retrieval errors over South Pole region. Mean retrieval errors over northern mid-latitudes over North Pole region. Results are averaged over all situations available during 2018.

- The smoothing error is very weak. Therefore, the error budget of the retrieval error (Figure 43) is dominated by the measurement error for **all values of SatZA;**

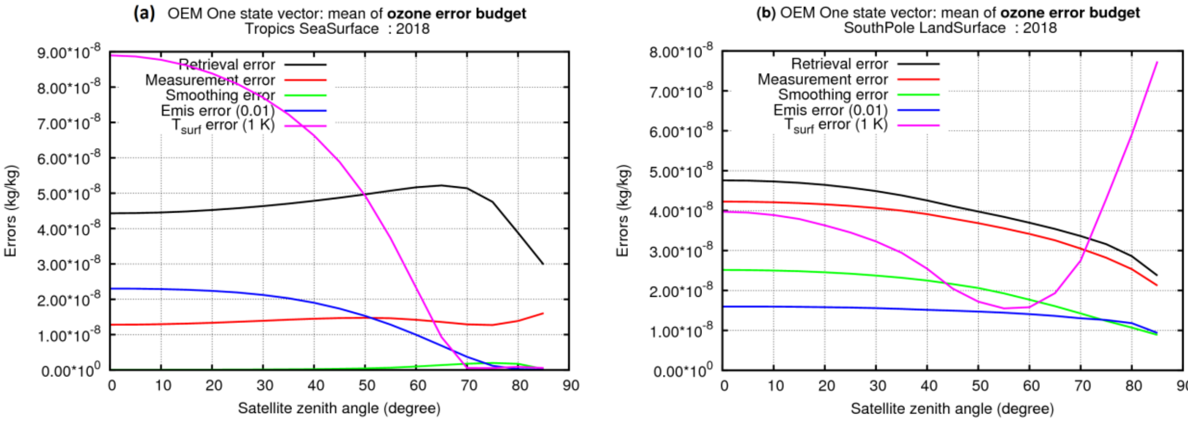

Figure 43: Retrieval error budget of water vapour in sub-column 0-103 hPa against the satellite zenith angle. (Black) Mean error of ozone column retrieval. (Red) Measurement error. (Green) Smoothing error. (Blue) Retrieval error induced by 0.01 emissivity incertitude. (Purple) Retrieval error induced by a 1 K surface temperature incertitude. All results are averaged over all situations in (a) the tropics and (b) South Pole region during 2018.

- A 0.01 random error on the emissivity (for each IRS channel) induces a mean retrieval error inferior or close to 2.4 10^{-8} (kg/kg) over the tropics over sea (blue line in Figure 43 (a)) and 1.5 10^{-8} kg/kg over South Pole over land (blue line in Figure 43 (b)); this error decreases to 0 kg/kg with increasing SatZA for SatZA > 20°;
- A 1 K random error on the surface temperature:
  - induces **an important error for the situations over the tropics** at nadir (about 9 10^{-8} kg/kg). This mean error decreases with increasing SatZA to 0 kg/kg,
  - At nadir, this mean error decreases poleward (about 4 10^{-8} kg/kg),
  - At high SatZA:
    - the error increases and becomes more important poleward,
    - North- and Poleward, this error is more important over land than over sea, with the highest values for SatZA around 70°;

- Per geographical zone and season, the mean retrieval errors (Figure 44):
  - Do not seem to depend strongly on months over tropics (Figure 44 (a)) and Southern mid-latitudes (Figure 44 (c));
  - are more important during January and less important during October in the Northern hemisphere (Figure 44 (b) and (d));
  - appear less important in January and October for South Pole;

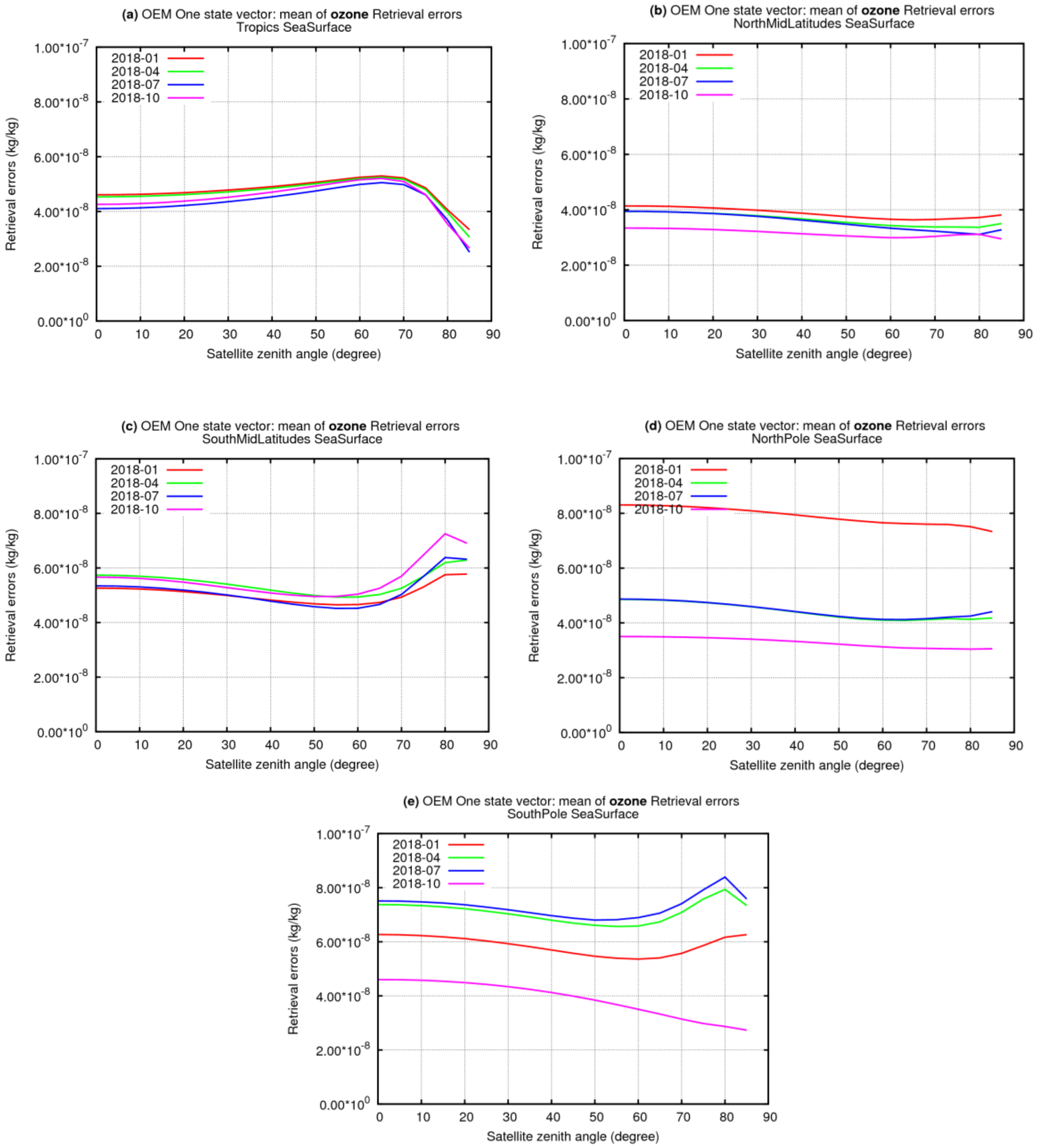

Figure 44: Retrieval errors for ozone according for different satellite zenith angles. Mean errors are shown for January (red line), April (green curve), July (blue line) and October (purple line) over tropics (a), northern (b) and southern mid-latitudes, North Pole (d) and (e) South Pole.

- Extreme situations exhibiting highest and lowest anomalies (see section 4.3 for the definition of anomalies), i.e. the situations that are most affected by the high SatZA, were extracted per day and per zone. Figure 45 regroups all the situations extracted during 2018.

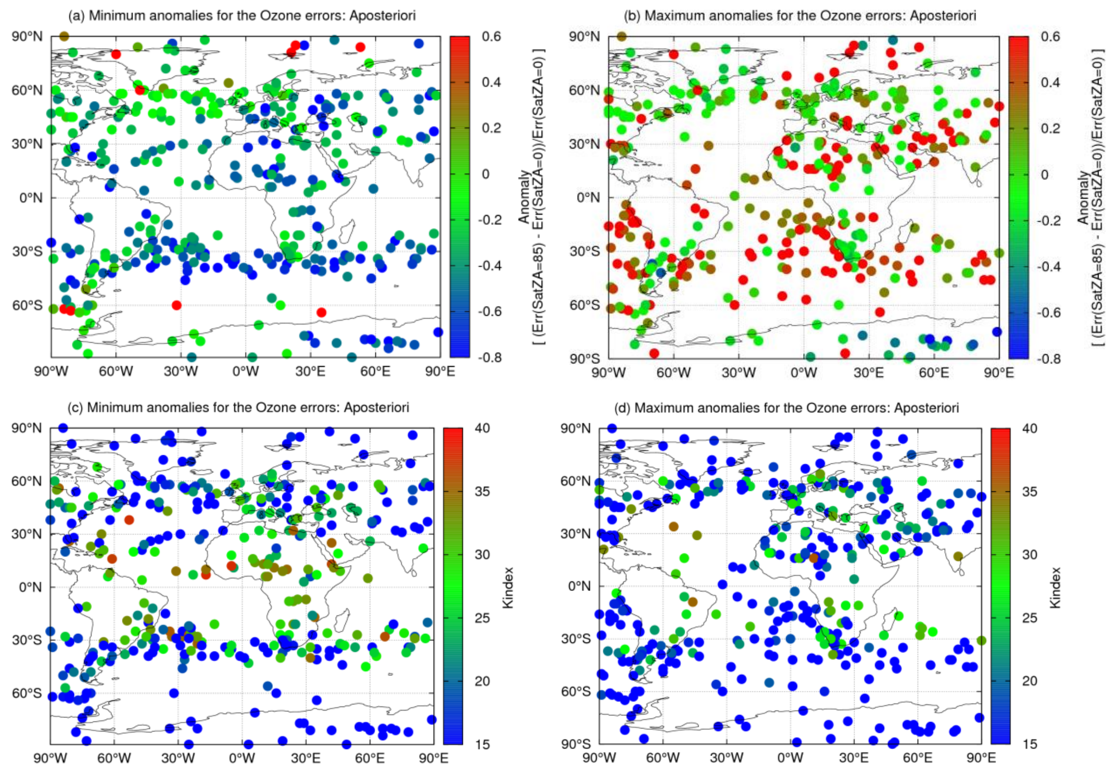

Figure 45: Maps of the extracted situations from the retrieval error dataset with the minimum (a) and maximum (b) anomalies. Associated K indices are displayed in (c) for minimum anomalies and in (d) for maximum anomalies, respectively.

- **The correlation between the anomalies values and the K index values are less clear than previously. The situations with positive anomalies values exhibit a K index above 30 and are found in the tropics and mid-latitudes, or exhibit a K index below 20 but are located in high latitudes. The situations with negative anomalies values exhibit a K index below 20 and are mainly found in the high latitudes bands.**

4.4.2 Impact of SatZA on retrieval profile errors

All the figures are available in ANNEXE B – All figures/§2.2.

4.4.2.1 Temperature

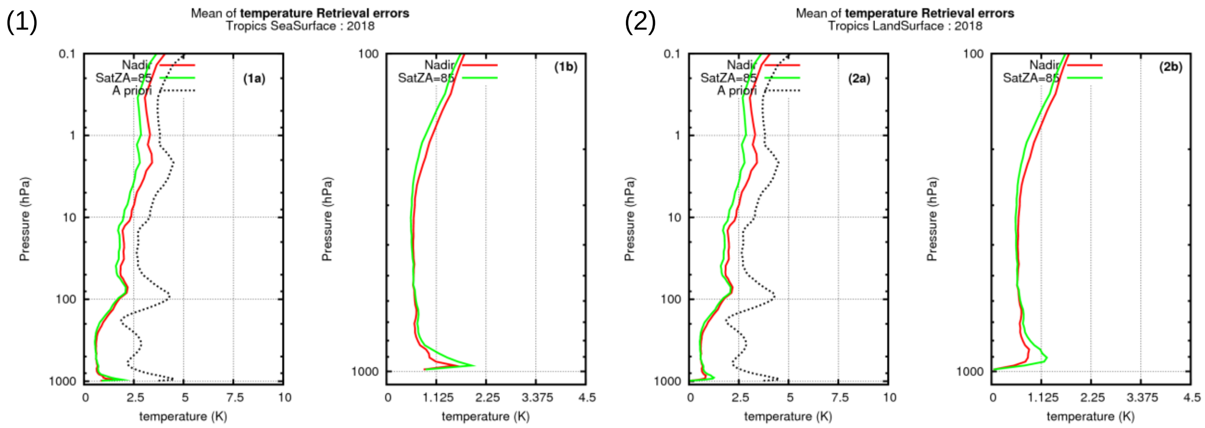

Figure 46: Retrieval errors at nadir (red curve) and at SatZA=85° (green curve) of the temperature profile over tropics (1) over sea and (2) over land. (1a) and (2a) Errors are displayed for altitudes from surface to 0.1 hPa. (1b) and (2b) Errors are displayed for altitudes from surface to 100 hPa.

Figure 46 compares the mean retrieval errors of temperature profiles at nadir and for SatZA=85° over the tropics over sea and over land. Between the surface and about 500 hPa, the mean retrieval errors at SatZA = 85° are greater than those obtained at nadir. Conversely, from about 500 hPa to TOA, the mean retrieval errors at SatZA = 85° are smaller than those obtained at nadir. This result is consistent with results obtained with sub-columns (see **Figure 31** and in Annex B/§2.1.1.1).

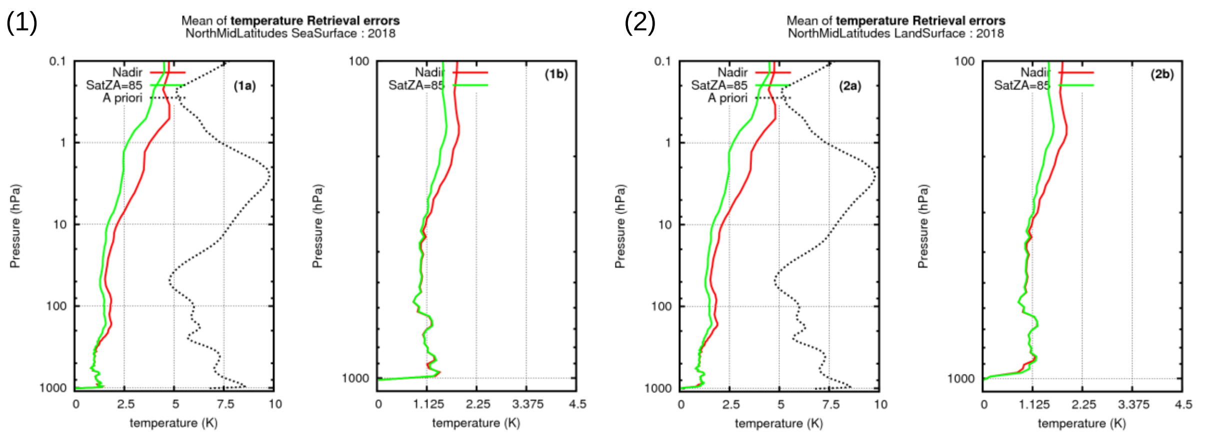

Figure 47: same as Figure 46 but errors are displayed for Northern Mid-latitudes

Figure 47 compares the mean retrieval errors of temperature profiles at nadir and for a SatZA=85° over northern mid-latitude over sea and over land. Between surface and approximately 500 hPa, the mean retrieval errors at SatZA = 85° are very close to the situations at nadir but a bit higher over land. For $p <$ 500 hPa, the mean retrieval errors at SatZA = 85° are smaller than those obtained at nadir. This result is consistent with results obtained with sub-columns (see Annex B/§2.1.2.1**).**

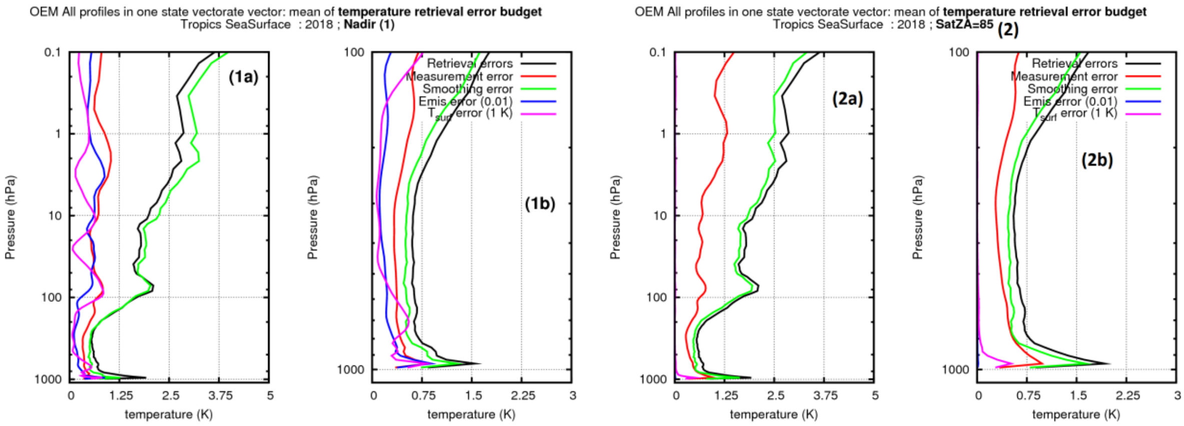

Figure 48: Mean retrieval error budget of temperature profiles over the tropics and sea for (1) nadir and (2) SatZA = 85°. (Black) Retrieval error profile. (Red) Measurement error. (Green) Smoothing error. (Blue) Error induced by a 0.01 incertitude on emissivity. (Purple) Error induced by a 1K incertitude on surface temperature. (1b) and (2b) Errors are displayed for altitudes from surface to 100 hPa.

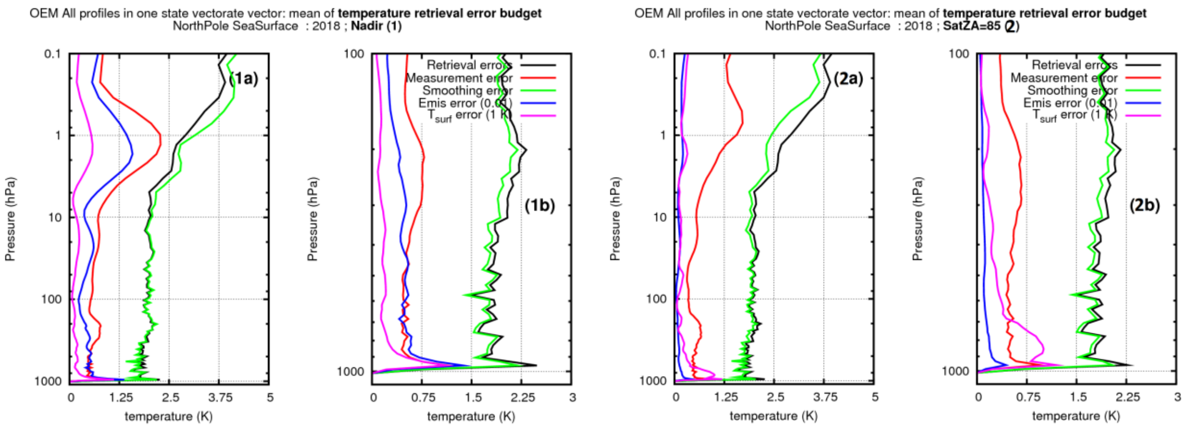

Figure 49: same as Figure 48, over North Pole

Figure 48 and Figure 49 reveal that:

- the retrieval error profiles (black lines) are dominated by the smoothing error (green curve) ,i.e. the *a priori* error. **That is, the retrieval error profiles depend mainly on the a priori error matrix.** Measurement errors (red line) are stronger at upper levels. **The observation error thus affects the error budget stronger at levels above 10 hPa (p < 10 hPa) than at tropospheric levels (between surface and about 100 hPa).**
- At nadir (Figure 48 (1) and Figure 49 (1)), a 0.01 emissivity incertitude (blue curve) affects all levels of the retrieval error profile and a 1 K incertitude has approximately the same impact on the retrieval error profile (purple curve) as a 0.01 emissivity incertitude;
- At SatZA=85° (Figure 49 (2) and Figure 48 (2)), only the retrieval errors of the levels close to the surface are affected by a 0.01 emissivity incertitude (blue curve). A 1 K incertitude has a more important impact on the retrieval error profile (purple curve) than a 0.01 emissivity incertitude mainly close the surface;
- At nadir and poleward, the impact of a 0.01 emissivity incertitude (blue curve) and a 1 K incertitude (purple curve) are greater than the impact found for the tropics.

Extreme situations exhibiting highest and lowest anomalies (see section 4.3 for the definition of anomalies), i.e. the situations that are most affected by the high SatZA, were extracted per day and per zone. Figure 50 regroups all the situations extracted during 2018.

For temperature, the anomalies have been computed for the levels at 986 hPa (Figure 50), at 661 hPa (Figure 51), at 400 hPa (Figure 52) and at 151 hPa (Figure 53). Subsequently, the situations that have the maximum/minimum anomaly values have been extracted during 2018.

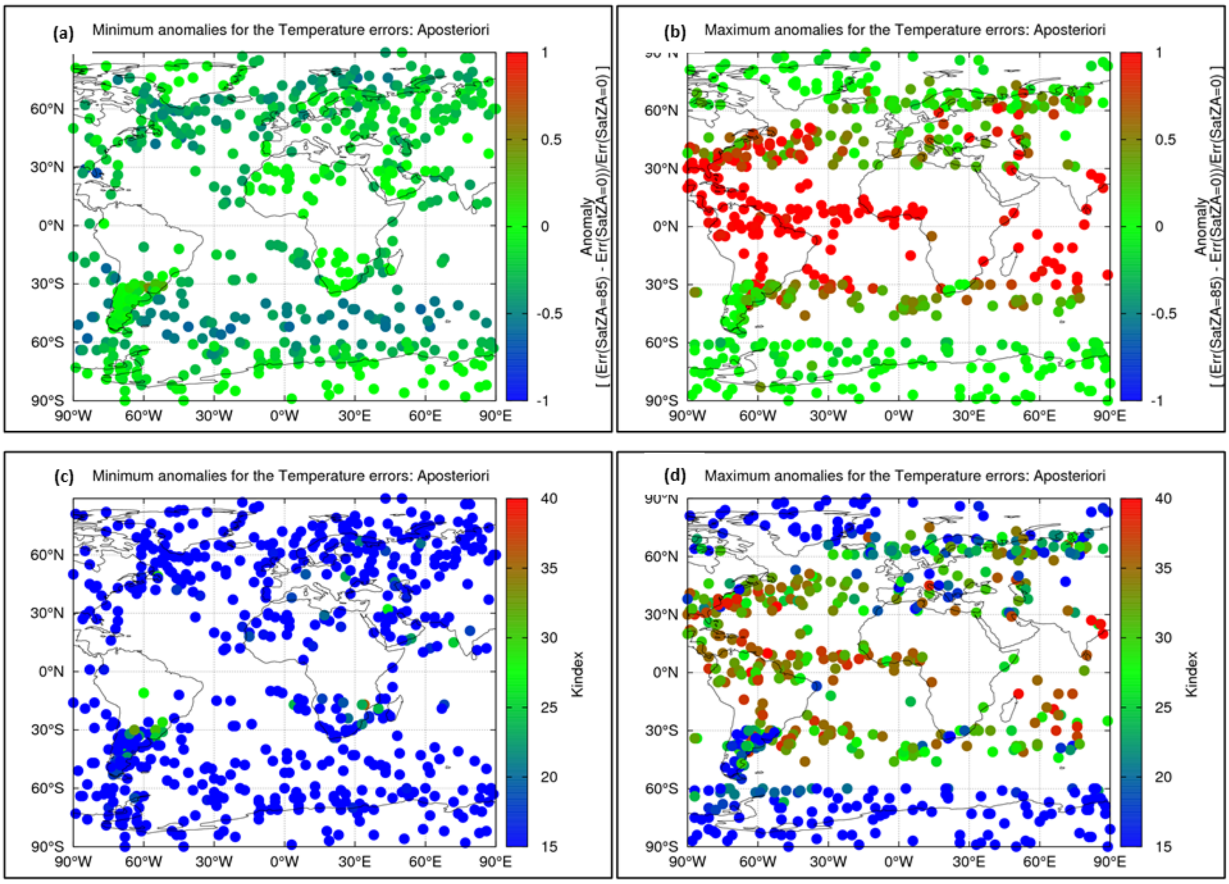

Figure 50: At level 986 hPa: Situations extracted from the generated dataset during 2018. One situation is extracted per day and zone. Upper panel: Location of the situations with (a) minimum anomalies and (b) maximum anomalies. Lower panel: Corresponding K indices

Figure 50 shows the results obtained at 986-hPa level.

The situations most impacted by higher satellite zenith angles have been extracted and displayed in Figure 50 (b). These situations are located mainly in the tropics and in the northern mid-latitudes. The retrieval error at this pressure level increases by than 100% (red colour). The Figure 50 (d) provides the associated values of K index for these situations. We observe that the situations with anomaly values close to 1 are associated to situations with K index value greater than 30, i.e. unstable situations.

Conversely, the situations with minimum anomaly values are shown in Figure 50 (a) and the associated K index values in Figure 50 (c). The anomalies are close to 0 and become even negative over the southern mid-latitudes. This means that the retrieval errors at 986 hPa are approximately similar at nadir and for SatZA = 85° and decrease weakly over the southern mid-latitudes. These situations correspond to stable situations since K indices are typically smaller than 20 (Figure 50 (c)).

Over the Polar Regions, the minimum (Figure 50 (a)) and the maximum (Figure 50 (b)) values of the anomalies are very close.

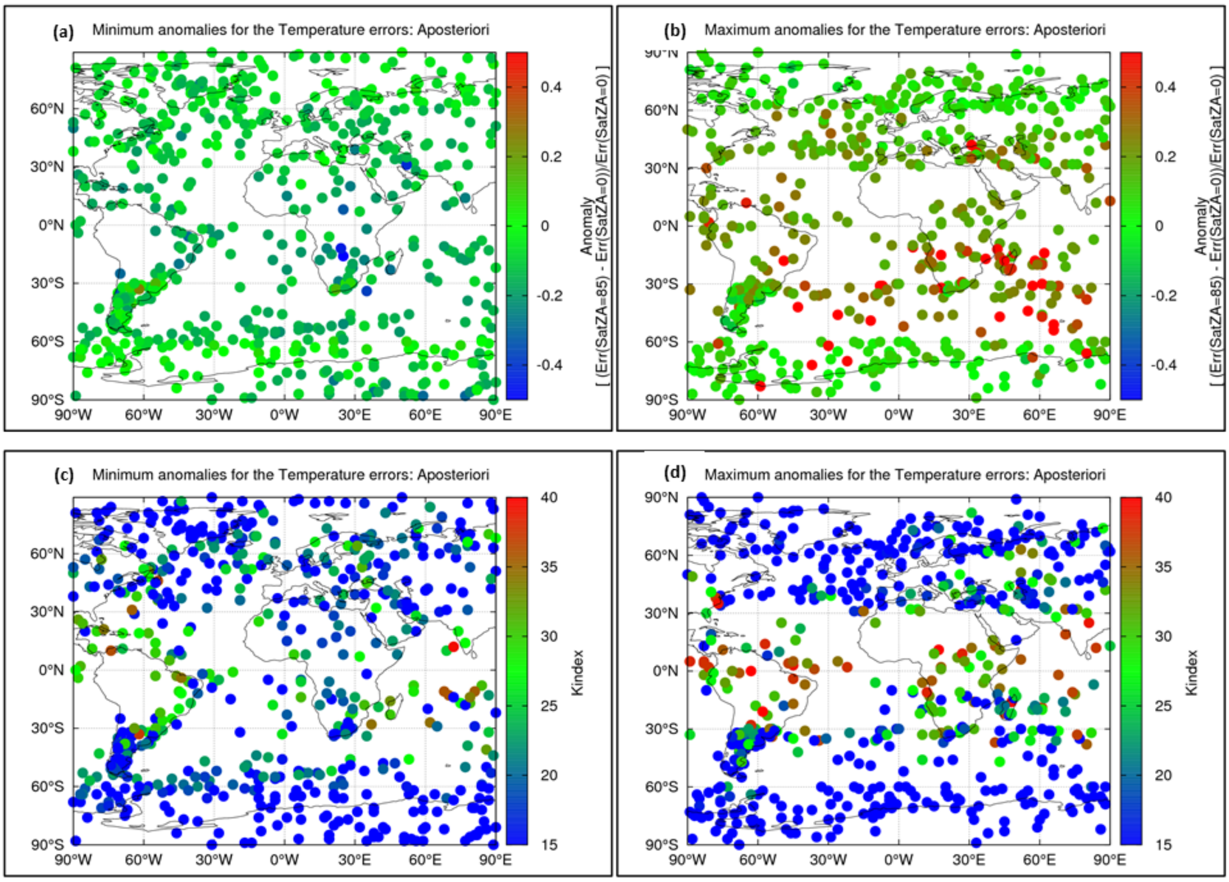

Figure 51: same as Figure 50 but for the 661-hPa level

Figure 51 reveals that for the 661-hPa level, the minimum (Figure 51 (a)) and the maximum (Figure 51 (b)) anomalies are very close for the main extracted situations. Associated K indices (Figure 51 (c) and (d)) are mainly below 30, but certain unstable situations (K indices above 30) are found. In the tropics, anomalies close or above 0.2 (Figure 51 (b)) correspond to situations with K indices between 25 and 40 (Figure 51 (d)), i.e. unstable situations. The situations with the minimum anomalies (Figure 51 (a)) are close to 0, i.e. these situations are not strongly affected by the higher satellite zenith angle. In the tropics, the anomalies are ≤ 0, i.e., for these situations, the retrieval error at 661 hPa is smaller for a SatAZ = 85° than at nadir (Figure 51 (a)). These situations correspond to situations with K indices < 30.

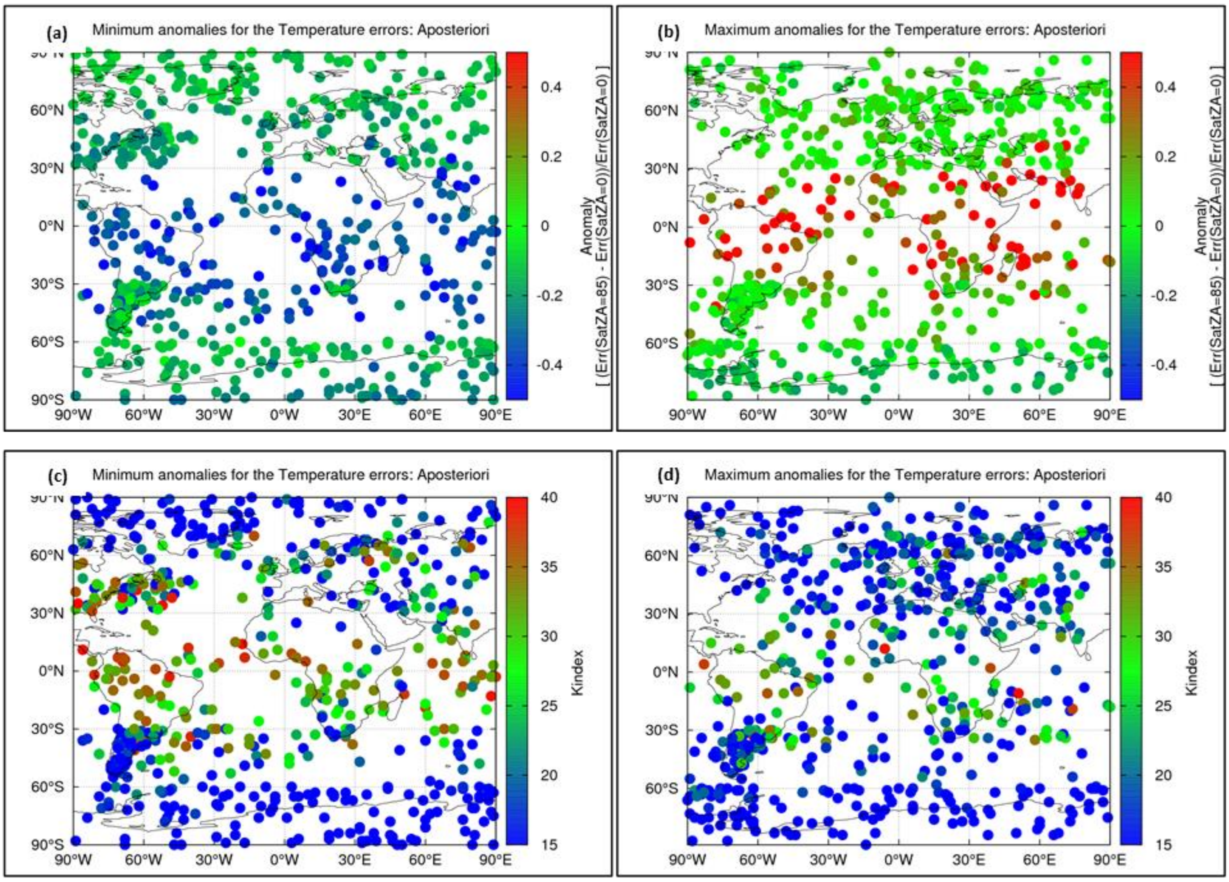

Figure 52: same as Figure 50, for the 400-hPa level.

Minimum (Figure 52 (a)) and maximum (Figure 52 (b)) anomalies of the extracted situations are very different over the tropics and the mid-latitudes at the 400-hPa level. The minimum values of anomalies are close or below -0.5, i.e., the retrieval error at 400 hPa for these situations can decrease by 50% or more (Figure 52 (a)). Conversely, maximum values of anomalies are close to or above 0.5, i.e., the retrieval error at 400 hPa for these situations can increase by 50% or more (Figure 52 (b)). Associated K indices (Figure 52 (c) and (d)) are typically between 25 and 40 for such situations in the tropics. At higher latitudes, the anomalies are close to 0 and correspond to stable situations (K indices below 20).

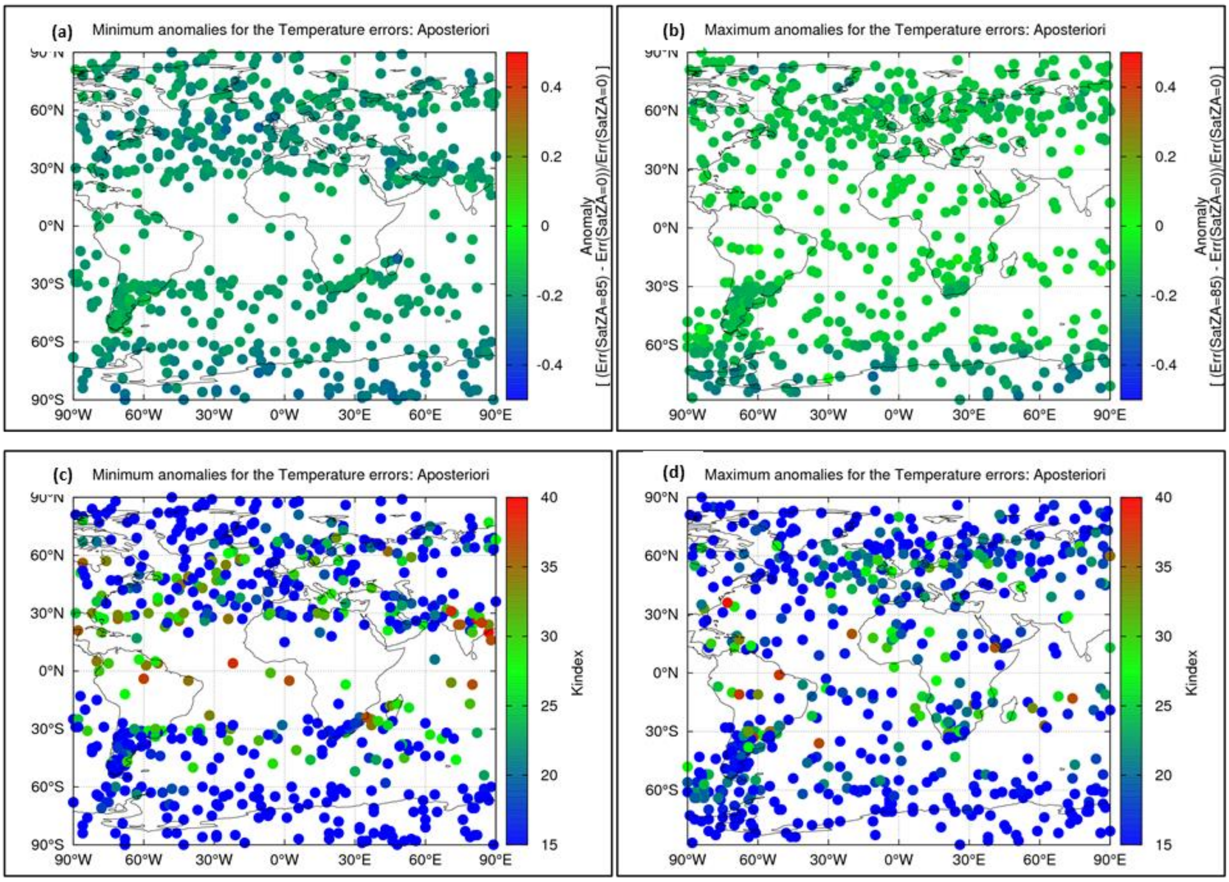

Figure 53: same as Figure 50 but for the 151-hPa level.

Figure 53 reveals that for the 151-hPa level, the minimum (Figure 53 (a)) and the maximum (Figure 53 (b)) values of the anomalies are very close to 0 for the extracted situations. The maximum (Figure 53 (b) values of the anomalies are mainly positive while the minimum (Figure 53 (a)) values are negative and generally found in the mid-latitudes. The associated K indices (Figure 53 (c) and (d)) are mainly below 35 in the tropics, and below 20 in the higher latitudes.

4.4.2.2 Water vapour

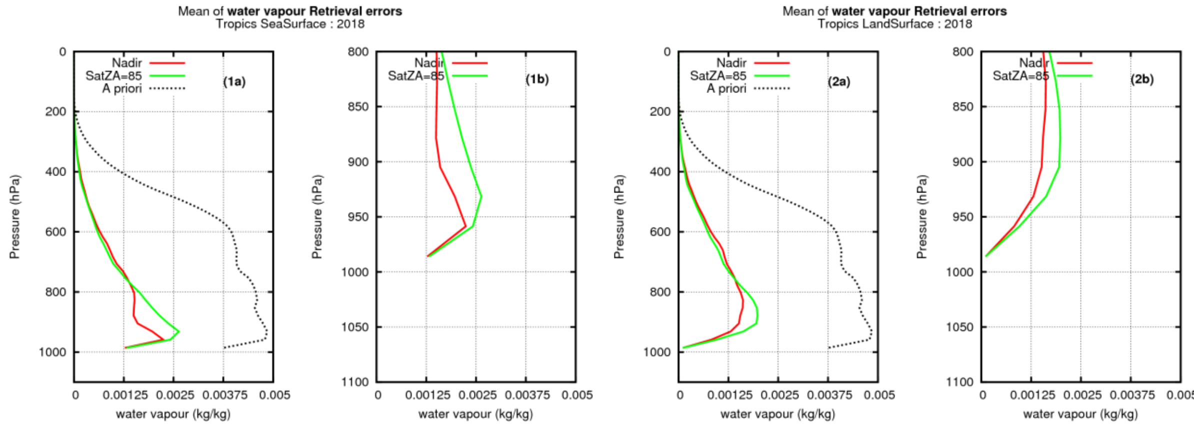

Figure 54: Retrieval errors at nadir (red curve) and at SatZA=85° (green curve) of the water vapour profile in the tropics over (1) sea and over (2) land. (a) Errors are displayed from surface to 0 hPa. (b) Errors are displayed from surface to 800 hPa.

Figure 54 compares the mean retrieval error profile of water vapour at nadir and for SatZA=85° in the tropics over sea and over land. The mean retrieval errors at SatZA = 85° are greater than those obtained at nadir for the levels between the surface and the level at about 800 hPa. In the mid-troposphere (800-400 hPa), the errors at nadir are slightly higher than at SatZA = 85°. From about 400 hPa to TOA, both retrieval error profiles are very close. This result is consistent with results obtained with sub-columns (see **Figure 32**, **Figure 38** and **Figure 39** (a) and Annex B/§2.1.1.2).

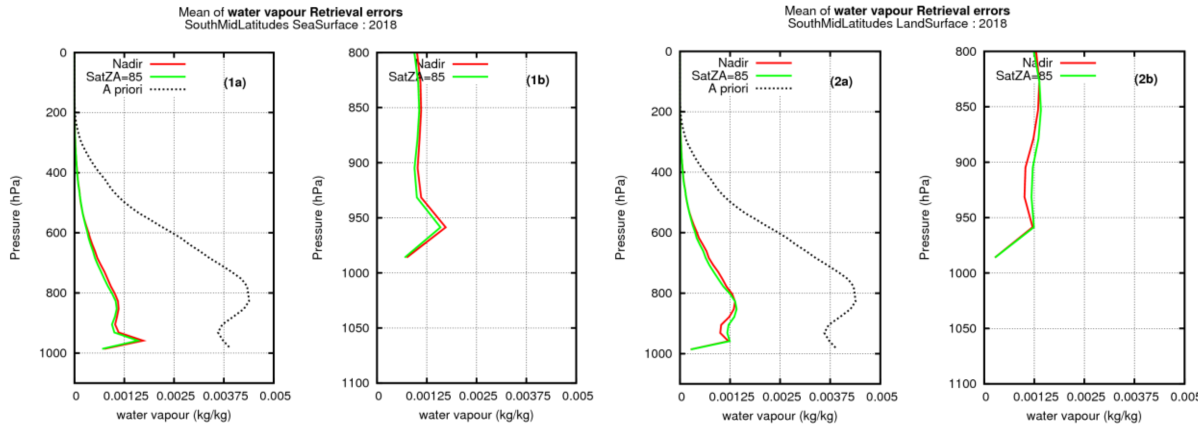

Figure 55: same as Figure 54 over Southern Mid-latitudes

The Figure 55 compares the mean retrieval error profile of water vapour at nadir and for SatZA=85° over Southern mid-latitude and over sea and land. The mean retrieval errors at SatZA = 85° are very close to the situations at nadir for all the levels. However, over sea, between the surface and approximately 800 hPa, the mean retrieval error profile at SatZA = 85° is smaller than at nadir, whereas over land, the mean retrieval error profile is greater at SatZA = 85° for those levels. This result is consistent with results obtained with sub-columns presented in **Figure 38** and Annex B/§2.1.3.2.

The different behaviours of the retrieval errors between land and sea surface still remain weak.

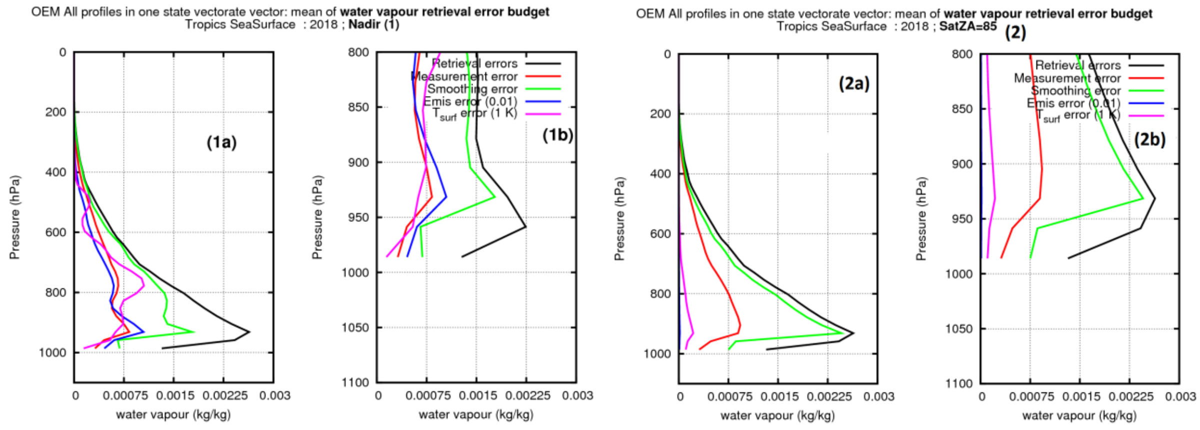

Figure 56: Retrieval error budget of water vapour profile in the tropics and over sea at (1) nadir and (2) SatZA=85°. (Black) Retrieval error profile. (Red) Measurement error. (Green) Smoothing error. (Blue) retrieval error induced by a 0.01 incertitude on emissivity. (Purple) retrieval error induced by a 1 K incertitude in surface temperature.

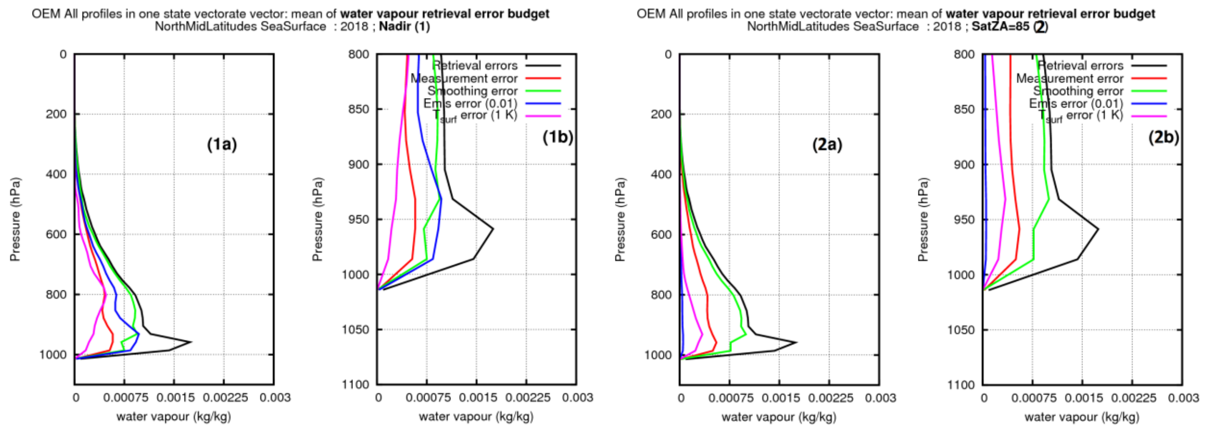

Figure 57: same as Figure 56 over Northern mid-latitudes

Figure 56 and Figure 57 reveal that:

- the retrieval error profiles (black lines) are dominated by the smoothing error (green curve), i.e. by the *a priori* error. In these cases, the **retrieval error profiles depend mainly on the *a priori* error because of the low space of the measurements. The observation error has a more significant impact for the levels close to the surface, and poleward** (see Annex B/§2.2);
- At nadir (Figure 56 (1) and Figure 57 (1)), a 0.01 emissivity incertitude (blue curve), impacts all retrieval error profiles. Levels close to the surface are more affected since the mixing ratio of H_2O is most pronounced. A 1 K incertitude on the surface temperature has a similar impact on the retrieval error profile (purple curve) as a 0.01 emissivity incertitude over the tropics but a lower impact over Northern mid-latitudes;
- At SatZA=85°(Figure 56 (2) and Figure 57 (2)), the impact of a 0.01 emissivity incertitude (blue curve) and a 1 K incertitude on the surface temperature (purple curve) induces retrieval errors close to 0 kg/kg and along all the vertical axis in the tropics. These errors, especially the one due to surface temperature, increase poleward but remain low in front of the total retrieval errors.

We have extracted extreme situations where anomalies exhibit the highest and lowest values, i.e. the situations that are most impacted by the high SatZA values are extracted per day and zone.

For water vapour, the anomalies have been computed for the 986-hPa (Figure 58), 802-hPa (Figure 59), and the 661-hPa level (Figure 60). Subsequently, those situations exhibiting maximum/minimum anomaly values have been extracted during 2018.

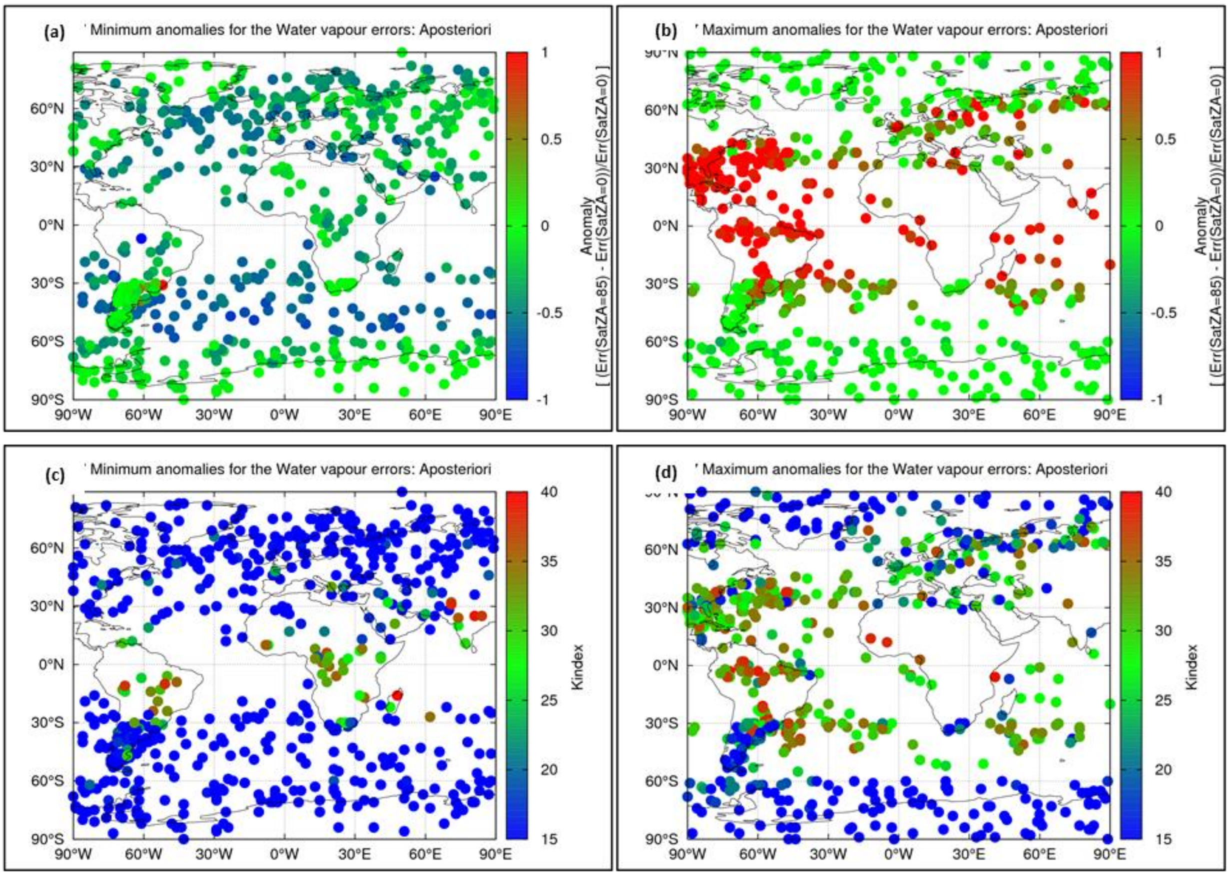

Figure 58: Situations extracted from the generated dataset at the 986-hPa level during 2018. (a, c) Situations exhibiting minimum values of anomalies and corresponding K indices. (b,d) Situations exhibiting maximum values of anomalies and corresponding K indices.

Figure 58 (b) shows the situations at the 986-hPa level that have highest anomaly values. These situations are found mainly in the tropics and northern mid-latitudes. The retrieval error at this pressure level increases by more than 100% (red coloured dots in Figure 58a, b). Figure 58 (d) provides the associated K indices for these situations. We observe that the situations impacted by the higher satellite zenith angles correspond to situations with K indices greater than 25, i.e. unstable situations.

The situations that have lowest anomaly values have been extracted and displayed together with corresponding K indices in Figure 58 (a, c). The anomalies are close to 0 and can even be negative over mid-latitudes. This means that the retrieval errors at 986-hPa level are approximately similar at nadir and for SatZA = 85° or decrease a few over in the mid-latitudes. These situations correspond to stable situations because the K indices (Figure 58 (c)) are smaller than 20.

Note in the polar regions, minimum (Figure 58 (a)) and maximum (Figure 58 (b)) values of the anomalies are very similar.

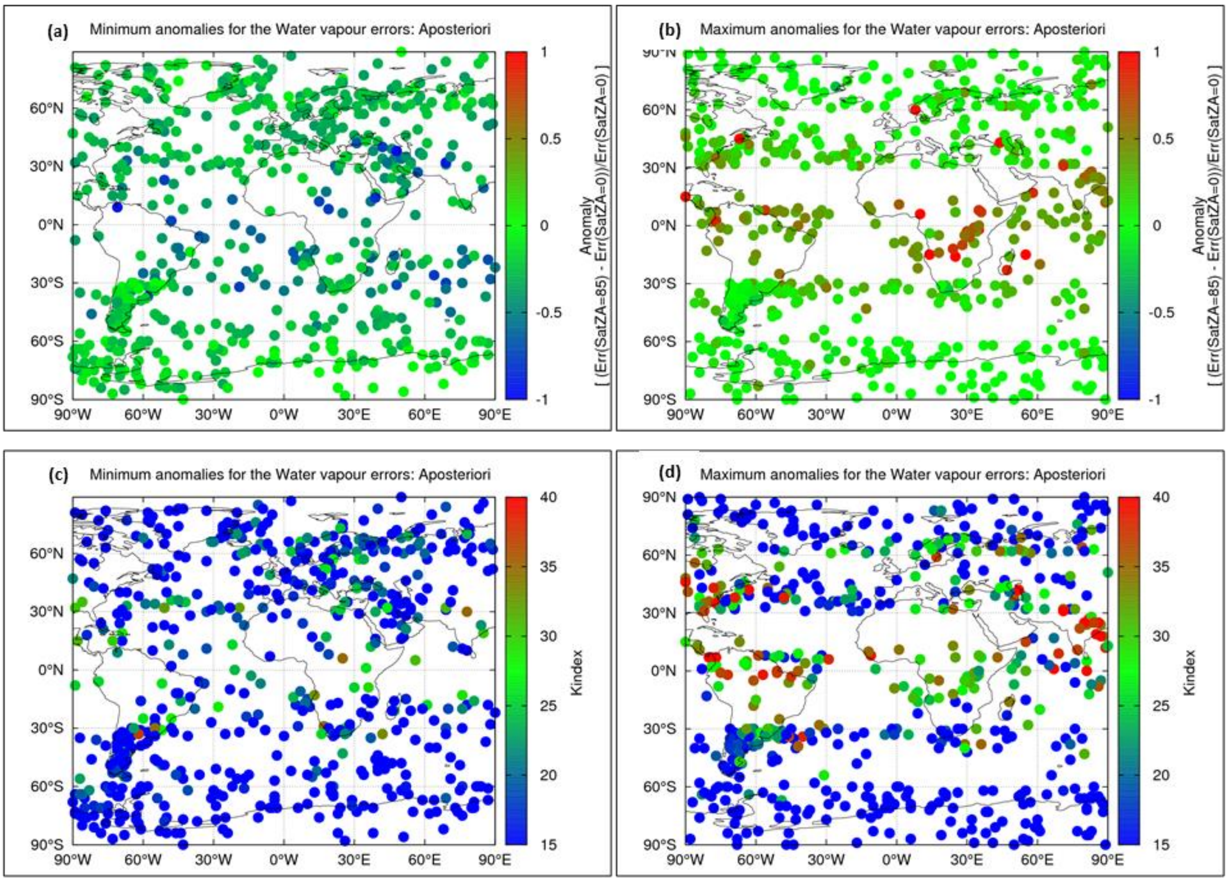

Figure 59: As Figure 58 but for the 802-hPa level.

Figure 59 (b) shows the situations at the 802-hPa level having the highest anomaly values. These situations are found mainly in the tropics and in the northern mid-latitudes. The retrieval error at this pressure level increases by more than 50%. Figure 59 (d) provides the associated K indices. We observe that the situations affected by the higher satellite zenith angles are associated to situations with K indices ≥ 30, i.e. unstable situations.

The situations exhibiting the lowest anomaly values are show in Figure 59 (a) and the associated K indices are given in Figure 59 (c). The anomalies are close to 0 and can even be negative over the tropics. This means that the retrieval errors at 802 hPa are approximately of similar magnitude at nadir and for SatZA = 85° or decrease for some situations over the tropics. These situations correspond to stable situations since the K indices (Figure 59 (c)) are mainly smaller than 30.

In the Polar Regions, the minimum (Figure 59 (a)) and the maximum (Figure 59 (b)) values of the anomalies are very close.

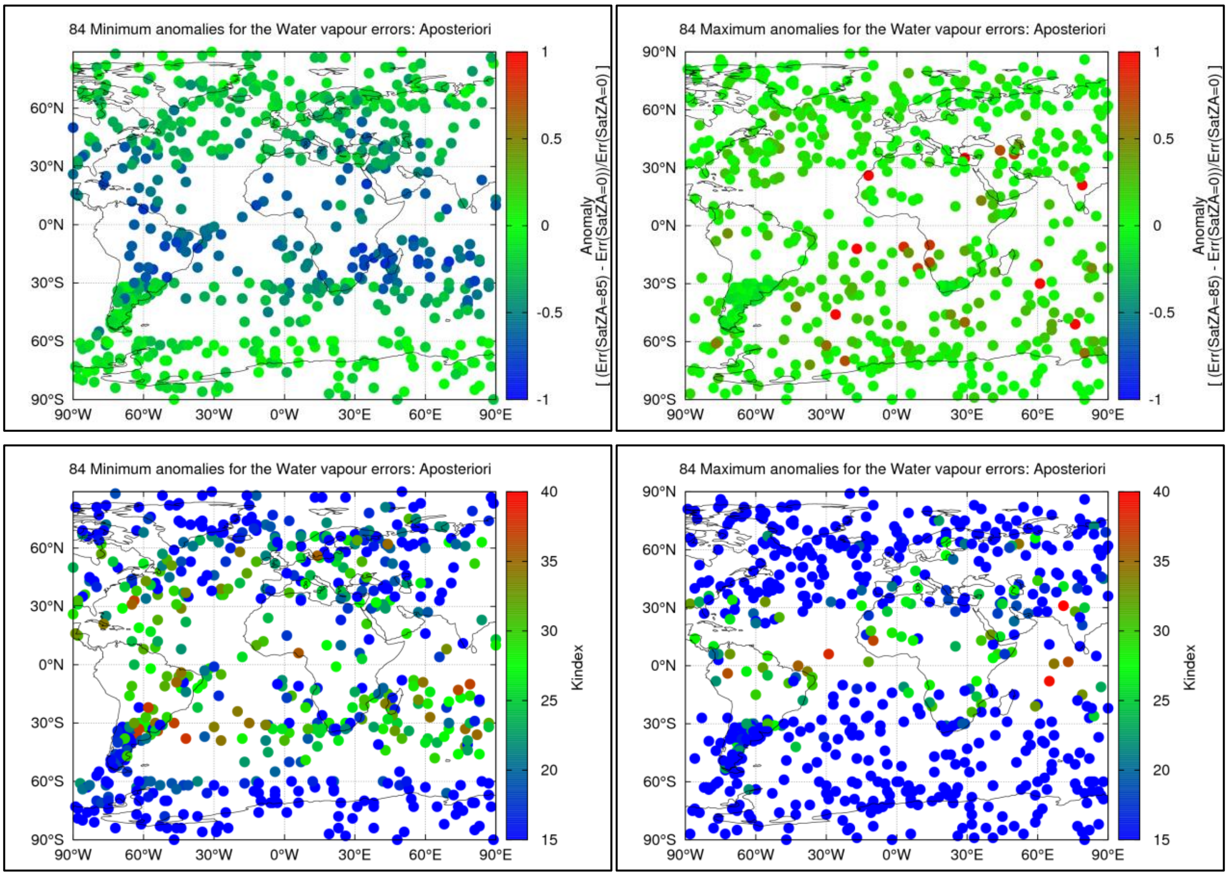

Figure 60: As Figure 58 but for the 661-hPa level.

At the 661-hPa level, retrieval errors for water vapour are close to 0. Figure 60 (b) shows the situations where the higher anomaly values. The most impacted situations do not seem to be localized in a particular geographical zone and the maximum anomalies are generally close to 0. We can note that there are some situations where the anomalies can be ≥ 1 (red points). Figure 60 (d) provides associated K indices for these situations. We observe that the situations impacted by higher satellite zenith angle values are associated to situations with K indices being smaller or close to 20, i.e. stable situations. In the tropics, some situations can have K indices between 20 and 30.

The situations that have the lowest anomalies and corresponding K indices are shown in Figure 60 (a) and Figure 60 (c), respectively. The anomalies are close to 0 and even negative anomalies can be found in the tropics. This means that the retrieval error at the 661-hPa level are smaller at SatZA = 85° than at nadir. Outside the tropics, these situations correspond to stable situations because the K indices (Figure 60 (c)) are mainly smaller than 20. In the tropics, these situations correspond to K indices between 25 and 35. In contrast to the 802-hPa level (Figure 59) and the 986-hPa level (Figure 58), these unstable situations are the situations where the retrieval errors decrease between nadir and SatZA = 85°.

In the Polar Regions, derived minimum (Figure 60 (a)) and maximum (Figure 60 (b)) values of the anomalies are very similar.

4.4.2.3 Ozone

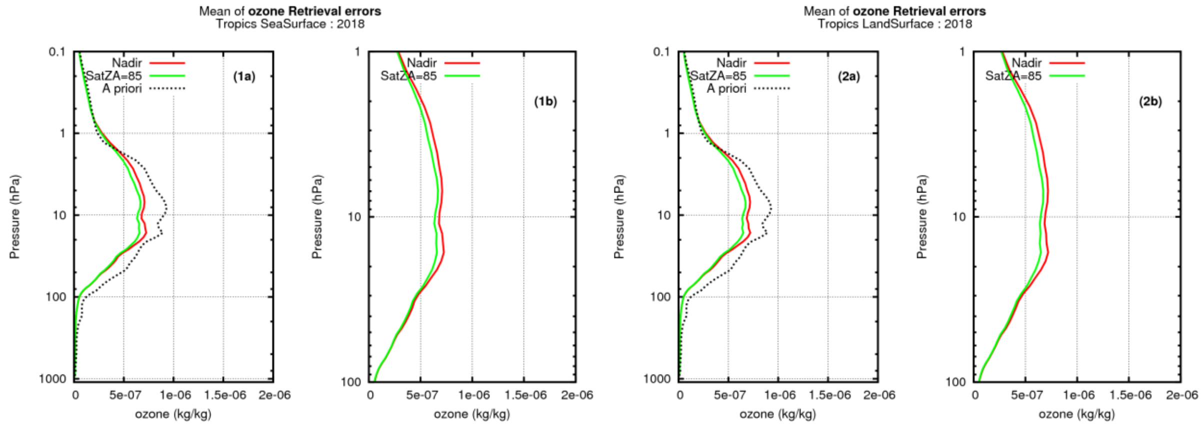

Figure 61: Retrieval errors at nadir (red curve) and at SatZA=85° (green curve) of the ozone profile over tropics. (1) Errors over sea. (2) Errors over land. (a) Altitude ranges from 1000 hPa to 0.1 hPa. (b) Altitude ranges from 100 to 1 hPa.

Figure 61 compares the mean retrieval error profile of the ozone at nadir and for SatZA=85°, in the tropics over sea and land. The mean retrieval errors at SatZA = 85° (green curve) are smaller than the mean retrieval errors at nadir (red curve) but both error profiles are very close. There is no significant difference between the behaviour of the retrieval errors over sea (Figure 61 (1)) and that over land (Figure 61 (2)) in the tropics. This result is consistent with results obtained with sub-columns (see **Figure 33** and in Annex B/§2.1.1.3).

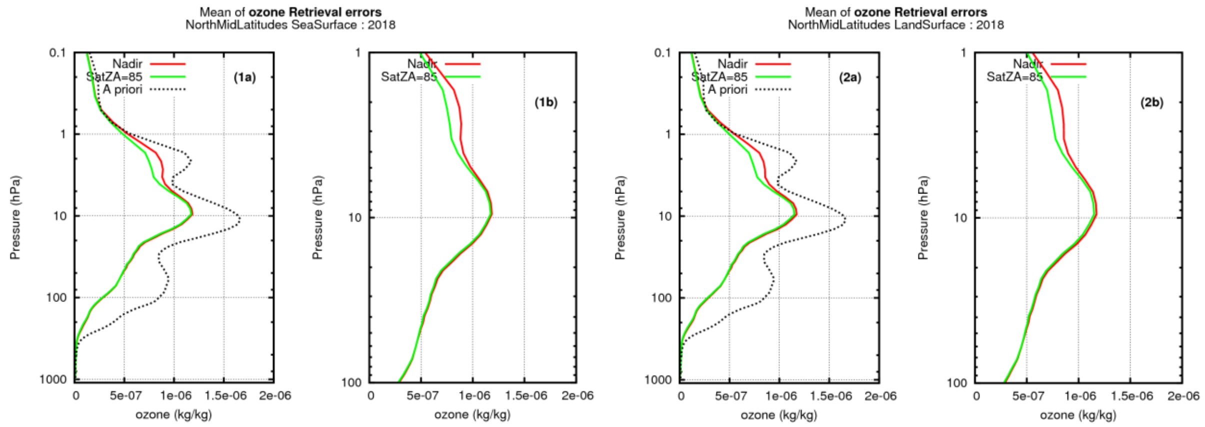

Figure 62: As Figure 61 but over Northern mid-latitudes

Figure 62 compares the mean retrieval error profile of ozone at nadir (red curve) and for SatZA=85° (green curve), at Northern mid-latitude over sea (Figure 62 (1)) and over land (Figure 62 (2)). Over sea (Figure 62 (1)) and over land (Figure 62 (2)), the error profiles are very close and appear similar.

The mean retrieval errors at SatZA = 85° (green curve) are very close to the situations at nadir (red curve) between 200 hPa and 10 hPa. From about 10 hPa to 0.5 hPa, mean retrieval errors at SatZA = 85° are quite smaller than those found at nadir.

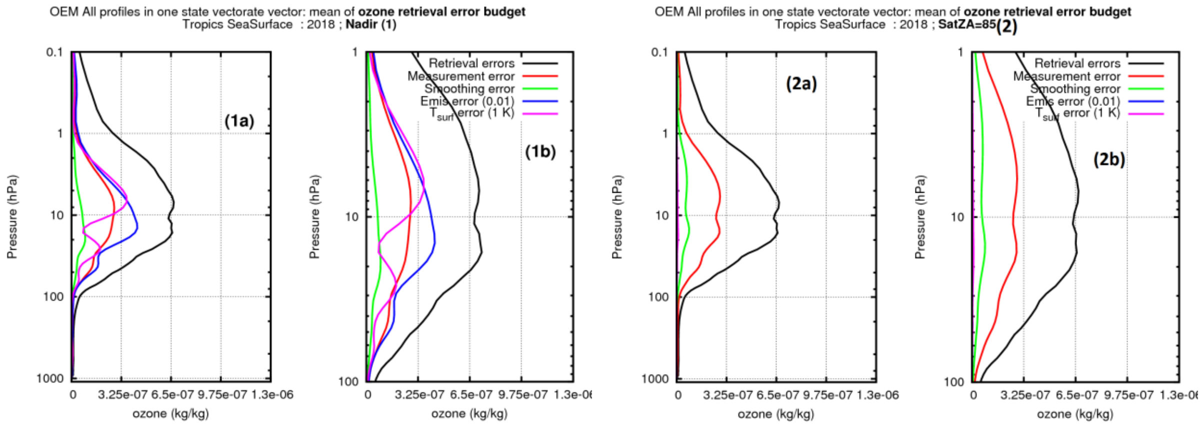

Figure 63: Error budget of ozone profile retrieval over the tropics and sea. (1) Error budget for a SatZA of 0° (nadir). (2) Error budget at SatZA=85°. (Black) Retrieval error profile of ozone. (Red) Measurement error. (Green) Smoothing error. (Blue) Retrieval error induced by a 0.01 incertitude on emissivity. (Purple) Retrieval error induced by a 0.01 incertitude on emissivity.

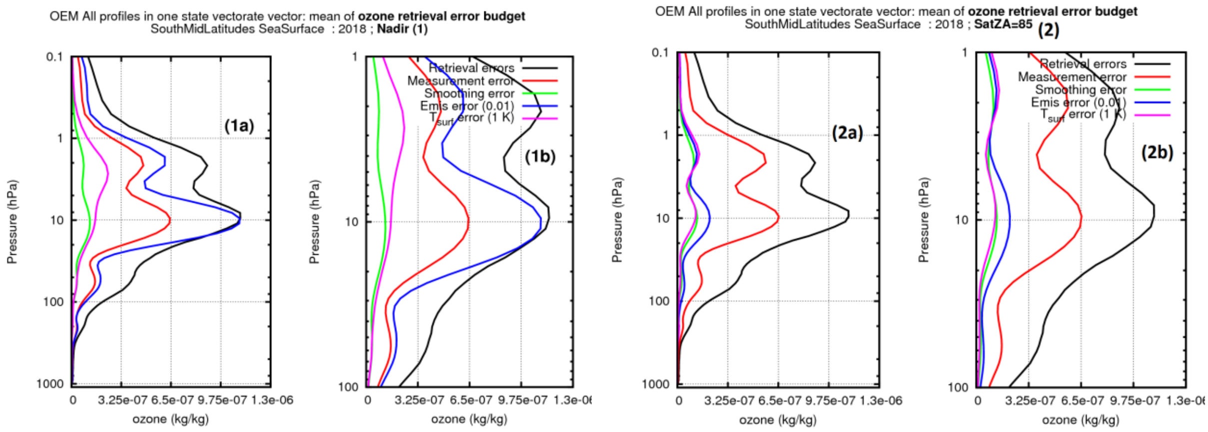

Figure 64 : As Figure 63 but over Southern Mid-latitudes

Figure 63 and Figure 64 reveal that:

- The retrieval error profiles (black lines) are dominated by the measurement error (red curve), i.e. the observation error. **The retrieval error profiles depend mainly on the observation error;**
- At nadir (Figure 63 (1) and Figure 64 (1)), a 0.01 emissivity incertitude (blue curve) impacts all retrieval error profiles, particularly levels close to 10 hPa are affected, where the mixing ratio of ozone is most pronounced. A 1 K incertitude on the surface temperature also impacts the retrieval error profiles (purple curve) for all the levels in a lesser extent;
- At SatZA=85° (Figure 63 (2) and Figure 64 (2)), the impact of both a 0.01 emissivity incertitude (blue curve) and a 1 K incertitude on the surface temperature (purple curve) induces retrieval errors close to 0 kg/kg along all the vertical axis in the tropics (Figure 63 (2)).These errors increase poleward but remain quite low in front of the retrieval errors for the levels above 100 hPa.

Extreme situations where anomalies exhibit high values, i.e. the situations which are the most impacted by the high SatZA values, have been extracted per day and zone. We reproduced this exercise for the minimum values of the anomalies in order to extract the situations which are least impacted by high SatZA values. For ozone, the anomalies have been computed for the 11- hPa level:

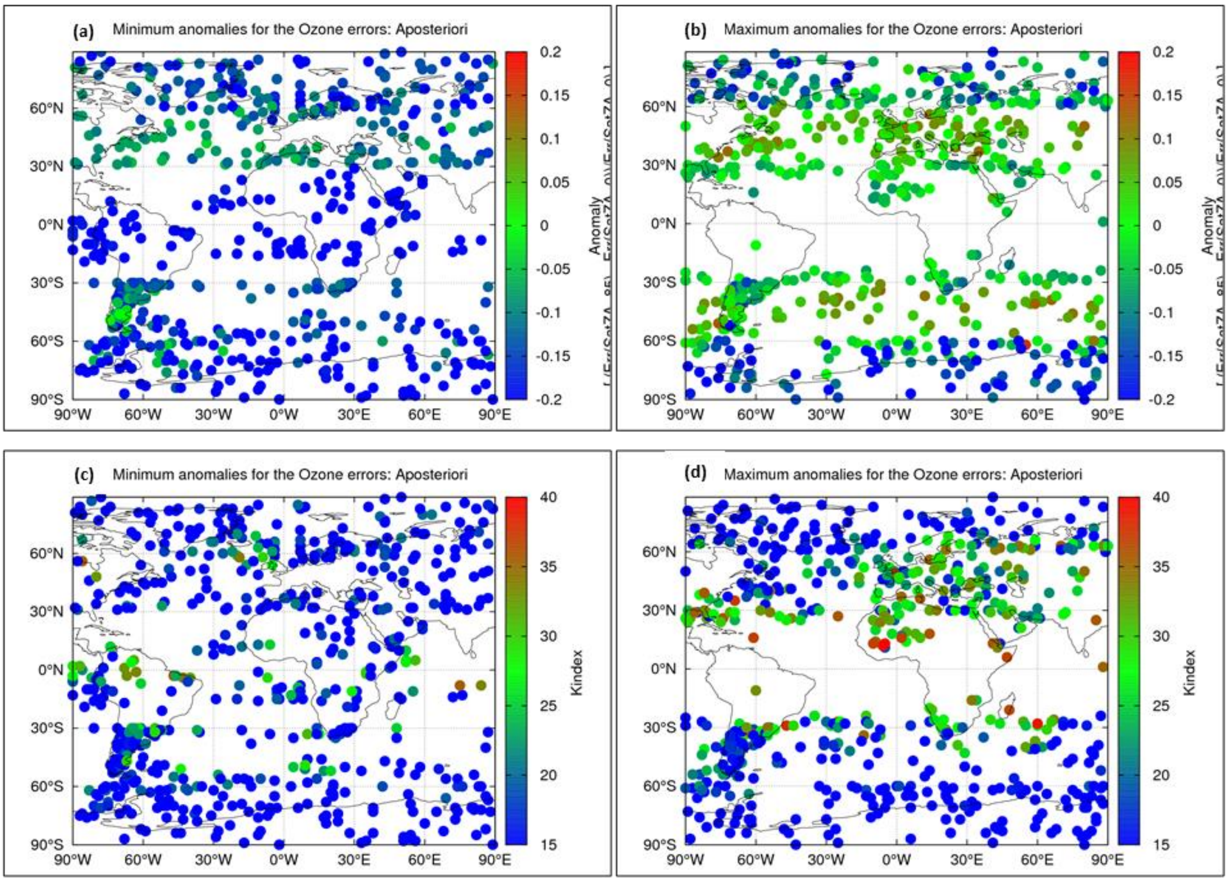

Figure 65: Situations extracted from the Generated data set during 2018 at the 11-hPa level. One situation is extracted per day and zone. Upper panel: (a) Situations with maximum anomaly values. (b) Situations with minimum anomaly values. Lower panel: Corresponding K indices.

The situations where the anomalies at 11 hPa are the highest are shown in Figure 65 (b). The most impacted situations are found at mid-latitudes (northern and southern) and the retrieval error at this level increases by about 10%. The Figure 65 (d) provides the associated K indices for these situations. We observe that the situations impacted by the higher satellite zenith angles are associated to situations with K index being greater or close to 30, i.e. unstable situations in the northern mid-latitudes. In the southern mid-latitudes, the situations are more stable (Figure 65 (d)) since K indices are generally below 20. These situations, however, are affected by the higher satellite zenith angles because certain anomalies close to 10% were found (Figure 65 (b)).

Conversely, the extracted situations where the anomalies at 11 hPa are the lowest are shown in Figure 65 (a) together with associated K indices given in Figure 65 (c). The anomalies are close to or smaller than 0 and some values drop by up to 20%. This means that the retrieval error at the 11-hPa level are less important for SatZA = 85° than at nadir. These situations correspond to stable situations because the K index values (Figure 65 (c)) are mainly smaller than 20. We can note that some situations have K indices between 25 and 30.

In the Polar Regions, the derived minimum (Figure 65 (a)) and the maximum (Figure 65 (b)) values of the anomalies are very close.

4.4.3 Impact of SatZA on Averaging Kernels and DOFS

The following section aims at illustrating the impact of the Satellite Zenith Angle on the Averaging Kernels (A) (see equation (8)) and the Degree Of Freedom For Signal (DOFS) for every geophysical product studied in the current study (T, W and O).

The Averaging Kernels represent the sensitivity of the retrieval to the true state, allowing the evaluation of the vertical resolution. The elements $A(i,j)$ of the Averaging Kernel matrix provide the relative contribution of the elements $x(i)$ of the true state vector to each element $\hat{x}(j)$ of the retrieved state vector.

The DOFS are obtained by calculating the trace of Averaging Kernels and provide global information, in particular on how many useful independent quantities can be found in a measurement. In addition, the cumulative degree of freedom (CDoF) is computed; the principle is to compute the sum along the diagonal of the Averaging Kernels from bottom to a pressure level which is increased incrementally as follows:

$$CDoF(j) = \sum_{j=bottom}^{j} A(j,j) \quad (19)$$

With *j* varying from the bottom to the top pressure level.

Since the impact of high satellite angles is generally higher in the tropical area, the following sections present the Averaging Kernels and the DOFS for this geographical region only. The whole set of plots (corresponding to all geographical areas and surface types) are gathered in Annexe C – All figures of Averaging Kernels and DOFS.

4.4.3.1 Temperature

The following figures (Figure 66) illustrate the annual mean of the Averaging Kernels and DOFS of the temperature in the tropics over sea at Nadir and for 85° for all levels and for the levels where the contrast between the two viewing geometry is the highest in each selected sub-column ([surface-700], [700-300], [300-100] hPa: see section 4.4.1).

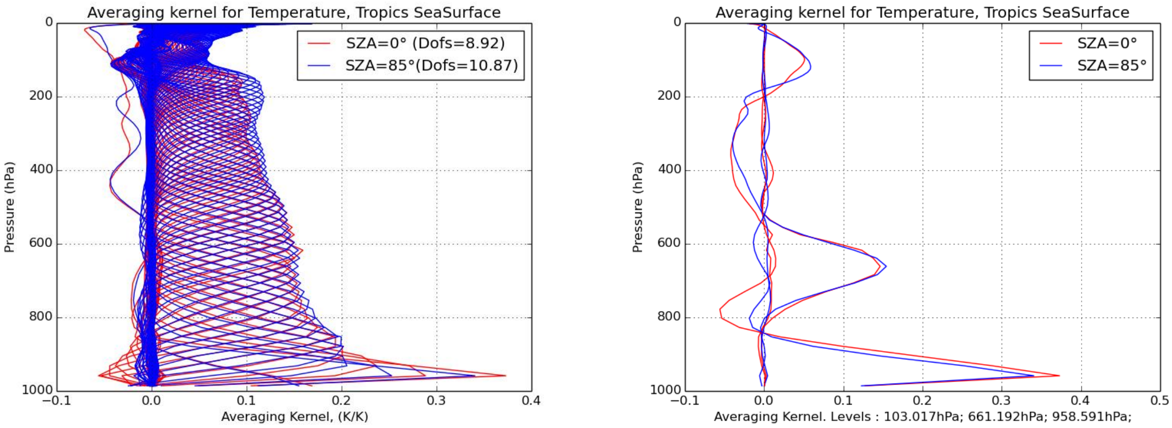

Figure 66: Annual mean of the Averaging Kernels of the temperature in the tropics over sea at Nadir (in red) and for 85° (in blue). Left side panel: all levels and corresponding DOFS; right side panel: levels where the contrast between the two viewing angles is the highest in each selected sub-column ([surface-700], [700-300], [300-100] hPa); the corresponding pressure value of each level is also provided in the x-axis text box.

Figure 66 and plots in Annexe C – All figures of Averaging Kernels and DOFS illustrate the change in the depth and width (vertical resolution) in the two viewing configurations: this result is consistent with the results presented in the previous sections, that is the vertical resolution of the temperature retrieval is slightly degraded close to surface in the tropics while it becomes better in the mid to upper troposphere at high SatZA. Close to surface, the impact at high angle depends on the geographical area and the surface type while in the upper troposphere the impact is the same whatever the region. The values of the DOFS show that the number of independent information is better at high SatZA.

The following figures (Figure 67) show the annual mean of the cumulative DoF of the temperature in the tropics over sea at Nadir and for 85° and a zoom in the mid-troposphere ([10^{-3} – 10^{-2}] hPa).

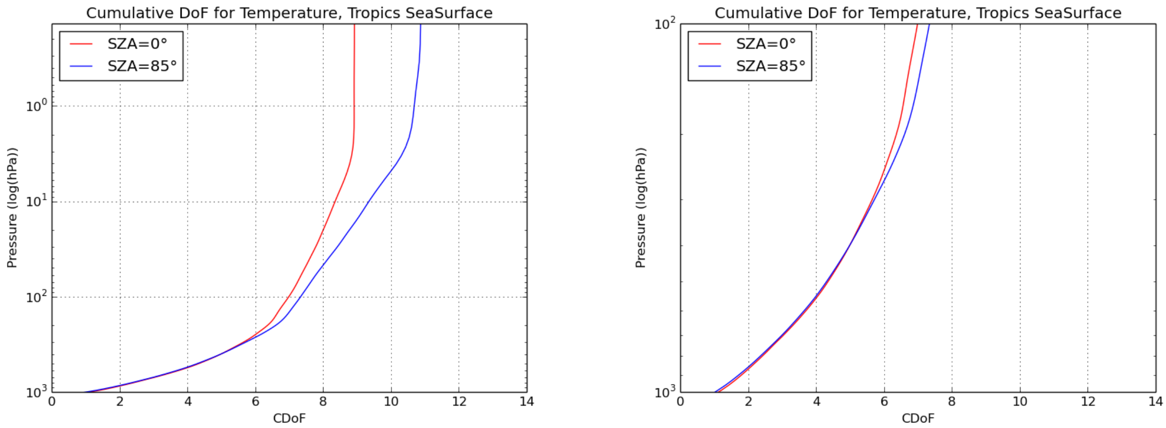

Figure 67: Annual mean of the cumulative DoF of the temperature in the tropics over sea at Nadir (in red) and for 85° (in blue). Left side panel: all levels; right side panel: zoom in the mid-troposphere.

Figure 67 and plots in Annexe C – All figures of Averaging Kernels and DOFS show that CDoF at Nadir are higher at bottom from the start and then decelerate while CDoF for 85° ramps up and overtakes in the upper troposphere and stays higher upwards.

4.4.3.2 Water vapour

The following figures (Figure 68) illustrate the annual mean of the Averaging Kernels and DOFS of the water vapour in the tropics over sea at Nadir and for 85° for all levels and for the levels where the contrast between the two viewing geometry is the highest in each selected sub-column ([surface-800], [800-500] hPa: see section 4.4.1).

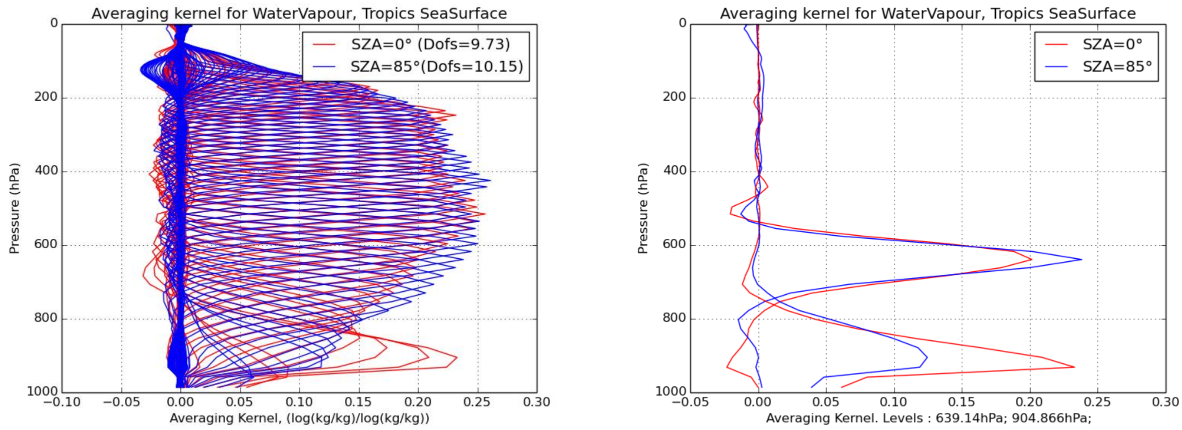

Figure 68: Same as Figure 66 for the water vapour.

Figure 68 and plots in Annexe C – All figures of Averaging Kernels and DOFS illustrate clearly the change in the depth and width (vertical resolution) in the two viewing configurations: this result is also consistent with the previous results, that is the accuracy of the water vapour retrieval is quite a lot degraded close to surface while it becomes better in the mid-troposphere at high SatZA.

The following figures (Figure 67) show the annual mean of the cumulative DoF of the water vapour in the tropics over sea at Nadir and for 85° and a zoom in the mid-troposphere ([10^{-3} – 10^{-2}] hPa).

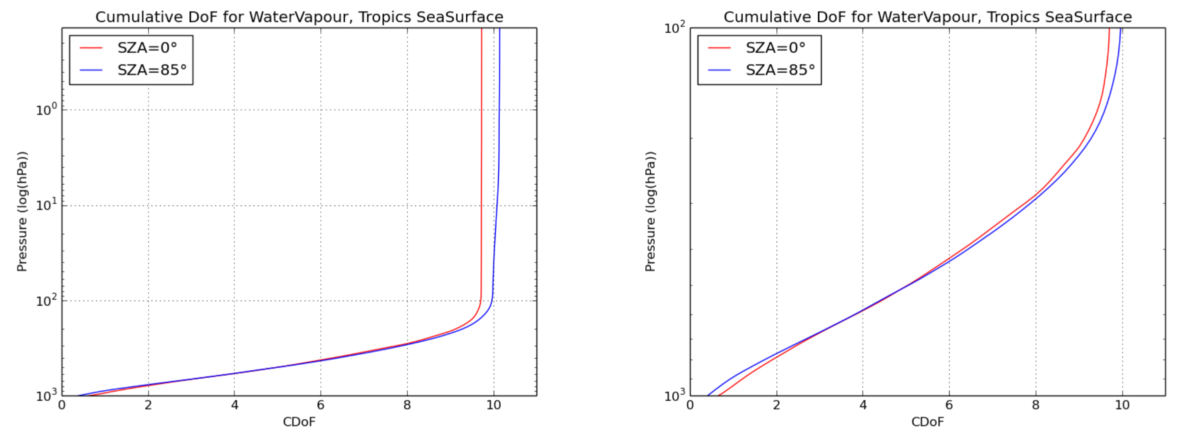

Figure 69: Same as Figure 67 for the water vapour.

4.4.3.3 Ozone

The following figures (Figure 68) illustrate the annual mean of the Averaging Kernels and DOFS of ozone in the tropics over sea at Nadir and for 85° for all levels and for the level where the contrast between the two viewing geometry is the highest in the selected sub-column ([100-1] hPa: see section 4.4.1).

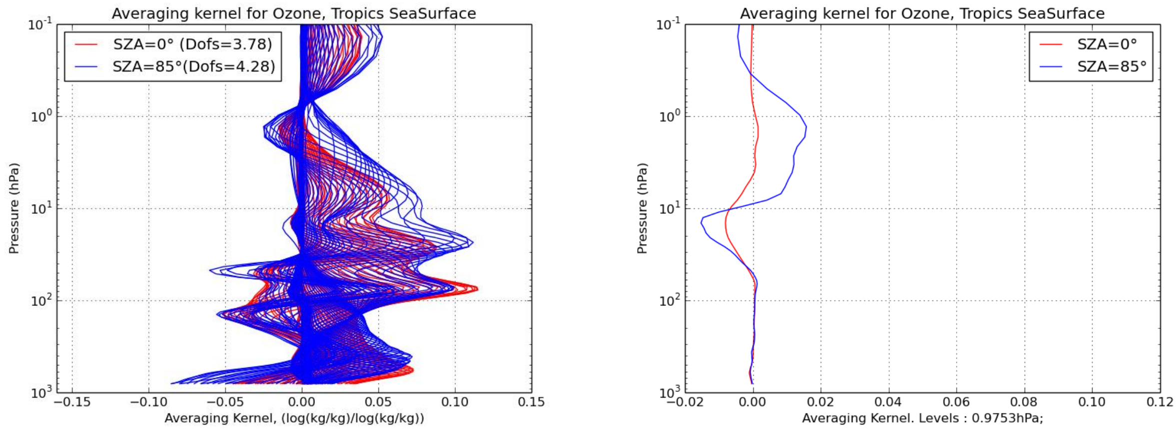

Figure 70: Same as Figure 66 for ozone.

The following figures (Figure 67) show the annual mean of the cumulative DoF of ozone in the tropics over sea at Nadir and for 85°.

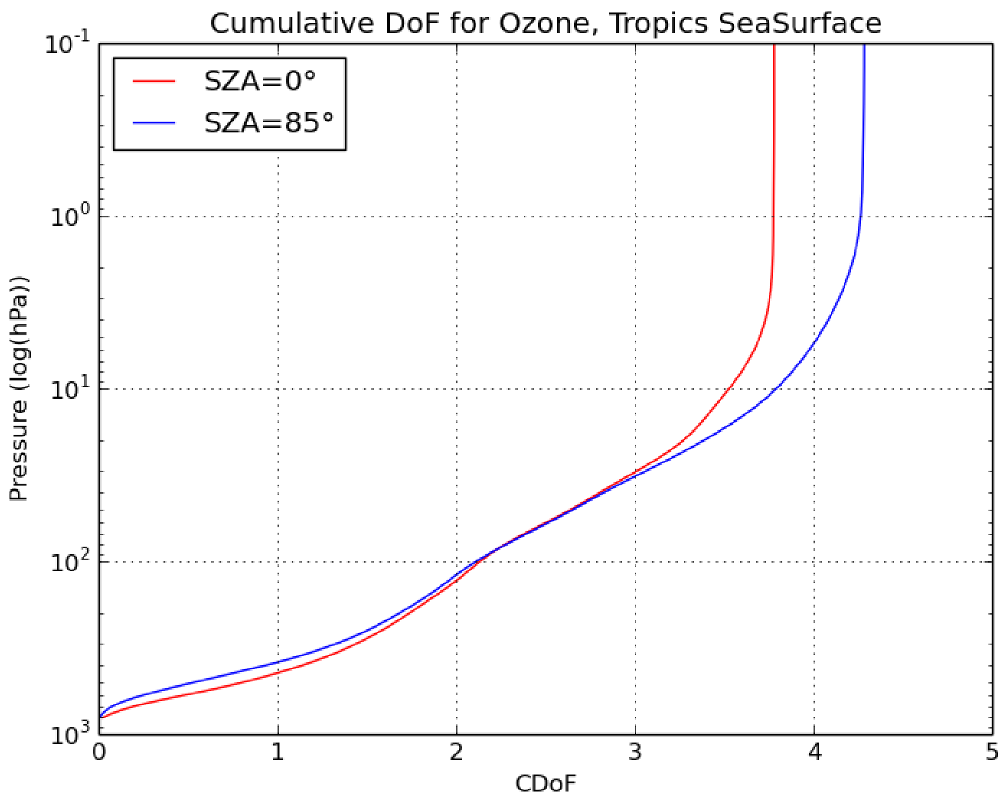

Figure 71: Annual mean of the cumulative DoF of ozone in the tropics over sea at Nadir (in red) and for 85° (in blue).

4.5 SUMMARY OF CONCLUSIONS

4.5.1 In terms of column errors

- The mean retrieval errors of temperature, water vapour and ozone are stable until SatZA reaches about 60°;
- In the tropics, above 60°, the mean retrieval errors of temperature, water vapour and ozone increase strongly, except for temperature in the upper troposphere and ozone over sea. This increase decreases towards the high latitudes;
- The retrieval error budgets of temperature, water vapour and ozone are predominantly dominated by the measurement error, i.e., driven by the observation error matrix;
- **For temperature:**
    - The retrieval error induced by a 0.01 random error on the emissivity seems to be stable for low values of SatZA and decreases above 50° in the tropics and above 70° over the Poles, mainly for upper atmospheric levels,
    - A 1 K random error on the surface temperature:
        - induces a **relatively large error for the situations over the tropics** at nadir (about 0.2 K). This mean error decreases with SatZA before increases until SatZA=80° and then decreasing again to about 0.1 K or below, depending on the sub-column level;
        - At nadir, this mean error decreases poleward,
        - At the higher SatZA values:
            - the error value increases and becomes important poleward,
            - This error is more important over sea than over land, probably because the emissivity decreases with SatZA,
    - Per geographical zone (latitude bands), the mean retrieval errors appear not depending strongly on the month, except for the North Pole over sea where the error is greater in January,
    - The situations that are most affected by the high satellite zenith angle are mainly in the tropics and mid-latitudes. These situations are unstable (important K index values);

- **For water vapour:**
    - Over sea: the mean retrieval error decreases until SatZA reaches about 70° and increases strongly in the tropics. This increase reduces poleward;
    - Over tropical land, the mean retrieval error is relatively stable for SatZA < 70° and increases strongly for SatZA > 70°. In the other geographical zones, this error is stable or decreases weakly over land;
    - The different behaviours between sea and land surface are probably induced by the different behaviour of the emissivity according to the SatZA (see section 6.2);
    - The retrieval error is mainly dominated by the observation error compared to the smoothing error;
    - A 0.01 random error on the emissivity (for each IRS channel) induces a mean retrieval error having the highest value at nadir and decreasing with increasing SatZA;
    - A 1 K random error on the surface temperature:
        - induces an important error for the situations over the tropics at nadir. This mean error decreases until SatZA reaches values between 50° and 60°; this error

increases until SatZA reaches values between 75° and 80° and then decreases again;
    - At nadir, this mean error decreases poleward;
    - At the high SatZA values, the error value decreases poleward,
  - Per geographical zone and season, the mean retrieval errors:
    - appear not depending strongly on the month,
    - appear more important during July (summer) and less important during January (winter) in the northern hemisphere over sea,
    - appear less important during July (winter) and more important during January (summer) and April (autumn) in the southern hemisphere over sea,
    - decrease slowly with increasing SatZA until about 75° and increase for SatZA>75° specially over sea; over land, the errors are quite stable for SatZA<70° and increase weakly for SatZA>70°;
  - The situations which correspond to maximum anomalies are those that have an important value of K index, above 25, and are located mainly in the tropics and mid-latitudes. Conversely, the situations which correspond to minimum anomalies are those that have a small values of K index, below 20, and are generally found in the high latitudes bands;

- <u>**For ozone:**</u>
  - The mean of the retrieval error depends slightly on the geographical zone and the surface type:
    - Over sea,
      - Over the tropics, the mean error appears stable until SatZA=70° and decreases for SatZA>70°,
      - In the southern hemisphere, the error decreases until SatZA reaches 60° and then increases weakly,
      - In the northern hemisphere, the error drops slowly until SatZA = 80°,
    - Over land:
      - Over the tropics and mid-latitudes, the mean error remains quite stable until SatZA = 70° and increases weakly beyond at mid-latitudes,
      - Poleward, the mean error decreases with an increasing SatZA,
  - The retrieval error is largely dominated by the measurement error;
  - A 0.01 random error on the emissivity (for each IRS channel) induces a mean retrieval error which decreases towards 0 kg/kg for SatZA > 20°, whatever the geographical zone and the surface type;
  - A 1 K random error on the surface temperature:
    - induces an important error at nadir for the situations over the tropics and South Mid-latitudes. This mean error decreases with increasing SatZA to 0 kg/kg,
    - At nadir, this mean error decreases poleward;
    - At the high SatZA values:
      - the error value increases and becomes important poleward,
      - North- and Poleward, this error is more important over land than over sea, with the highest values for SatZA around 70°,
  - Per geographical zone, the mean retrieval errors, in terms of season:

    - Do not seem to depend strongly on months over the tropics and Southern mid-latitudes,
    - are more important during January and less important during October in the northern hemisphere,
    - appear less important in January and October for South Pole,
  - The correlation between the anomalies values and the K index values are not very clear. The situations with positive anomalies values exhibit a K index above 30 and are found in the tropics and mid-latitudes, or exhibit a K index below 20 but are located in high latitudes. The situations with negative anomalies values exhibit a K index below 20 and are mainly found in the high latitudes bands but also in the mid-latitudes.

4.5.2 In terms of profile errors

- **For temperature:**
  - In the tropics: the mean retrieval errors at SatZA = 85° are greater than at nadir for the level between surface and about 500 hPa. From about 500 hPa to TOA, it is the opposite, that is the mean retrieval errors at SatZA = 85° are smaller than at nadir,
  - In higher latitudes: the mean retrieval errors at SatZA = 85° are very close to the situations at nadir for the level between surface and about 500 hPa. From 500 hPa to TOA, the mean retrieval errors at SatZA = 85° are smaller than at nadir,
  - The retrieval error profiles is mainly dominated by the *a priori* error, except close to surface in the tropics,
  - At nadir: a 0.01 emissivity incertitude impacts all the retrieval error profiles; a 1 K incertitude has approximately the same impact on the retrieval error profile,
  - At SatZA=85°, only the retrieval errors of the levels close to the surface are affected by a 0.01 emissivity incertitude and a 1 K incertitude. Both errors have approximately the same impact on the retrieval error profile,
  - At 986 hPa level:
    - The situations with the maximum values of anomalies at 986 hPa are mainly in the tropics and in the northern mid-latitudes. The retrieval errors at this level increase by than 100%,
    - The retrieval errors at level 986 hPa are approximately the same at nadir and for SatZA = 85°, or decrease a little, at polar and southern mid-latitudes. These situations correspond to stable situations,
  - At 661 hPa level:
    - The minimum and maximum anomalies are very close and mainly close to 0, i.e. these situations are not very affected by the higher satellite zenith angle,
    - In the tropics, the anomalies with values close to or above 0.2 corresponds to the situations with K index values between 25 and 40, i.e. unstable situations,
    - In the tropics, the minimum anomalies become negative, i.e., for these situations, the retrieval errors at 661 hPa are smaller for a SatZA = 85° than at nadir. These situations corresponds to situations with K index values below 30,
  - At 400 hPa level:
    - Minimum and maximum anomalies of the extracted situations are very different in the tropics and mid-latitudes,
    - The maximum values of anomalies are close to or above 0.5, i.e., the retrieval errors at 400 hPa for these situations can increase by 50% or more,

        - Conversely, the minimum values of anomalies are close or below to -0.5, i.e., the retrieval errors at 400 hPa for these situations can decrease by 50% or more. The associated K index values are mainly situations with K index values between 25 and 40 in the tropics,
        - In higher latitudes, the anomalies are close to 0 and correspond to stable situations (K index below 20).
    - At 151 hPa level:
        - The minimum and the maximum values of the anomalies for the extracted situations are very close to 0,
        - The maximum values of the anomalies are mainly positive while the minimum values are negative and generally found in the mid-latitudes. The associated K indices are mainly below 35 in the tropics, and below 20 in higher latitudes;

- **For water vapour:**
    - In the tropics over sea and over land: the mean retrieval errors at SatZA = 85° are higher than at nadir for the levels between the surface and about 800 hPa. In the mid-troposphere (800-400 hPa), the errors at nadir are slightly higher than at SatZA = 85°. From about 400 hPa to TOA, both retrieval error profiles are very close,
    - In the mid-latitude regions over sea and land: the mean retrieval errors at SatZA = 85° are very close to the situations at nadir for all the levels. However, over sea, between the surface and approximately 800 hPa, the mean retrieval error profile at SatZA = 85° is slightly smaller than at nadir, whereas over land, the mean retrieval error profile is greater at SatZA = 85° for those levels,
    - There is no significant difference between the behaviour of the retrieval errors over land and that over sea. The retrieval errors at nadir and for SatZA=85° are also quite close,
    - The retrieval error profiles depend mainly on the *a priori* error because of the low space of the measurements. The observation error has a more significant impact for the levels very close to the surface, and poleward. The observation error affects also the error budget stronger at upper tropospheric levels (p < 500 hPa) than at lower tropospheric levels,
    - At nadir: a 0.01 emissivity incertitude, impacts all the retrieval error profiles, mainly the levels close to the surface, where the mixing ratio of H_2O is the most pronounced. A 1 K incertitude on the surface temperature has approximately the same impact on the retrieval error profile,
    - At SatZA=85°: the impact of a 0.01 emissivity incertitude induces retrieval errors close to 0 kg/kg and along all the vertical axis in the tropics. A 1 K incertitude on the surface temperature has a small impact on the retrieval error. Poleward, these errors increase but remain low,
    - At 986 hPa level:
        - The most impacted situations (maximum anomalies) are generally in the tropics and northern mid-latitudes. The retrieval errors at this pressure level increase by more than 100%. The situations impacted (maximum anomalies) by the higher satellite zenith angle values are associated to situations with K index value above 25, i.e. unstable situations,
        - Conversely, the situations with the minimum anomalies have anomalies close to 0 and can even be negative over mid-latitudes. This means that the retrieval error at 986 hPa are similar at nadir and for SatZA = 85° or decrease weakly at mid-latitudes. These situations correspond to stable situations since the K index values are mainly smaller than 20,

- At 802 hPa level:
  - The most impacted situations (maximum anomalies) are generally in the tropics and in the northern mid-latitudes. The retrieval error at this pressure level increases by more than 50%. These situations are associated to situations with K indices ≥ 30, i.e. unstable situations,
  - Conversely, the situations with the minimum anomalies are close to 0 and can be negative in the tropics. This means that the retrieval error at 802 hPa are approximately the same at nadir and for SatZA = 85° or decrease for some situations over tropics. These situations correspond to stable situations, K index values mainly being smaller than 30,
- At 661 hPa level:
  - The situations with the maximum values of anomalies do not seem to be located in a particular geographical zone and the maximum anomalies are generally close to 0. The situations impacted by higher satellite zenith angle values are associated to situations with K indices being smaller or close to 20, i.e. stable situations,
  - Over the tropics: the anomalies are negative. This means that the retrieval error at 661-hPa are smaller at SatZA = 85° than at nadir. These situations correspond to K index values between 25 and 35,
  - Outside the tropics, these situations correspond to stable situations since the K index values are mainly inferior to 20,
  - In contrast to the 802-hPa level and the 986-hPa level, the unstable situations with K index values between 25 and 35 are the situations where the retrieval errors decrease between nadir and SatZA = 85°,
- In the Polar Regions, the minimum and the maximum values of the anomalies are very close;

- **For ozone:**
  - Over the tropics:
    - The mean retrieval errors at SatZA = 85° are smaller than the mean retrieval errors at nadir but both error profiles are close,
    - There is no significant difference between the behaviour of the retrieval errors over sea and that over land,
  - At mid-latitudes: the mean retrieval errors at SatZA = 85° are very close to the situations at nadir between about 200 hPa and 10 hPa. From about 10 hPa to 0.5 hPa, mean retrieval errors at SatZA = 85° are smaller than those found at nadir, whatever the surface type and the geographical zone,
  - The retrieval error profiles depends mainly of the observation error,
  - At nadir: a 0.01 emissivity incertitude, impacts all the retrieval error profiles, mainly the levels close to 10 hPa, where ozone is the most abundant; a 1 K incertitude on the surface temperature has a smaller impact on the retrieval error profile than a 0.01 emissivity incertitude except in the tropics where the impact is similar,
  - At SatZA=85: the impact of a 0.01 emissivity incertitude and a 1 K incertitude on the surface temperature induce retrieval errors close to 0 kg/kg along all the vertical pressure levels in the tropics. Poleward, these errors increase significantly but remain relatively low except in the South Pole over land where the impact of the surface temperature seems strong,

- At 11 hPa level:
  - The most impacted situations are found at mid-latitudes (northern and southern) and the retrieval error at this level increases by about 10%. The situations impacted by the higher satellite zenith angles are associated to situations with K index being greater than or close to 30, i.e. unstable situations in the northern mid-latitudes. In the southern mid-latitudes, the situations are more stable,
  - Conversely, the minimum values of anomalies in the majority are close to or less than 0 for any latitudes with some values dropping by up to 20%. This means that the retrieval error at level 11 hPa are less important for SatZA = 85° than at nadir. These situations correspond to stable situations since the K index values are mainly less than 20. We can note that some situations correspond to K index values between 25 and 30,
  - In the Polar Regions, the minimum and the maximum values of the anomalies are very close.

4.5.3 In terms of DOFS

For temperature:

Table 4: Mean DOFS of temperature per geographical area and surface type at SatZA=0° and 85°

Surface type	Sea surface		Land surface	
SatZA	0°	85°	0°	85°
Tropics	8.92	10.87	8.50	10.31
Northern Mid-latitudes	9.79	11.73	9.42	11.28
Southern Mid-latitudes	9.45	11.40	9.37	11.24
North Pole	9.26	10.98	9.23	10.90
South Pole	10.66	12.44	7.09	8.91

For water vapour:

Table 5: Mean DOFS of water vapour per geographical area and surface type at SatZA=0° and 85°

Surface type	Sea surface		Land surface	
SatZA	0°	85°	0°	85°
Tropics	9.73	10.15	9.68	10.37
Northern Mid-latitudes	8.01	8.29	7.88	8.12
Southern Mid-latitudes	7.97	8.31	8.41	8.63
North Pole	5.90	6.32	5.99	6.25
South Pole	6.06	6.61	3.74	4.27

For ozone:

Table 6: Mean DOFS of ozone per geographical area and surface type at SatZA=0° and 85°

Surface type	Sea surface		Land surface	
SatZA	0°	85°	0°	85°
Tropics	3.78	4.28	3.37	4.07
Northern Mid-latitudes	4.30	4.89	3.75	4.57
Southern Mid-latitudes	4.16	4.63	3.95	4.73
North Pole	4.03	4.88	3.83	4.78
South Pole	4.19	4.78	2.39	3.59

4.6 POTENTIAL AND LIMITATIONS OF THE IRS PRODUCTS AT HIGH ZENITH ANGLES

For temperature:

- For the unstable situations, i.e., with important K index values, the impact of high satellite zenith angle on the temperature retrieval can be large in the lower troposphere, mainly in the tropics: the retrieval accuracy is degraded. At higher latitudes, the impact on the temperature retrievals becomes weak;
- At upper pressure levels, i.e. above 400 hPa, the temperature retrievals should be more accurate at high zenith angle whatever the geographical zone, mainly over sea.

For water vapour:

- In the tropics, for the levels close to surface and up to about 800 hPa, the retrieval errors of the water vapour for a satellite zenith angle of 85° can increase by up to a factor 2 in comparison with the retrieval errors at nadir;
- Conversely, at higher latitudes over sea, the accuracy of the water vapour retrievals close to surface and up to about 800 hPa can slightly increase at high zenith angle;
- At higher pressure levels i.e. lower than 800 hPa, the retrieval errors of the water vapour decrease at high zenith angle, except in the tropics where the retrievals errors are quite stable;
- The situations most impacted at high zenith angle are generally located in the tropics and in a lesser extent at mid-latitudes, depending on the season, and correspond to unstable atmospheric scenes.

For ozone:

- Largest errors were found in the Polar Regions but these errors can decrease at high SZA for some situations. The mean retrieval errors for a satellite zenith angle of 85° are mostly smaller than at nadir even if the values are very close, except over land at mid-latitudes and over sea in the southern hemisphere where the mean retrieval errors can increase but very weakly;
- In most stable atmospheric situations (with low values of K index) whatever the geographical zone, the retrieval errors found for a satellite zenith angle of 85° can decrease by up to 20% or more (at about 10 hPa) compared to retrieval errors found at nadir;
- For unstable situations, the retrieval errors can increase weakly (about 5-10 %) at high zenith angle, mainly in the tropics and at mid-latitudes.

5 STUDY OF PRACTICAL IMPLEMENTATION ASPECTS OF OPERATIONAL ALGORITHMS FOR MTG-IRS RETRIEVALS AT VERY HIGH ZENITH ANGLES

5.1 STUDY OF THE ROLE OF SURFACE EMISSIVITY AT HIGH ZENITHAL ANGLES

At high satellite zenith angles (SZA), surface emissivity may be insufficiently known. In this section, the impact of surface emissivity variations at high zenith angles on retrieval errors is studied.

Firstly, we analyse the variation of the emissivity Jacobians with various zenith angle values, considering 10% variation of the surface emissivity (see §2.3.2.2.4). We perform this exercise on the five geographical zones for each surface type. The emissivity is assumed to be Lambertian. Since the IRS channels sensitive to the surface emissivity are also sensitive to the surface temperature, the surface temperature Jacobians are computed as well (see §2.3.2.2.5). For each zone and each surface type, we compute the average of those Jacobians over the whole year. In order to observe them in the best way, the Jacobians are expressed in brightness temperature. The quality flag stored previously (see 2.2.4) as a RTTOV output is also used to select the Jacobians. If the quality flag, given by channel, is equal to 2, the RTTOV simulation failed and the Jacobian is not taken into account in the average.

Figure 72 shows the emissivity Jacobians simulated for a tropical situation for three different satellite zenith angle values: 0°, 65° and 85°. The sensitivity of the IRS channels decreases with respect to SZA. At SZA equal to 85°, the IRS channels are nearly not sensitive to emissivity: at SZA=0°, for a wavenumber equal to 1100 cm^{-1}, a variation of 10% of emissivity conduces to a variation of ~35K in the spectrum expressed in brightness temperature, whereas it involves a variation of only 2K at SZA=85°.

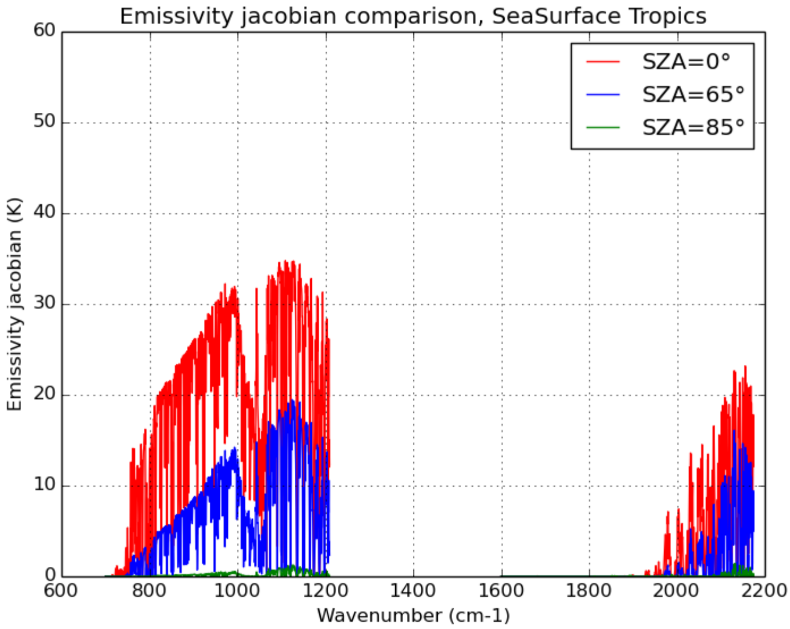

Figure 72: Jacobian w.r.t. the surface emissivity for a tropical situation over sea for three satellite zenith angles: 0° (in red), 65° (in blue) and 85° (in green)

Figure 73 shows the emissivity Jacobians simulated in the Southern mid-latitudes over land. Although the IRS channels are more sensitive to the surface emissivity in Southern mid-latitudes than in the tropics at high satellite zenith angles, the sensitivity remains weak compared to low satellite zenith angles.

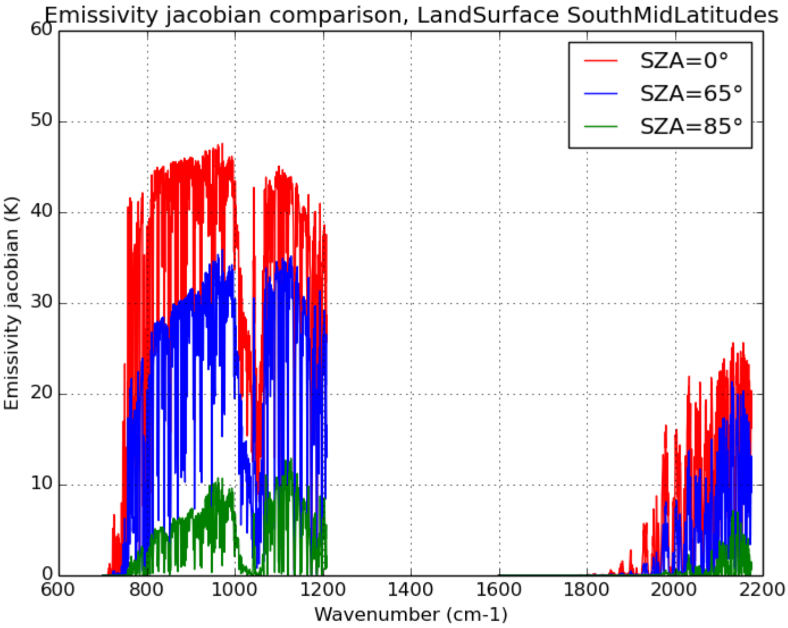

Figure 73: Same as Figure 72 for Southern mid-latitudes over

Figure 74 and Figure 75 show the Jacobian with respect to the surface temperature in the tropics over sea (Figure 74) and in Southern mid-latitudes over land (Figure 75). These figures reveal that the IRS channels are not very sensitive to the surface temperature either at high SZA. For example, for a tropical situation over sea, the variation of the spectrum induced by a variation of 1K of the surface temperature is about 0.75K at SZA=0° for a wavenumber of 1100 cm^{-1}; this variation drops to values smaller than 0.1K in the spectrum at SZA=85°.

All figures corresponding to the whole set of the geographical areas and surface types are available in Annexe D – All figures for jacobians w.r.t. surface emissivity and surface temperature.

IRS channels are less sensitive to the surface emissivity and to the surface temperature at high satellite zenith angle, mainly in the tropics. Note that sensitivities are quite close in the South Pole. At high SZA, the IRS channels contain little information on surface properties and on layers close to surface. As a consequence, the accuracy of temperature, water vapour and ozone retrieval errors could be degraded at such high SZA (> 60-70°) in the tropics, as shown in the previous sections.

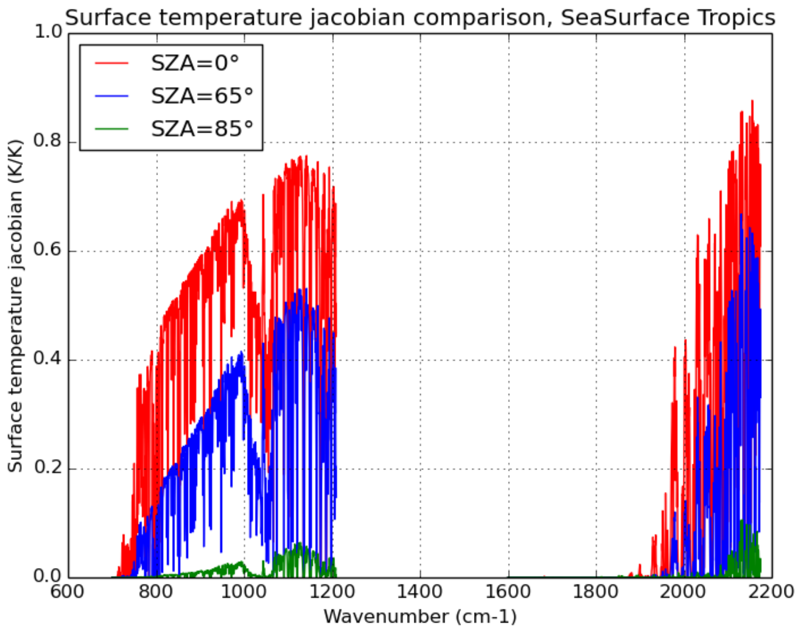

Figure 74: Jacobian w.r.t. the surface temperature for a tropical situation over sea for three satellite zenith angles: 0° (in red), 65° (in blue) and 85° (in green)

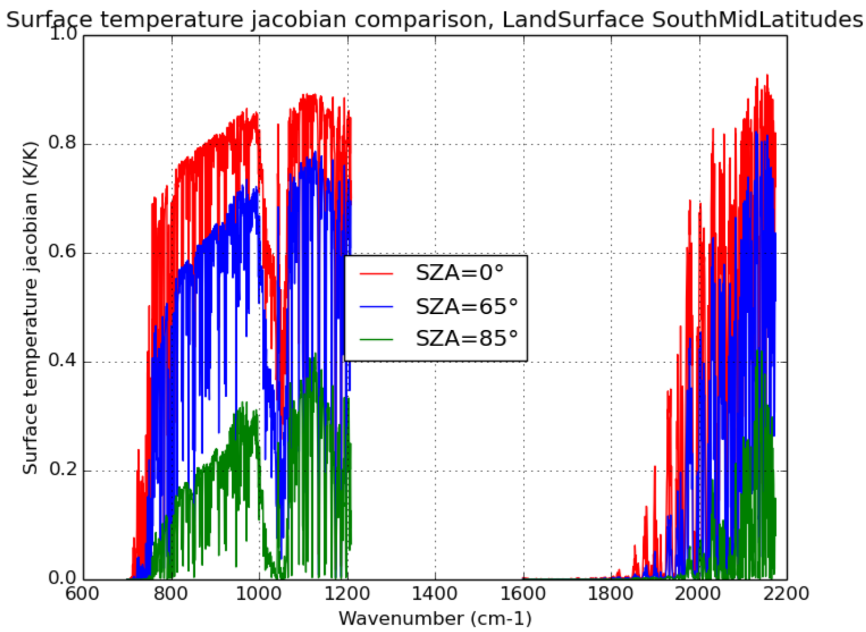

Figure 75: Same as Figure 74 in South Mid-Latitudes over land

5.2 RETRIEVAL TECHNIQUES FOR LIMB SOUNDER APPLICABLE TO MTG-IRS

The results shown in sections 3 and 4 show that, on average, most of the ozone, water vapour and temperature retrieval errors are relatively stable and constant when the satellite zenith angle remains below 60°. Some disparities are observed between tropical regions and mid-latitudes. However, these differences are essentially linked to the meteorological variations of the scenes considered. Indeed, in the tropics, the atmosphere is more unstable with convective phenomena being stronger pronounced than at mid-latitudes. This stronger convection is associated with higher water vapour content and greater temperature gradients, leading to a higher risk of retrieval error. This is typically what was observed in the results. The ozone error is also correlated to geographic areas, whereby largest errors were found in the polar region.

An interesting result stems from the evaluation of retrieval errors of profile estimates. It was noted that the bottom of the retrieved profile (between the surface up to 500 hPa) is systematically of lower quality when the satellite zenith angle is very high (SatZA = 85°) compared to that obtained with nadir. On the other hand, the top of the temperature profile (pressure < 500 hPa) systematically is of better quality at a very high satellite zenith angle than at nadir.

In summary, results show that at high zenith angle satellite, the bottom of the profile (close to the surface) is of poor quality, while the upper part is of similar quality as at nadir, probably of even higher quality.

This indicates that at high satellite zenith angle, the IRS channels are not sensitive to surface properties. This would explain the larger errors found at the bottom of the profile and the fact that the top of the profile is of same quality as at nadir, even sometimes of higher quality. Indeed, if the retrieval were little constrained by the surface, more freedom at the top of the profile would be left, potentially leading to a product more in agreement with channels strongly sensitive at high altitudes.

The study performed in the previous section (5.1) on surface emissivity sensitivities shows that at very high zenith angles, IRS channels have almost no sensitivity to variations of surface emissivity. In other words, IRS observations become indifferent to the properties of the surface.

At very high zenith angles, the observation configurations are similar to limb sounder measurements. Under these conditions, the retrieval method used is no longer suitable. The RTTOV radiative transfer model needs to consider the entire profile (from the ground to the top of the atmosphere). However, as demonstrated earlier, at very high zenith angles the IRS channels are no longer sensitive to surface properties. Consequently, a different restitution method should be considered. Several methods of restitution to the limb sounding can be found in the literature:

Launched in 2003, the SciSAt satellite carries the ACE-FTS instrument (Atmospheric Chemistry Experiment – Fourier Transform Spectrometer). In order to retrieve atmospheric pressure, temperature and profiles of some species, a method based on a modified global fit approach in which the parameters are determined with the Levenberg–Marquardt nonlinear least-squares method is employed (Boone *et al*. 2005). However, the method is not suitable for a fine restitution in the lower atmosphere (troposphere and lower stratosphere).

Other methods based on the Optimal Estimation Method with Tikhonov Regularisation can be applied to limb measurement. Such methods are employed by the Earth Observing System Microwave Limb Sounder (OSM-MLS) on board the Aura satellite launched in 2004 (Livesey and Wu, 2004), and also by the Michelson Interferometer for Passive Atmospheric Sounding (MIPAS) (Raspollini *et al*. 2013). As the Levenberg–Marquardt method, the Tikhonov Regularisation allows non-linear behaviours to be taken into account during the retrieval process.

The first drawback of these iterative methods is the required digital resources, in particular computation times. For each iteration it is necessary to use a direct model (forward model) to project the state vector into the observation space, this most often involves a radiative transfer model. However, for hyperspectral infrared instruments, this results in the simulation of several thousand channels, which can take a very long time to calculate. Then, most of the retrieval methods use subsets of the recorded spectra (micro-windows) to reduce the computing time.

Other studies show the possibility of obtaining retrieved products without going through an iterative method. Millán and Dudhia (2013) offer a fast linear restitution method using the entire spectral signature of the instrument. Based on a linear least-squares fit constrained by a Twomey–Tikhonov regularisation, the scheme inverts atmospheric temperature, pressure and species. To avoid running the radiative transfer model during the linear inversion scheme, the simulated spectra are linearly adjusted using the pressure-temperature scene conditions and their dependence on the Jacobians. An evaluation of this method applied to the MIPAS observations, reports retrieved products with an error of 20% compared to an iterative method for atmospheric pressure and temperature.

Statistical methods are also a possible solution. For instance, the first estimate of IRS products are performed by means of a non-linear statistical retrieval. Based on a Piece-Wise Linear Regression (PWLR), the approximation of the overall non-linear relationship between observations and state vector parameters is done in different classes. Since all statistical methods require an offline training phase, the PWLR approach is trained by a dataset linking real IASI observations to co-located ECMWF reanalysis profiles. These first retrieved products provide a first estimate of fairly good quality and can even be used as a first guess for the OEM. However, this technique is mainly limited by the IASI observations used as training data set. As the satellite zenith angle of IASI is less than 60°, not all satellite zenith angles of IRS are covered. One can imagine reusing this method and adapt it to high satellite zenith angles and close to limb sounding. To this end, a source of limb sounding observations for the learning process such as the MIPAS data are required. Consequently, PWLR could be used for all configurations. While the restitutions with a SatZA below 60° is trained with IASI data, the restitution with higher SatZA (up to 85°) could be trained with MIPAS data.

We mentioned above the limitation to use RTTOV as a radiative transfer model in this configuration close to the limb measurement. As the IRS channels are almost or no longer sensitive to surface properties, the use of RTTOV as radiative transfer model may be not appropriate. Several other radiative transfer models exist that are better suited to this configuration, for instance the Reference Forward Model (RFM) model (Dudhia 2017). This line-by-line model comes from an ESA project to provide reference spectral calculations for the Envisat/MIPAS instrument. This model is said to be 'easy' to use and free to access (http://eodg.atm.ox.ac.uk/RFM/). Since its first development in mid-1990s, it has undergone numerous updates and improvements. It is able to take into account different field of view geometries (from nadir to Limb) and different spectral fields. It also provides the Jacobians of p, T and of the different mixing ratios of the gases considered, which makes it an interesting candidate as a direct model in an iterative retrieval method. One has to note however, that this model does not take into account scattering, which limits its use in clear sky only.

References:

- Boone Chris D., Ray Nassar, Kaley A. Walker, Yves Rochon, Sean D. McLeod, Curtis P. Rinsland, and Peter F. Bernath, "Retrievals for the atmospheric chemistry experiment Fourier-transform spectrometer," Appl. Opt. 44, 7218-7231 (2005).

- Livesey N.J., D.L. Wu. EOS MLS Retrieval Processes Algorithm Theoretical Basis. ATBD-MLS-03. EOS MLS DRL 601 (part 3). JPL D-16159 / CL #04-2043. 2004.

- Raspollini, P., Carli, B., Carlotti, M., Ceccherini, S., Dehn, A., Dinelli, B. M., Dudhia, A., Flaud, J.-M., López-Puertas, M., Niro, F., Remedios, J. J., Ridolfi, M., Sembhi, H., Sgheri, L., and von Clarmann, T.: Ten years of MIPAS measurements with ESA Level 2 processor V6 – Part 1: Retrieval algorithm and diagnostics of the products, Atmos. Meas. Tech., 6, 2419–2439, https://doi.org/10.5194/amt-6-2419-2013, 2013.

- Millán, L. and Dudhia, A.: A non-iterative linear retrieval for infrared high-resolution limb sounders, Atmos. Meas. Tech., 6, 1381–1396, https://doi.org/10.5194/amt-6-1381-2013, 2013.

- Dudhia A. The Reference Forward Model (RFM), J Quant. Spec. R. T., 186, 243-253, https://doi.org/10.1016/j.jqsrt.2016.06.018. 2017.

1 ANNEXE A - COEFFICIENTS DEFINING THE 137 MODEL LEVELS

Table 7: a(n) and b(n) coefficients defining the 137 ECMWF model levels

Level number	a [Pa]	B
0	0.000000	0.000000
1	2.000365	0.000000
2	3.102241	0.000000
3	4.666084	0.000000
4	6.827977	0.000000
5	9.746966	0.000000
6	13.605424	0.000000
7	18.608931	0.000000
8	24.985718	0.000000
9	32.985710	0.000000
10	42.879242	0.000000
11	54.955463	0.000000
12	69.520576	0.000000
13	86.895882	0.000000
14	107.415741	0.000000
15	131.425507	0.000000
16	159.279404	0.000000
17	191.338562	0.000000
18	227.968948	0.000000
19	269.539581	0.000000
20	316.420746	0.000000
21	368.982361	0.000000

Level number	a [Pa]	B
22	427.592499	0.000000
23	492.616028	0.000000
24	564.413452	0.000000
25	643.339905	0.000000
26	729.744141	0.000000
27	823.967834	0.000000
28	926.344910	0.000000
29	1037.201172	0.000000
30	1156.853638	0.000000
31	1285.610352	0.000000
32	1423.770142	0.000000
33	1571.622925	0.000000
34	1729.448975	0.000000
35	1897.519287	0.000000
36	2076.095947	0.000000
37	2265.431641	0.000000
38	2465.770508	0.000000
39	2677.348145	0.000000
40	2900.391357	0.000000
41	3135.119385	0.000000
42	3381.743652	0.000000
43	3640.468262	0.000000
44	3911.490479	0.000000
45	4194.930664	0.000000
46	4490.817383	0.000000
47	4799.149414	0.000000

Level number	a [Pa]	B
48	5119.895020	0.000000
49	5452.990723	0.000000
50	5798.344727	0.000000
51	6156.074219	0.000000
52	6526.946777	0.000000
53	6911.870605	0.000000
54	7311.869141	0.000000
55	7727.412109	0.000007
56	8159.354004	0.000024
57	8608.525391	0.000059
58	9076.400391	0.000112
59	9562.682617	0.000199
60	10065.978516	0.000340
61	10584.631836	0.000562
62	11116.662109	0.000890
63	11660.067383	0.001353
64	12211.547852	0.001992
65	12766.873047	0.002857
66	13324.668945	0.003971
67	13881.331055	0.005378
68	14432.139648	0.007133
69	14975.615234	0.009261
70	15508.256836	0.011806
71	16026.115234	0.014816
72	16527.322266	0.018318
73	17008.789063	0.022355

Level number	a [Pa]	B
74	17467.613281	0.026964
75	17901.621094	0.032176
76	18308.433594	0.038026
77	18685.718750	0.044548
78	19031.289063	0.051773
79	19343.511719	0.059728
80	19620.042969	0.068448
81	19859.390625	0.077958
82	20059.931641	0.088286
83	20219.664063	0.099462
84	20337.863281	0.111505
85	20412.308594	0.124448
86	20442.078125	0.138313
87	20425.718750	0.153125
88	20361.816406	0.168910
89	20249.511719	0.185689
90	20087.085938	0.203491
91	19874.025391	0.222333
92	19608.572266	0.242244
93	19290.226563	0.263242
94	18917.460938	0.285354
95	18489.707031	0.308598
96	18006.925781	0.332939
97	17471.839844	0.358254
98	16888.687500	0.384363
99	16262.046875	0.411125

Level number	a [Pa]	B
100	15596.695313	0.438391
101	14898.453125	0.466003
102	14173.324219	0.493800
103	13427.769531	0.521619
104	12668.257813	0.549301
105	11901.339844	0.576692
106	11133.304688	0.603648
107	10370.175781	0.630036
108	9617.515625	0.655736
109	8880.453125	0.680643
110	8163.375000	0.704669
111	7470.343750	0.727739
112	6804.421875	0.749797
113	6168.531250	0.770798
114	5564.382813	0.790717
115	4993.796875	0.809536
116	4457.375000	0.827256
117	3955.960938	0.843881
118	3489.234375	0.859432
119	3057.265625	0.873929
120	2659.140625	0.887408
121	2294.242188	0.899900
122	1961.500000	0.911448
123	1659.476563	0.922096
124	1387.546875	0.931881
125	1143.250000	0.940860

Level number	a [Pa]	B
126	926.507813	0.949064
127	734.992188	0.956550
128	568.062500	0.963352
129	424.414063	0.969513
130	302.476563	0.975078
131	202.484375	0.980072
132	122.101563	0.984542
133	62.781250	0.988500
134	22.835938	0.991984
135	3.757813	0.995003
136	0.000000	0.997630
137	0.000000	1.000000

2 ANNEXE B – ALL FIGURES OF RETRIEVAL ERRORS SUB-COLUMNS AND PROFILES

2.1 ANALYSIS IN TERMS OF SUB-COLUMN RETRIEVAL ERRORS

2.1.1 Column analysis: Tropics

2.1.1.1 Temperature

2.1.1.1.1 Over sea

2.1.1.1.1.1 Sub-column 103-300 hPa

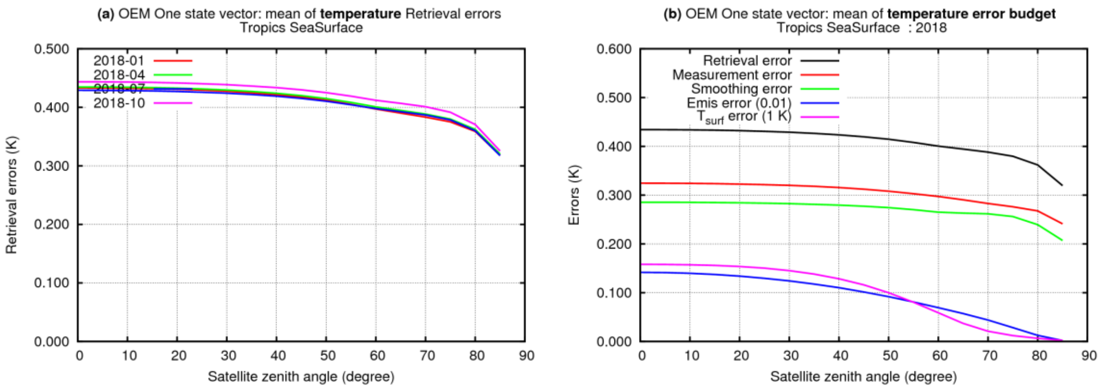

Figure 76: (a) Means of the temperature column error over the tropics/sea according to the value of the satellite zenith angle; (b) the temperature column error (black), the measurement error (red), the smoothing error (green), the errors induced by a 0.01 random error on the emissivity (blue) and induced by a 1 K random surface temperature error (purple) according to the satellite zenith angle

2.1.1.1.1.2 Sub-column 300-706 hPa

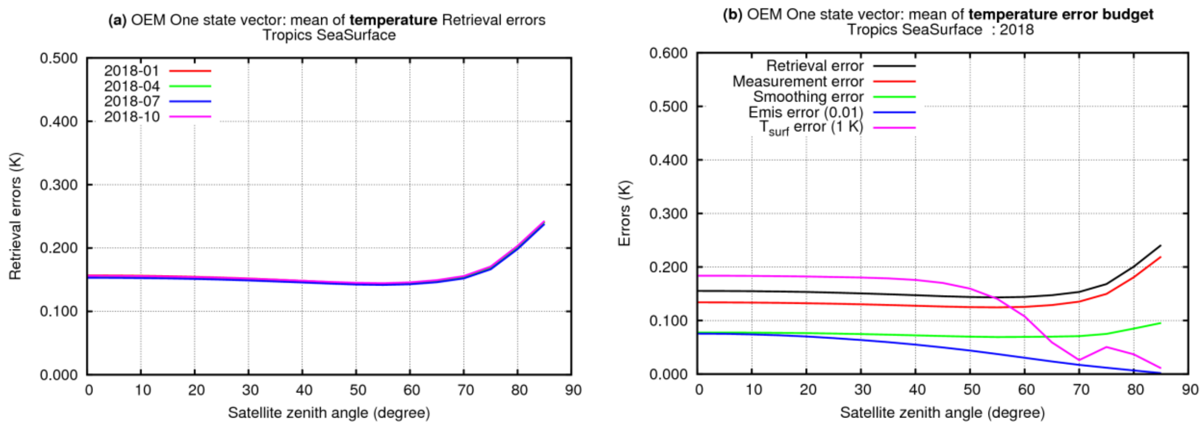

Figure 77 : (a) the means of the temperature column error over the tropics/sea according to the value of the satellite zenith angle; (b) the temperature column error (black), the measurement error (red), the smoothing error (green), the errors induced by a 0.01 random error on the emissivity (blue) and induced by a 1 K random surface temperature error (purple) according to the satellite zenith angle

2.1.1.1.1.3 Sub-column 706-1013 hPa

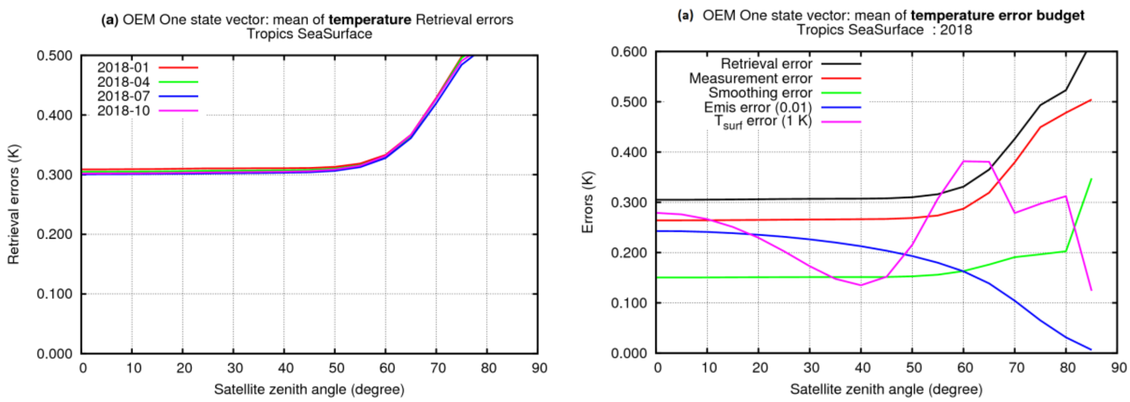

Figure 78 : (a) the means of the temperature column error over the tropics/sea according to the value of the satellite zenith angle; (b) the temperature column error (black), the measurement error (red), the smoothing error (green), the errors induced by a 0.01 random error on the emissivity (blue) and induced by a 1 K random surface temperature error (purple) according to the satellite zenith angle

2.1.1.1.2 Over land

2.1.1.1.2.1 Sub-column 103-300 hPa

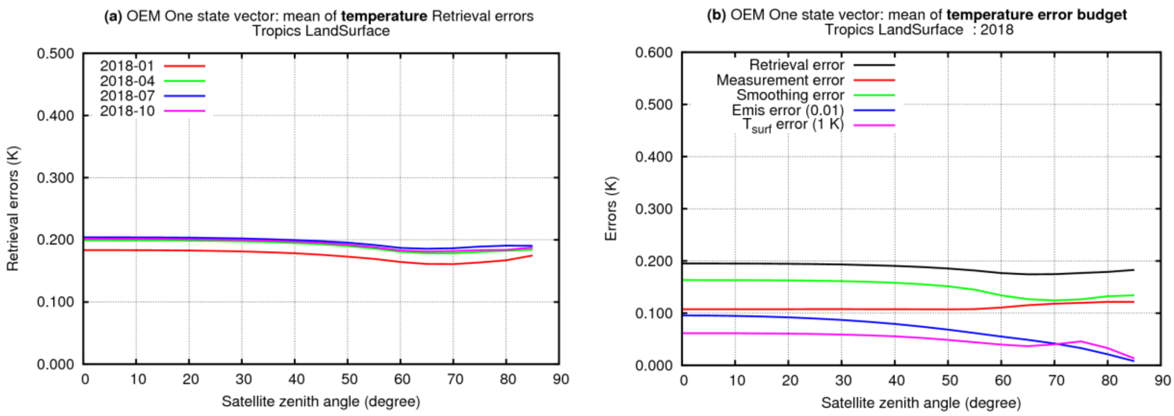

Figure 79: as Figure 76 over tropics/land.

2.1.1.1.2.2 Sub-column 300-706 hPa

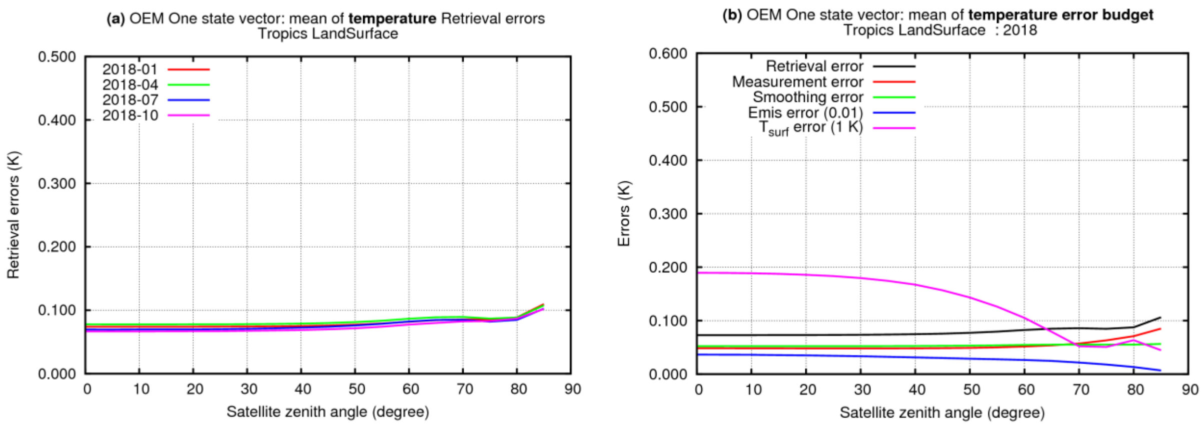

Figure 80: as Figure 77 over tropics/land.

2.1.1.1.2.3 *Sub-column 706-1013 hPa*

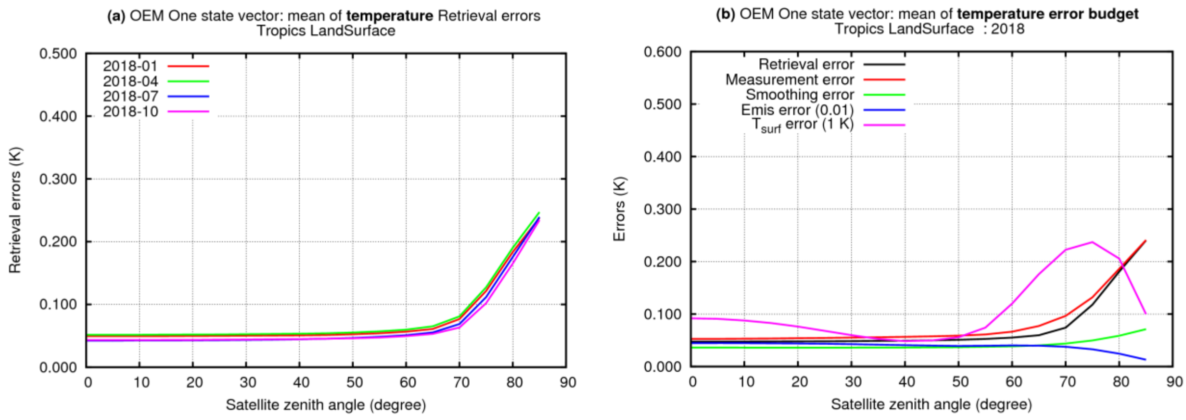

Figure 81 : as Figure 78 over tropics/land

2.1.1.2 Water vapour

2.1.1.2.1 Over sea

2.1.1.2.1.1 *Sub-column 496-802 hPa*

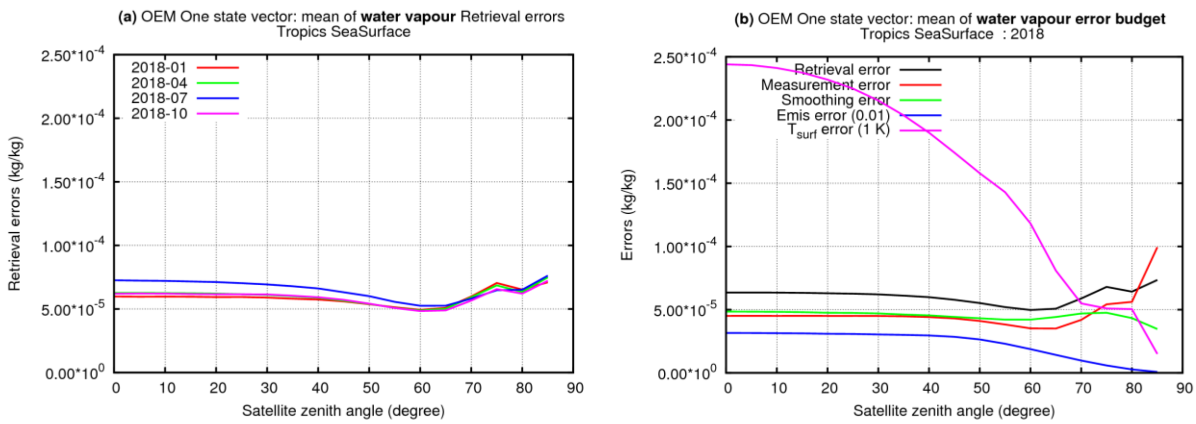

Figure 82: as Figure 76 for water vapour

2.1.1.2.1.2 Sub-column 802-1013 hPa

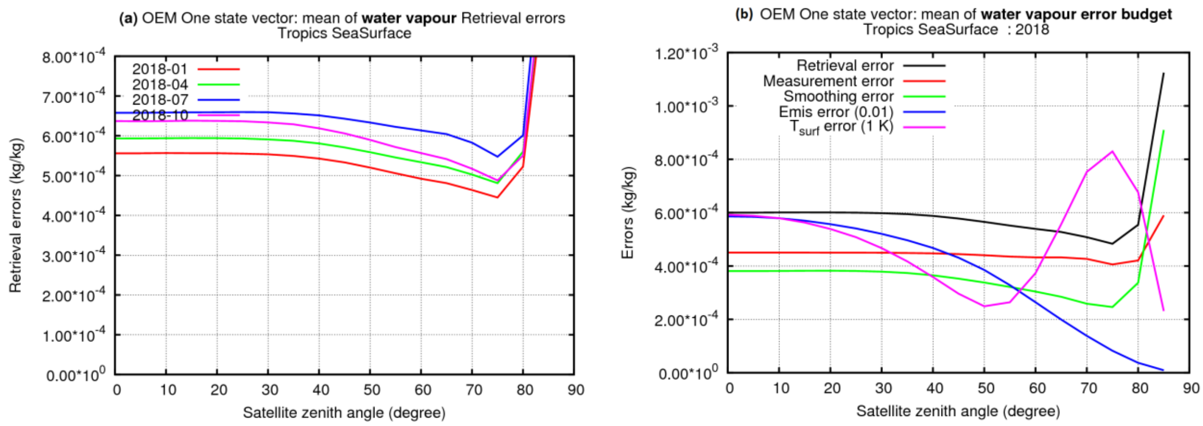

Figure 83 : as Figure 82 for sub-column 802-1013

2.1.1.2.2 Over land

2.1.1.2.2.1 Sub-column 496-802 hPa

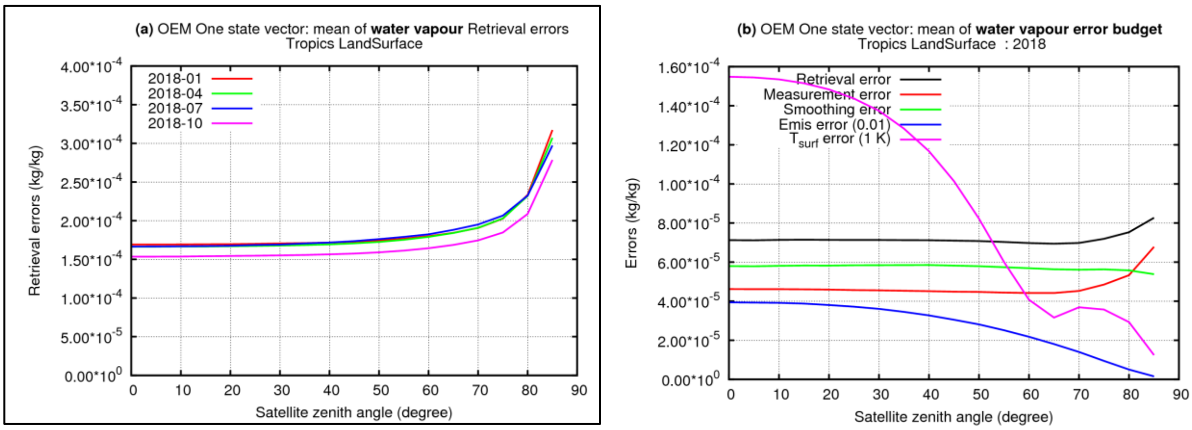

Figure 84: as Figure 82 over tropics/land

2.1.1.2.2.2 Sub-column 802-1013 hPa

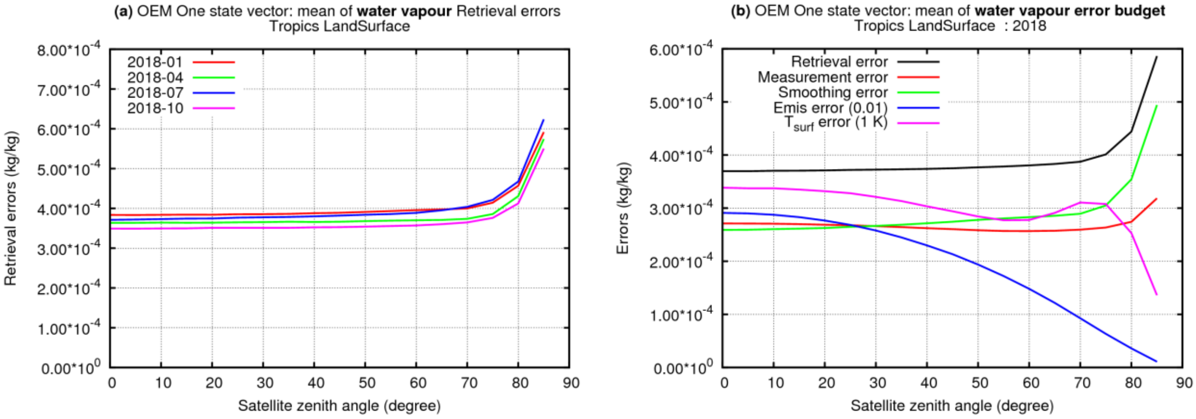

Figure 85 : as Figure 84 for sub-column 802-1013 hPa

2.1.1.3 Ozone

2.1.1.3.1 Over sea

2.1.1.3.1.1 Sub-column 0-103

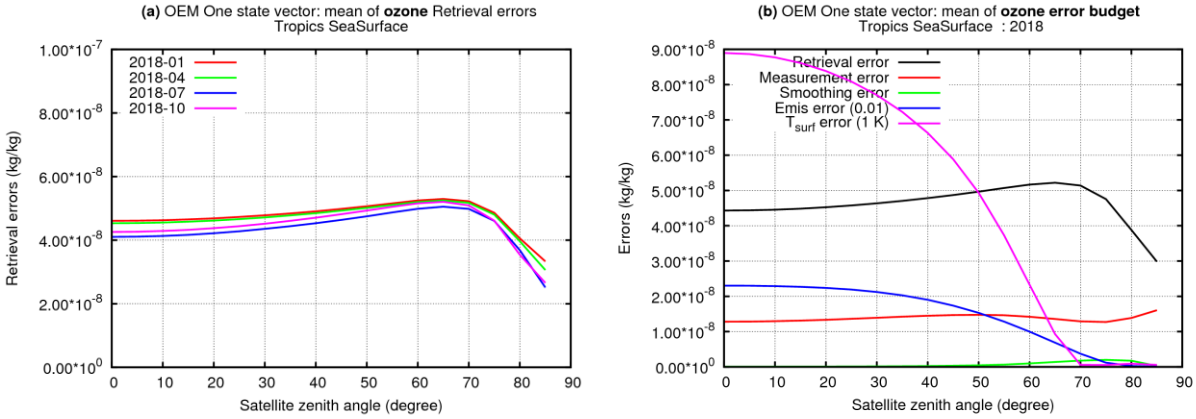

Figure 86: as Figure 76 for ozone

2.1.1.3.2 Over land

2.1.1.3.2.1 Sub-column 0-103

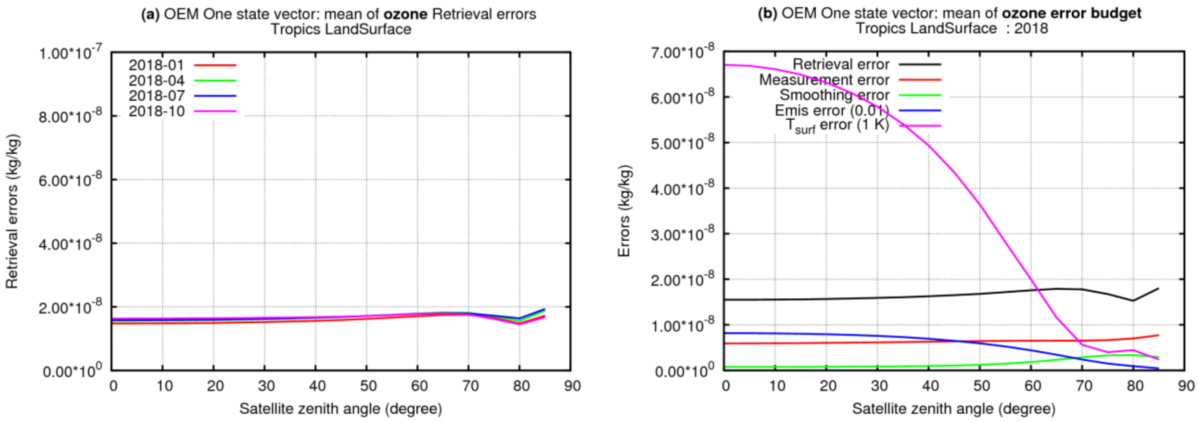

Figure 87: as Figure 86, over tropics/land

2.1.2 Column analysis: Northern Mid-latitudes

2.1.2.1 Temperature

2.1.2.1.1 Over sea

2.1.2.1.1.1 Sub-column 103-300 hPa

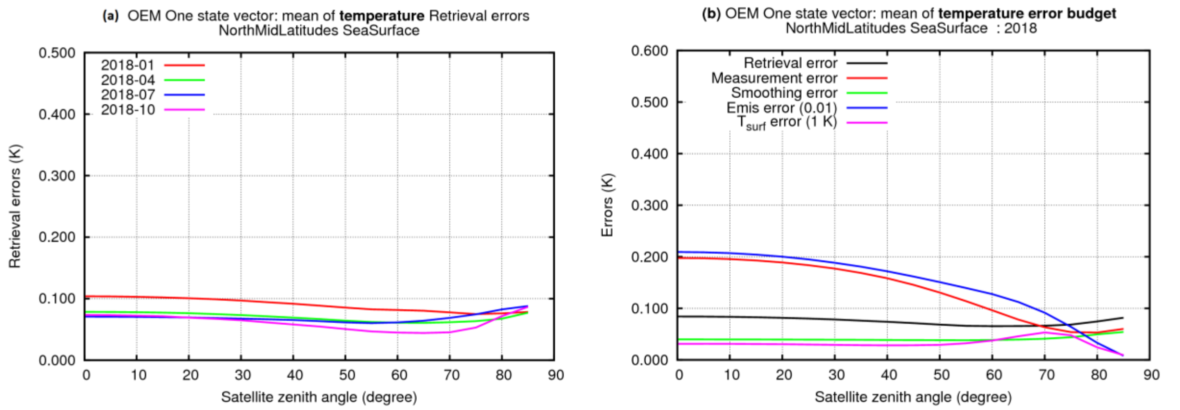

Figure 88: (a) the means of the temperature column error over the Norhern latitudes/sea according to the value of the satellite zenith angle; (b) the temperature column error (black), the measurement error (red), the smoothing error (green), the errors induced by a 0.01 random error on the emissivity (blue) and induced by a 1 K random error (purple) according to the satellite zenith angle

2.1.2.1.1.2 Sub-column 300-706 hPa

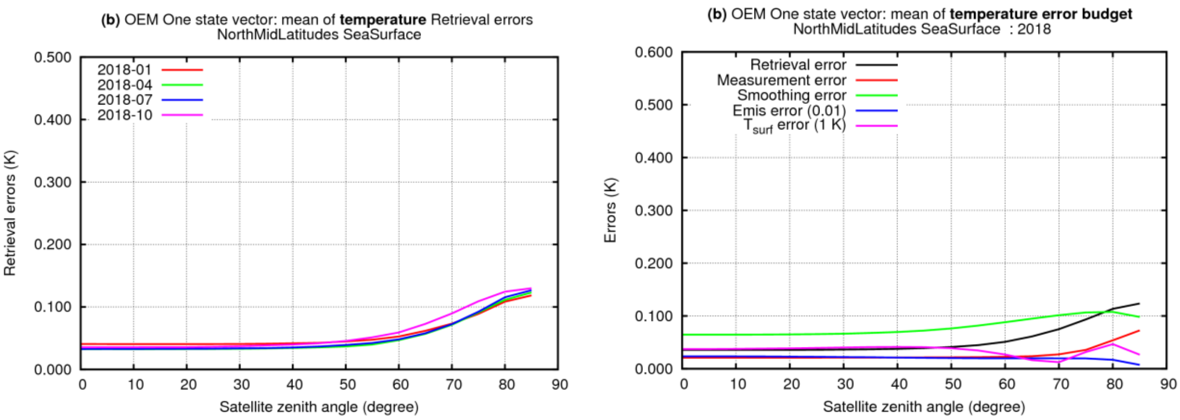

Figure 89 : same as Figure 88 for sub-column 300-706 hPa

2.1.2.1.1.3 Sub-column 706-1013

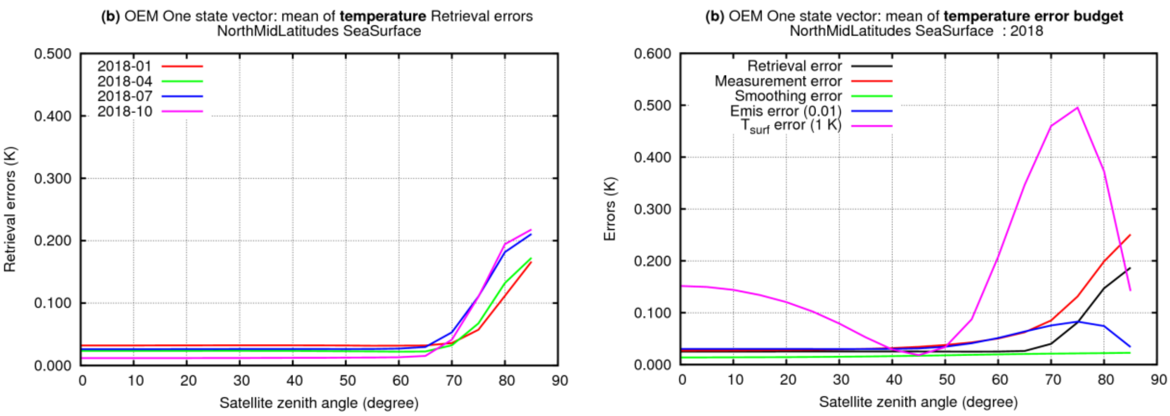

Figure 90 : same as Figure 89 for sub-column 706-1013

2.1.2.1.2 Over land

2.1.2.1.2.1 Sub-column 103-300 hPa

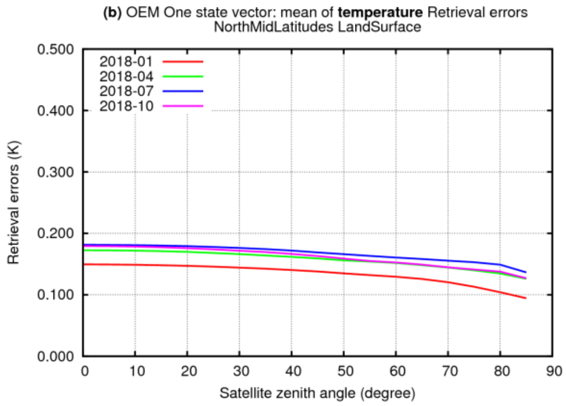

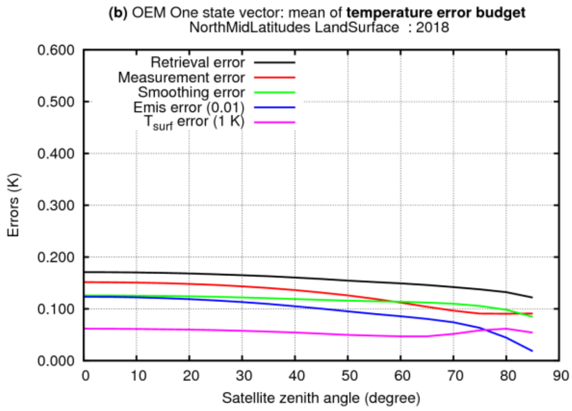

Figure 91: as Figure 88 over Northern mid-latitudes/land

2.1.2.1.2.2 Sub-column 300-706 hPa

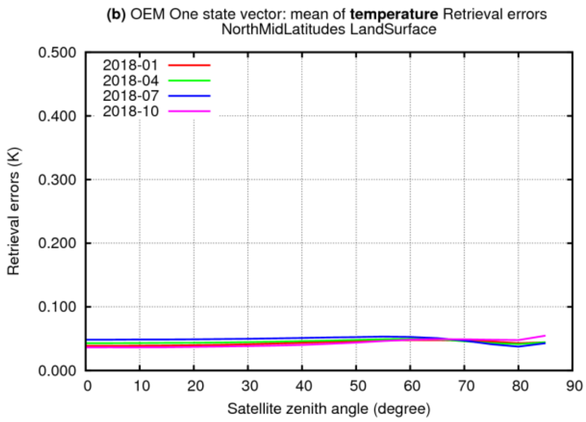

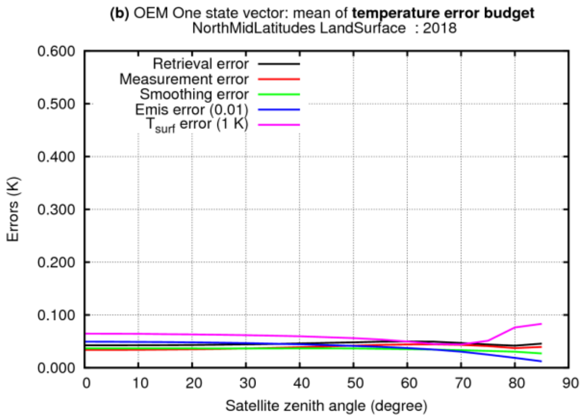

Figure 92 : same as Figure 91 for sub-column 300-706

2.1.2.1.2.3 Sub-column 706-1013 hPa

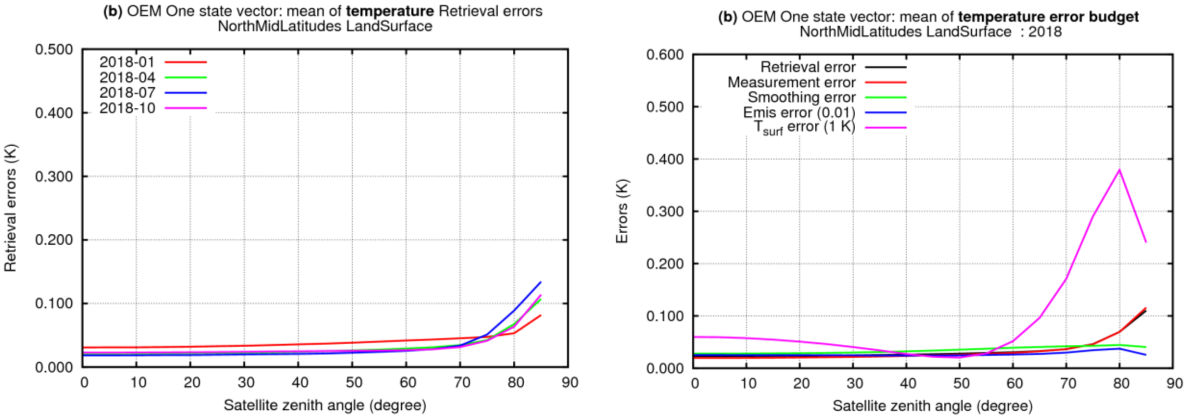

Figure 93 : same as Figure 92 for sub-column 706-1013 hPa

2.1.2.2 Water vapour

2.1.2.2.1 Over sea

2.1.2.2.1.1 Sub-column 496-802 hPa

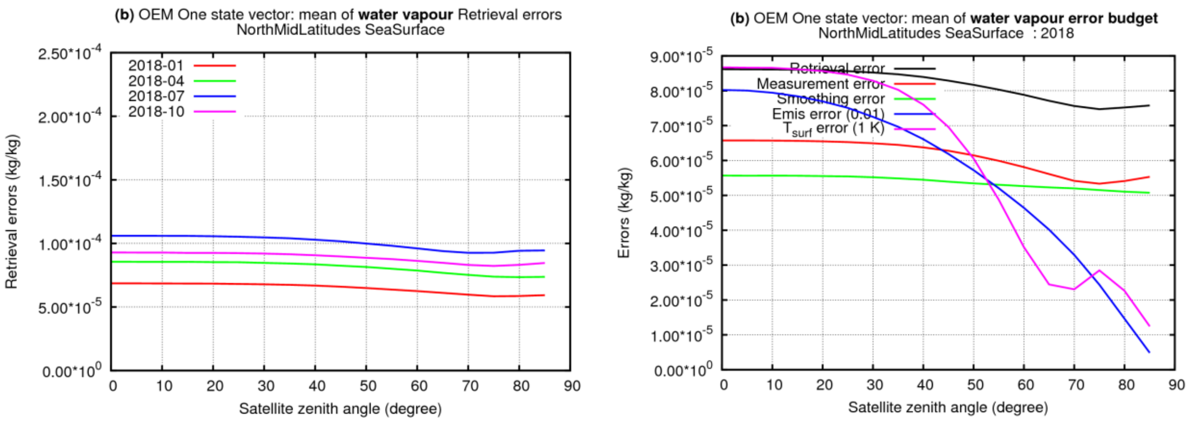

Figure 94: as Figure 88 for water vapour

2.1.2.2.1.2 Sub-column 802-1013 hPa

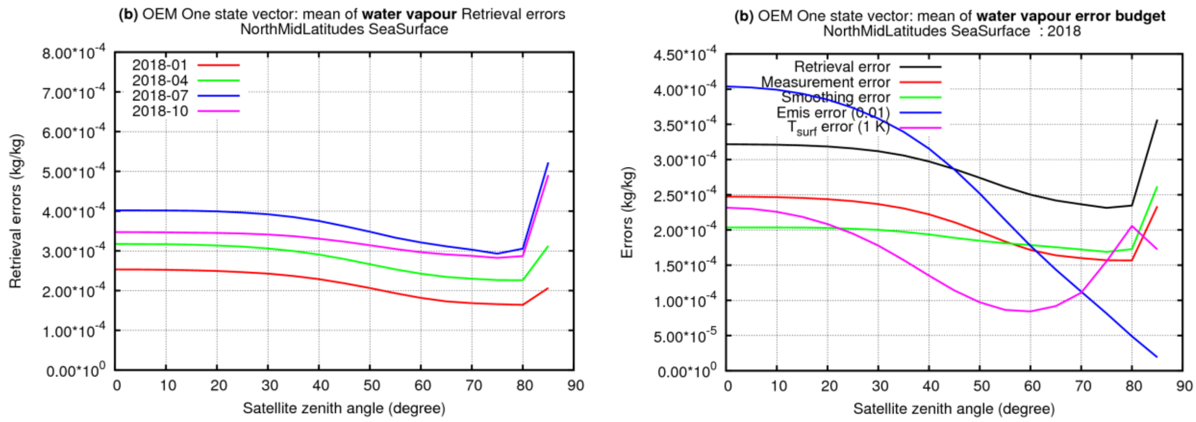

Figure 95 : same as Figure 94 for sub-column 802-1013 hPa

2.1.2.2.2 Over land

2.1.2.2.2.1 Sub-column 496-802 hPa

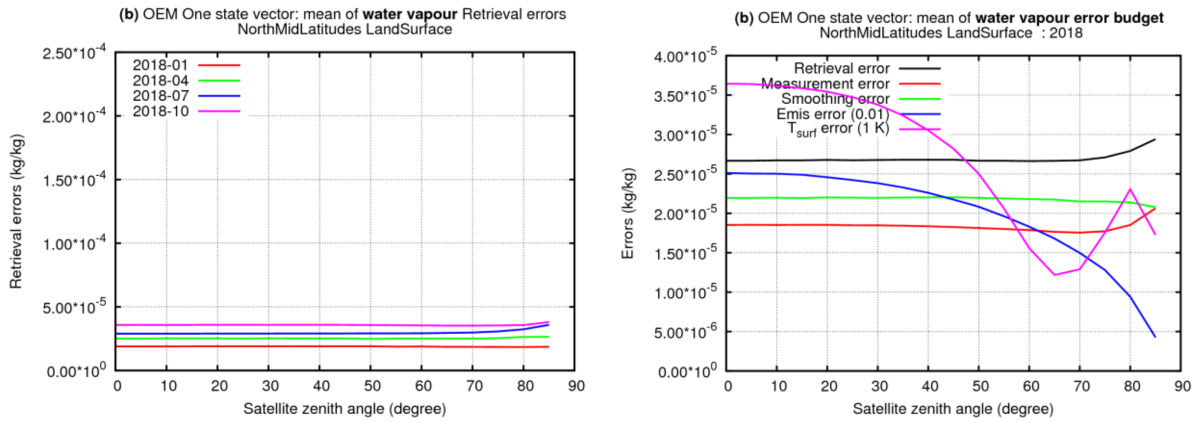

Figure 96: as Figure 94 over northern latitudes/land

2.1.2.2.2.2 Sub-column 802-1013 hPa

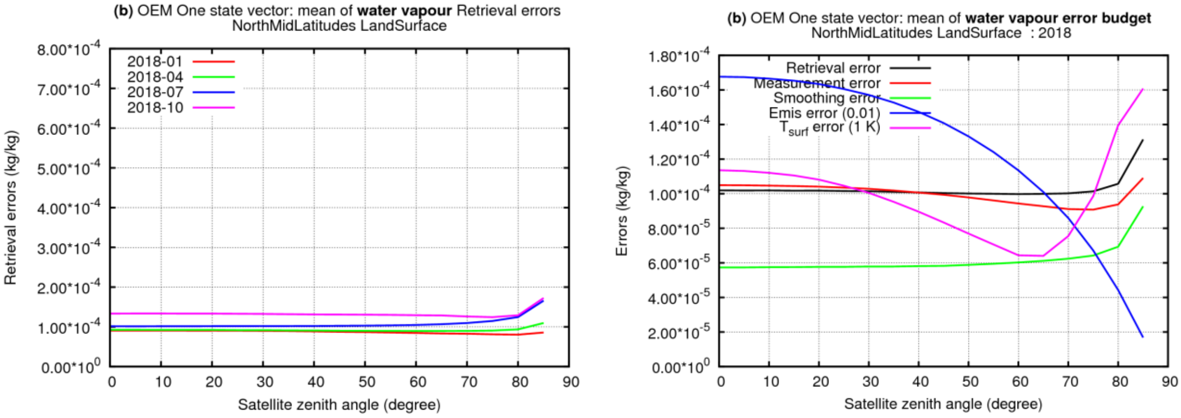

Figure 97 : same as Figure 96 fo sub-column 802-1013 hPa

2.1.2.3 Ozone

2.1.2.3.1 Over sea

2.1.2.3.1.1 Sub-column 0-103 hPa

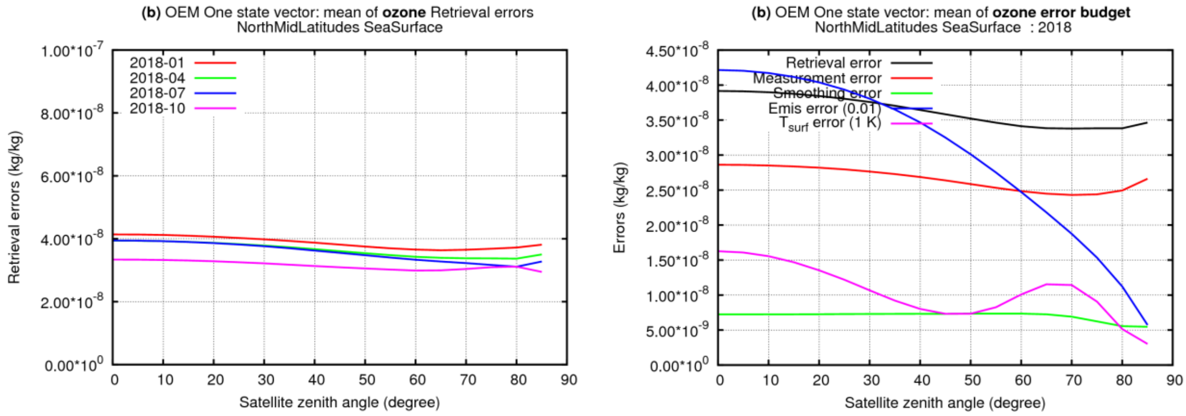

Figure 98: as Figure 94 for ozone

2.1.2.3.2 Over land

2.1.2.3.2.1 Sub-column 0-103 hPa

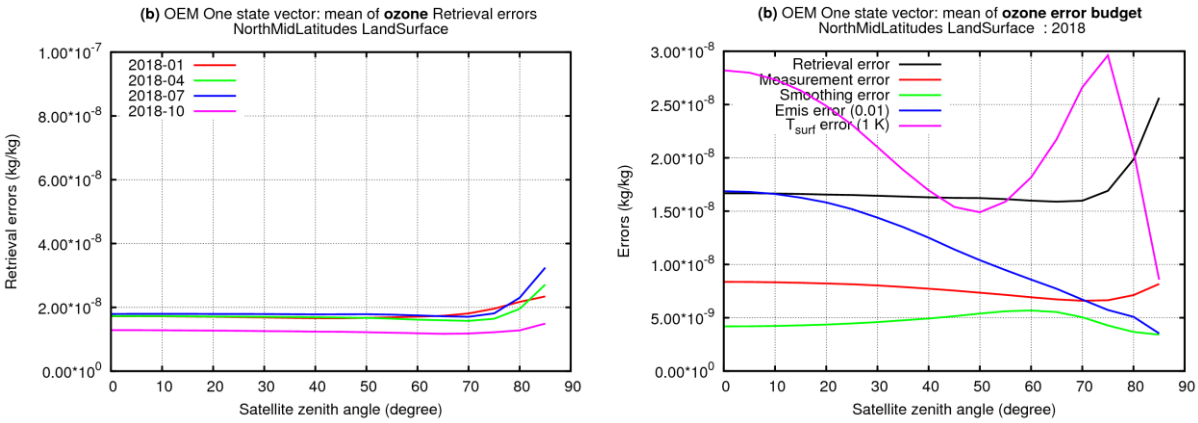

Figure 99: as Figure 98 over land

2.1.3 Column analysis: Southern Mid-latitudes

2.1.3.1 Temperature

2.1.3.1.1 Over sea

2.1.3.1.1.1 Sub-column 103-300 hPa

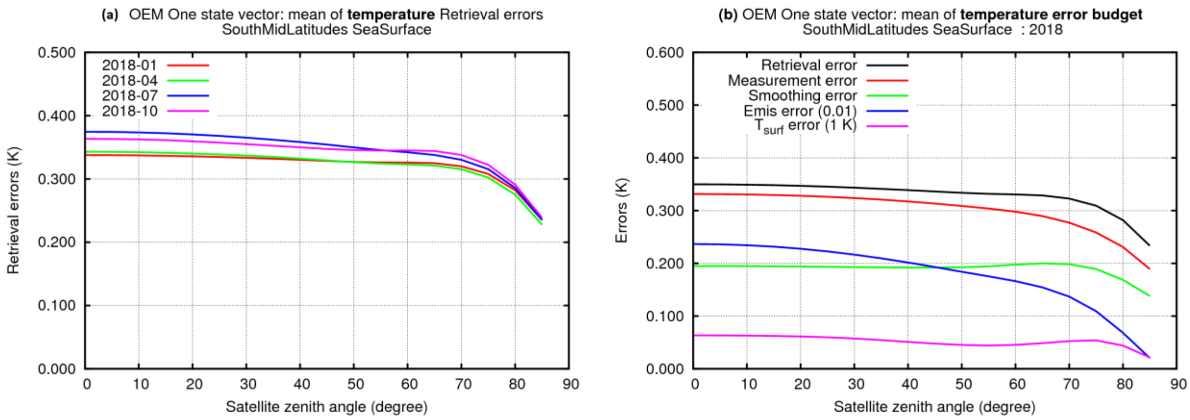

Figure 100: (a) the means of the temperature column error over the Southern latitudes/sea according to the value of the satellite zenith angle; (b) the temperature column error (black), the measurement error (red), the smoothing error (green), the errors induced by a 0.01 random error on the emissivity (blue) and induced by a 1 K random error (purple) according to the satellite zenith angle

2.1.3.1.1.2 Sub-column 300-706 hPa

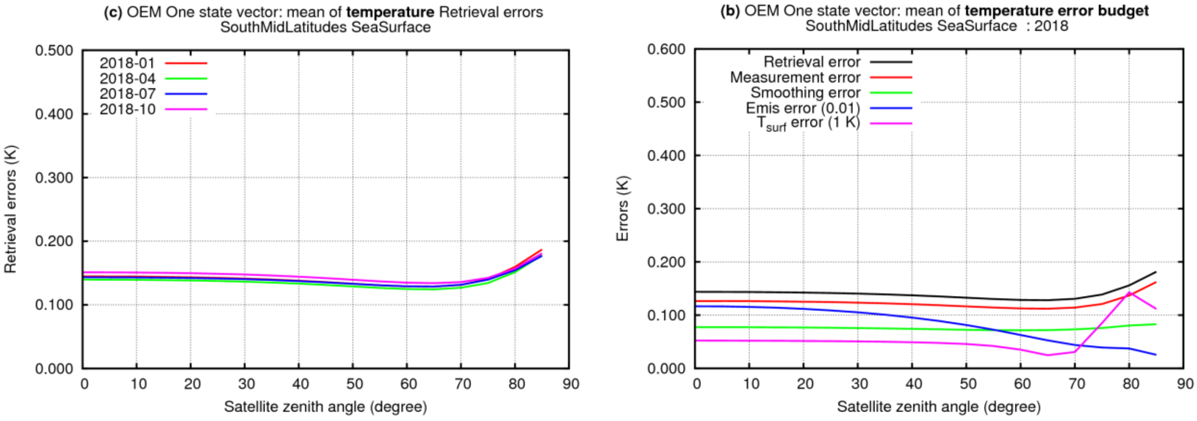

Figure 101 : same as Figure 100 for sub-column 300-706 hPa

2.1.3.1.1.3 Sub-column 706-1013 hPa

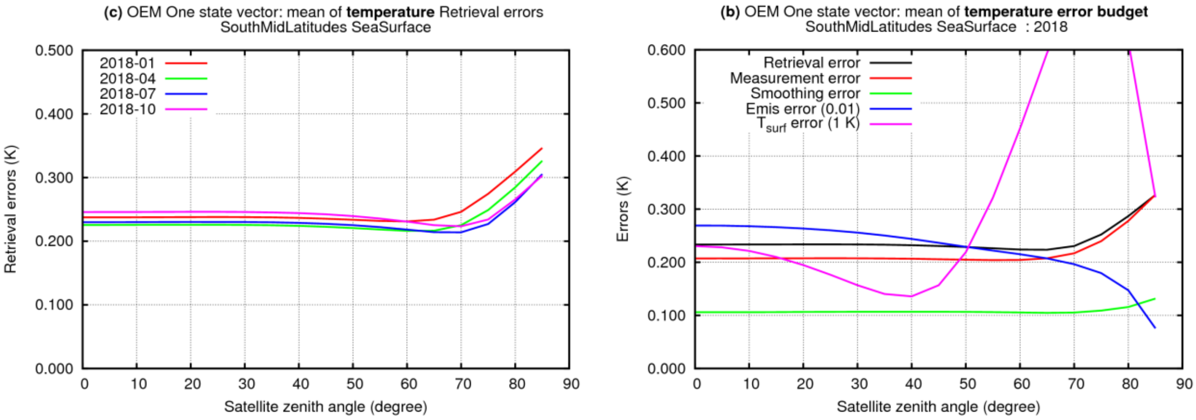

Figure 102 : same as Figure 101 for sub-column 706-1013 hPa

2.1.3.1.2 Over land

2.1.3.1.2.1 Sub-column 103-300 hPa

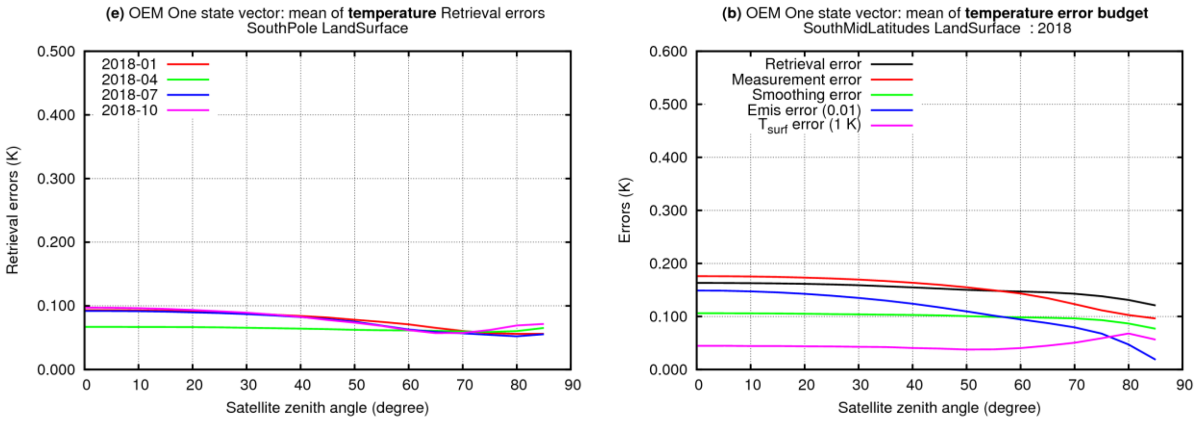

Figure 103: as Figure 100 over land

2.1.3.1.2.2 Sub-column 300-706 hPa

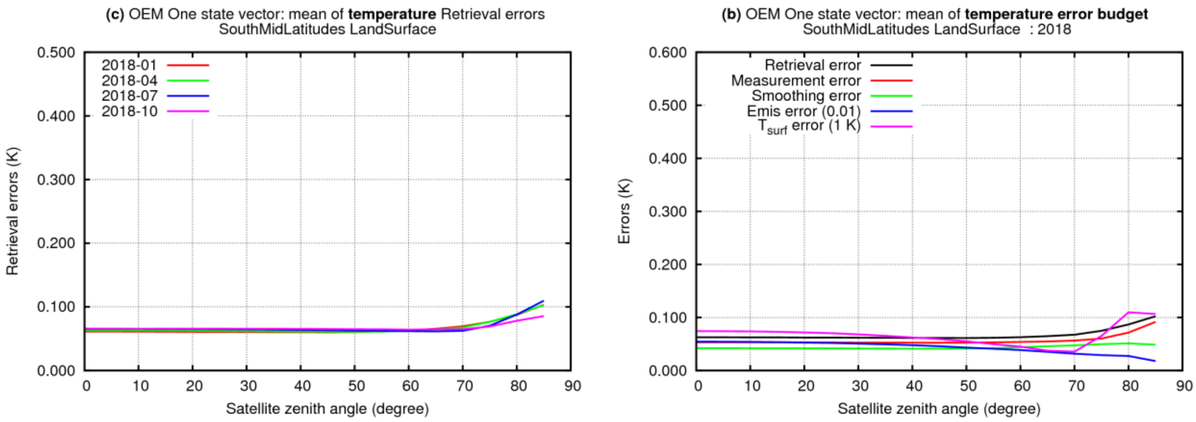

Figure 104 : same as Figure 103 for sub-column 300-706 hPa

2.1.3.1.2.3 Sub-column 706-1013 hPa

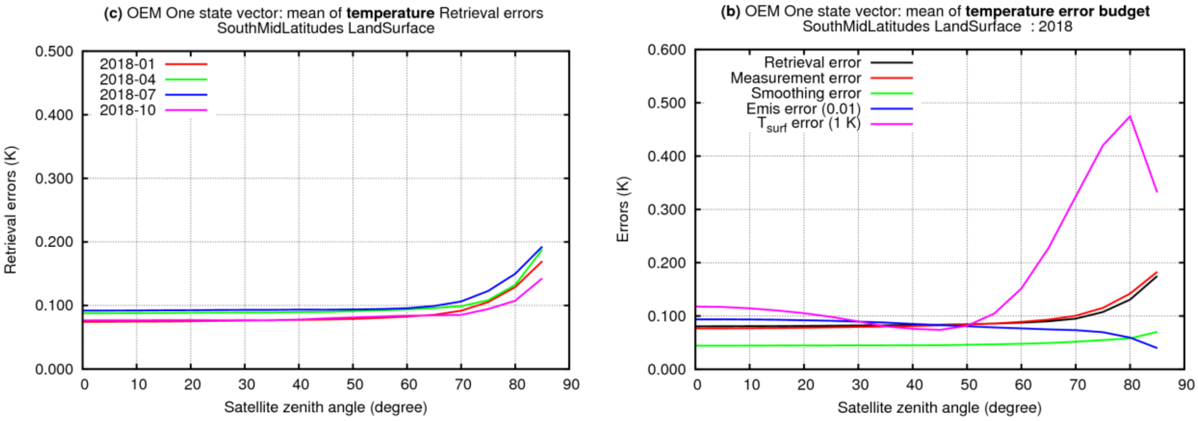

Figure 105 : same as Figure 104 for sub-column 706-1013 hPa

2.1.3.2 Water vapour

2.1.3.2.1 Over sea

2.1.3.2.1.1 Sub-column 496-802 hPa

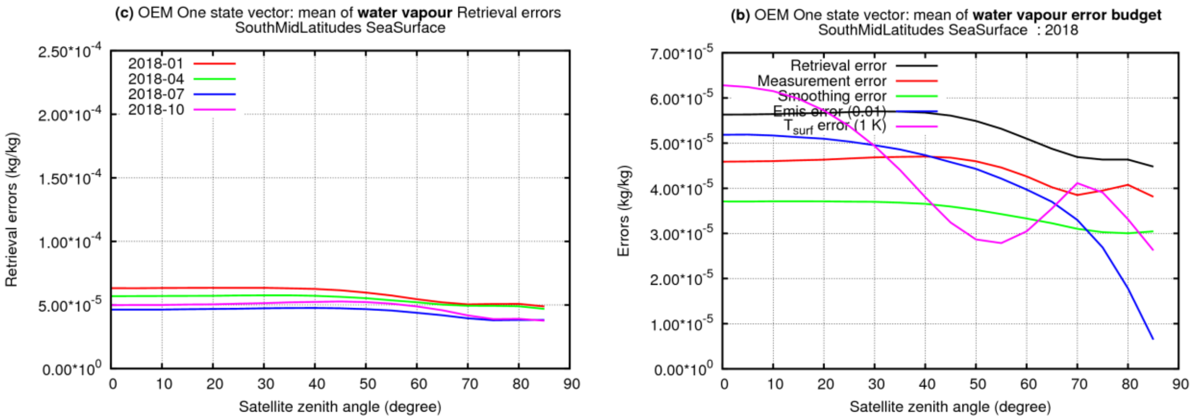

Figure 106: as Figure 100 for water vapour

2.1.3.2.1.2 Sub-column 802-1013 hPa

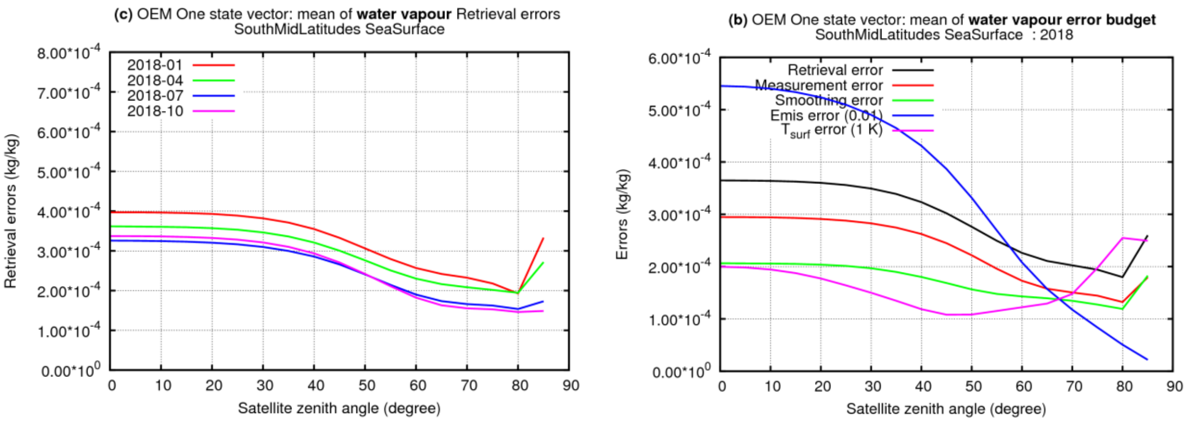

Figure 107 : same as Figure 106 for sub-column 802-1013 hPa

2.1.3.2.2 Over land

2.1.3.2.2.1 Sub-column 496-802 hPa

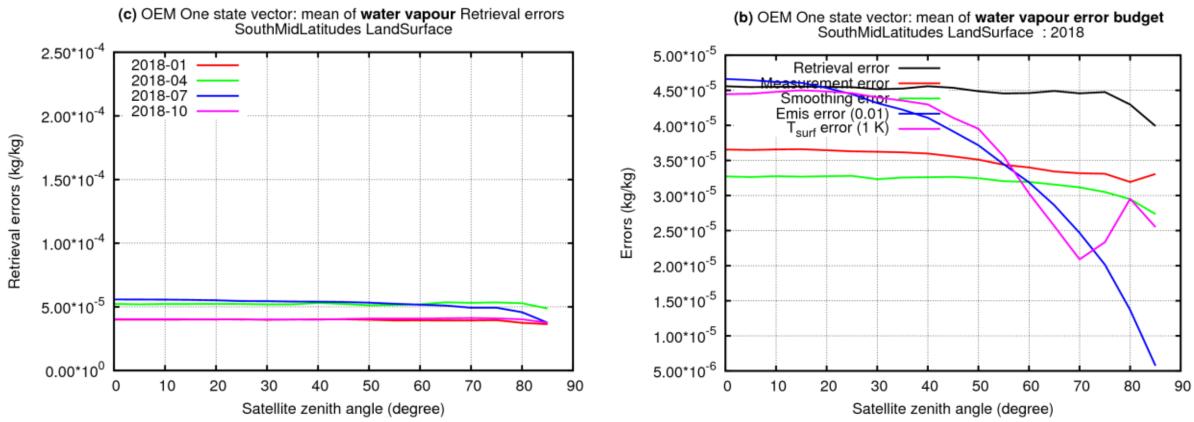

Figure 108: as Figure 106 over land

2.1.3.2.2.2 Sub-column 802-1013 hPa

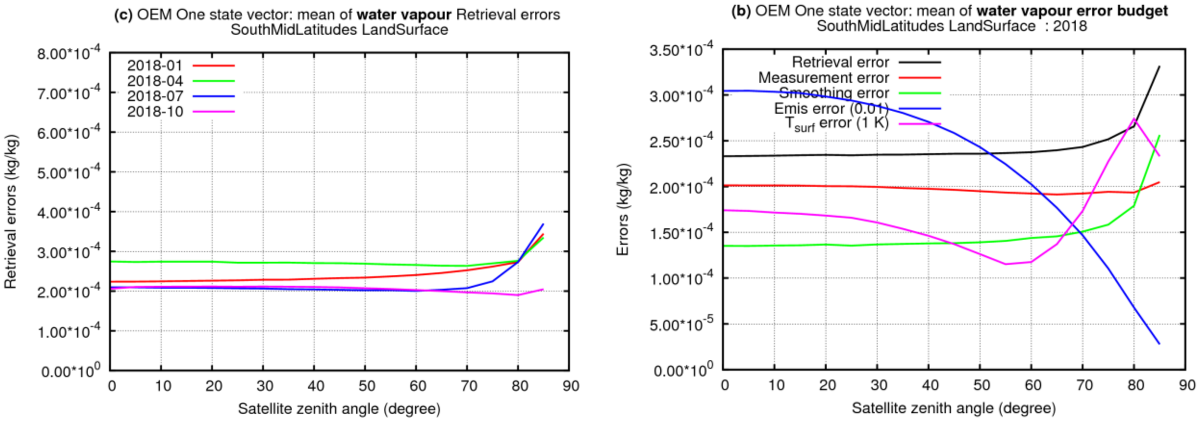

Figure 109 : same as Figure 108 for sub-column 802-1013 hPa

2.1.3.3 Ozone

2.1.3.3.1 Over sea

2.1.3.3.1.1 Sub-column 0-103 hPa

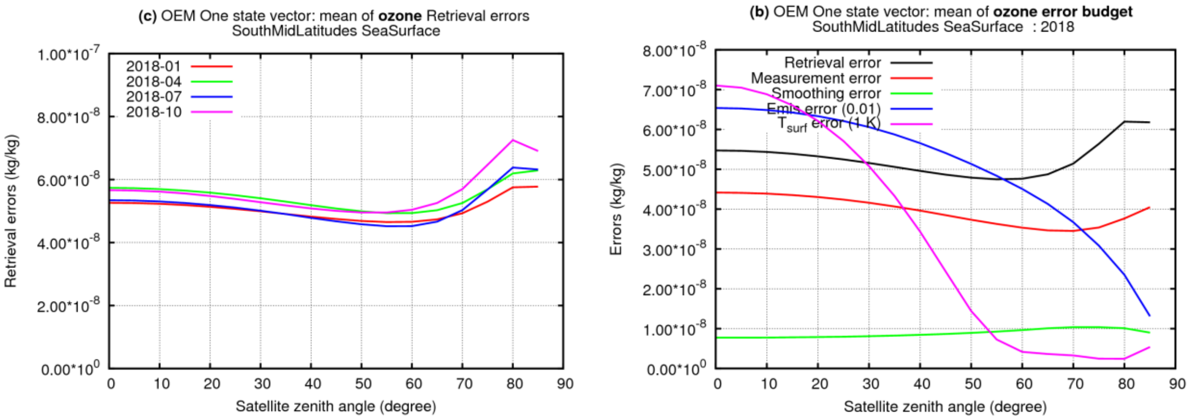

Figure 110: as Figure 100 for ozone

2.1.3.3.2 Over land

2.1.3.3.2.1 Sub-column 0-103 hPa

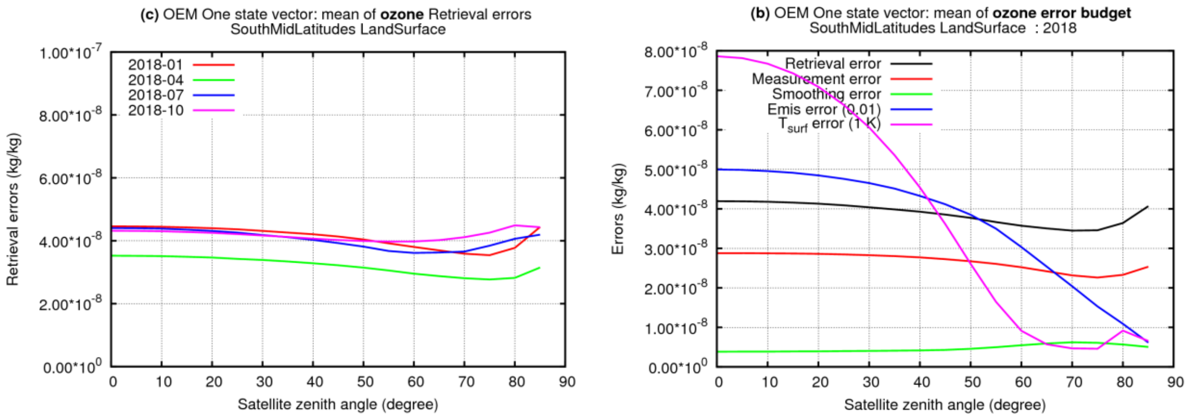

Figure 111: as Figure 110 over land

2.1.4 Column analysis: North Pole

2.1.4.1 Temperature

2.1.4.1.1 Over sea

2.1.4.1.1.1 Sub-column 103-300 hPa

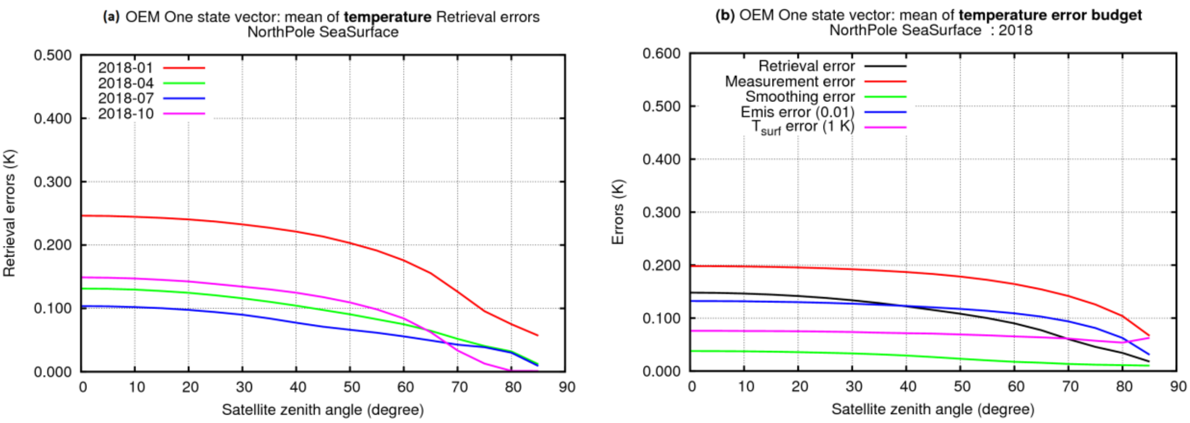

Figure 112: (a) the means of the temperature column error over the North Pole/sea according to the value of the satellite zenith angle; (b) the temperature column error (black), the measurement error (red), the smoothing error (green), the errors induced by a 0.01 random error on the emissivity (blue) and induced by a 1 K random error (purple) according to the satellite zenith angle

2.1.4.1.1.2 Sub-column 300-706 hPa

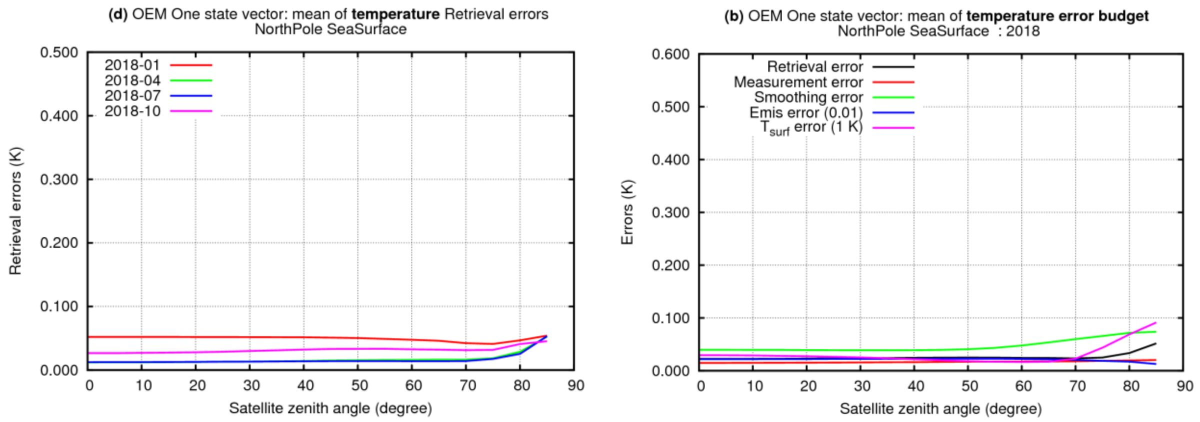

Figure 113 : same as for Figure 112 for sub-column 300-706 hPa

2.1.4.1.1.3 Sub-column 706-1013 hPa

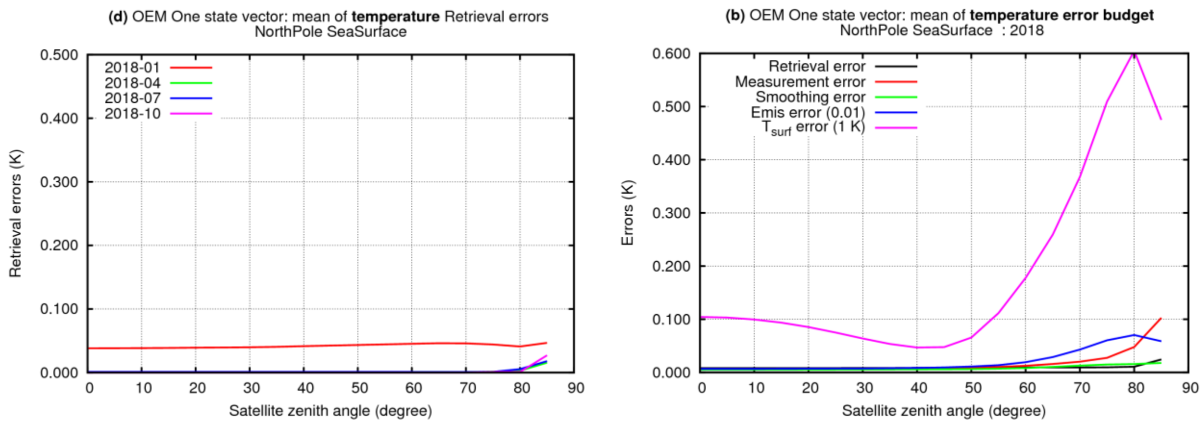

Figure 114 : same as for Figure 113 for sub-column 706-1013 hPa

2.1.4.1.2 Over land

2.1.4.1.2.1 Sub-column 103-300 hPa

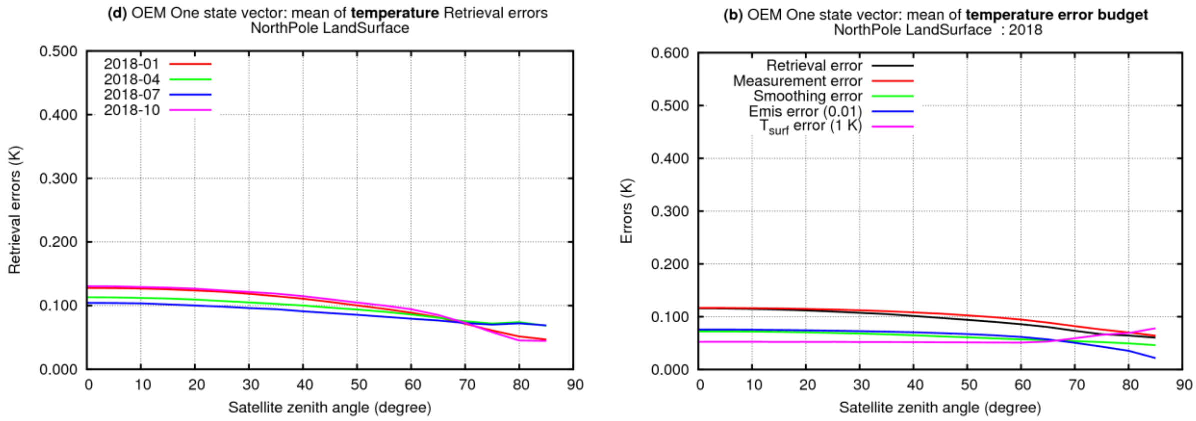

Figure 115: as Figure 112 over land

2.1.4.1.2.2 Sub-column 300-706 hPa

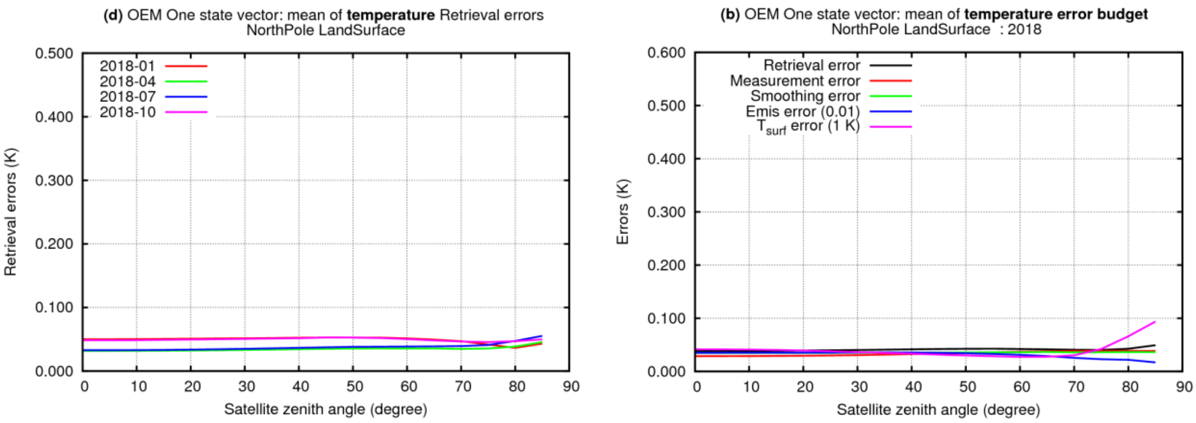

Figure 116 : same as for Figure 115 for sub-column 300-706

2.1.4.1.2.3 Sub-column 706-1013 hPa

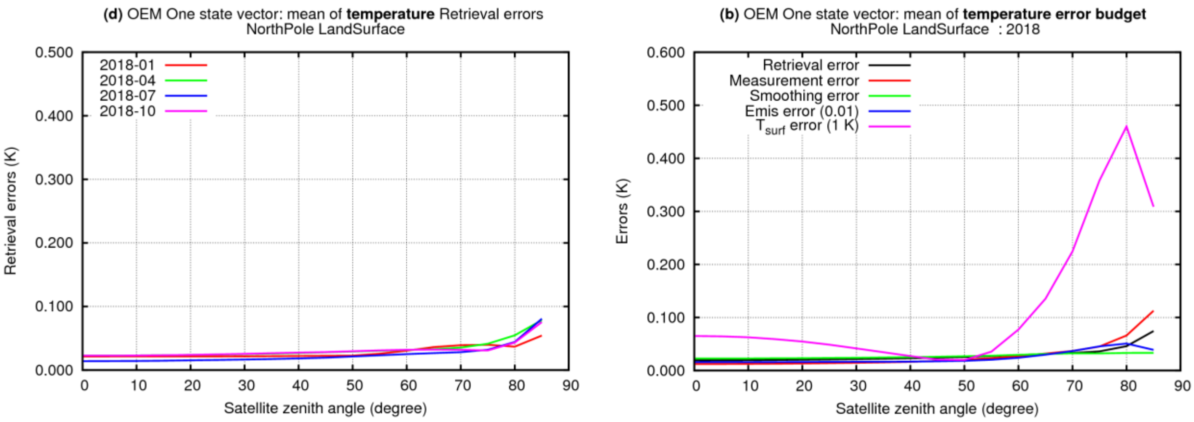

Figure 117 : same as Figure 116 for sub-column 706-1013 hPa

2.1.4.2 Water vapour

2.1.4.2.1 Over sea

2.1.4.2.1.1 Sub-column 496-802 hPa

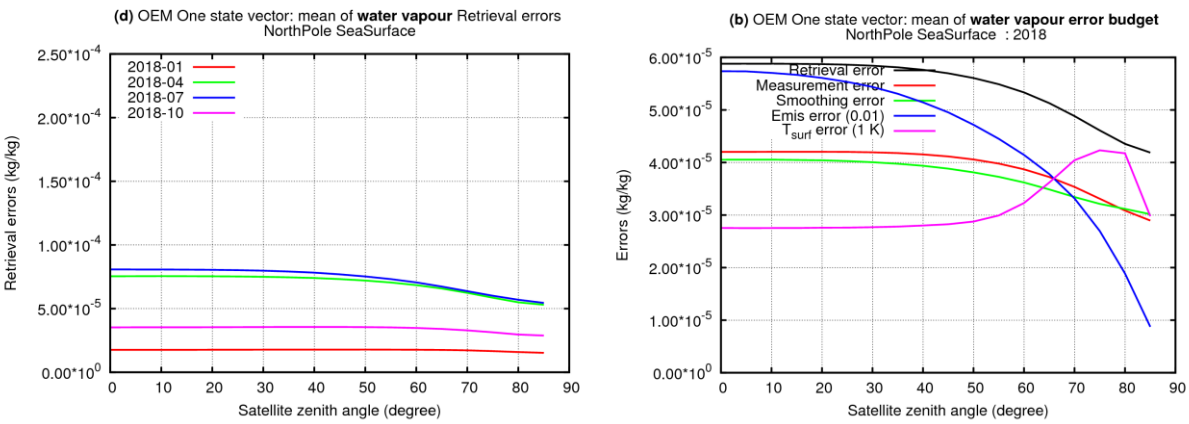

Figure 118: as Figure 112 for water vapour

2.1.4.2.1.2 Sub-column 802-1013 hPa

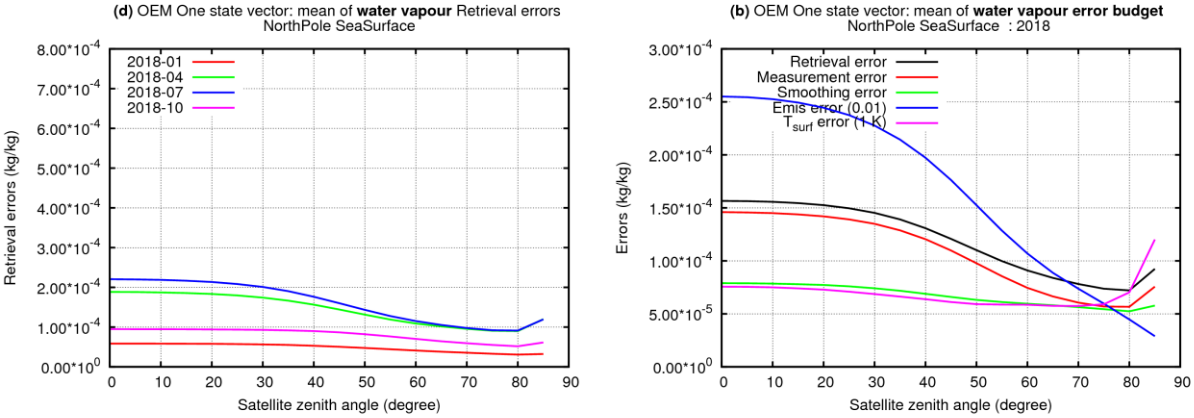

Figure 119 : same as Figure 118 for sub-column 802-1013 hPa

2.1.4.2.2 Over land

2.1.4.2.2.1 Sub-column 496-802 hPa

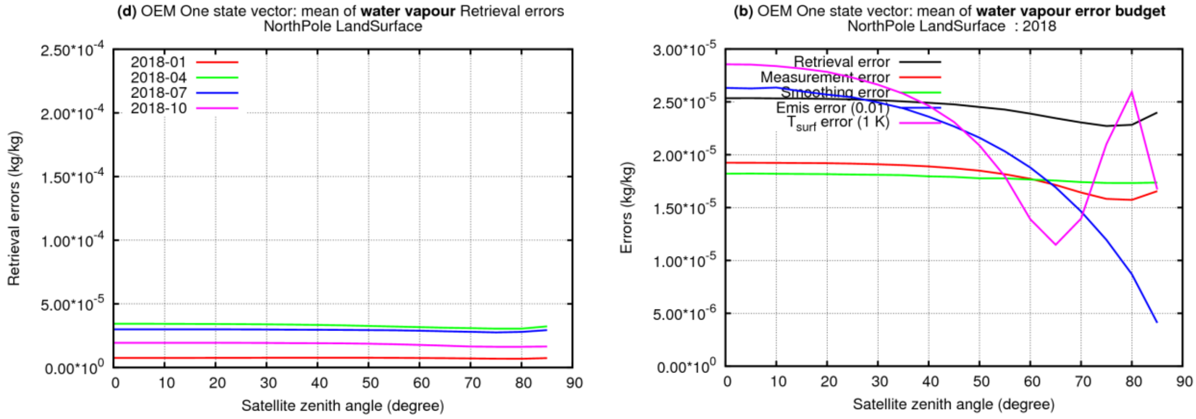

Figure 120: as Figure 118 over land

2.1.4.2.2.2 Sub-column 802-1013 hPa

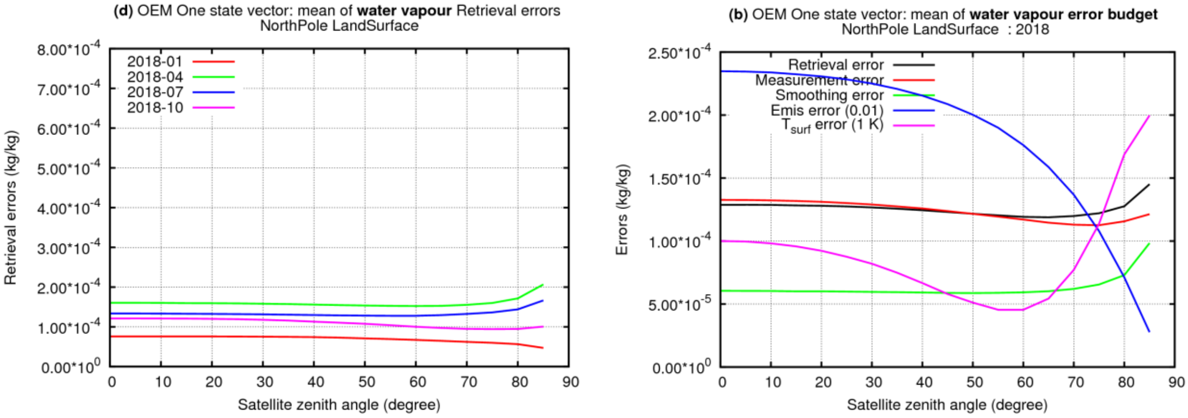

Figure 121 : same as Figure 120 for sub-column 802-1013 hPa

2.1.4.3 Ozone

2.1.4.3.1 Over sea

2.1.4.3.1.1 Sub-column 0-103 hPa

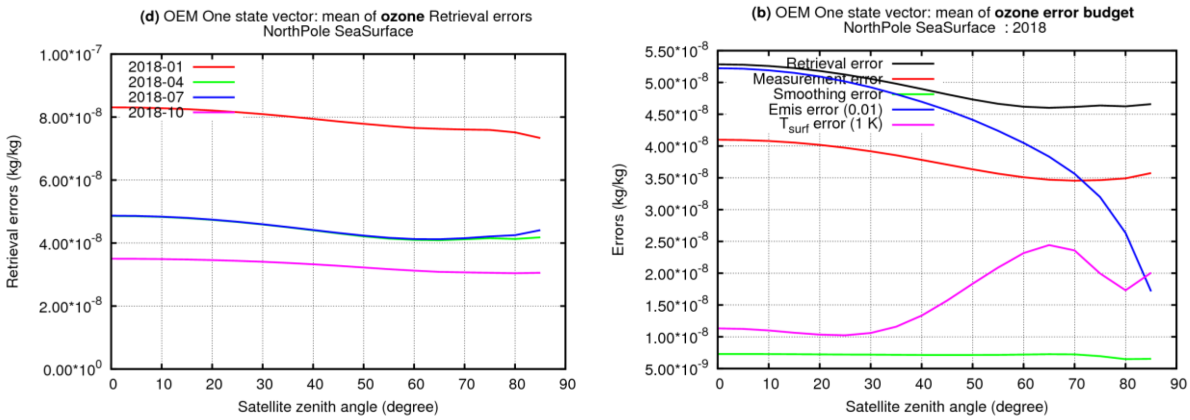

Figure 122: as Figure 112 for water vapour

2.1.4.3.2 Over land

2.1.4.3.2.1 Sub-column 0-103 hPa

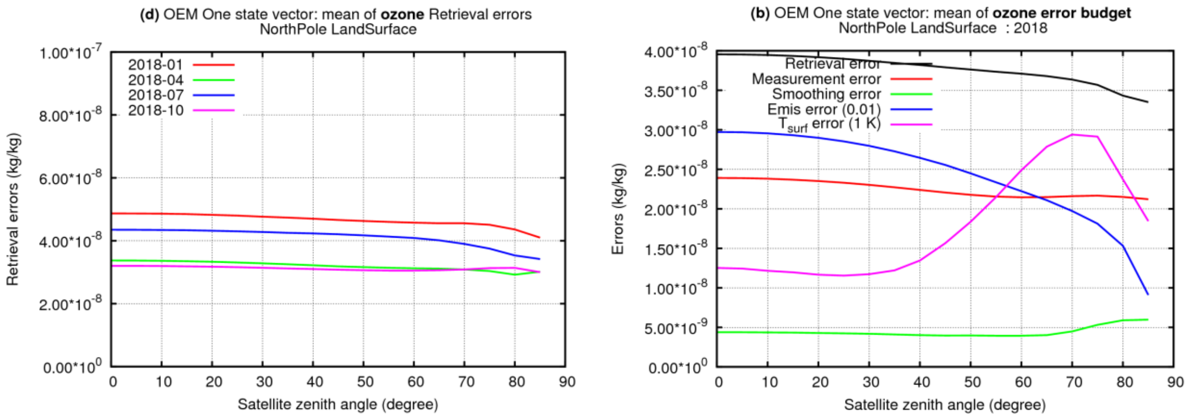

Figure 123: as Figure 122 over land

2.1.5 Column analysis: South Pole

2.1.5.1 Temperature

2.1.5.1.1 Over sea

2.1.5.1.1.1 Sub-column 103-300 hPa

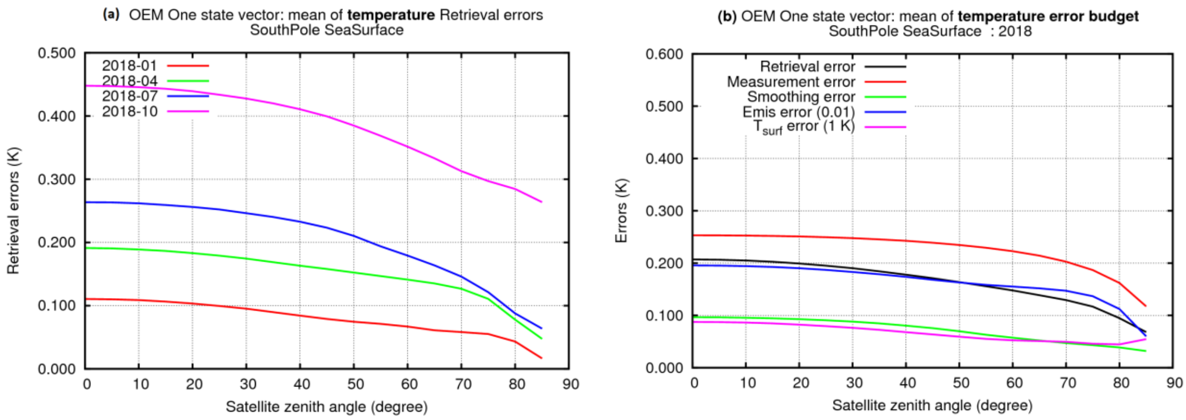

Figure 124: (a) the means of the temperature column error over the South Pole/sea according to the value of the satellite zenith angle; (b) the temperature column error (black), the measurement error (red), the smoothing error (green), the errors induced by a 0.01 random error on the emissivity (blue) and induced by a 1 K random surface temperature error (purple) according to the satellite zenith angle

2.1.5.1.1.2 Sub-column 300-706 hPa

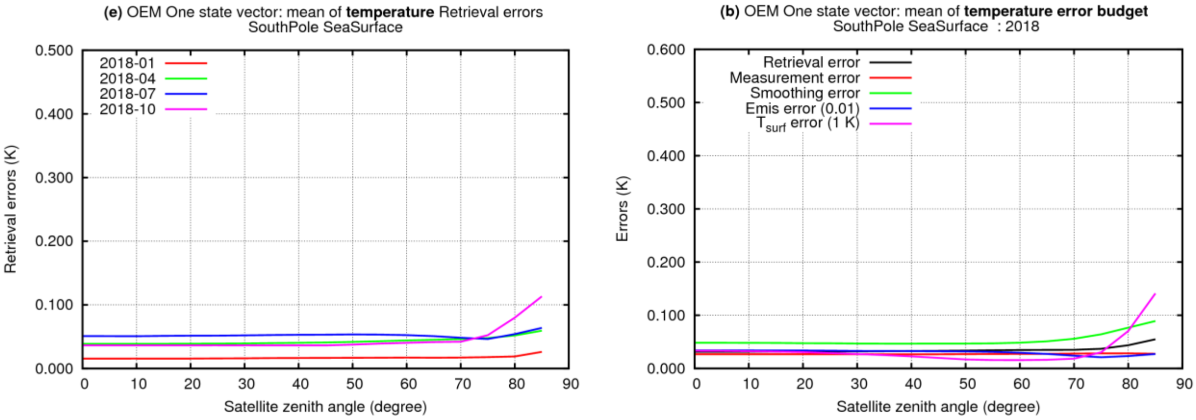

Figure 125 : same as Figure 124 for sub-column 300-706

2.1.5.1.1.3 Sub-column 706-1013 hPa

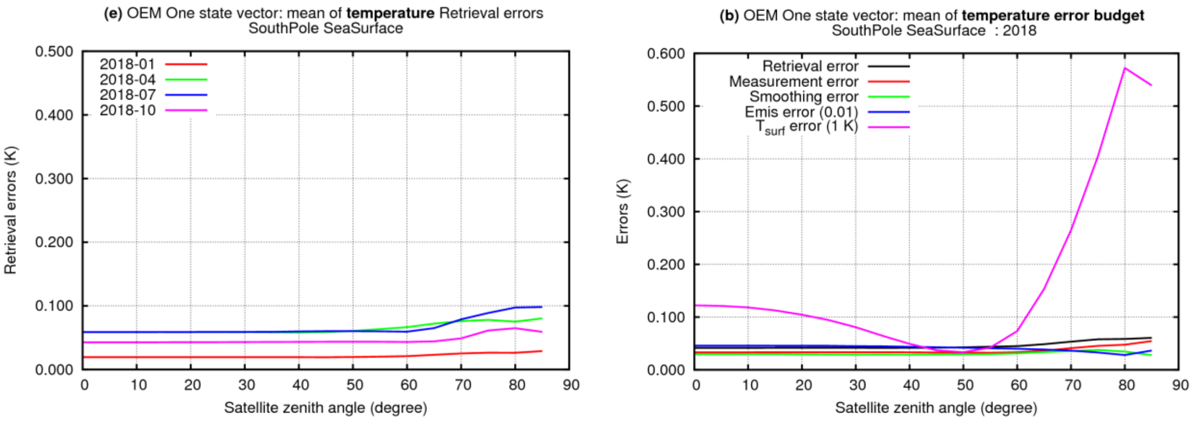

Figure 126 : same as Figure 125 for sub-column 706-1013 hPa

2.1.5.1.2 Over land

2.1.5.1.2.1 Sub-column 103-300 hPa

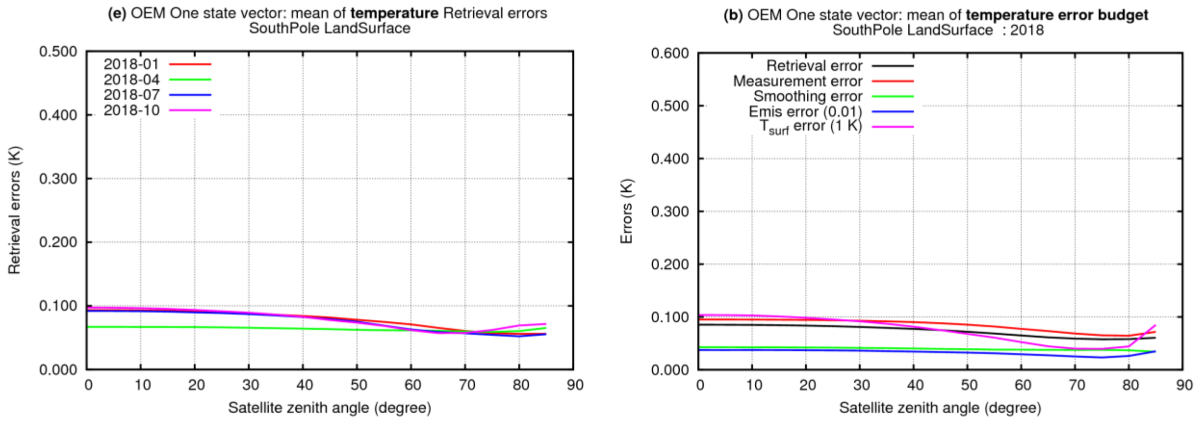

Figure 127: as Figure 124 over land

2.1.5.1.2.2 Sub-column 300-706 hPa

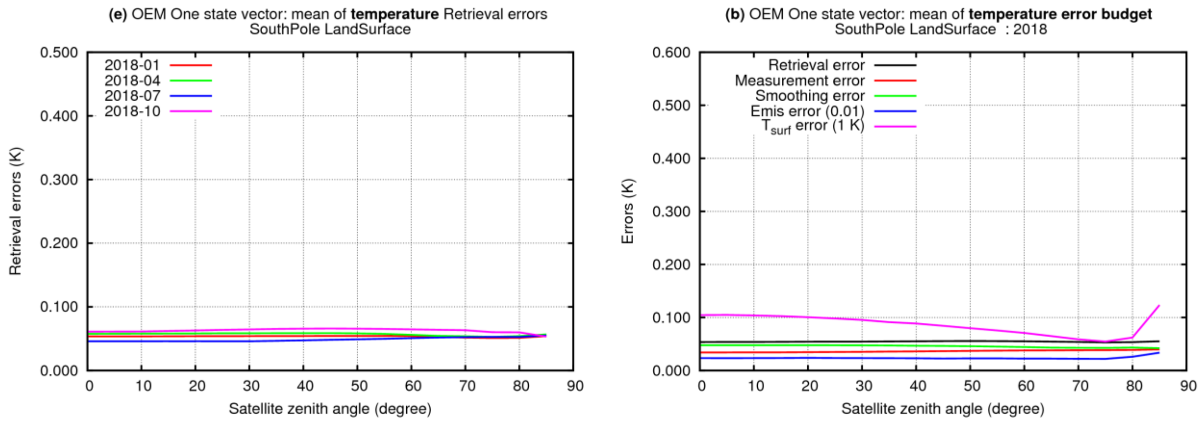

Figure 128 : same as for Figure 127 for sub-column 300-706 hPa

2.1.5.1.2.3 Sub-column 706-1013 hPa

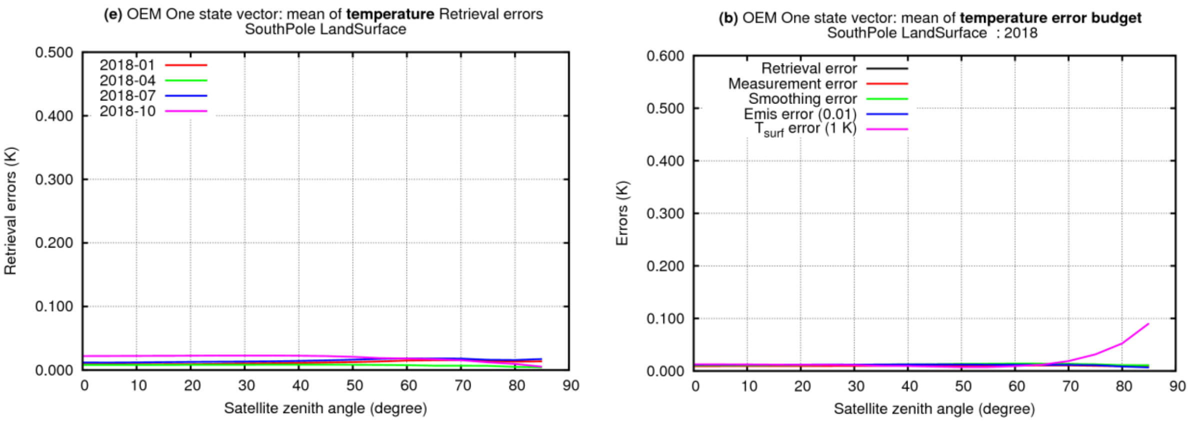

Figure 129 : same as Figure 127 for sub-column 706-1013 hPa

2.1.5.2 Water vapour

2.1.5.2.1 Over sea

2.1.5.2.1.1 Sub-column 496-802 hPa

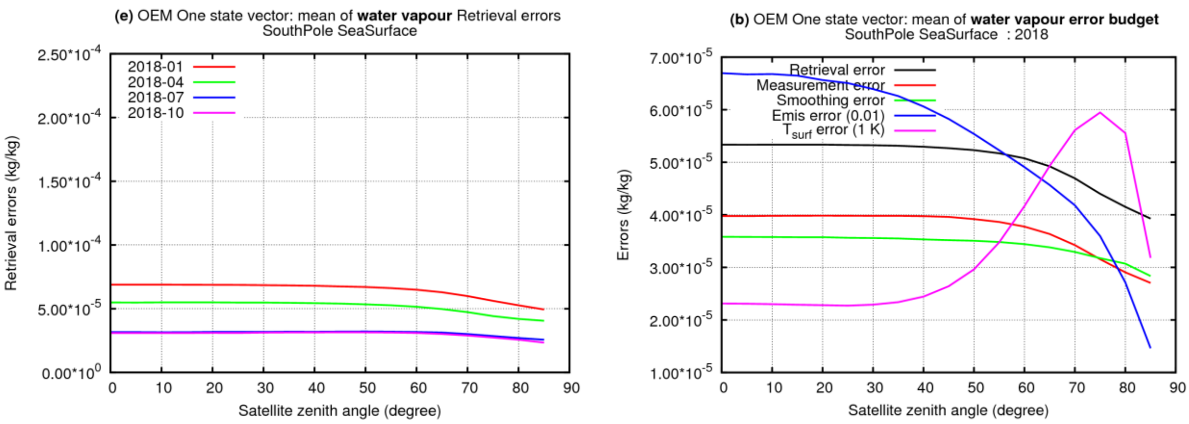

Figure 130: as Figure 124 for water vapour

2.1.5.2.1.2 Sub-column 802-1013 hPa

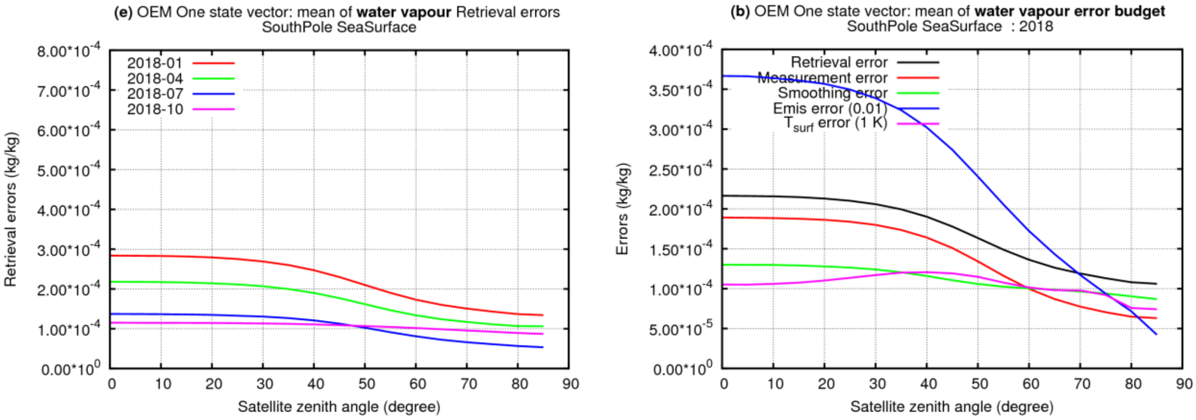

Figure 131 : same as Figure 130 for sub-column 802-1013 hPa

2.1.5.2.2 Over land

2.1.5.2.2.1 Sub-column 496-802 hPa

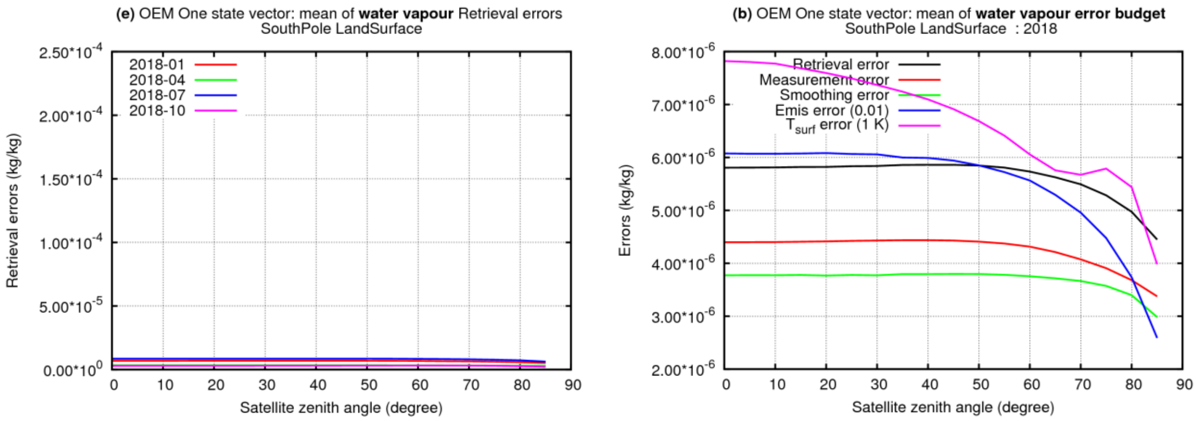

Figure 132: as Figure 130 over land

2.1.5.2.2.2 Sub-column 802-1013 hPa

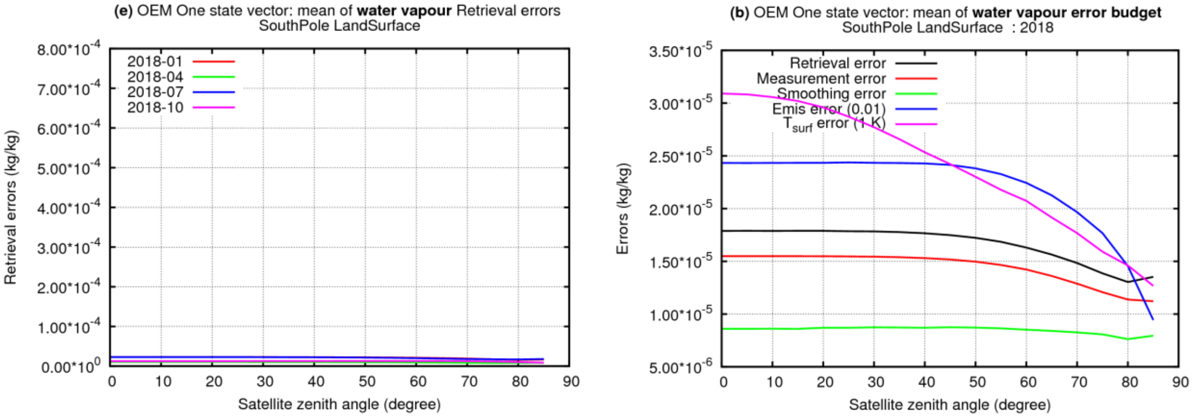

Figure 133 : same as Figure 132 for sub-column 802-1013 hPa

2.1.5.3 Ozone

2.1.5.3.1 Over sea

2.1.5.3.1.1 Sub-column 0-103 hPa

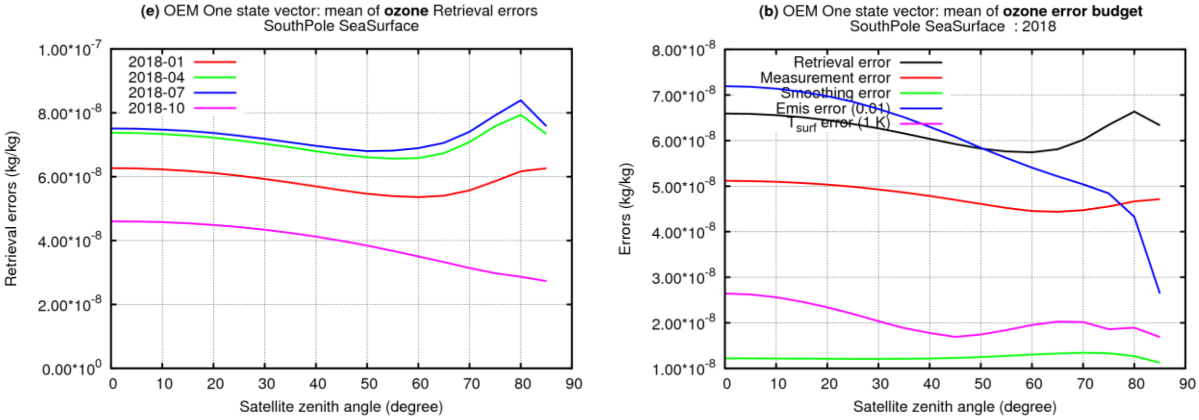

Figure 134: Figure 124 for ozone

2.1.5.3.2 Over land

2.1.5.3.2.1 Sub-column 0-103 hPa

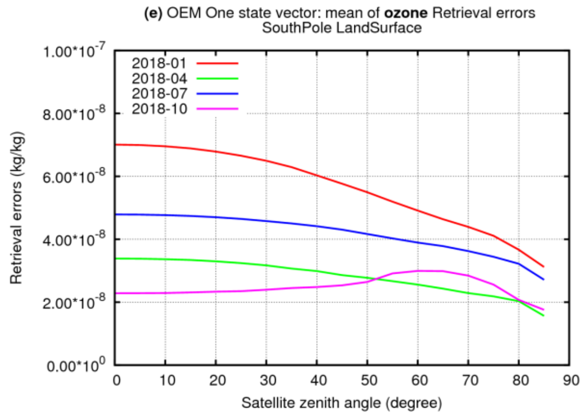

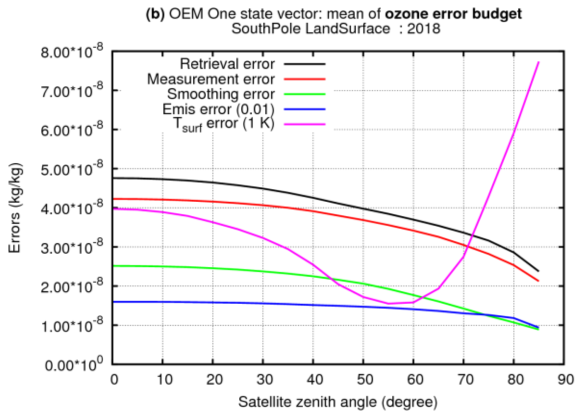

Figure 135: as Figure 134 over land

2.1.6 Maps of the scenes with the minimum/maximum anomalies: temperature

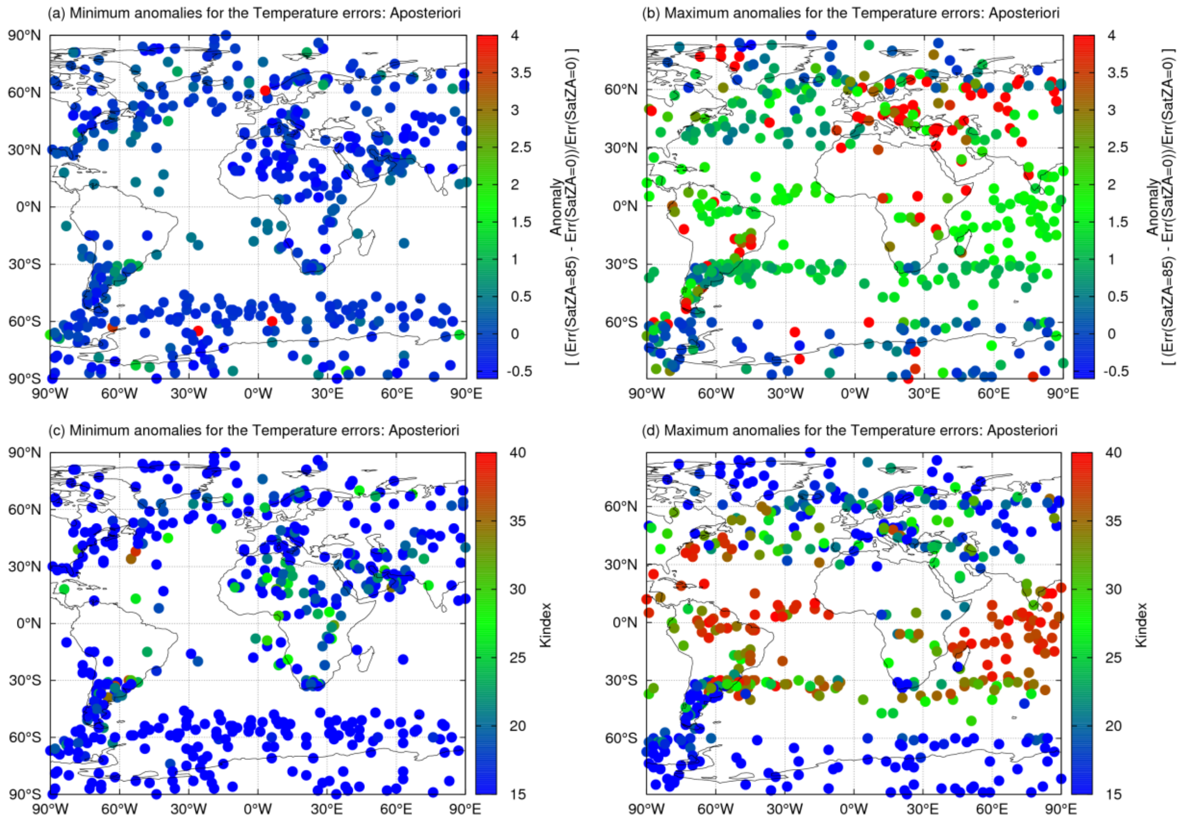

Figure 136 : Maps of the extracted situations from the generated dataset with the minimum (a) and maximum (b) anomalies values. Associated K index values for these situations are given for minimum anomaly dataset (c) and the maximum anomaly dataset (d).

2.1.7 Maps of the scenes with the minimum/maximum anomalies: water vapour

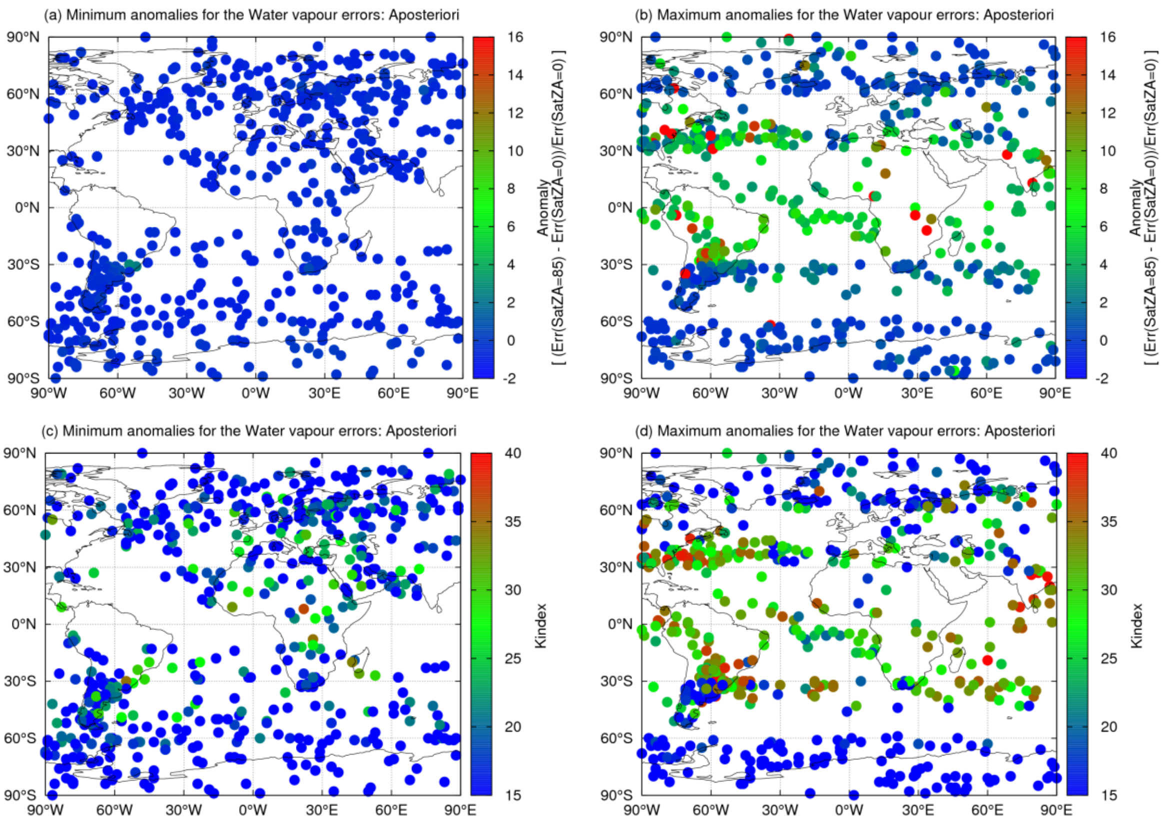

Figure 137: Maps of the extracted situations from the generated dataset with the minimum (a) and maximum (b) anomalies values. Associated K index values for these situations are given for minimum anomaly dataset (c) and the maximum anomaly dataset (d).

2.1.8 Maps of the scenes with the minimum/maximum anomalies: ozone

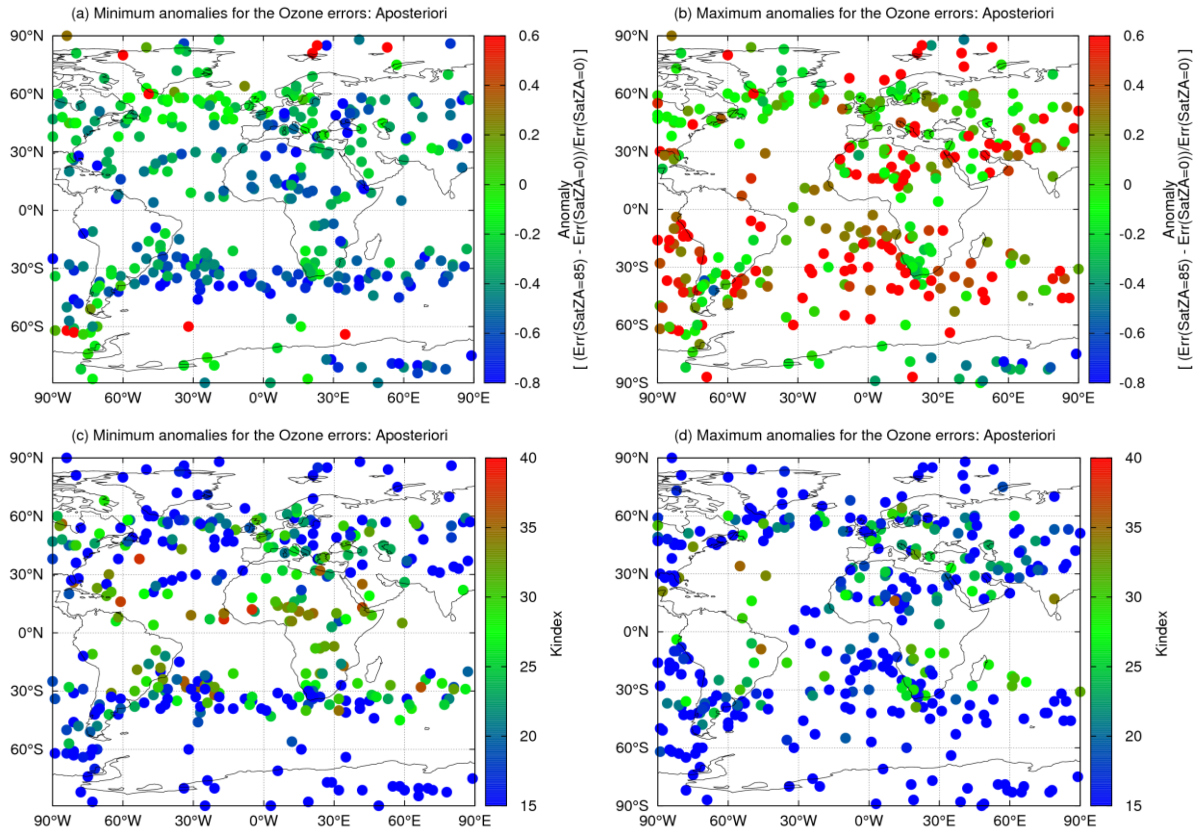

Figure 138: Maps of the extracted situations from the generated dataset with the minimum (a) and maximum (b) anomalies values. Associated K index values for these situations are given for minimum anomaly dataset (c) and the maximum anomaly dataset (d).

2.2 ANALYSIS IN TERMS OF PROFILE RETRIEVAL ERRORS

2.2.1 Profile analysis: Tropics, over sea

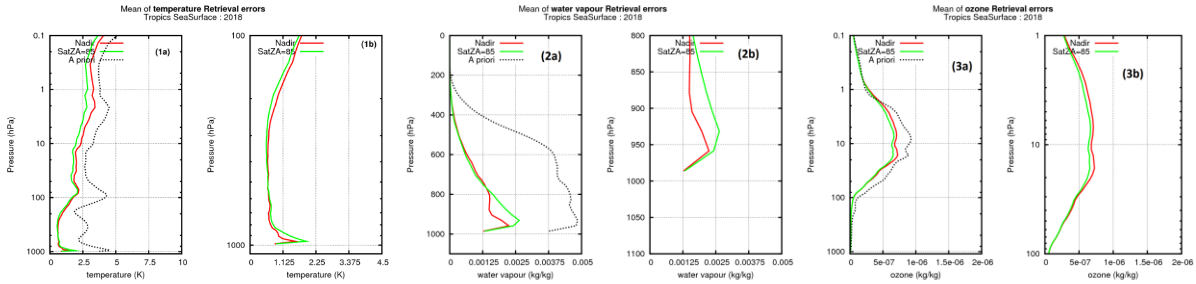

Figure 139: Profiles of the retrieval errors at nadir (red), for SatZA = 85° (green) and the a priori error (black, dot line) for the temperature profile (1a, zoom 1b), for the water vapour (2a, zoom 2b) and for ozone (3a, zoom 3b) over tropics/sea

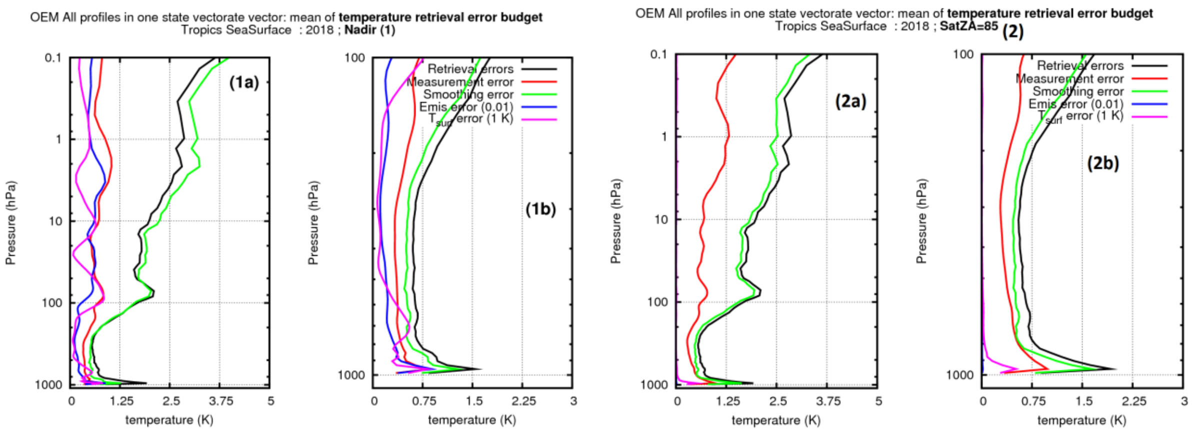

Figure 140: Mean retrieval error budget of temperature profiles over tropics and sea for (1) nadir and (2) for a SatZA of 85°. (Black) Retrieval error profile. (Red) Measurement error. (Green) Smoothing error. (Blue) Error induced by a 0.01 incertitude on emissivity. (Purple) Error induced by a 1K incertitude on surface temperature.

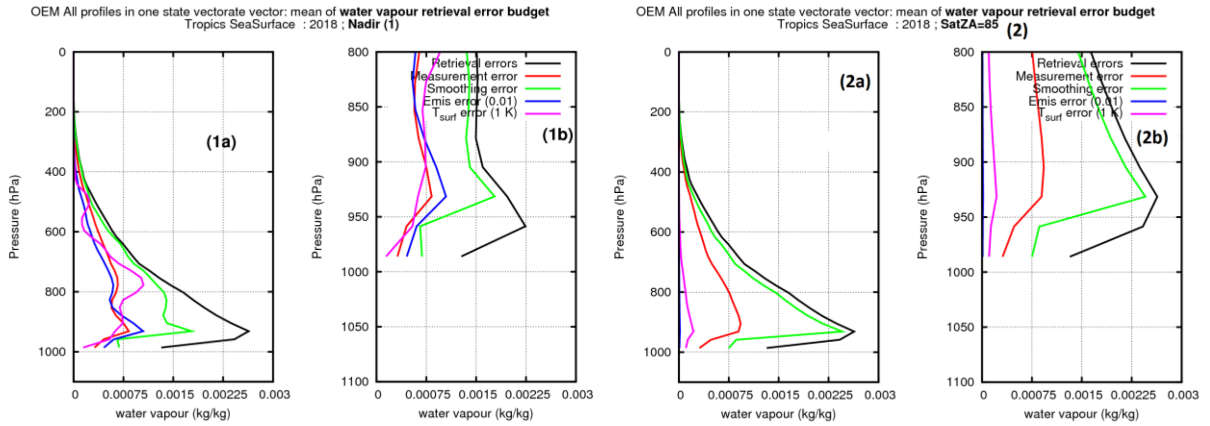

Figure 141: Mean retrieval error budget of water vapour profiles over tropics and sea for (1) nadir and (2) for a SatZA of 85°. (Black) Retrieval error profile. (Red) Measurement error. (Green) Smoothing error. (Blue) Error induced by a 0.01 incertitude on emissivity. (Purple) Error induced by a 1 K incertitude on surface temperature.

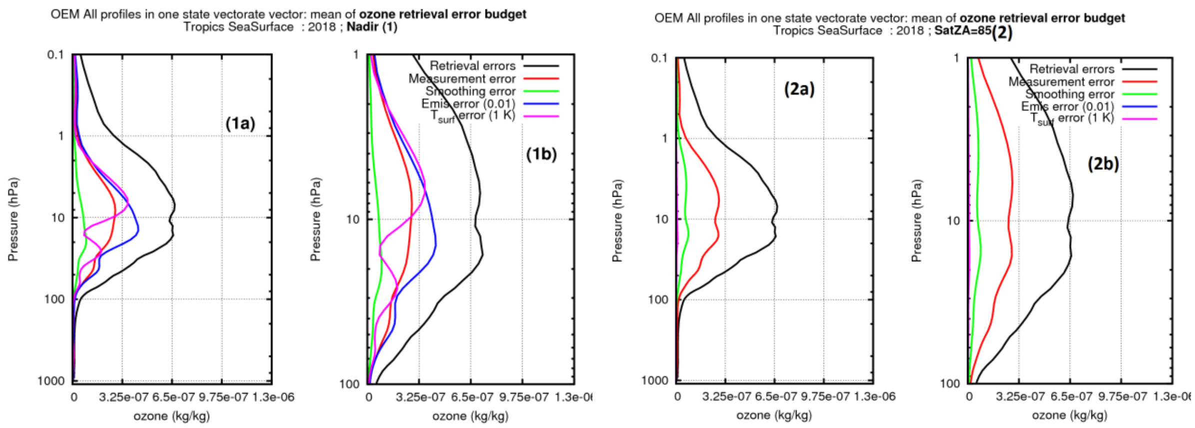

Figure 142: Mean retrieval error budget of ozone profiles over tropics and sea for (1) nadir and (2) for a SatZA of 85°. (Black) Retrieval error profile. (Red) Measurement error. (Green) Smoothing error. (Blue) Error induced by a 0.01 incertitude on emissivity. (Purple) Error induced by a 1 K incertitude on surface temperature.

2.2.2 Profile analysis: Tropics, over land

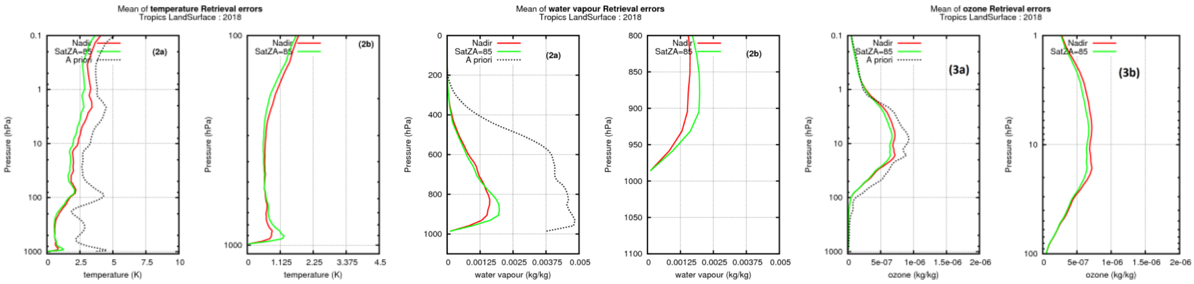

Figure 143: as Figure 139 over tropics/land

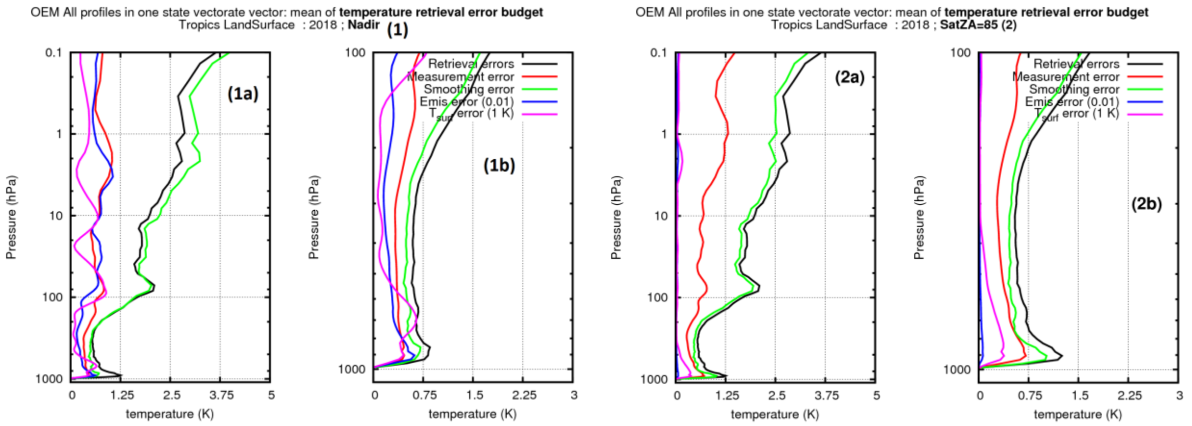

Figure 144: Mean retrieval error budget of temperature profiles over tropics and land for (1) nadir and (2) for a SatZA of 85°. (Black) Retrieval error profile. (Red) Measurement error. (Green) Smoothing error. (Blue) Error induced by a 0.01 incertitude on emissivity. (Purple) Error induced by a 1K incertitude on surface temperature.

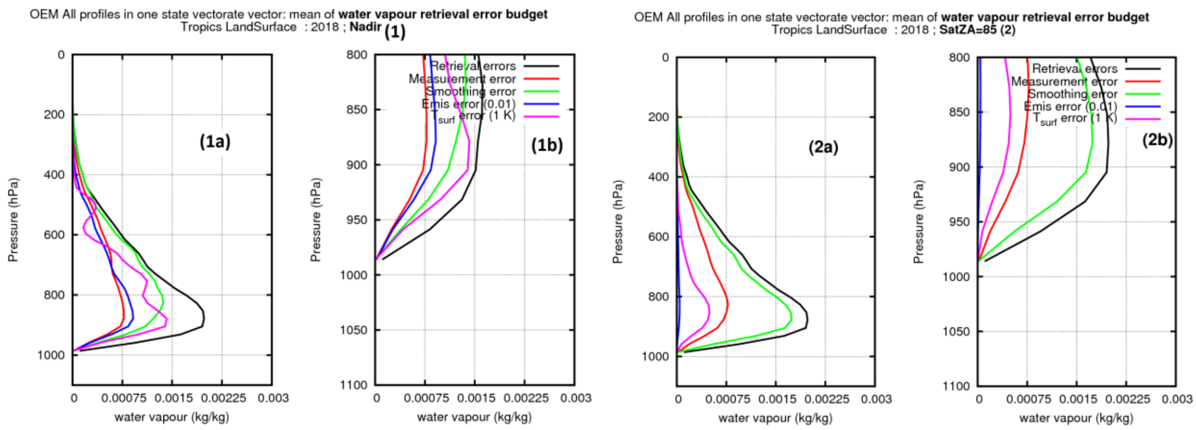

Figure 145: Mean retrieval error budget of water vapour profiles over tropics and land for (1) nadir and (2) for a SatZA of 85°. (Black) Retrieval error profile. (Red) Measurement error. (Green) Smoothing error. (Blue) Error induced by a 0.01 incertitude on emissivity. (Purple) Error induced by a 1K incertitude on surface temperature.

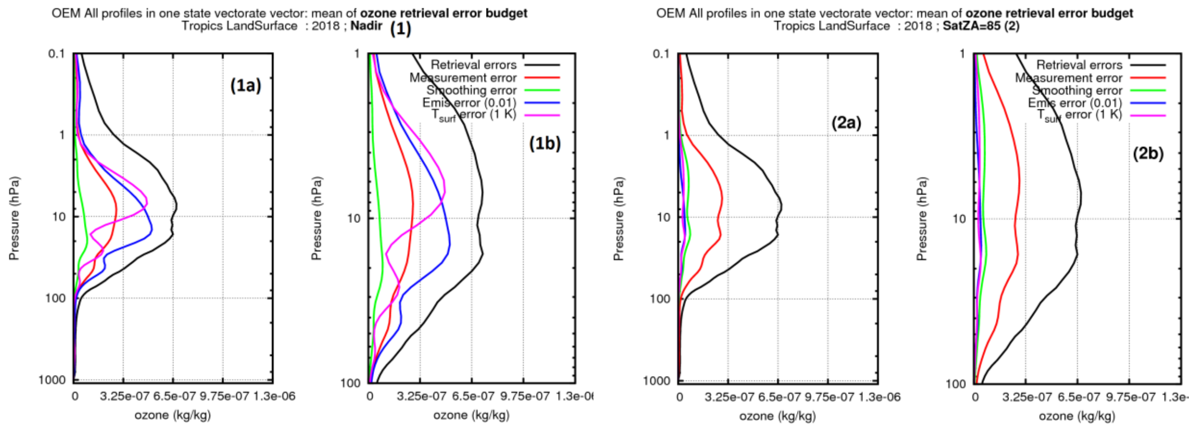

Figure 146: Mean retrieval error budget of ozone profiles over tropics and land for (1) nadir and (2) for a SatZA of 85°. (Black) Retrieval error profile. (Red) Measurement error. (Green) Smoothing error. (Blue) Error induced by a 0.01 incertitude on emissivity. (Purple) Error induced by a 1K incertitude on surface temperature.

2.2.3 Profile analysis: Northern Mid-latitudes, over sea

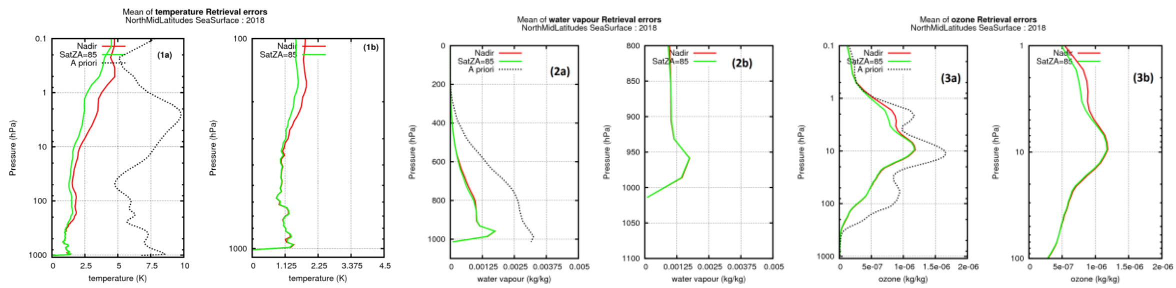

Figure 147: as Figure 139 over Northern Mid-latitudes/sea

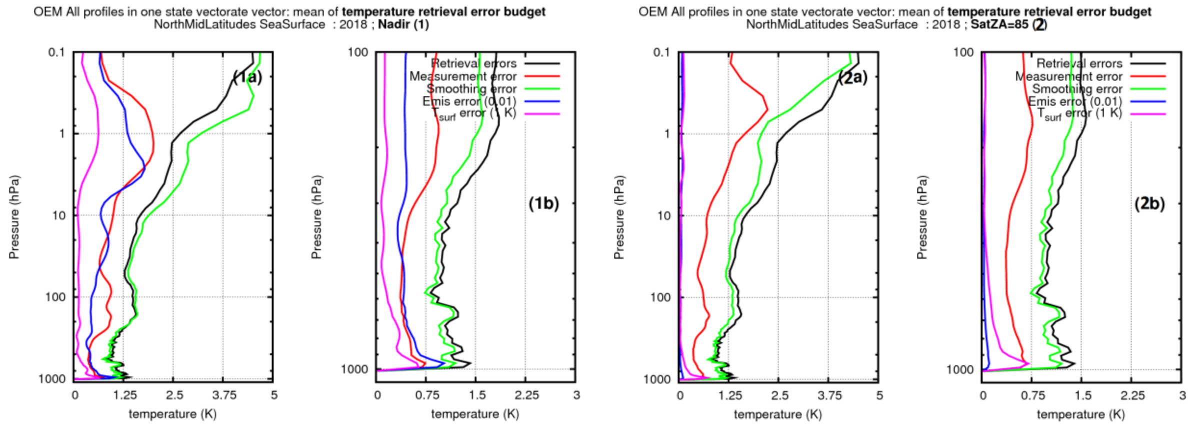

Figure 148: Mean retrieval error budget of temperature profiles over northern mid-latitudes and sea for (1) nadir and (2) for a SatZA of 85°. (Black) Retrieval error profile. (Red) Measurement error. (Green) Smoothing error. (Blue) Error induced by a 0.01 incertitude on emissivity. (Purple) Error induced by a 1K incertitude on surface temperature.

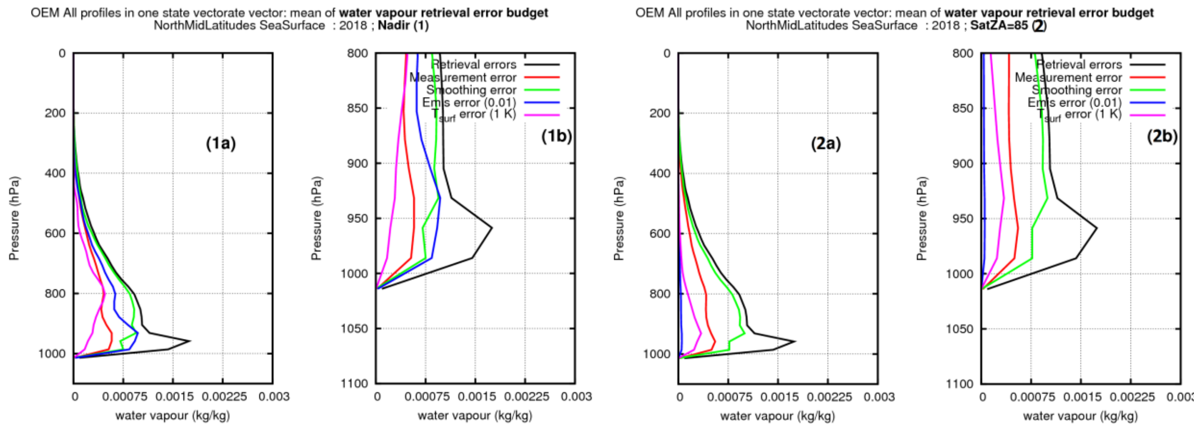

Figure 149: Mean retrieval error budget of water vapour profiles over northern mid-latitudes and sea for (1) nadir and (2) for a SatZA of 85°. (Black) Retrieval error profile. (Red) Measurement error. (Green) Smoothing error. (Blue) Error induced by a 0.01 incertitude on emissivity. (Purple) Error induced by a 1K incertitude on surface temperature.

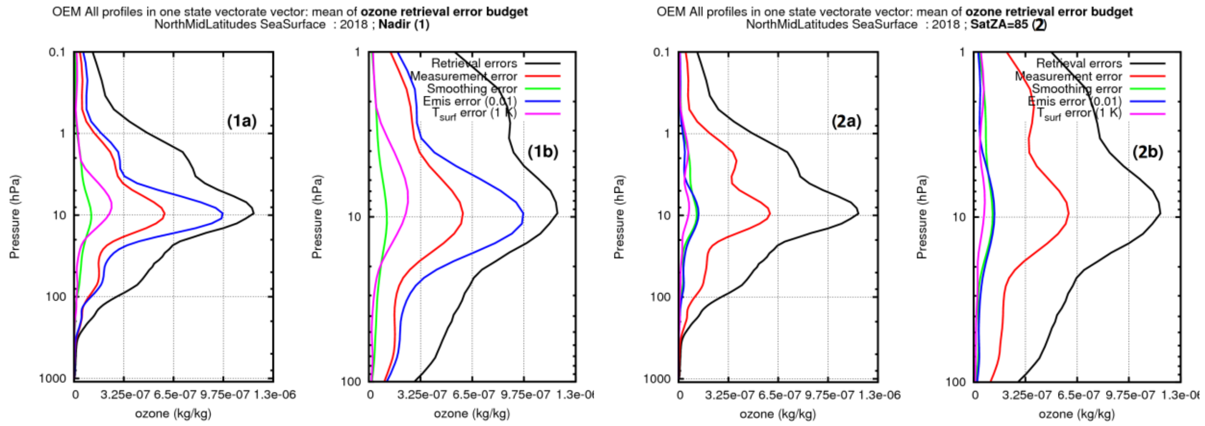

Figure 150: Mean retrieval error budget of ozone profiles over northern mid-latitudes and sea for (1) nadir and (2) for a SatZA of 85°. (Black) Retrieval error profile. (Red) Measurement error. (Green) Smoothing error. (Blue) Error induced by a 0.01 incertitude on emissivity. (Purple) Error induced by a 1K incertitude on surface temperature.

2.2.4 Profile analysis: Northern Mid-latitudes, over land

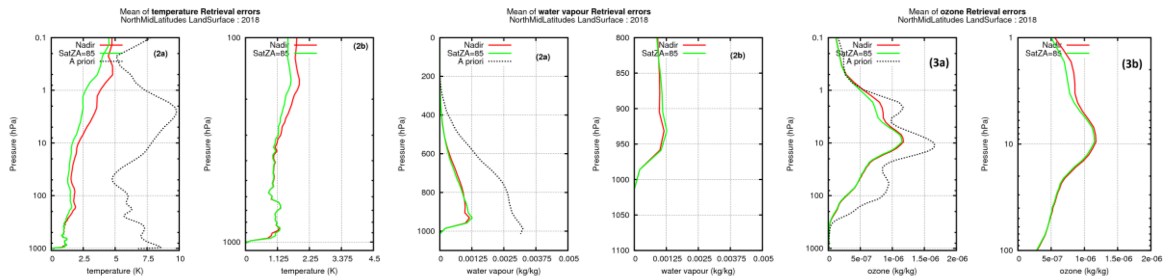

Figure 151: as Figure 139 over Northern Mid-latitudes/land

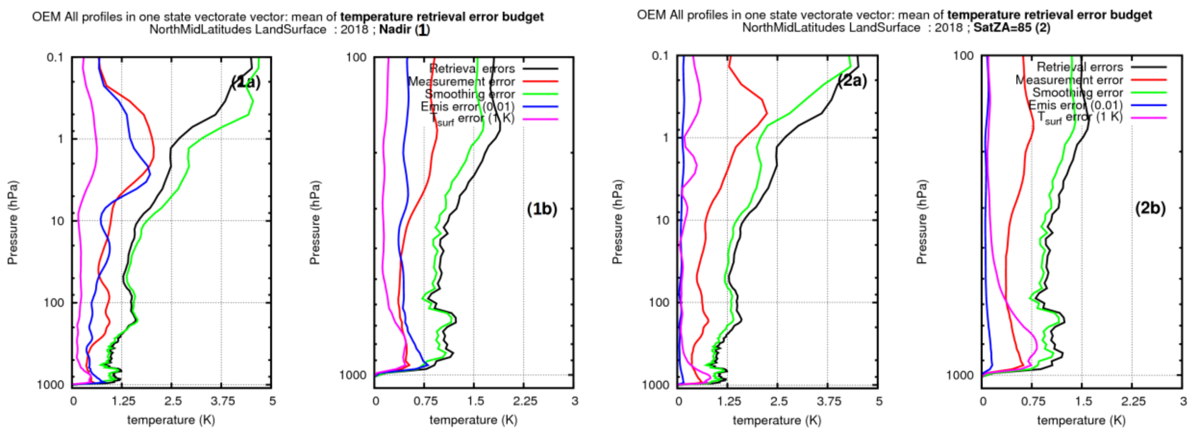

Figure 152: Mean retrieval error budget of temperature profiles over northern mid-latitudes and land for (1) nadir and (2) for a SatZA of 85°. (Black) Retrieval error profile. (Red) Measurement error. (Green) Smoothing error. (Blue) Error induced by a 0.01 incertitude on emissivity. (Purple) Error induced by a 1K incertitude on surface temperature.

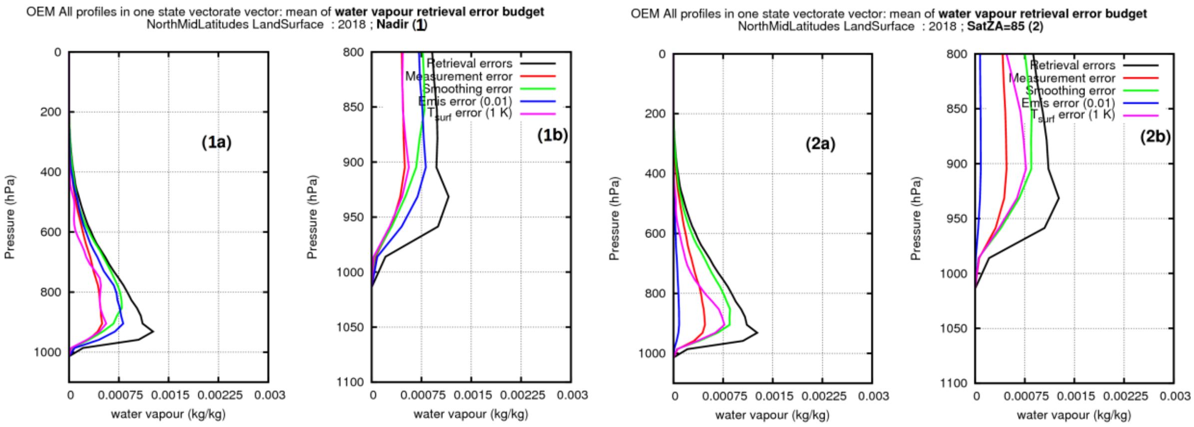

Figure 153: Mean retrieval error budget of water vapour profiles over northern mid-latitudes and land for (1) nadir and (2) for a SatZA of 85°. (Black) Retrieval error profile. (Red) Measurement error. (Green) Smoothing error. (Blue) Error induced by a 0.01 incertitude on emissivity. (Purple) Error induced by 1K incertitude on surface temperature.

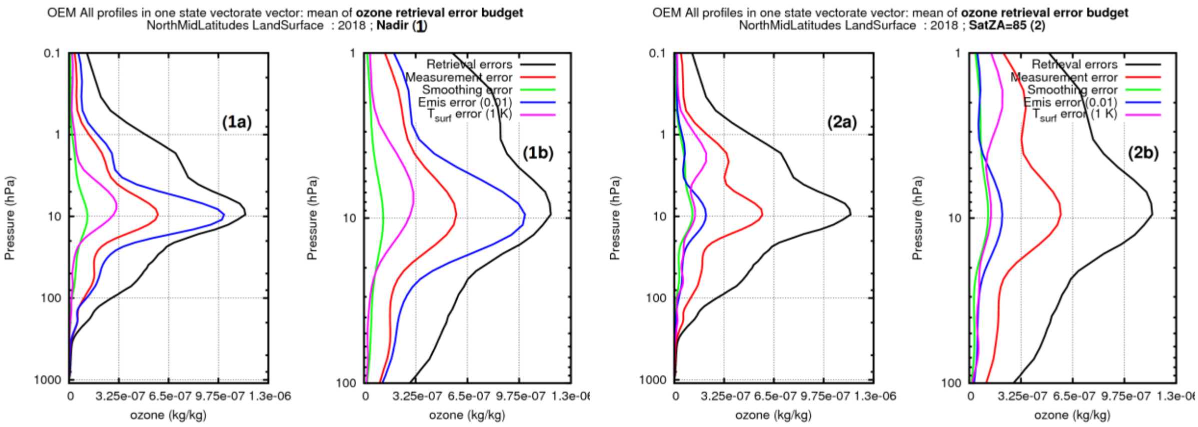

Figure 154: Mean retrieval error budget of ozone profiles over northern mid-latitudes and land for (1) nadir and (2) for a SatZA of 85°. (Black) Retrieval error profile. (Red) Measurement error. (Green) Smoothing error. (Blue) Error induced by a 0.01 incertitude on emissivity. (Purple) Error induced by a 1K incertitude on surface temperature.

2.2.5 Profile analysis: Southern Mid-latitudes, over sea

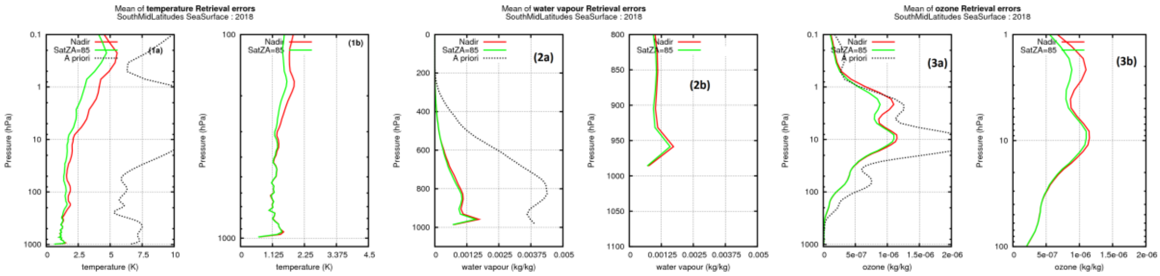

Figure 155: as Figure 139 over Southern Mid-latitudes/sea

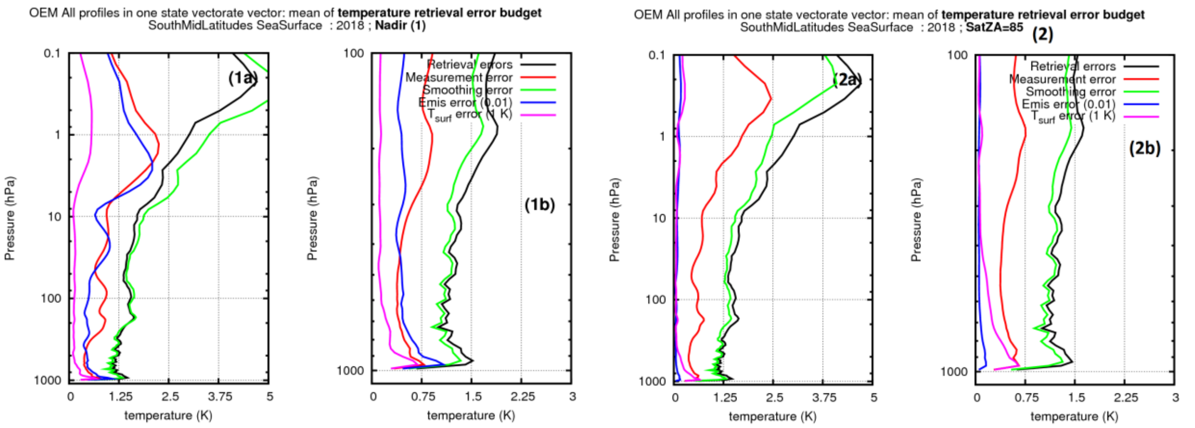

Figure 156: Mean retrieval error budget of temperature profiles over southern mid-latitudes and sea for (1) nadir and (2) for a SatZA of 85°. (Black) Retrieval error profile. (Red) Measurement error. (Green) Smoothing error. (Blue) Error induced by a 0.01 incertitude on emissivity. (Purple) Error induced by a 1K incertitude on surface temperature.

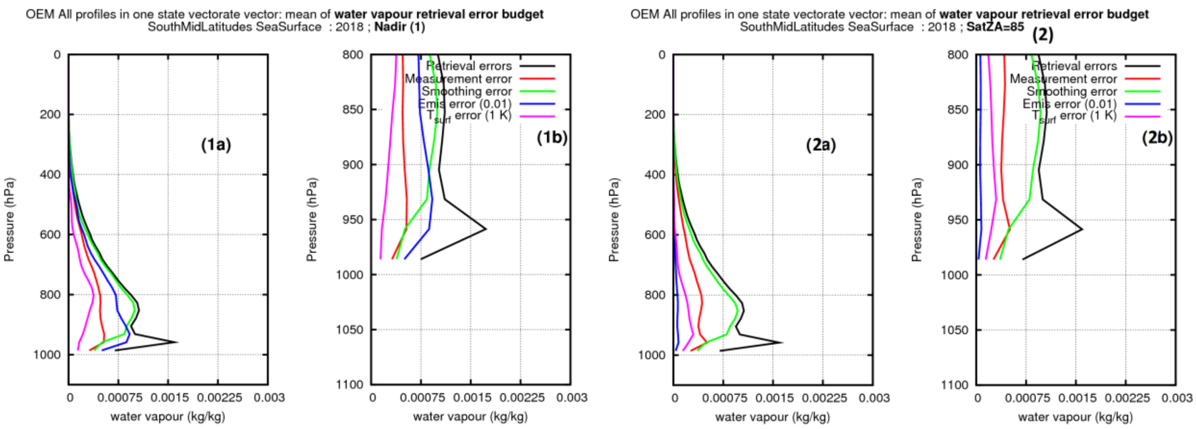

Figure 157: Mean retrieval error budget of water vapour profiles over southern mid-latitudes and sea for (1) nadir and (2) for a SatZA of 85°. (Black) Retrieval error profile. (Red) Measurement error. (Green) Smoothing error. (Blue) Error induced by a 0.01 incertitude on emissivity. (Purple) Error induced by a 1K incertitude on surface temperature.

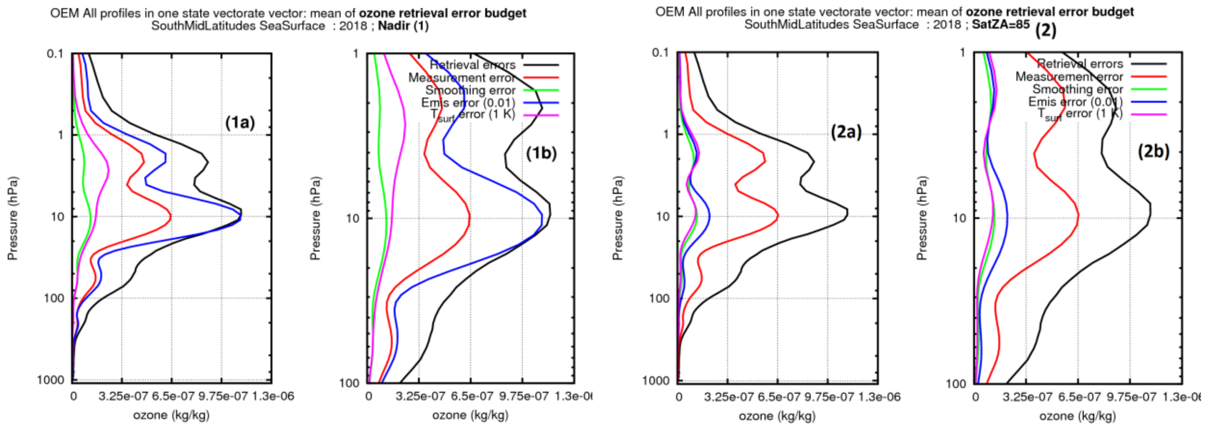

Figure 158: Mean retrieval error budget of ozone profiles over southern mid-latitudes and sea for (1) nadir and (2) for a SatZA of 85°. (Black) Retrieval error profile. (Red) Measurement error. (Green) Smoothing error. (Blue) Error induced by a 0.01 incertitude on emissivity. (Purple) Error induced by a 1K incertitude on surface temperature.

2.2.6 Profile analysis: Southern Mid-latitudes, over land

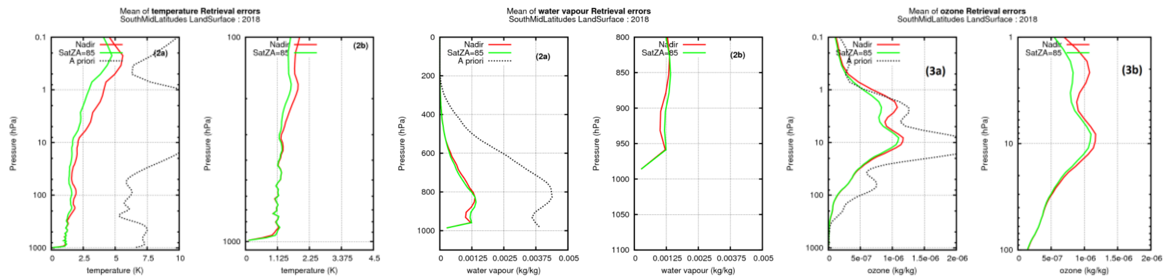

Figure 159: as Figure 139 over Southern Mid-latitudes/land

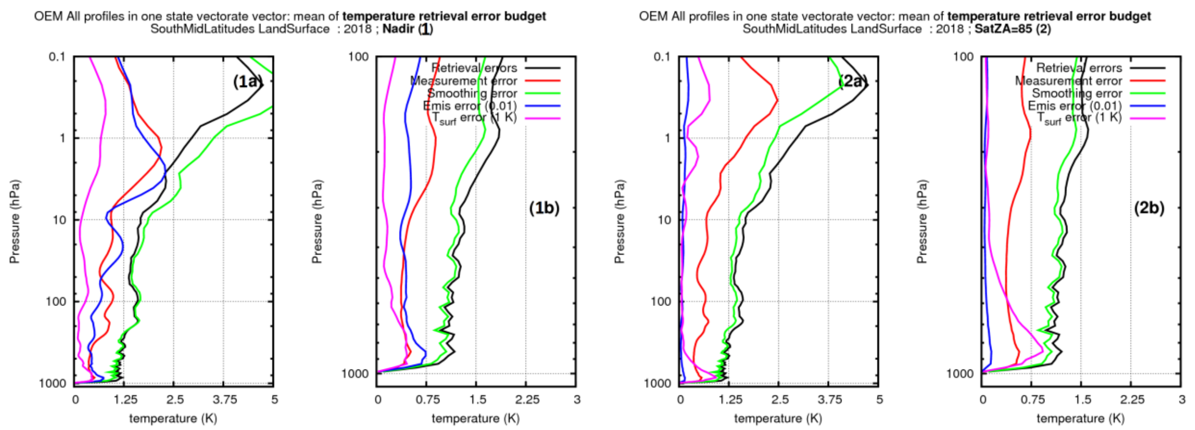

Figure 160: Mean retrieval error budget of temperature profiles over southern mid-latitudes and sea for (1) nadir and (2) for a SatZA of 85°. (Black) Retrieval error profile. (Red) Measurement error. (Green) Smoothing error. (Blue) Error induced by a 0.01 incertitude on emissivity. (Purple) Error induced by a 1K incertitude on surface temperature.

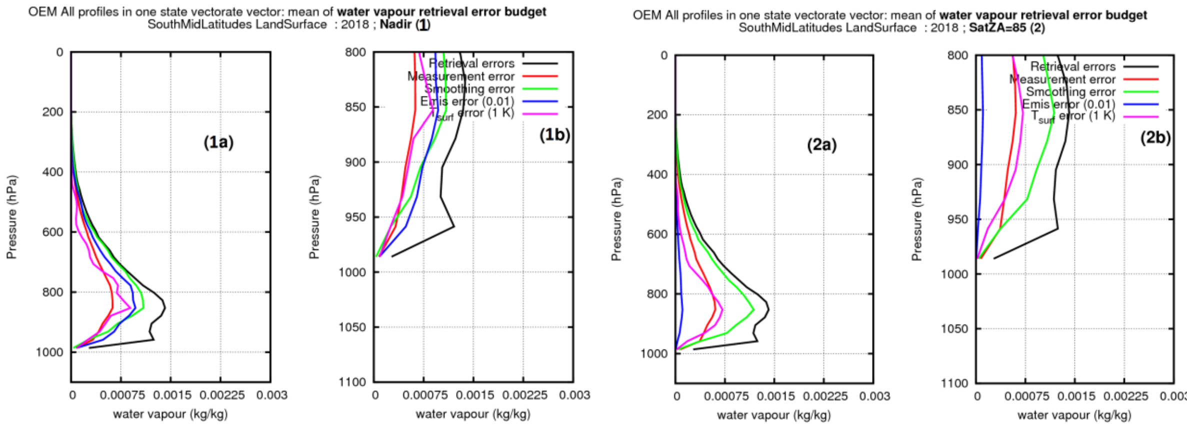

Figure 161: Mean retrieval error budget of water vapour profiles over southern mid-latitudes and sea for (1) nadir and (2) for a SatZA of 85°. (Black) Retrieval error profile. (Red) Measurement error. (Green) Smoothing error. (Blue) Error induced by a 0.01 incertitude on emissivity. (Purple) Error induced by a 1K incertitude on surface temperature.

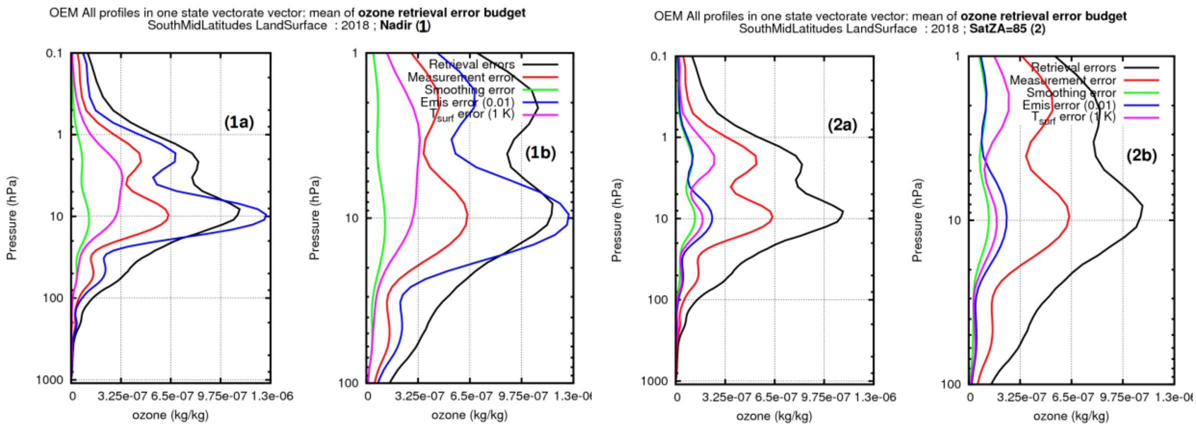

Figure 162: Mean retrieval error budget of ozone profiles over southern mid-latitudes and sea for (1) nadir and (2) for a SatZA of 85°. (Black) Retrieval error profile. (Red) Measurement error. (Green) Smoothing error. (Blue) Error induced by a 0.01 incertitude on emissivity. (Purple) Error induced by a 1K incertitude on surface temperature.

2.2.7 Profile analysis: North Pole, over sea

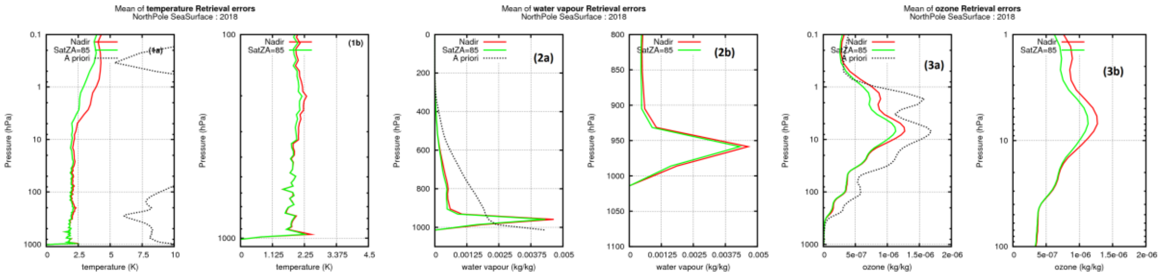

Figure 163: as Figure 139 over North Pole/sea

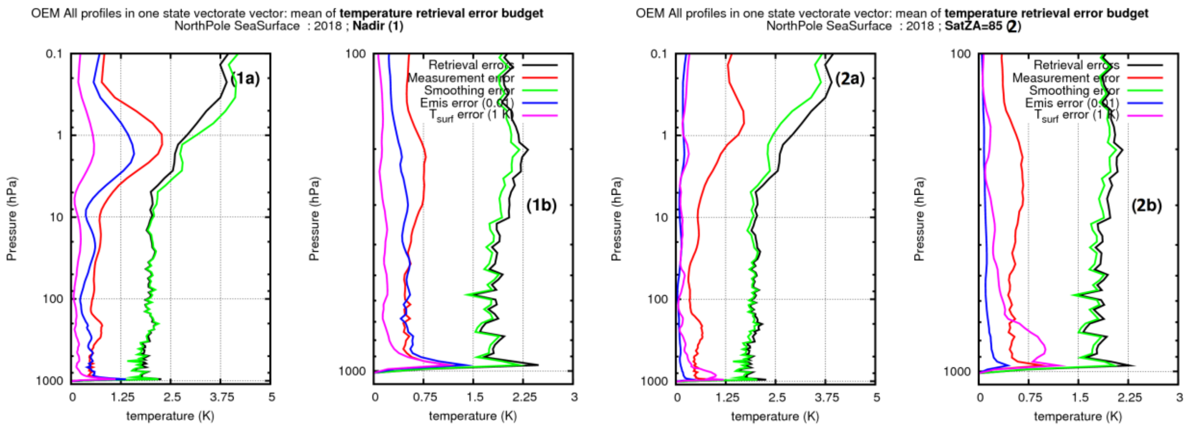

Figure 164: Mean retrieval error budget of temperature profiles over North Pole and sea for (1) nadir and (2) for a SatZA of 85°. (Black) Retrieval error profile. (Red) Measurement error. (Green) Smoothing error. (Blue) Error induced by a 0.01 incertitude on emissivity. (Purple) Error induced by a 1K incertitude on surface temperature.

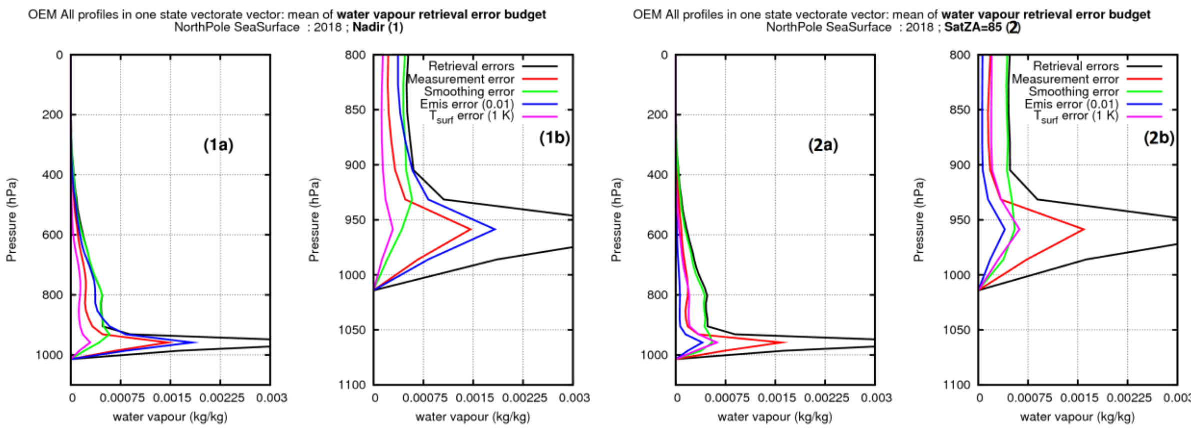

Figure 165: Mean retrieval error budget of water vapour profiles over North Pole and sea for (1) nadir and (2) for a SatZA of 85°. (Black) Retrieval error profile. (Red) Measurement error. (Green) Smoothing error. (Blue) Error induced by a 0.01 incertitude on emissivity. (Purple) Error induced by a 1K incertitude on surface temperature.

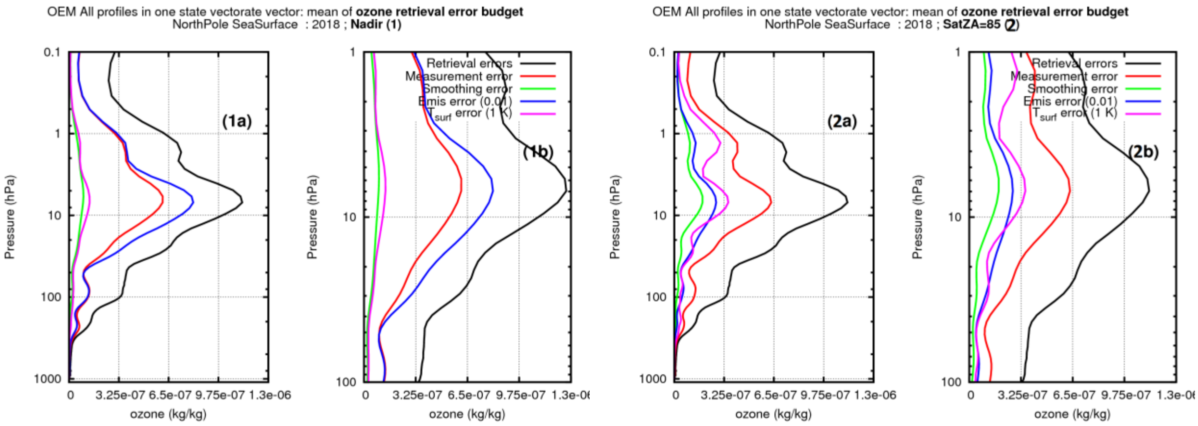

Figure 166: Mean retrieval error budget of ozone profiles over North Pole and sea for (1) nadir and (2) for a SatZA of 85°. (Black) Retrieval error profile. (Red) Measurement error. (Green) Smoothing error. (Blue) Error induced by a 0.01 incertitude on emissivity. (Purple) Error induced by a 1K incertitude on surface temperature.

2.2.8 Profile analysis: North Pole, over land

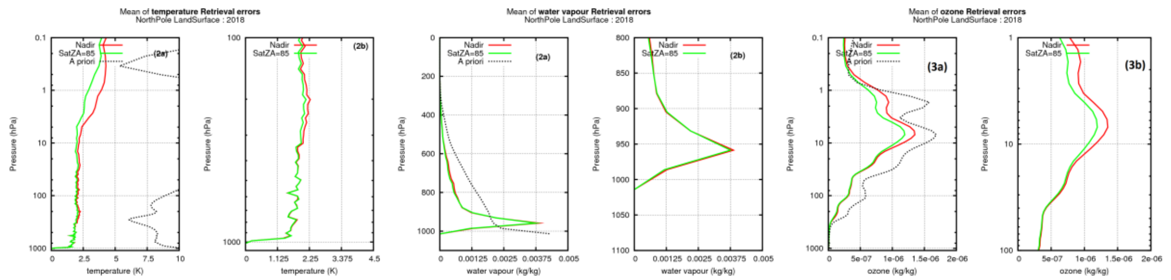

Figure 167: as Figure 139 over North Pole/land

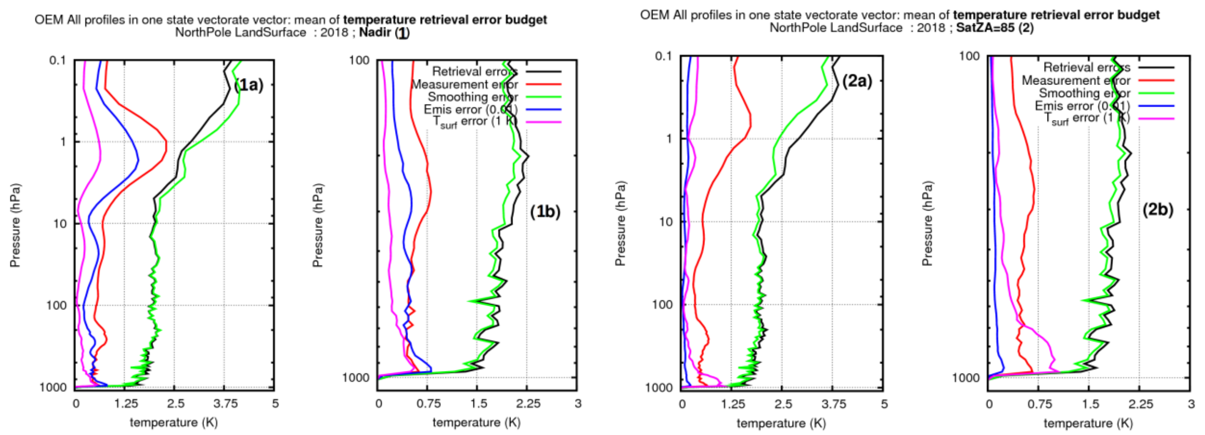

Figure 168: Mean retrieval error budget of temperature profiles over North Pole and land for (1) nadir and (2) for a SatZA of 85°. (Black) Retrieval error profile. (Red) Measurement error. (Green) Smoothing error. (Blue) Error induced by a 0.01 incertitude on emissivity. (Purple) Error induced by a 1K incertitude on surface temperature.

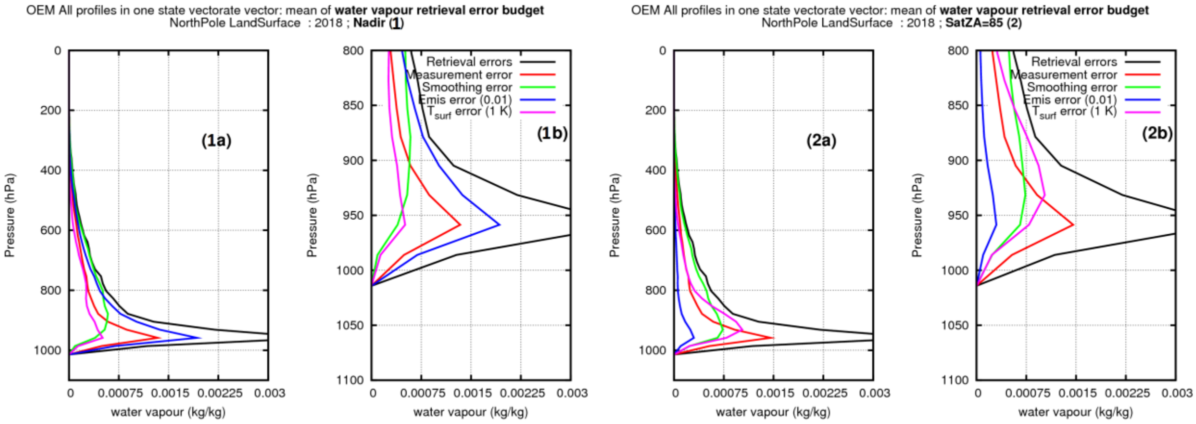

Figure 169: Mean retrieval error budget of water vapour profiles over North Pole and land for (1) nadir and (2) for a SatZA of 85°. (Black) Retrieval error profile. (Red) Measurement error. (Green) Smoothing error. (Blue) Error induced by a 0.01 incertitude on emissivity. (Purple) Error induced by a 1K incertitude on surface temperature.

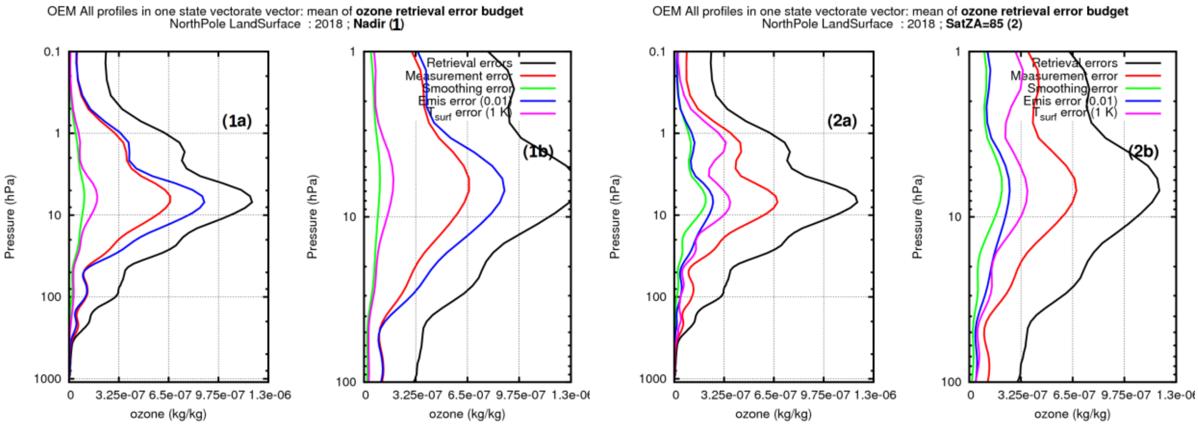

Figure 170: Mean retrieval error budget of ozone profiles over North Pole and land for (1) nadir and (2) for a SatZA of 85°. (Black) Retrieval error profile. (Red) Measurement error. (Green) Smoothing error. (Blue) Error induced by a 0.01 incertitude on emissivity. (Purple) Error induced by a 1K incertitude on surface temperature.

2.2.9 Profile analysis: South Pole, over sea

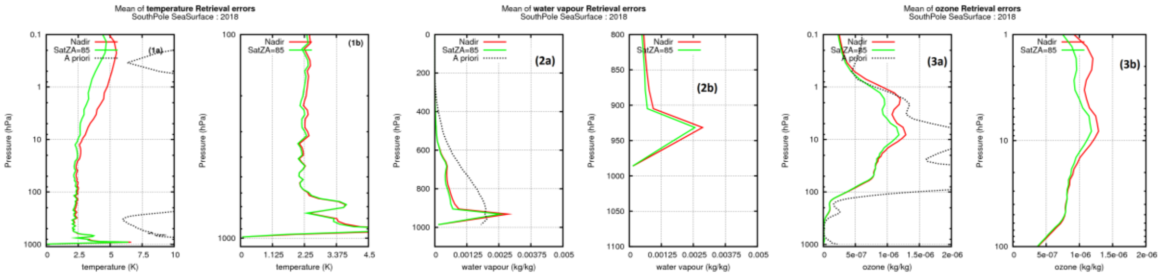

Figure 171: as Figure 139 over South Pole/sea

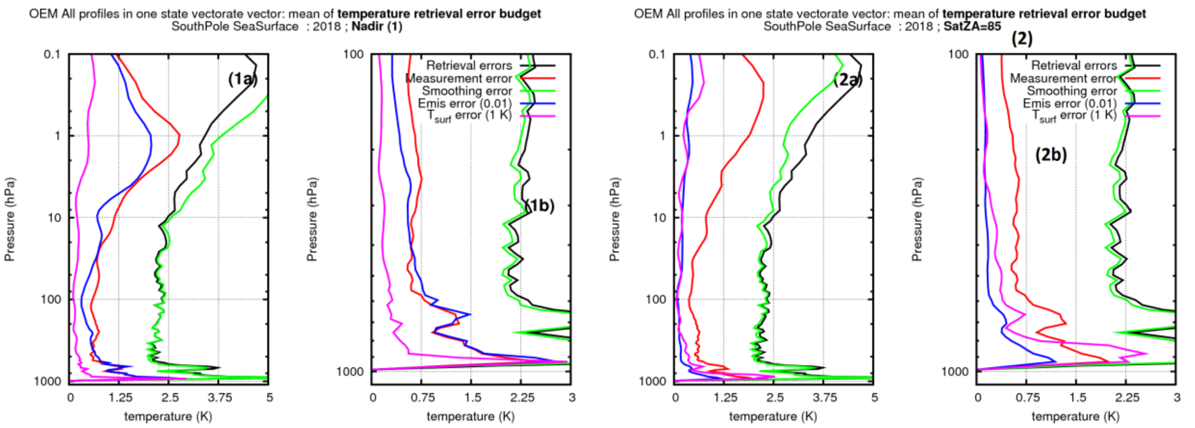

Figure 172: Mean retrieval error budget of temperature profiles over South Pole and sea for (1) nadir and (2) for a SatZA of 85°. (Black) Retrieval error profile. (Red) Measurement error. (Green) Smoothing error. (Blue) Error induced by a 0.01 incertitude on emissivity. (Purple) Error induced by a 1K incertitude on surface temperature.

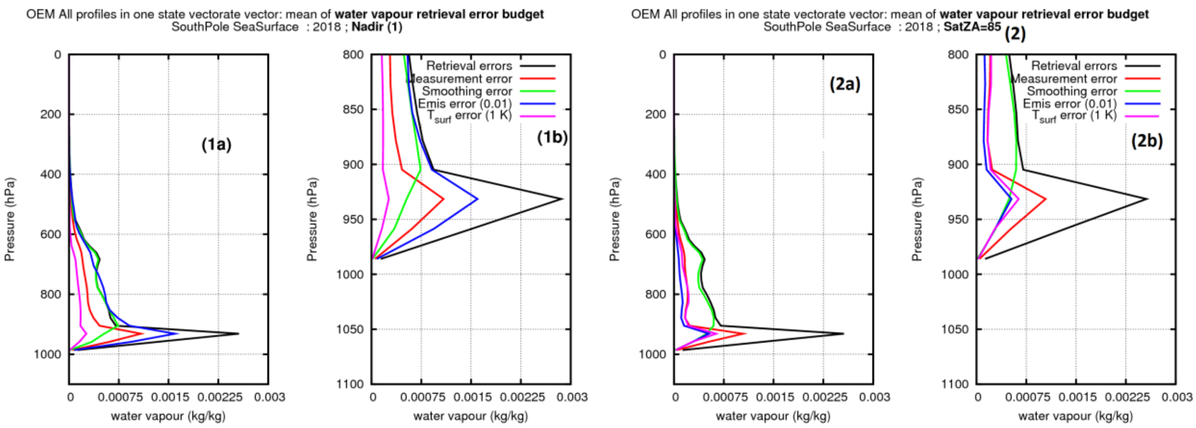

Figure 173: Mean retrieval error budget of water vapour profiles over South Pole and sea for (1) nadir and (2) for a SatZA of 85°. (Black) Retrieval error profile. (Red) Measurement error. (Green) Smoothing error. (Blue) Error induced by a 0.01 incertitude on emissivity. (Purple) Error induced by a 01K incertitude on surface temperature.

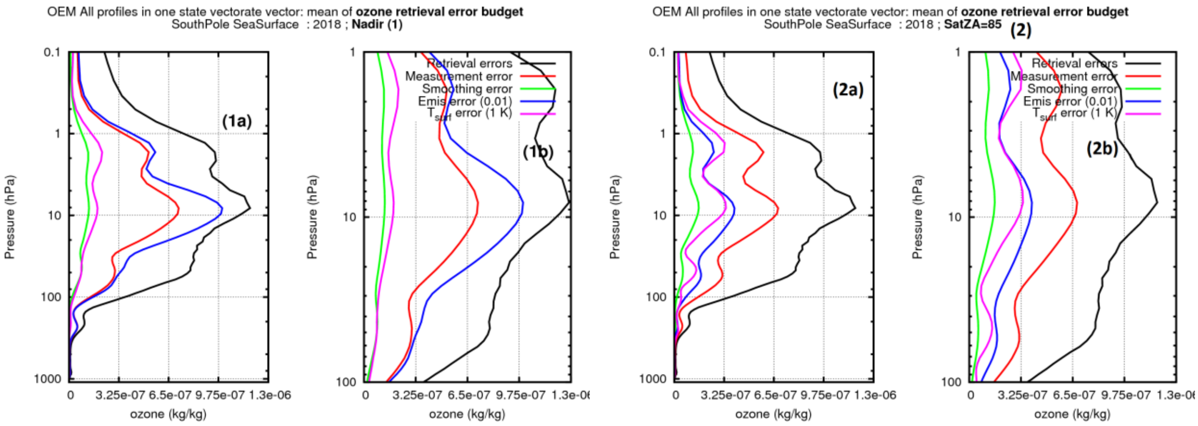

Figure 174: Mean retrieval error budget of ozone profiles over South Pole and sea for (1) nadir and (2) for a SatZA of 85°. (Black) Retrieval error profile. (Red) Measurement error. (Green) Smoothing error. (Blue) Error induced by a 0.01 incertitude on emissivity. (Purple) Error induced by a 1K incertitude on surface temperature.

2.2.10 Profile analysis: South Pole, over land

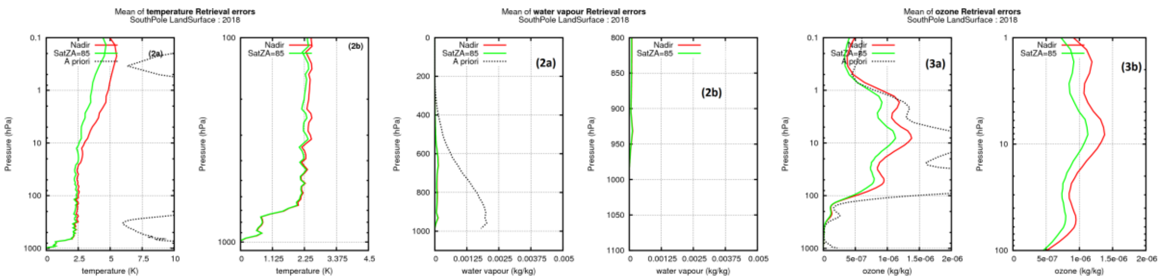

Figure 175: as Figure 139 over South Pole/land

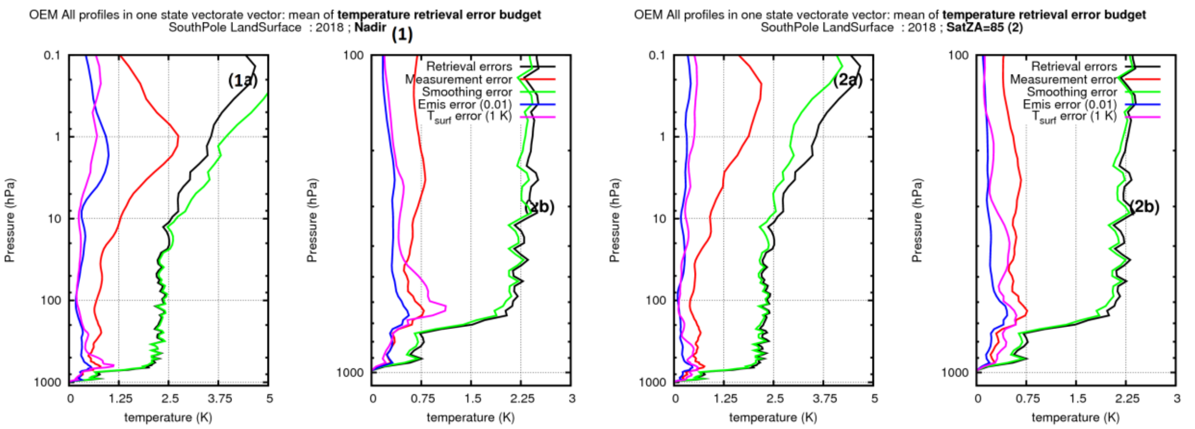

Figure 176: Mean retrieval error budget of temperature profiles over South Pole and land for (1) nadir and (2) for a SatZA of 85°. (Black) Retrieval error profile. (Red) Measurement error. (Green) Smoothing error. (Blue) Error induced by a 0.01 incertitude on emissivity. (Purple) Error induced by a 1K incertitude on surface temperature.

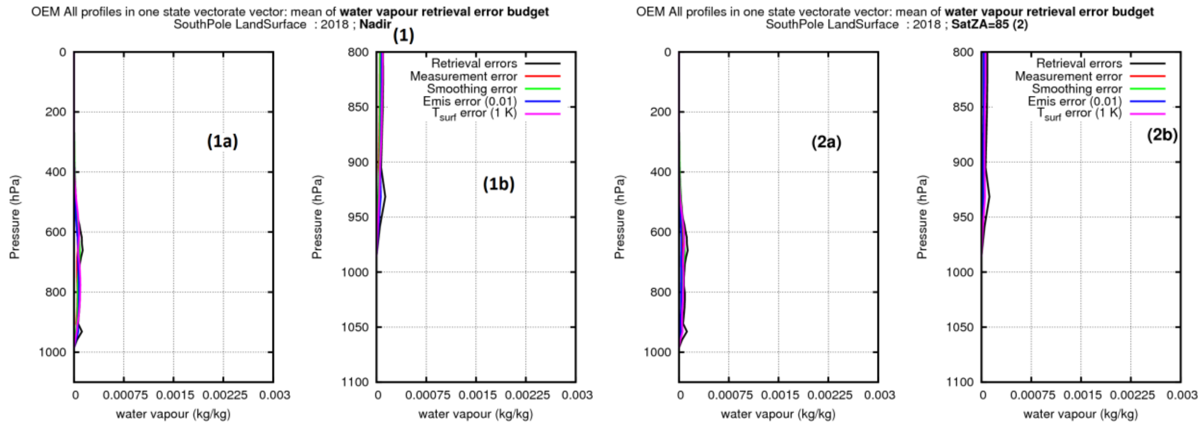

Figure 177: Mean retrieval error budget of water vapour profiles over South Pole and land for (1) nadir and (2) for a SatZA of 85°. (Black) Retrieval error profile. (Red) Measurement error. (Green) Smoothing error. (Blue) Error induced by a 0.01 incertitude on emissivity. (Purple) Error induced by a 1K incertitude on surface temperature.

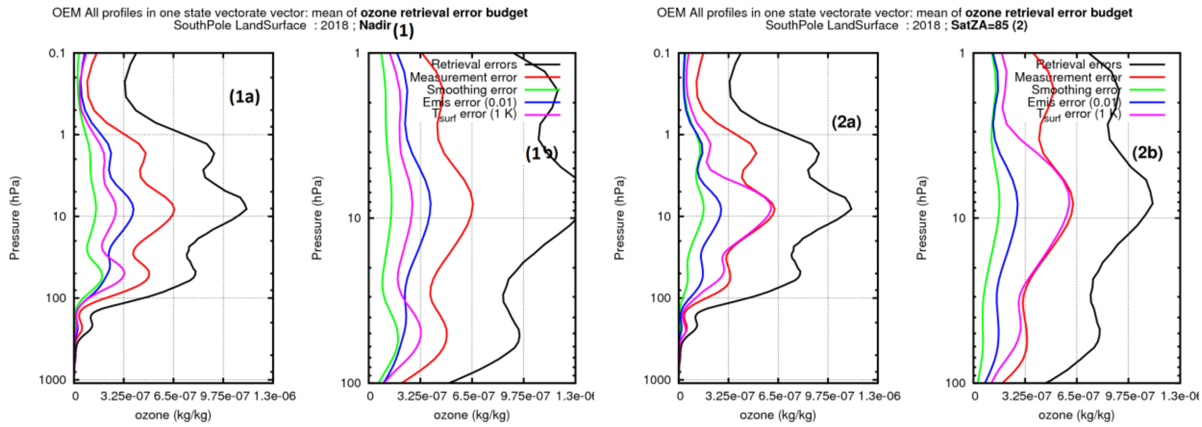

Figure 178: Mean retrieval error budget of ozone profiles over South Pole and land for (1) nadir and (2) for a SatZA of 85°. (Black) Retrieval error profile. (Red) Measurement error. (Green) Smoothing error. (Blue) Error induced by a 0.01 incertitude on emissivity. (Purple) Error induced by a 1K incertitude on surface temperature.

3 ANNEXE C – ALL FIGURES OF AVERAGING KERNELS AND DOFS

3.1 TEMPERATURE

3.1.1 Tropics over sea

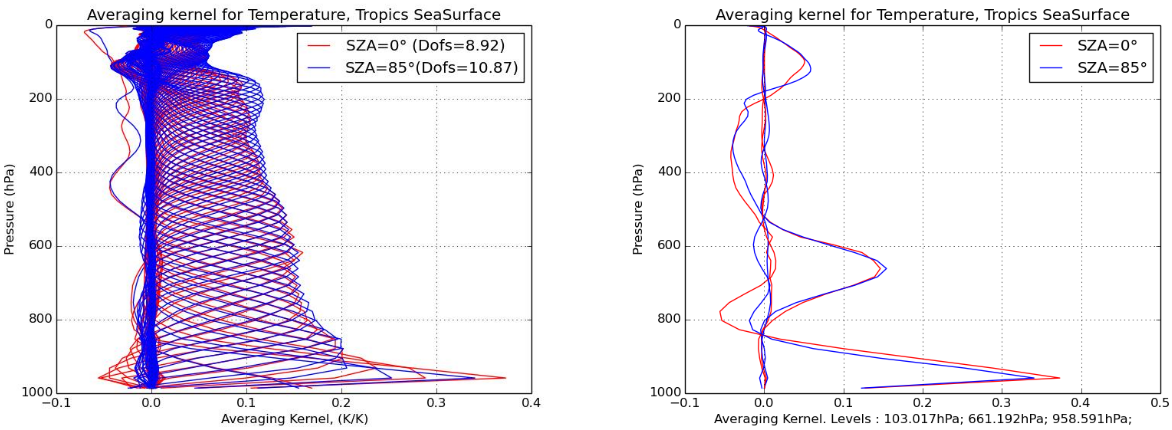

Figure 179: Annual mean of the Averaging Kernels of the temperature in the tropics over sea at Nadir (in red) and for 85° (in blue). Left side panel: all levels and corresponding DOFS; right side panel: levels where the contrast between the two viewing angles is the highest in each selected sub-column ([surface-700], [700-300], [300-100] hPa); the corresponding pressure value of each level is also provided in the x-axis text box.

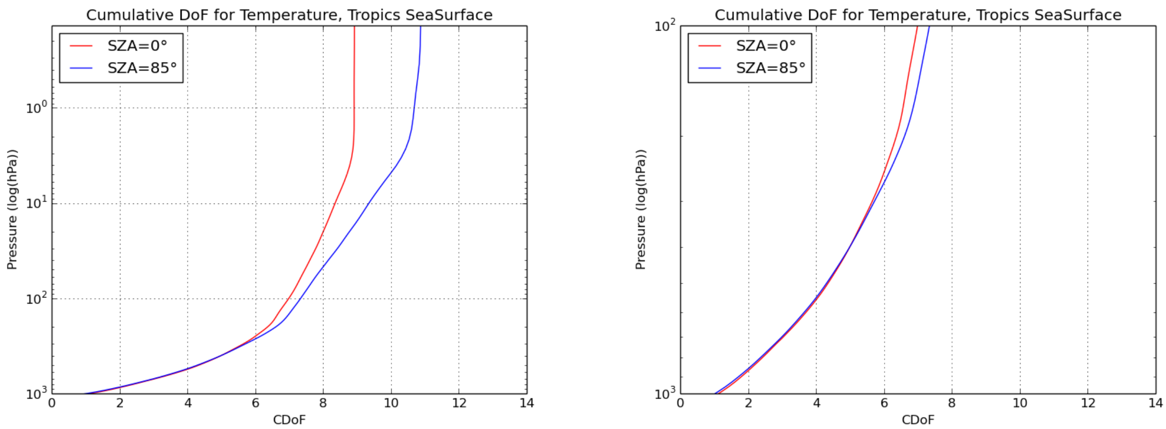

Figure 180: Annual mean of the cumulative DoF of the temperature in the tropics over sea at Nadir (in red) and for 85° (in blue). Left side panel: all levels; right side panel: zoom in the mid-troposphere.

3.1.2 Tropics over land

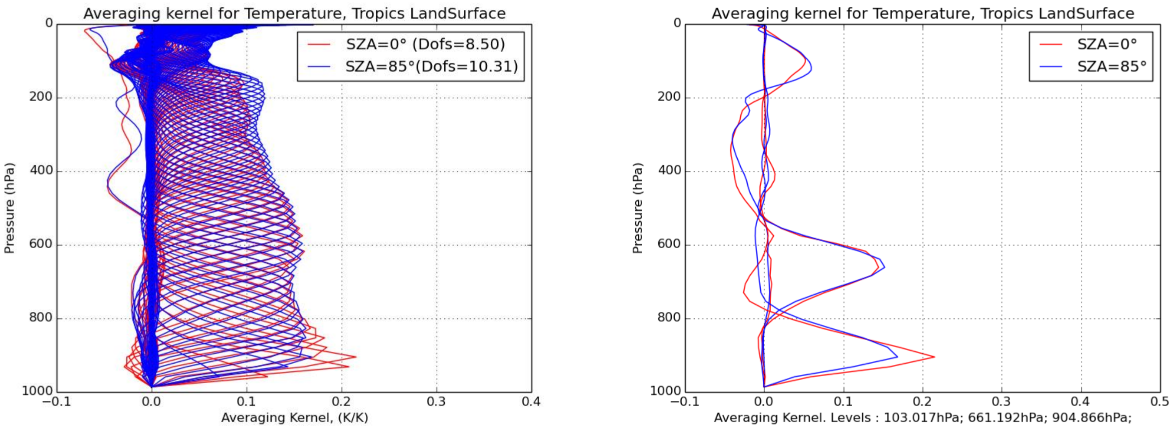

Figure 181: Same as Figure 179 over land.

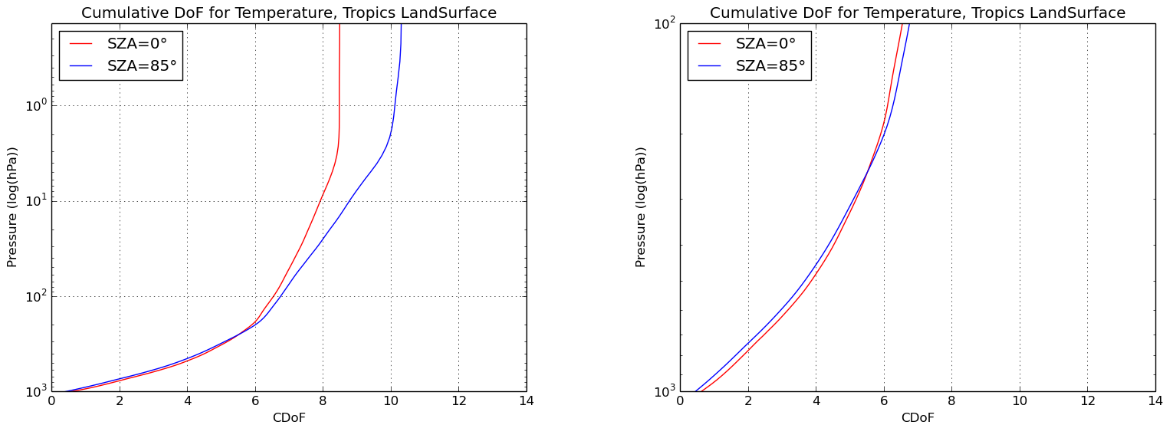

Figure 182: Same as Figure 180 over land.

3.1.3 Northern Mid-latitudes over sea

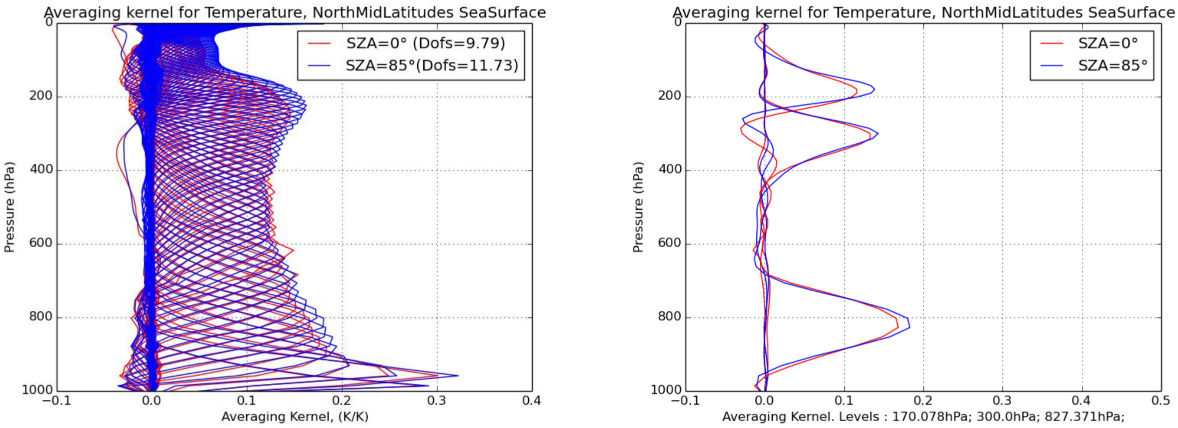

Figure 183: Same as Figure 179 in the Northern Mid-latitudes over sea.

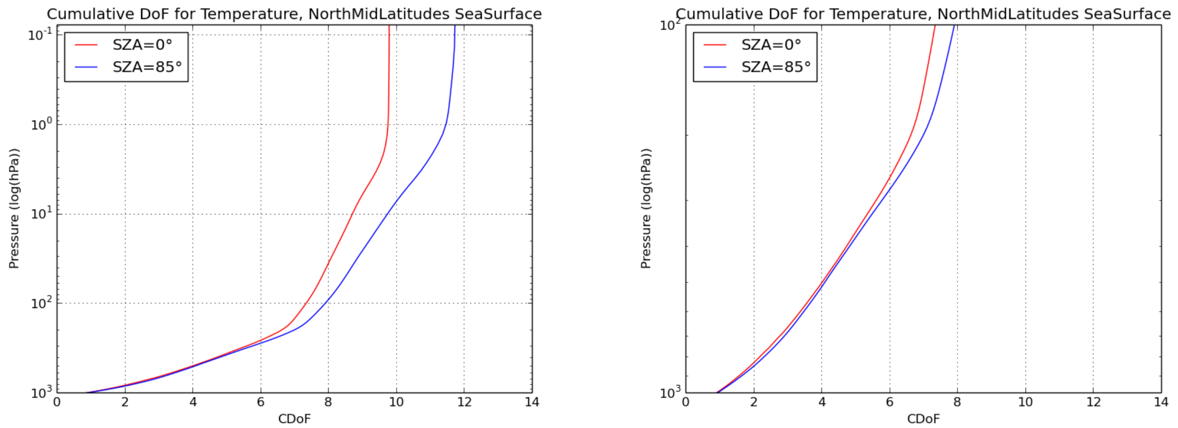

Figure 184: Same as Figure 180 in the Northern Mid-latitudes over sea.

3.1.4 Northern Mid-latitudes over land

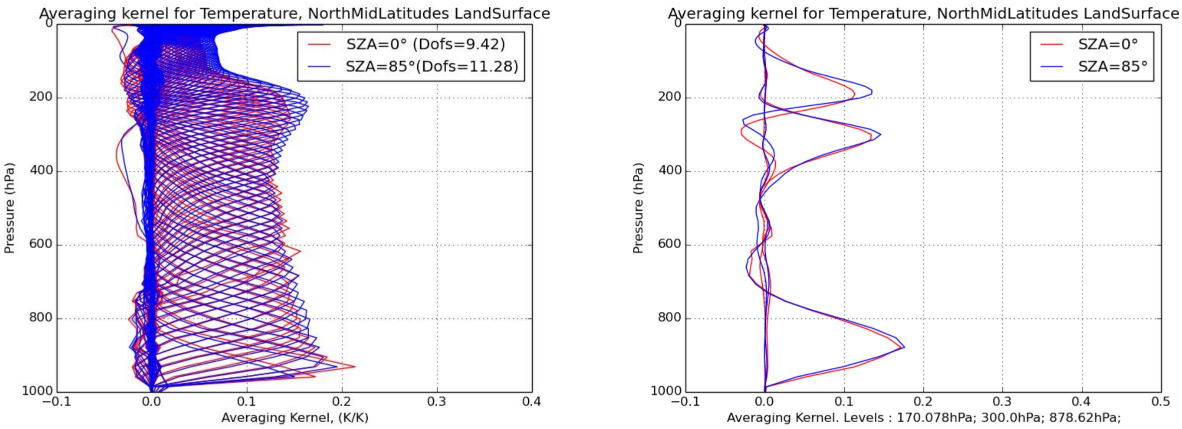

Figure 185: Same as Figure 179 in the Northern Mid-latitudes over land.

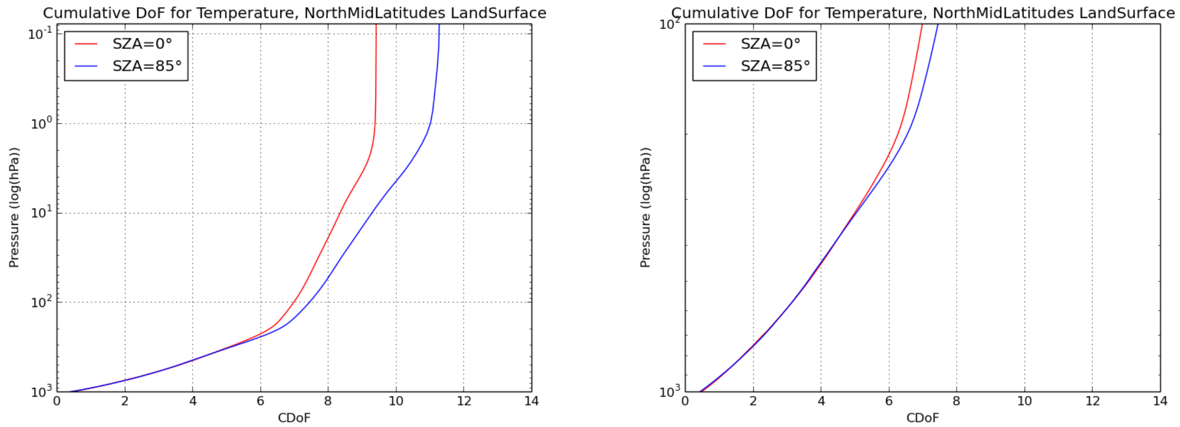

Figure 186: Same as Figure 180 in the Northern Mid-latitudes over land.

3.1.5 Southern Mid-latitudes over sea

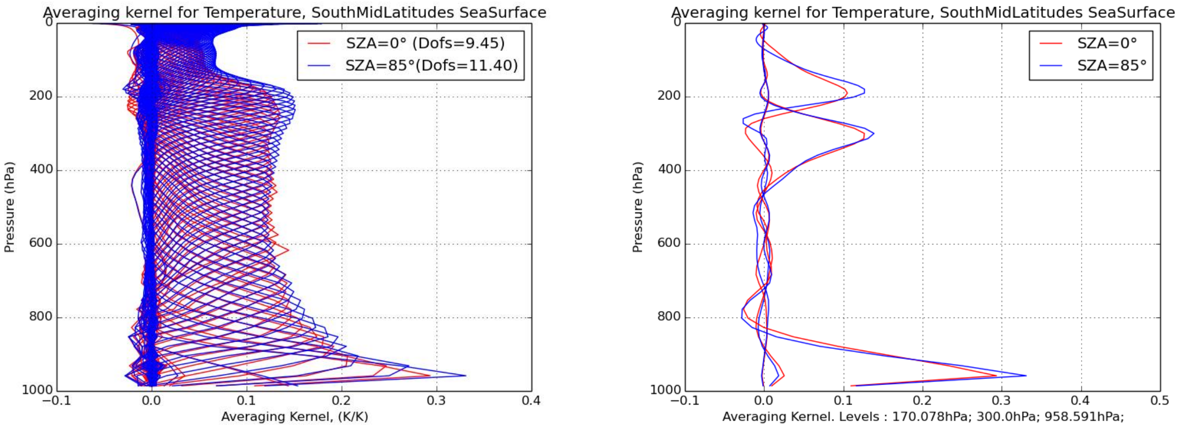

Figure 187: Same as Figure 179 in the Southern Mid-latitudes over sea.

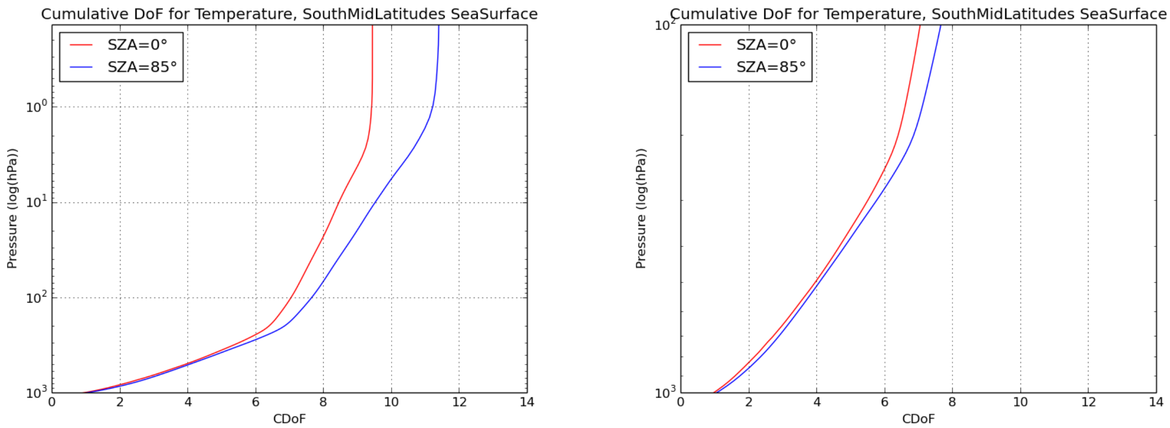

Figure 188: Same as Figure 180 in the Southern Mid-latitudes over sea.

3.1.6 Southern Mid-latitudes over land

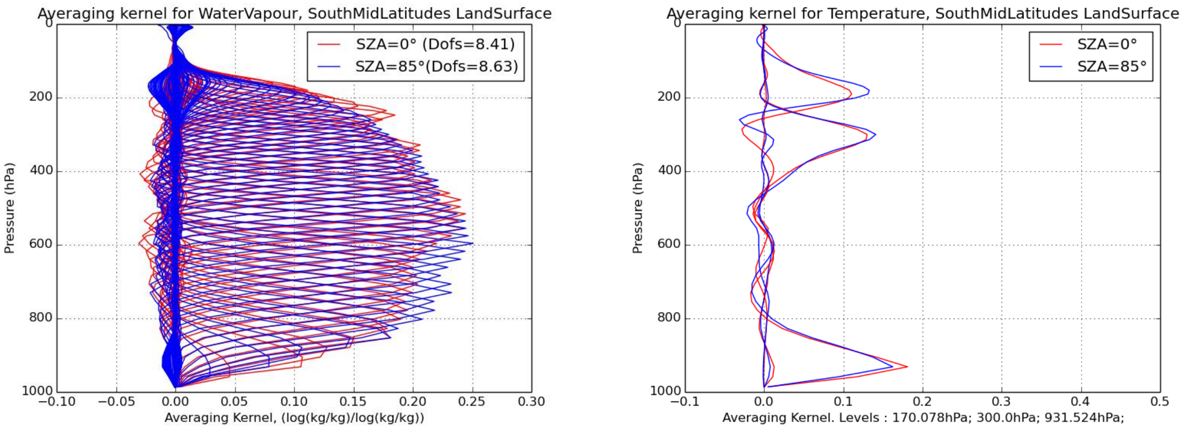

Figure 189: Same as Figure 179 in the Southern Mid-latitudes over land.

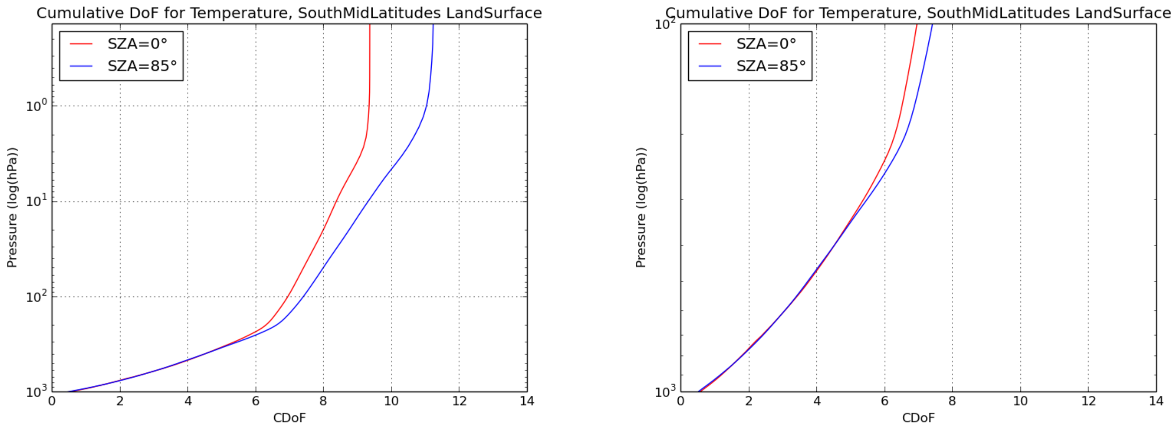

Figure 190: Same as Figure 180 in the Southern Mid-latitudes over land.

3.1.7 North Pole over sea

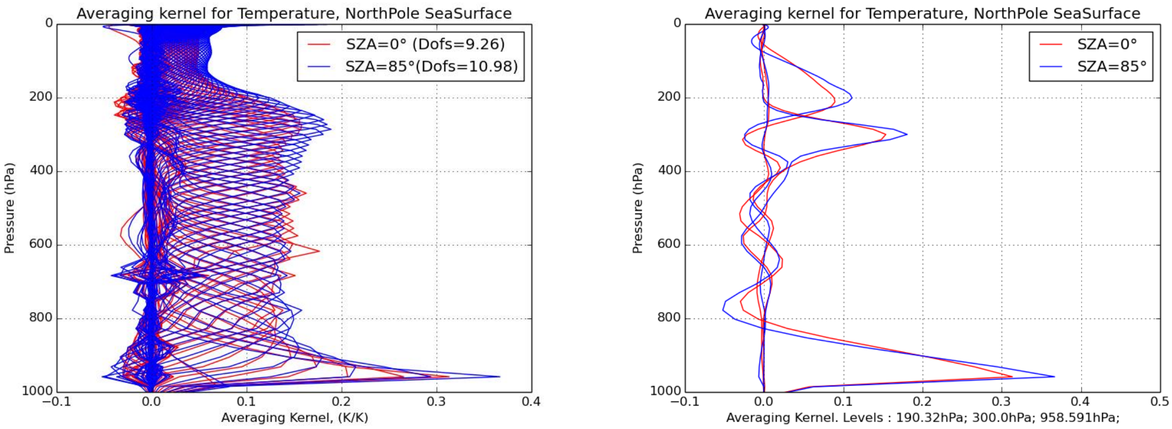

Figure 191: Same as Figure 179 in the North Pole over sea.

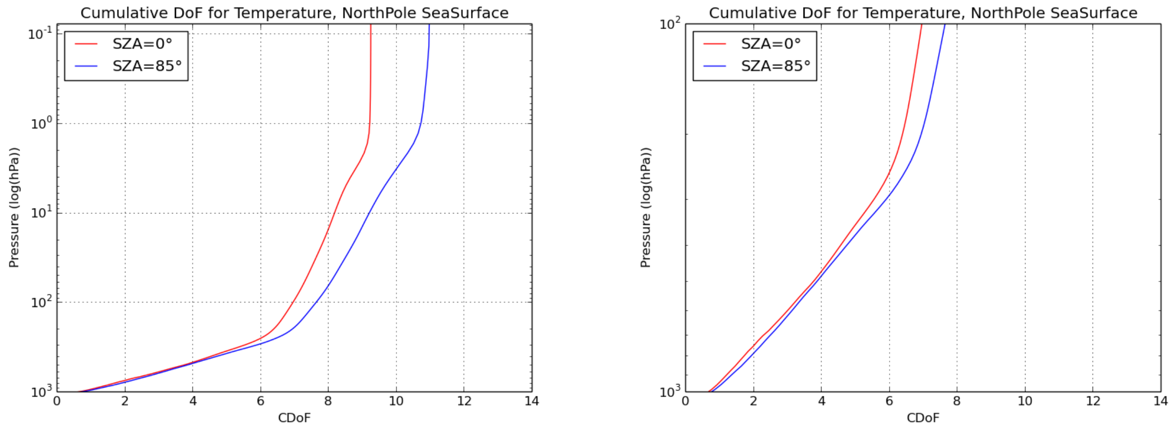

Figure 192: Same as Figure 180 in the North Pole over sea.

3.1.8 North Pole over land

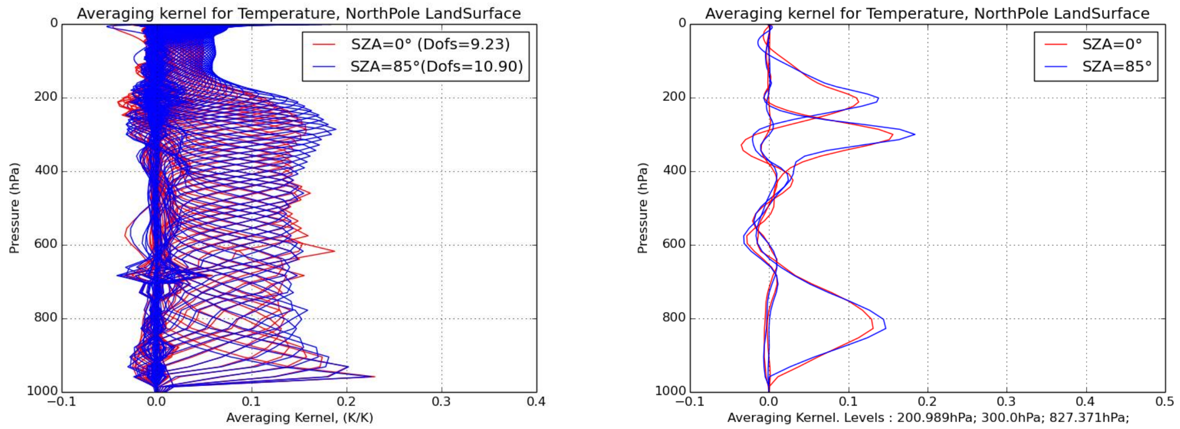

Figure 193: Same as Figure 179 in the North Pole over land.

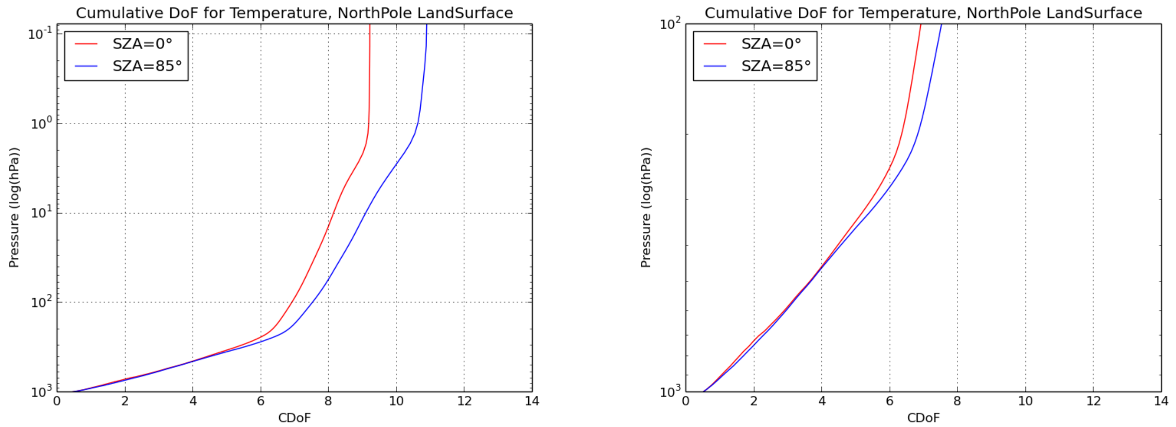

Figure 194: Same as Figure 180 in the North Pole over land.

3.1.9 South Pole over sea

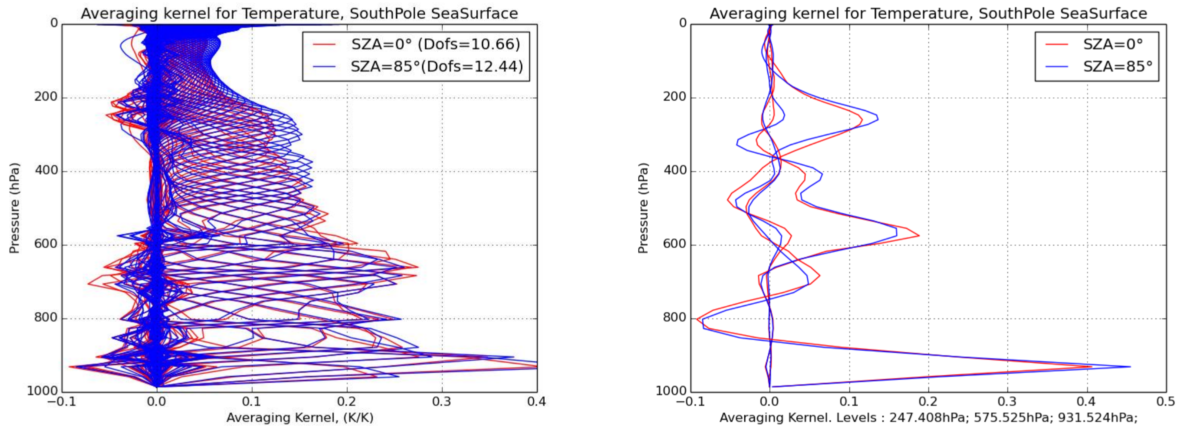

Figure 195: Same as Figure 179 in the South Pole over sea.

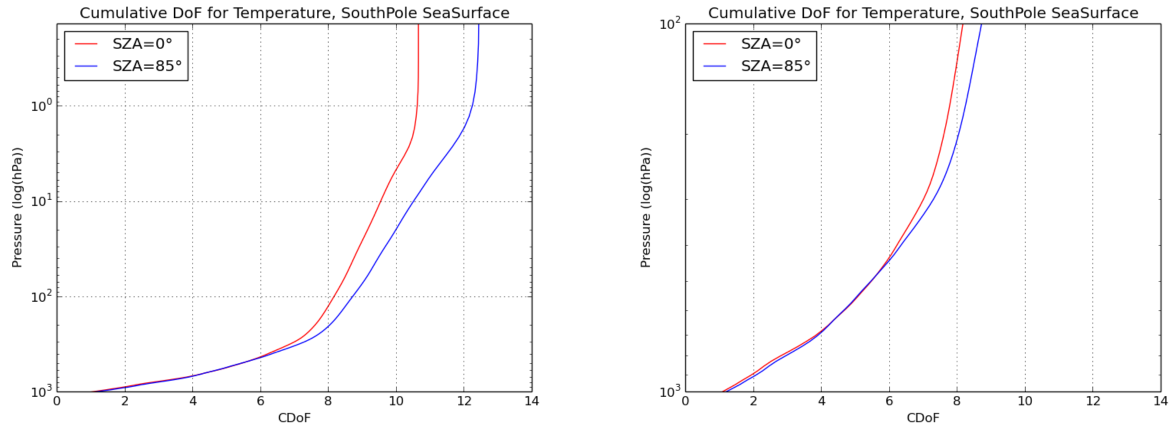

Figure 196: Same as Figure 180 in the South Pole over sea.

3.1.10 South Pole over land

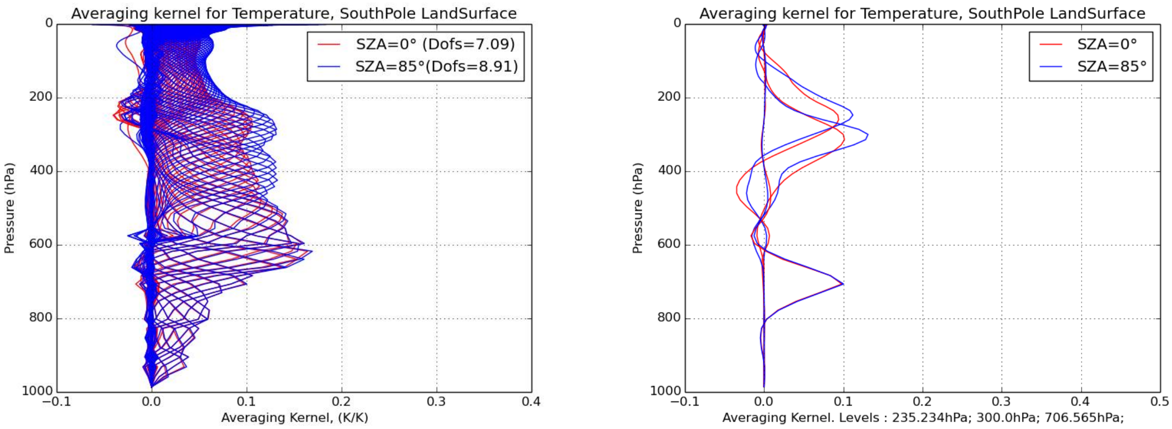

Figure 197: Same as Figure 179 in the South Pole over land.

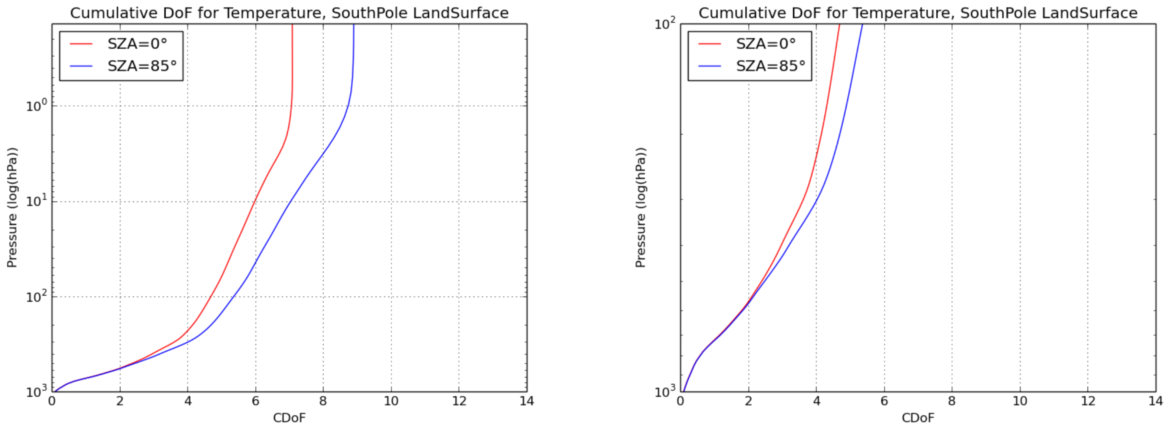

Figure 198: Same as Figure 180 in the South Pole over land.

3.2 WATER VAPOUR

3.2.1 Tropics over sea

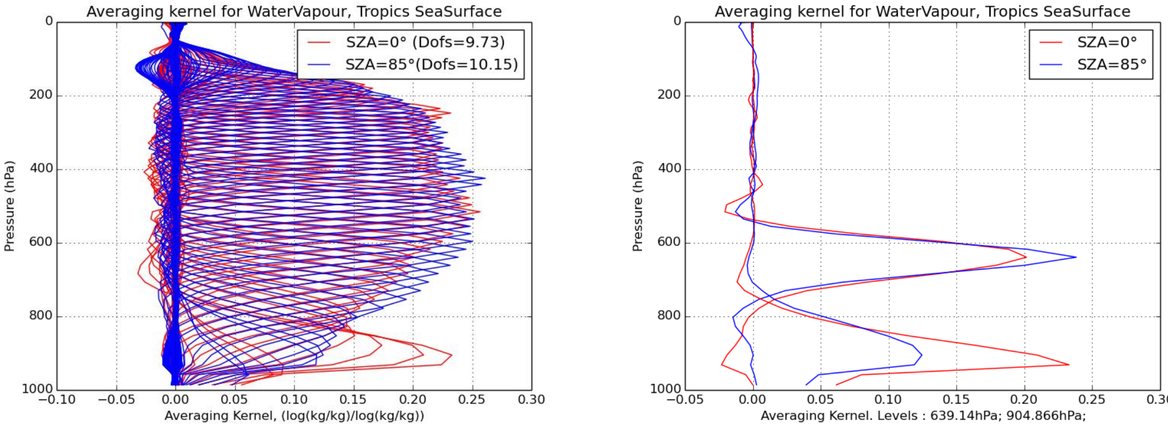

Figure 199: Same as Figure 179 for the water vapour.

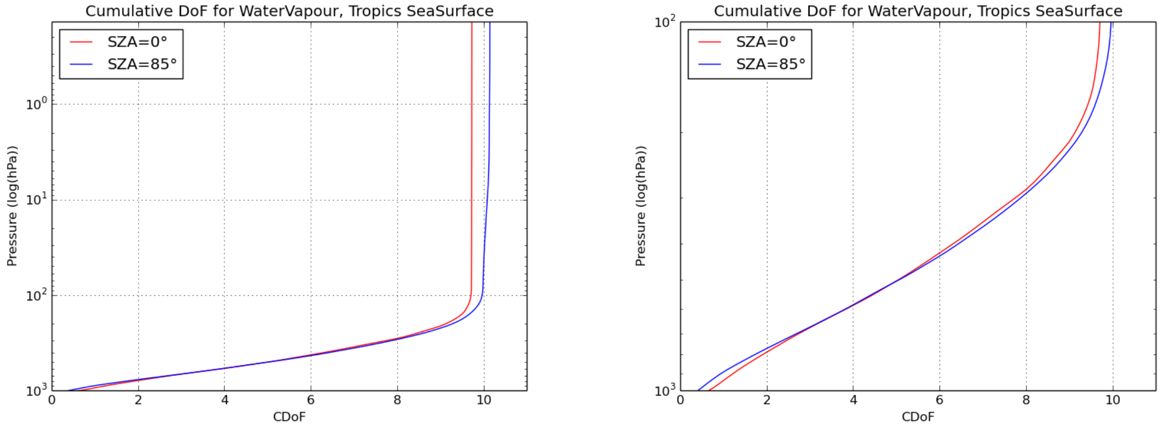

Figure 200: Same as Figure 180 for the water vapour.

3.2.2 Tropics over land

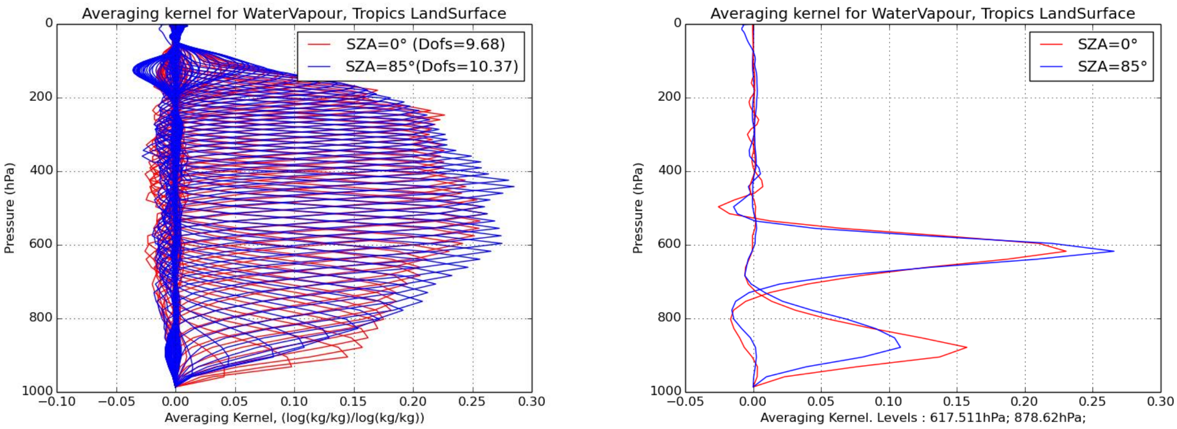

Figure 201: Same as Figure 199 over land.

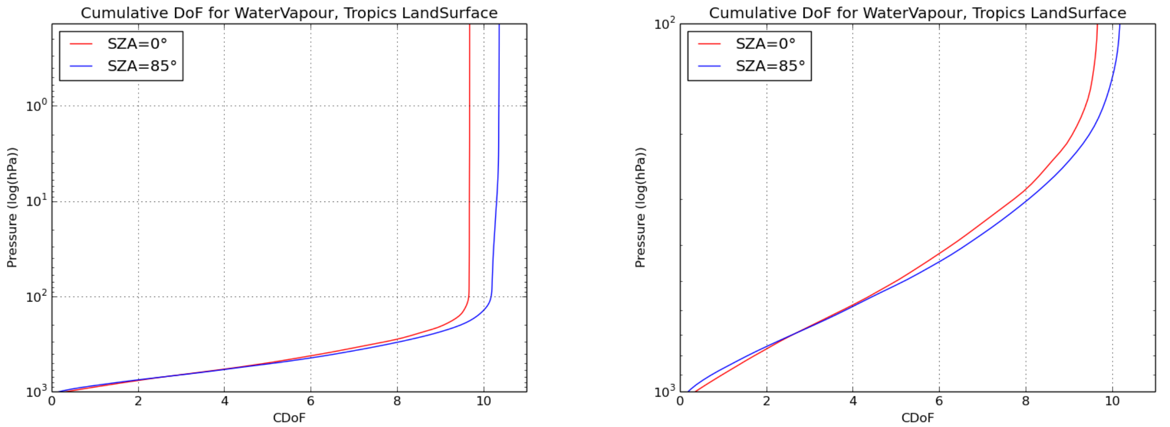

Figure 202: Same as Figure 200 over land.

3.2.3 Northern Mid-latitudes over sea

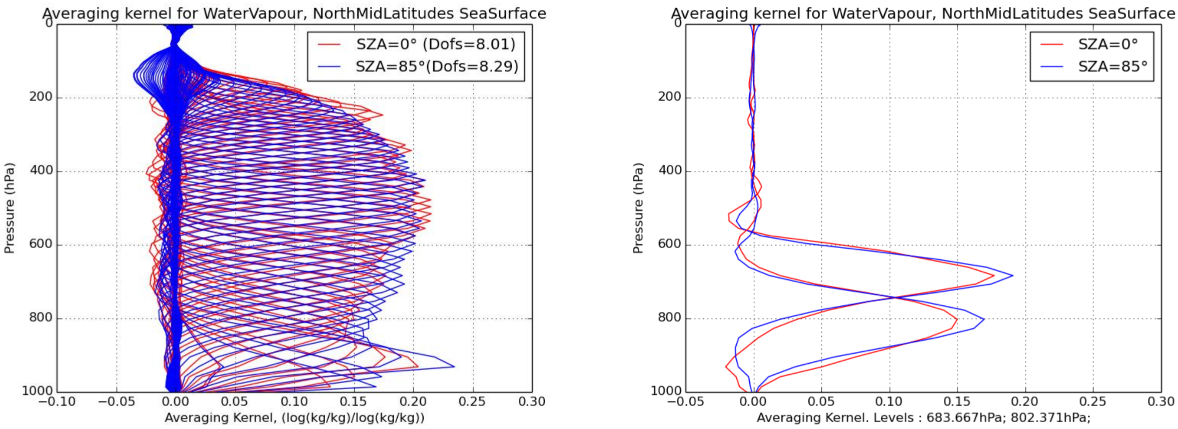

Figure 203: Same as Figure 199 in the Northern Mid-latitudes over sea.

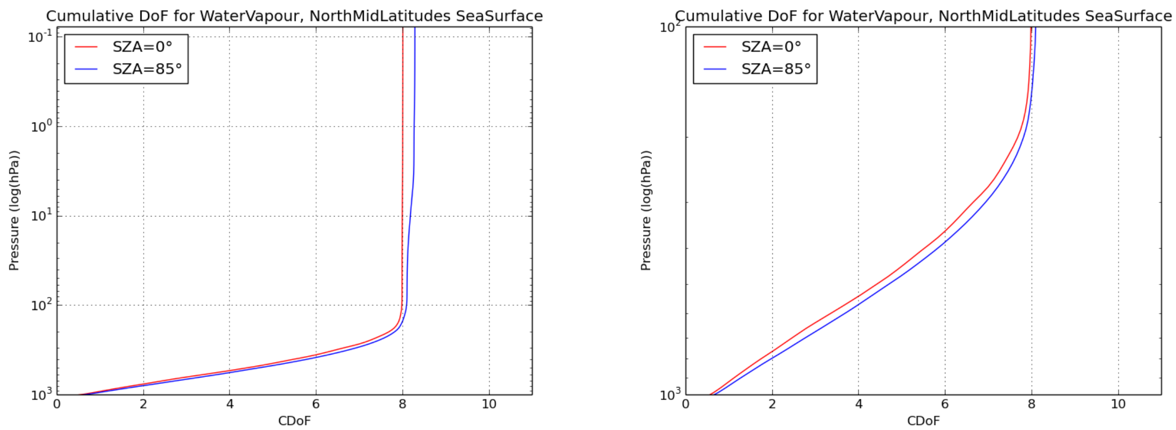

Figure 204: Same as Figure 200 in the Northern Mid-latitudes over sea.

3.2.4 Northern Mid-latitudes over land

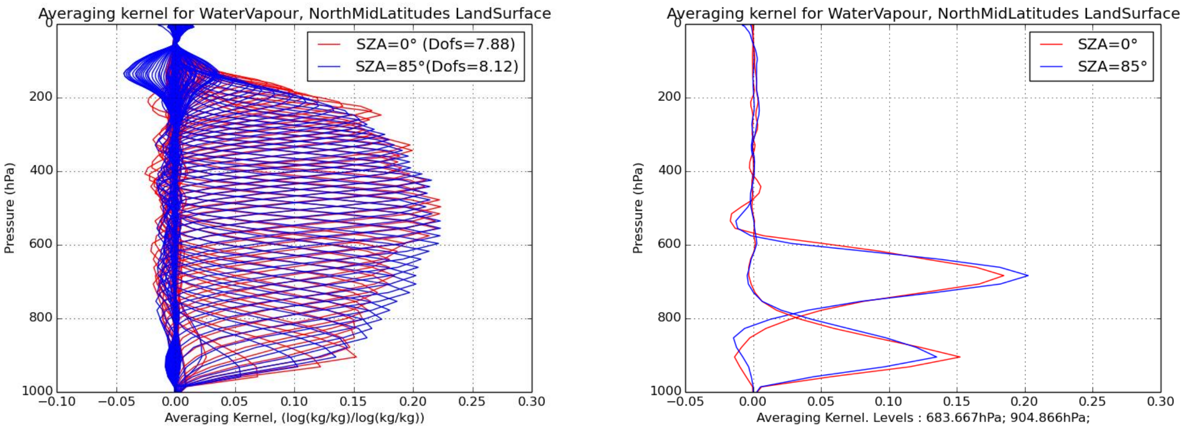

Figure 205: Same as Figure 199 in the Northern Mid-latitudes over land.

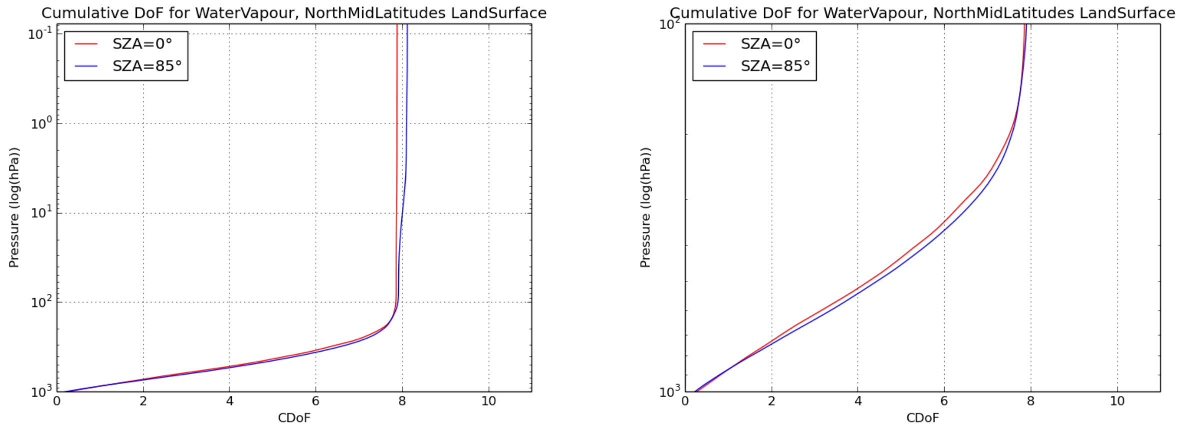

Figure 206: Same as Figure 200 in the Northern Mid-latitudes over land.

3.2.5 Southern Mid-latitudes over sea

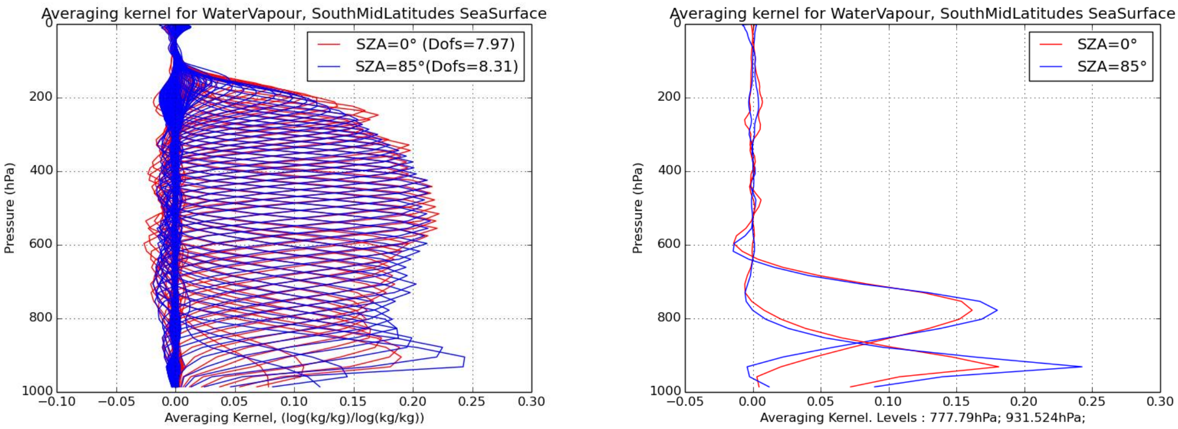

Figure 207: Same as Figure 199 in the Southern Mid-latitudes over sea.

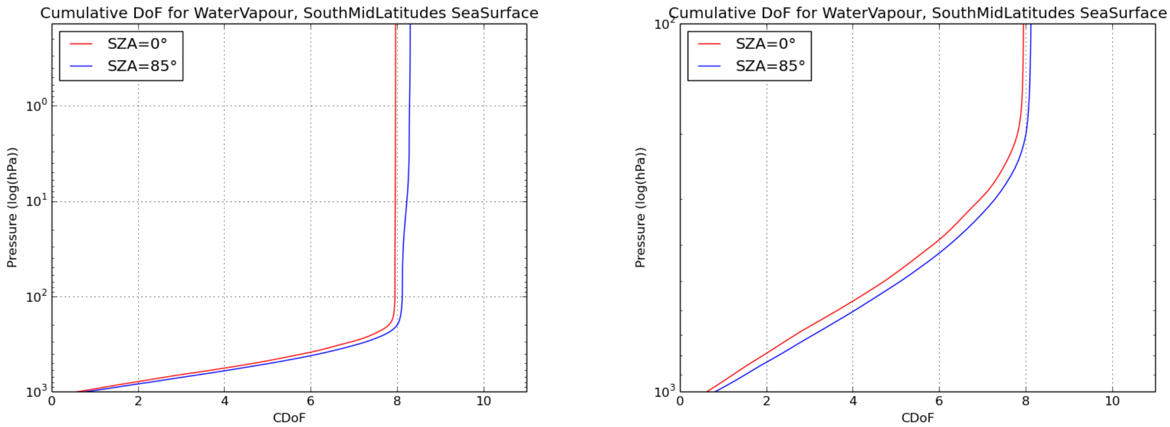

Figure 208: Same as Figure 200 in the Southern Mid-latitudes over sea.

3.2.6 Southern Mid-latitudes over land

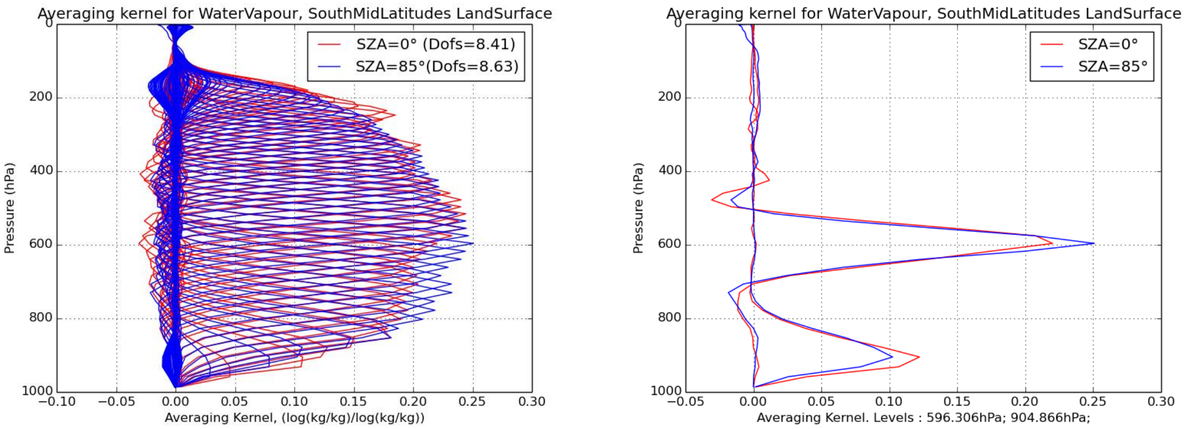

Figure 209: Same as Figure 199 in the Southern Mid-latitudes over land.

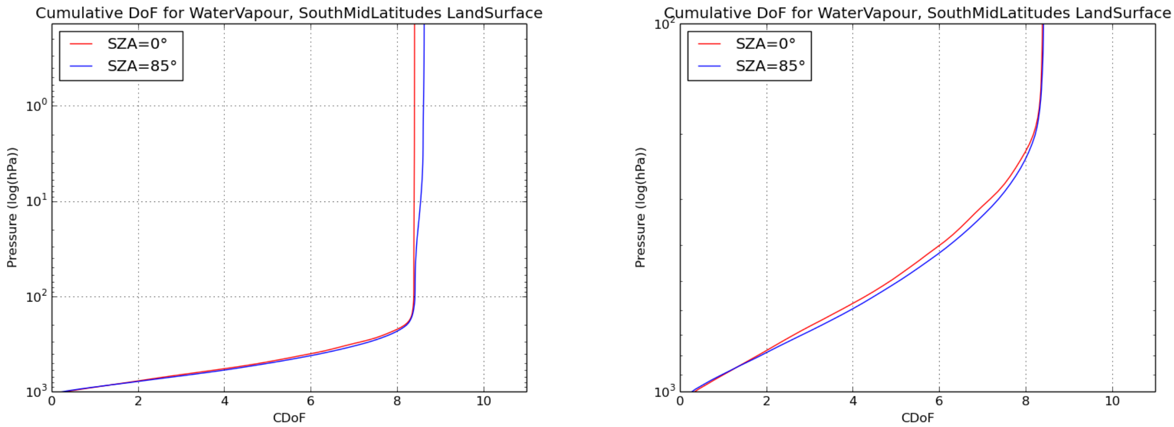

Figure 210: Same as Figure 200 in the Southern Mid-latitudes over land.

3.2.7 North Pole over sea

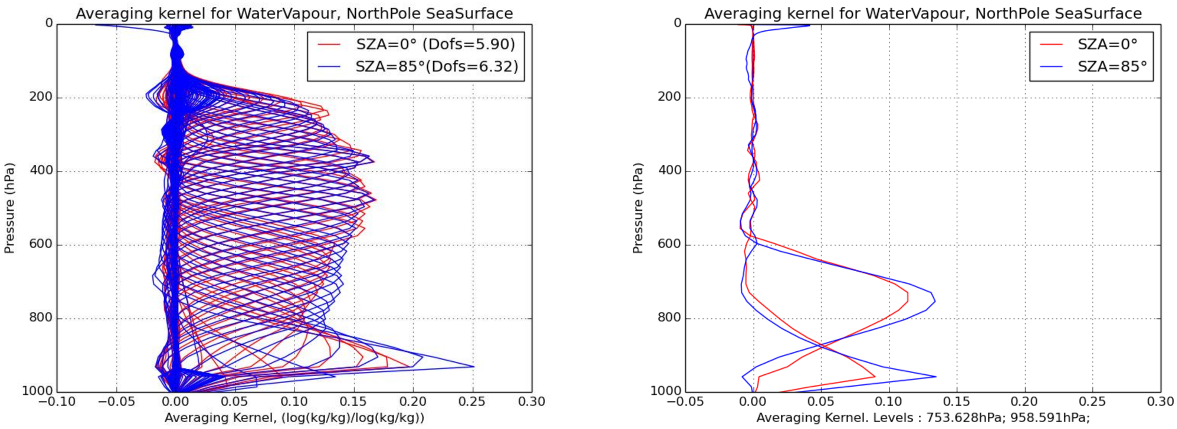

Figure 211: Same as Figure 199 in the North Pole over sea.

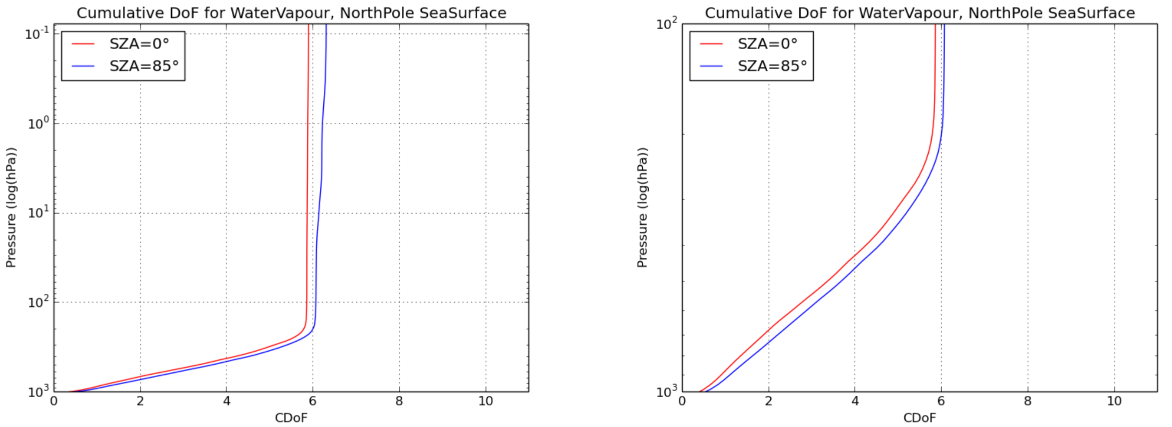

Figure 212: Same as Figure 200 in the North Pole over sea.

3.2.8 North Pole over land

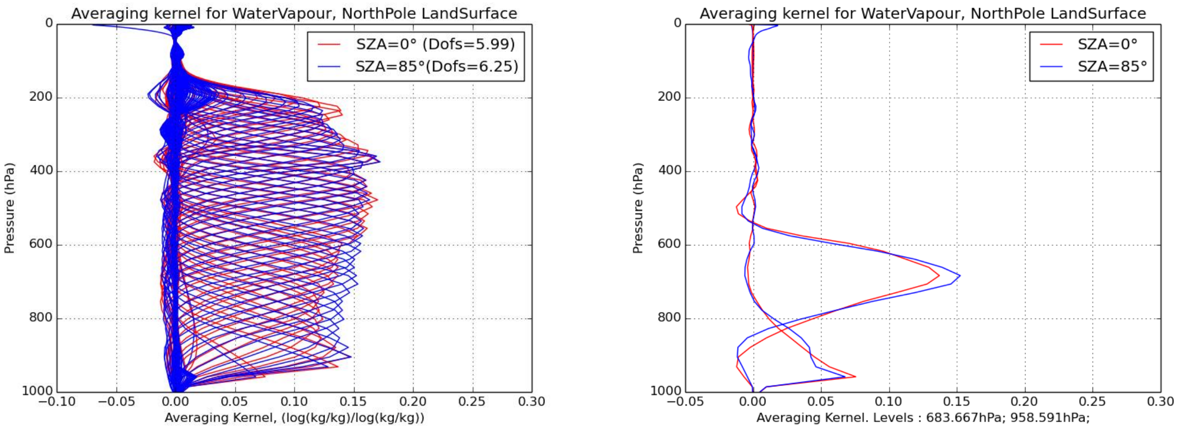

Figure 213: Same as Figure 199 in the North Pole over land.

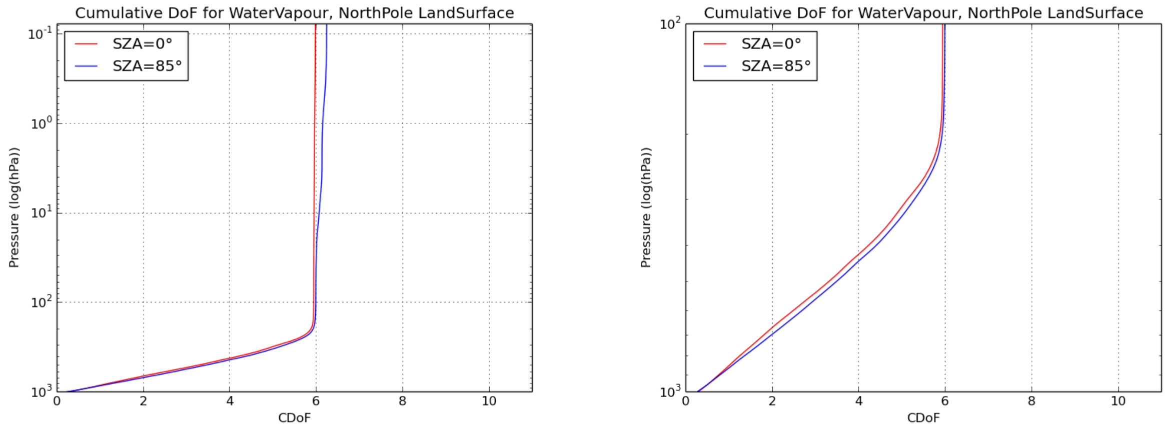

Figure 214: Same as Figure 200 in the North Pole over land.

3.2.9 South Pole over sea

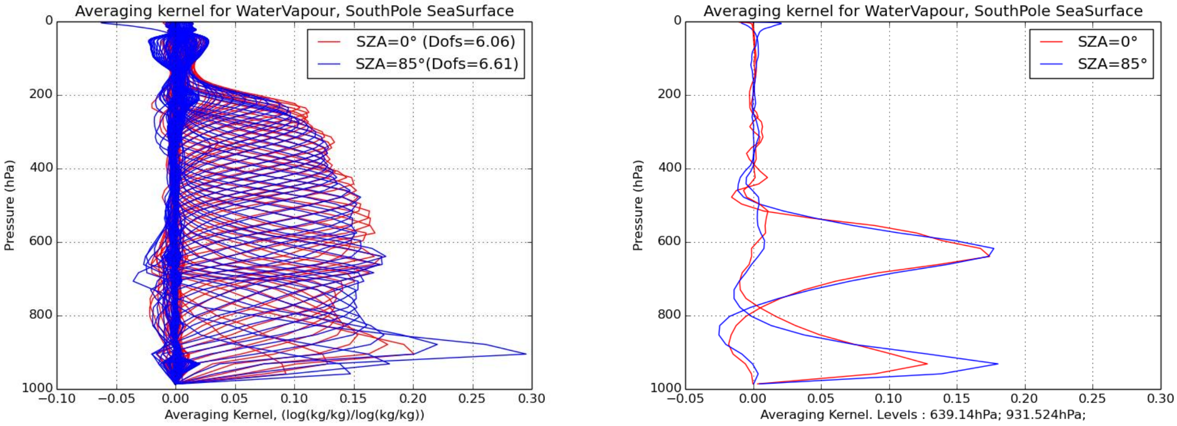

Figure 215: Same as Figure 199 in the South Pole over sea.

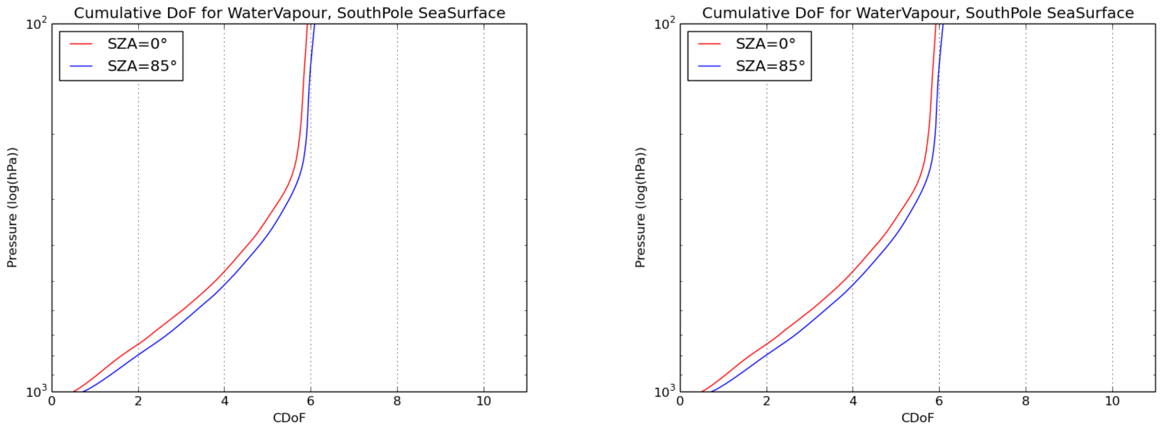

Figure 216: Same as Figure 200 in the South Pole over sea.

3.2.10 South Pole over land

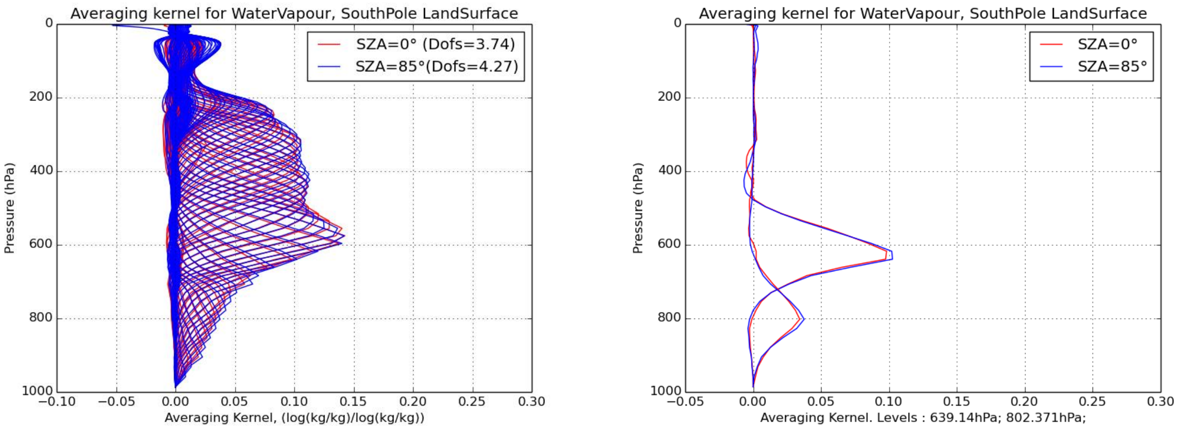

Figure 217: Same as Figure 199 in the South Pole over land.

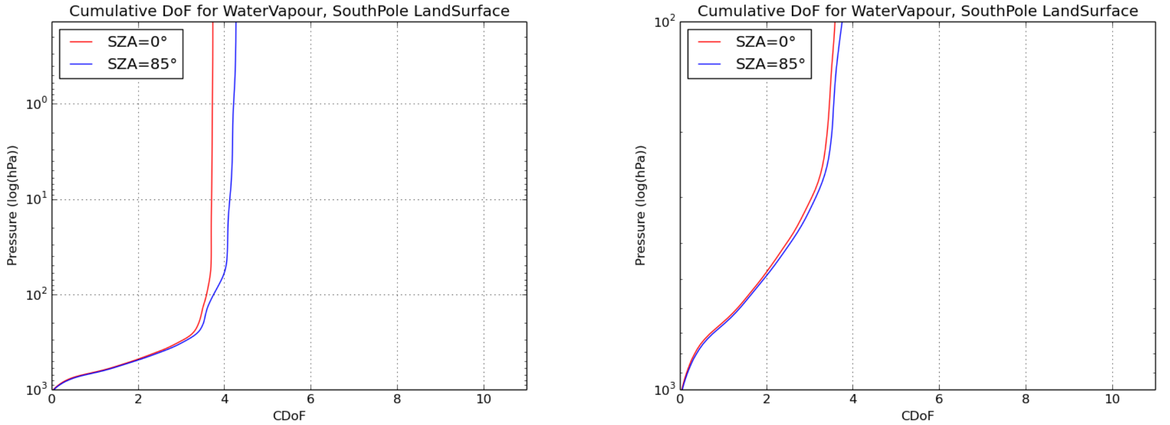

Figure 218: Same as Figure 200 in the South Pole over land.

3.3 OZONE

3.3.1 Tropics over sea

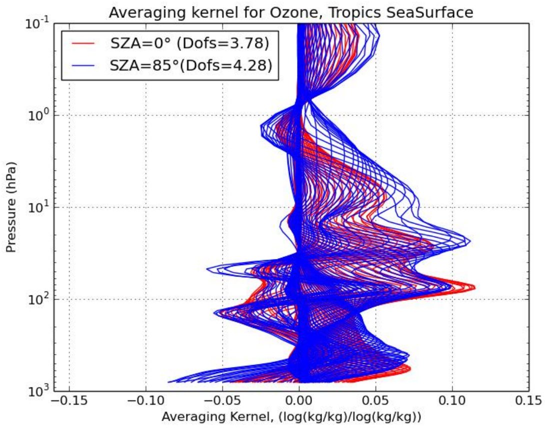

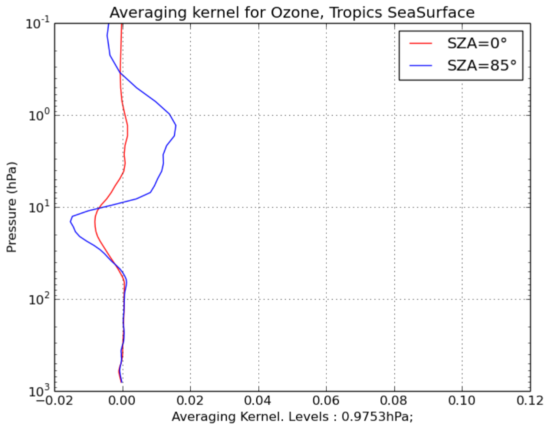

Figure 219: Same as Figure 179 for ozone.

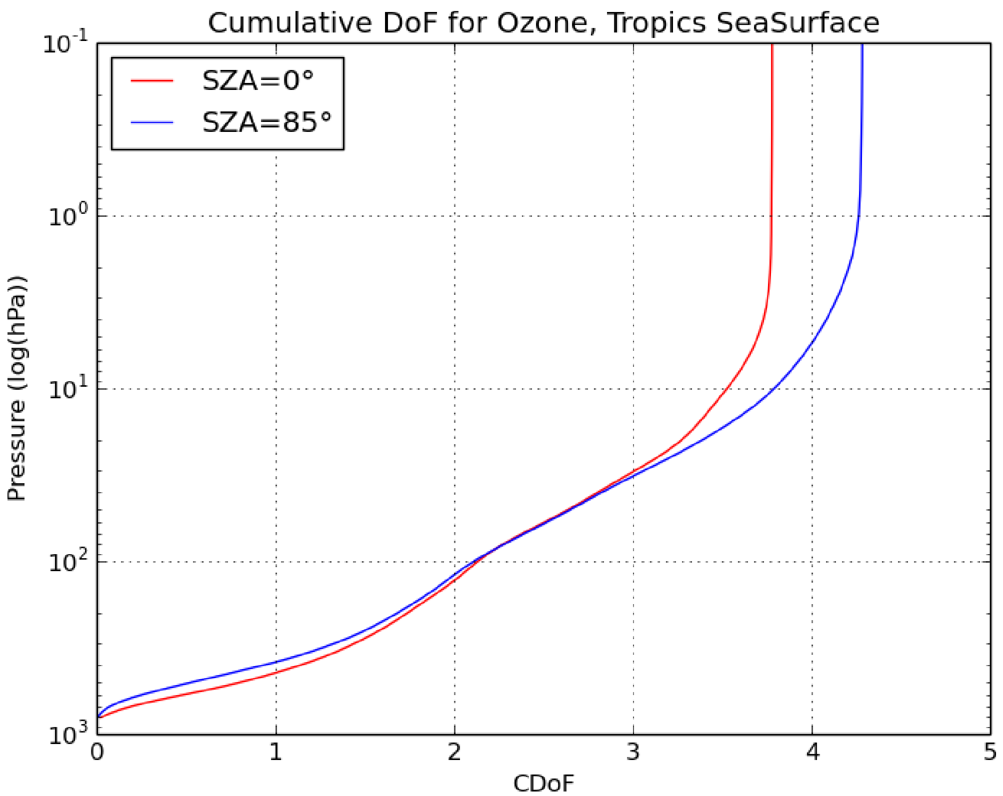

Figure 220: Annual mean of the cumulative DoF of ozone in the tropics over sea at Nadir (in red) and for 85° (in blue).

3.3.2 Tropics over land

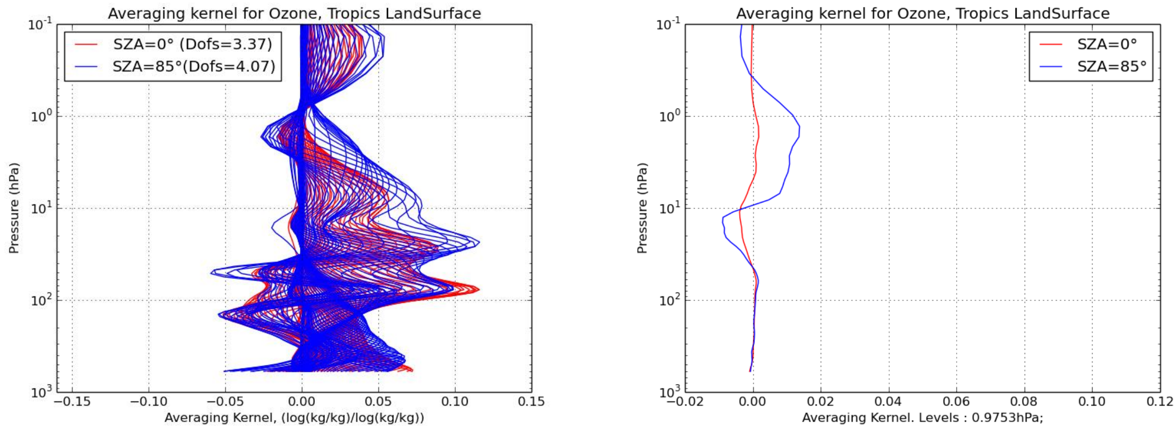

Figure 221: Same as Figure 219 over land.

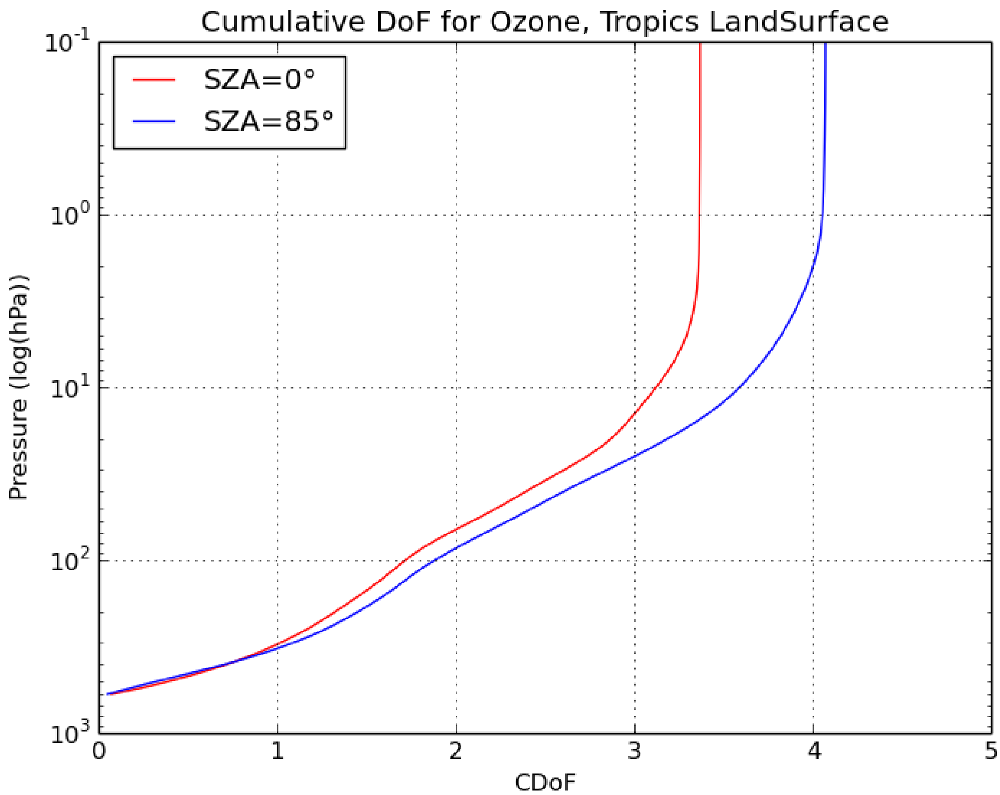

Figure 222: Same as Figure 220 over land.

3.3.3 Northern Mid-latitudes over sea

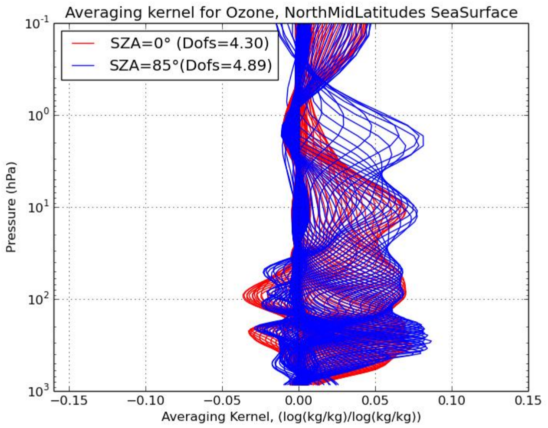

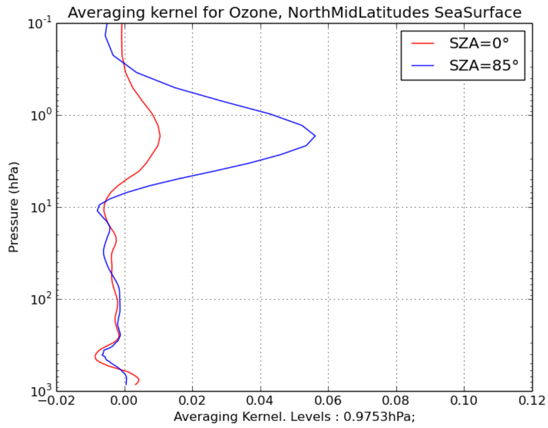

Figure 223: Same as Figure 219 in the Northern Mid-latitudes over sea.

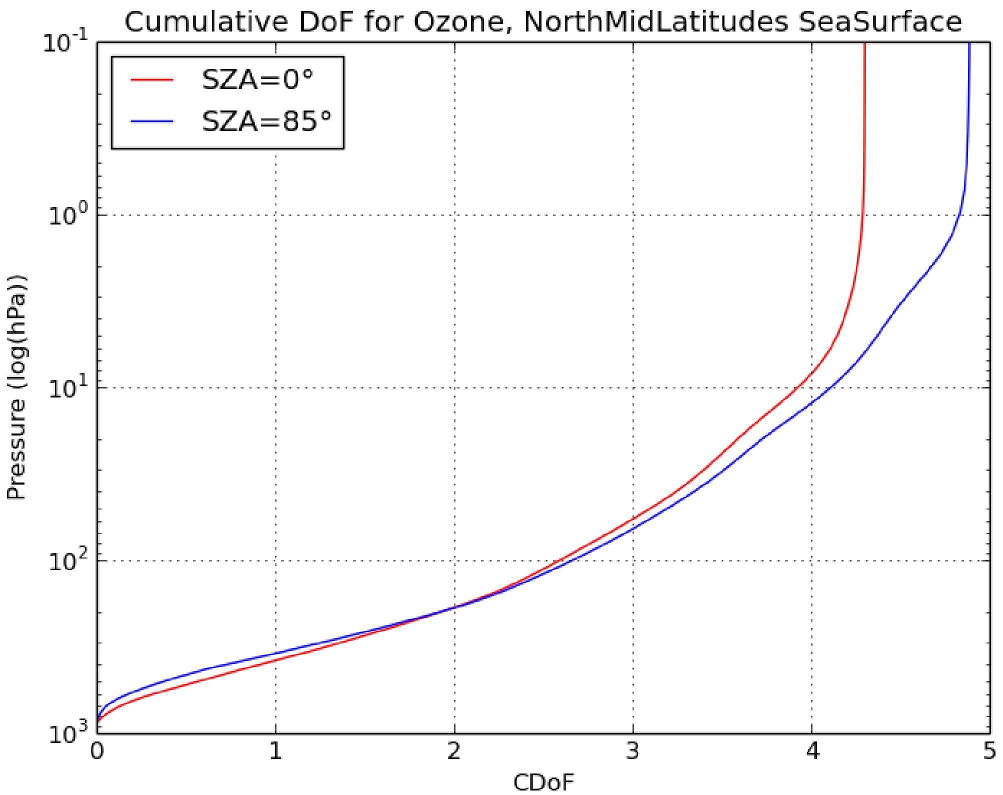

Figure 224: Same as Figure 220 in the Northern Mid-latitudes over sea.

3.3.4 Northern Mid-latitudes over land

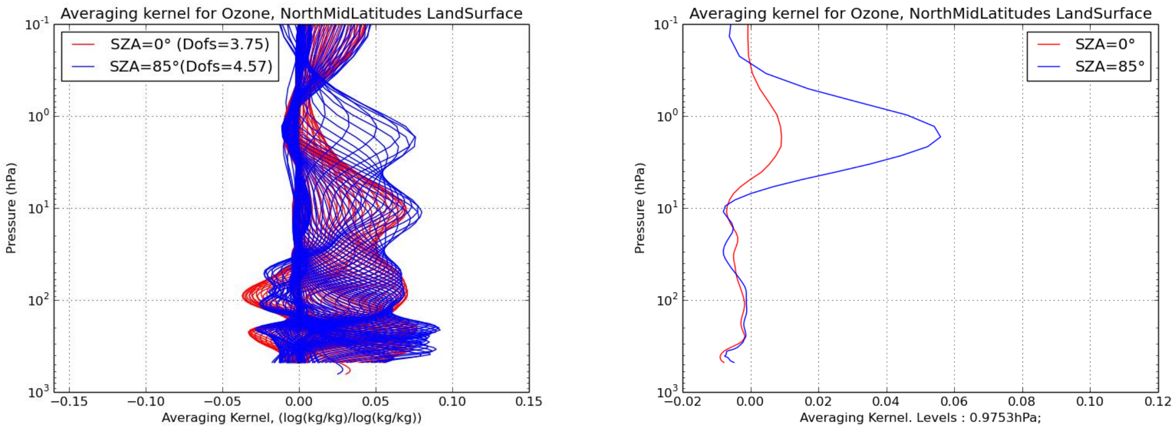

Figure 225: Same as Figure 219 in the Northern Mid-latitudes over land.

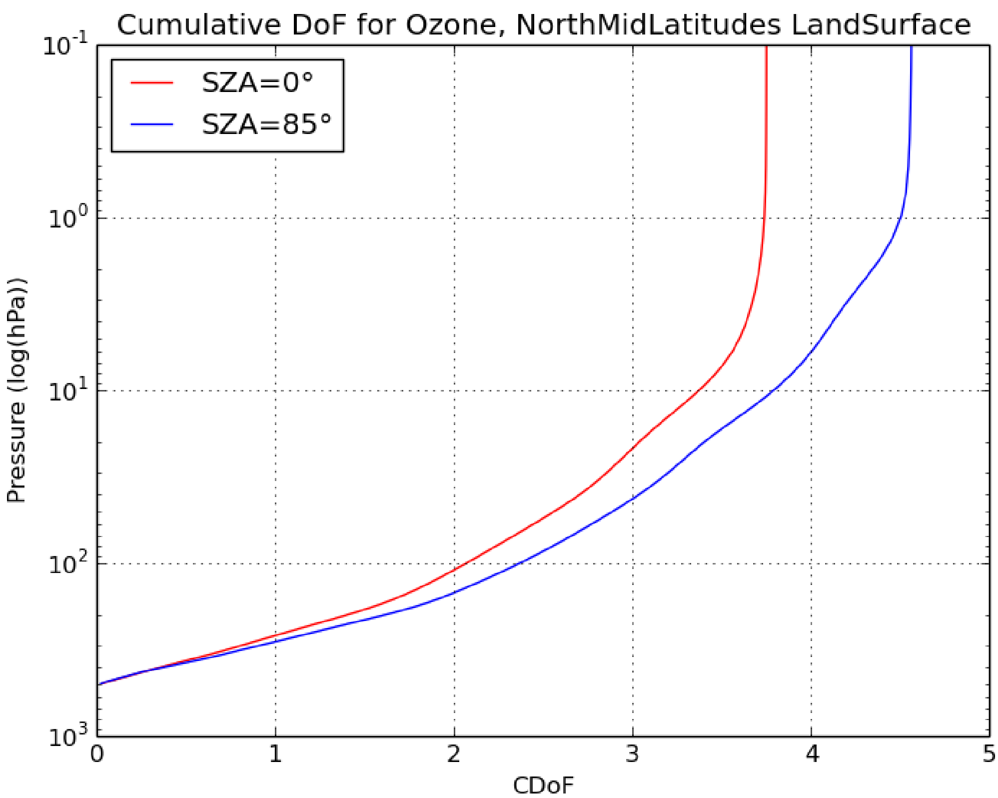

Figure 226: Same as Figure 220 in the Northern Mid-latitudes over land.

3.3.5 Southern Mid-latitudes over sea

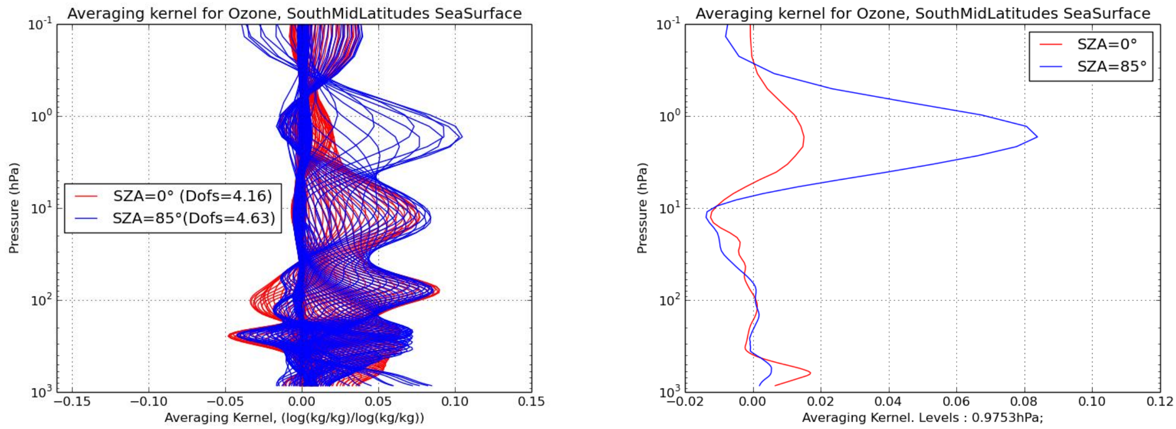

Figure 227: Same as Figure 219 in the Southern Mid-latitudes over sea.

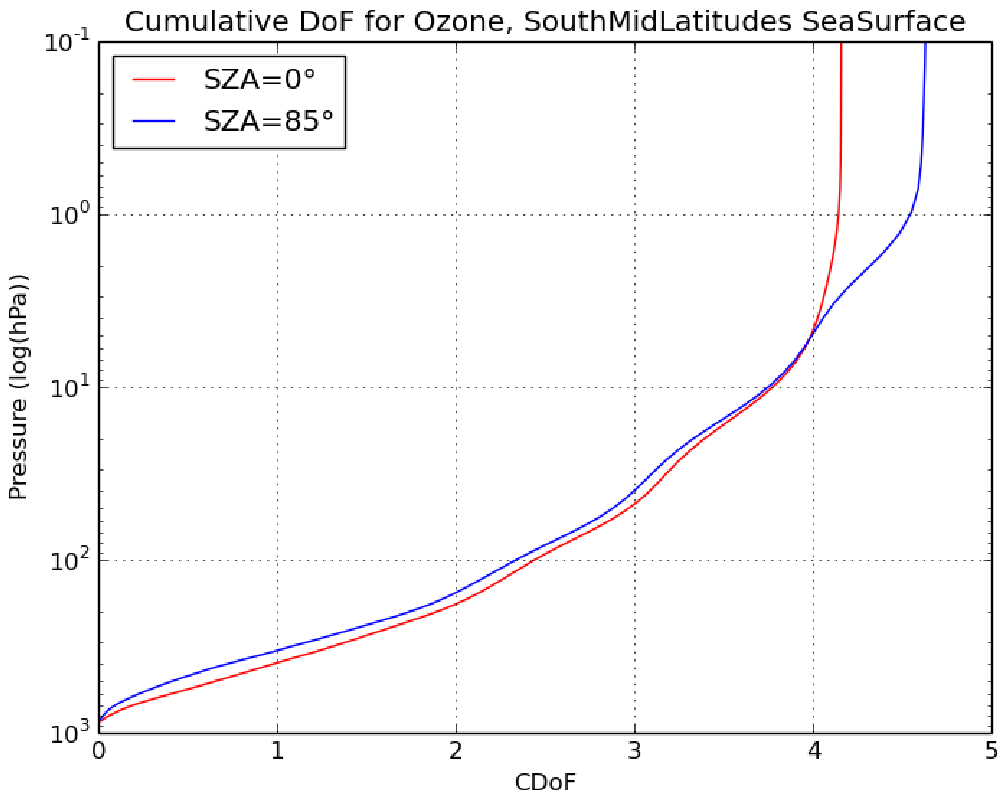

Figure 228: Same as Figure 220 in the Southern Mid-latitudes over sea.

3.3.6 Southern Mid-latitudes over land

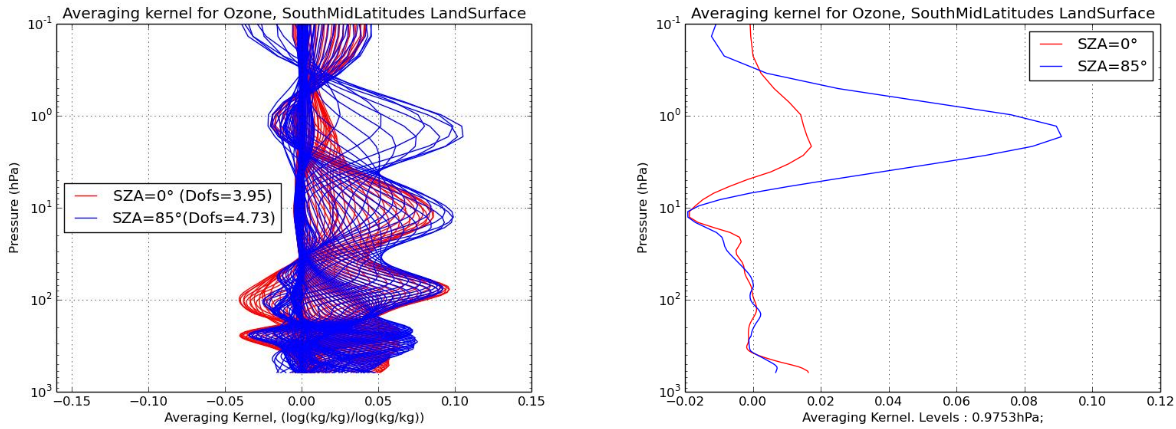

Figure 229: Same as Figure 219 in the Southern Mid-latitudes over land.

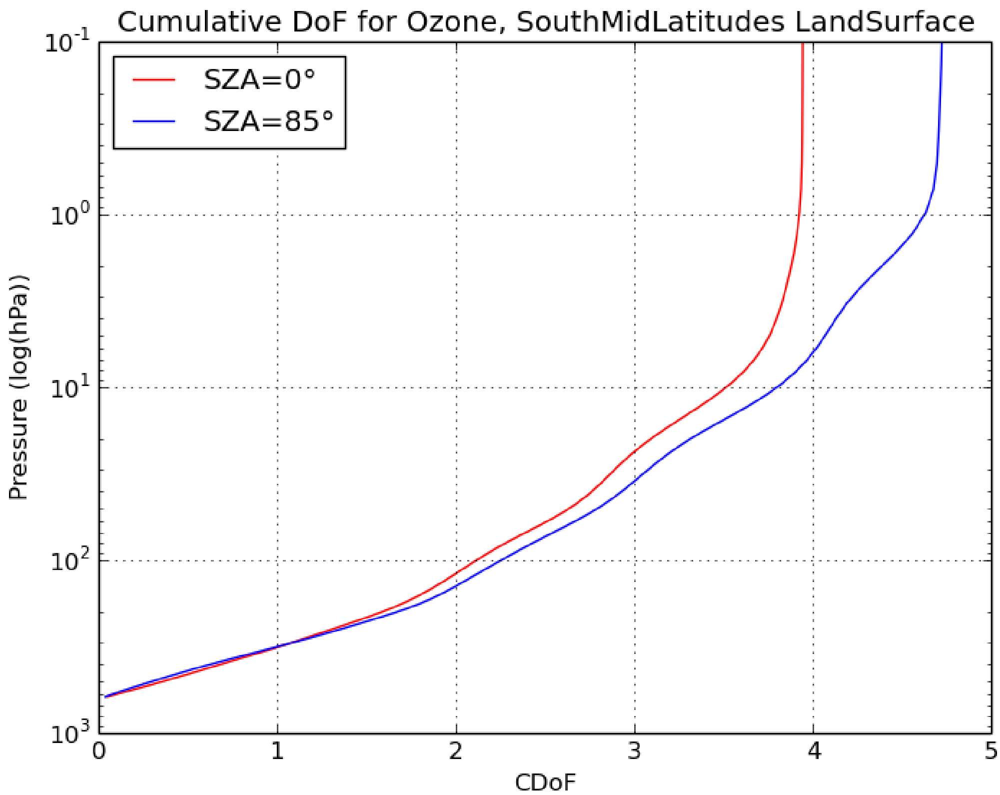

Figure 230: Same as Figure 220 in the Southern Mid-latitudes over land.

3.3.7 North Pole over sea

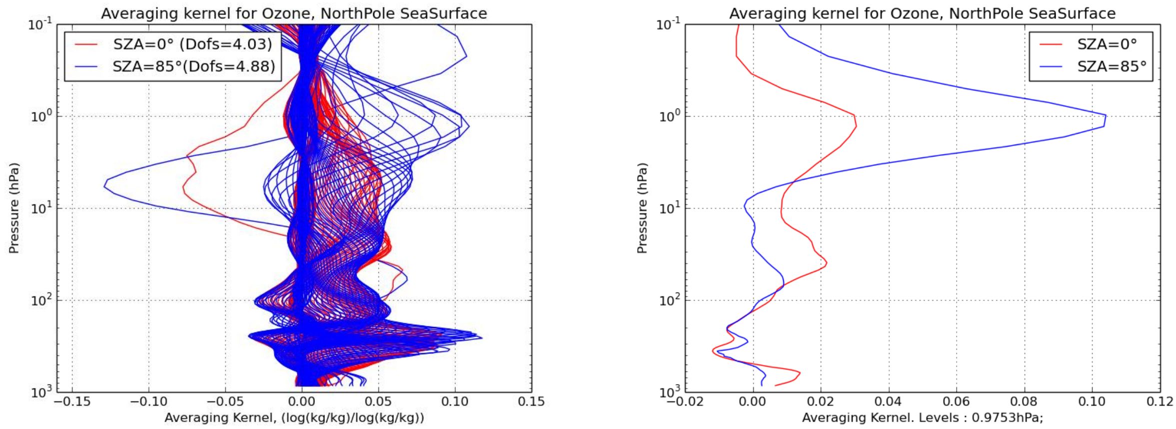

Figure 231: Same as Figure 219 in the North Pole over sea.

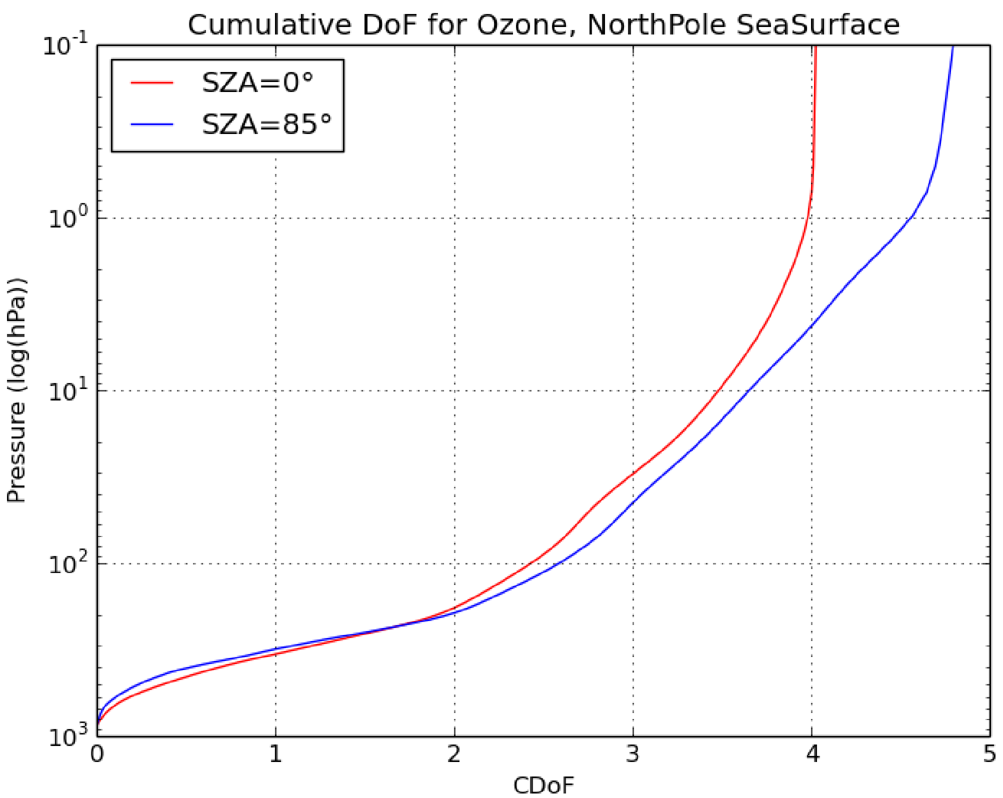

Figure 232: Same as Figure 220 in the North Pole over sea.

3.3.8 North Pole over land

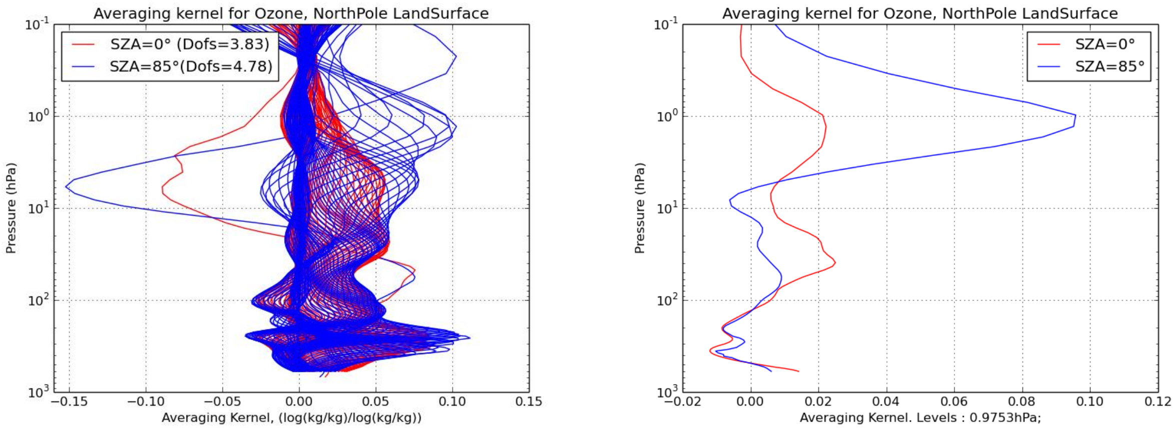

Figure 233: Same as Figure 219 in the North Pole over land.

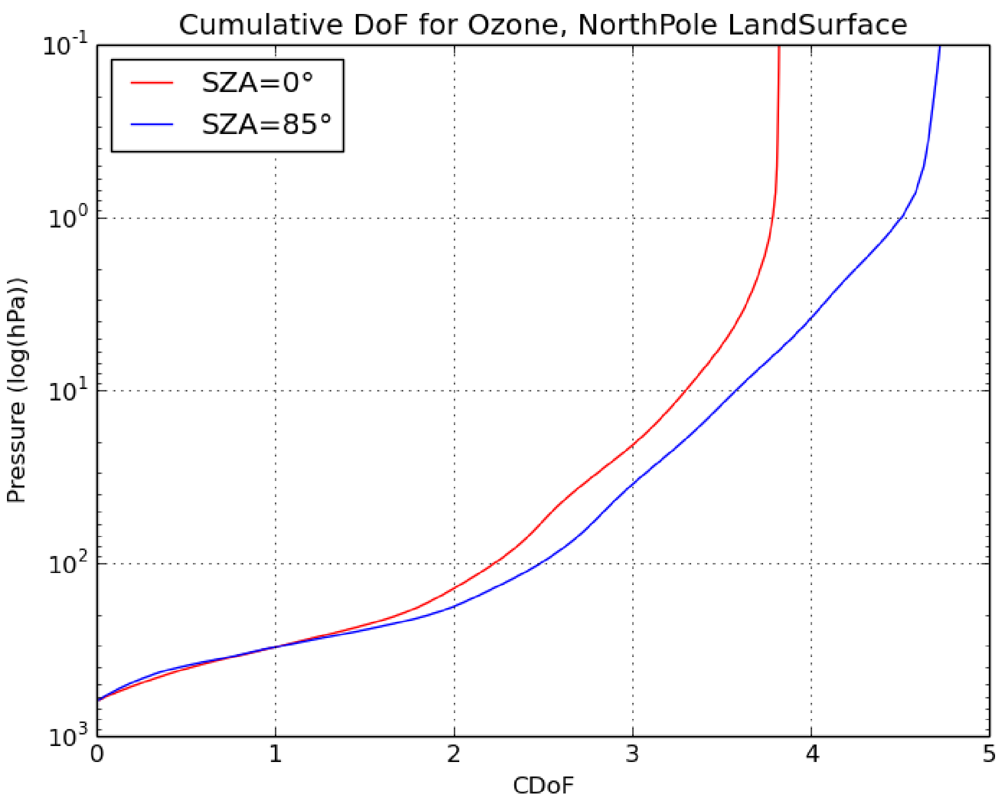

Figure 234: Same as Figure 220 in the North Pole over land.

3.3.9 South Pole over sea

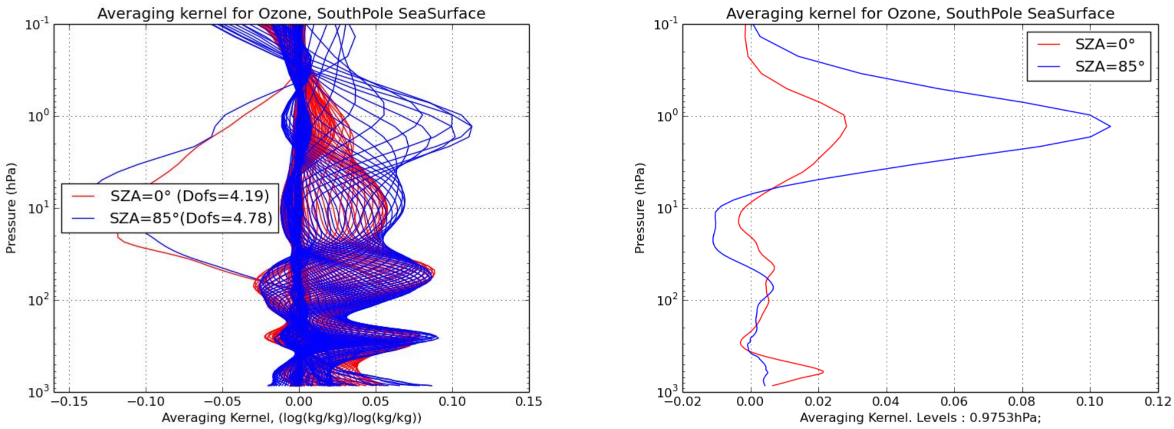

Figure 235: Same as Figure 219 in the South Pole over sea.

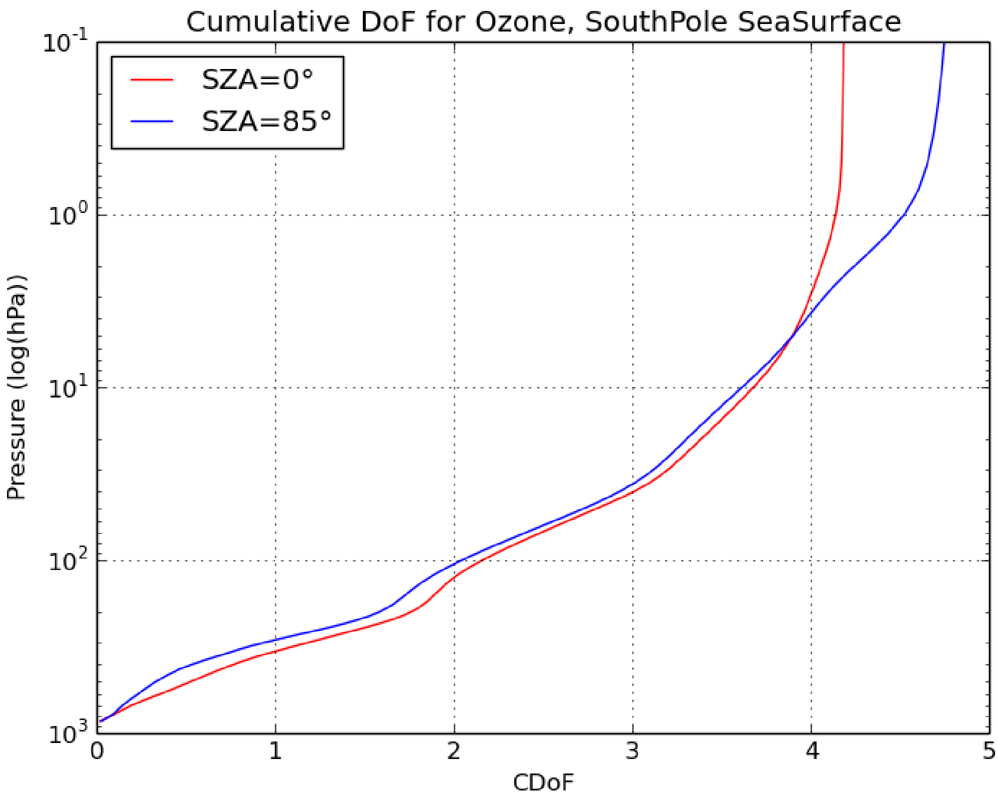

Figure 236: Same as Figure 220 in the South Pole over sea.

3.3.10 South Pole over land

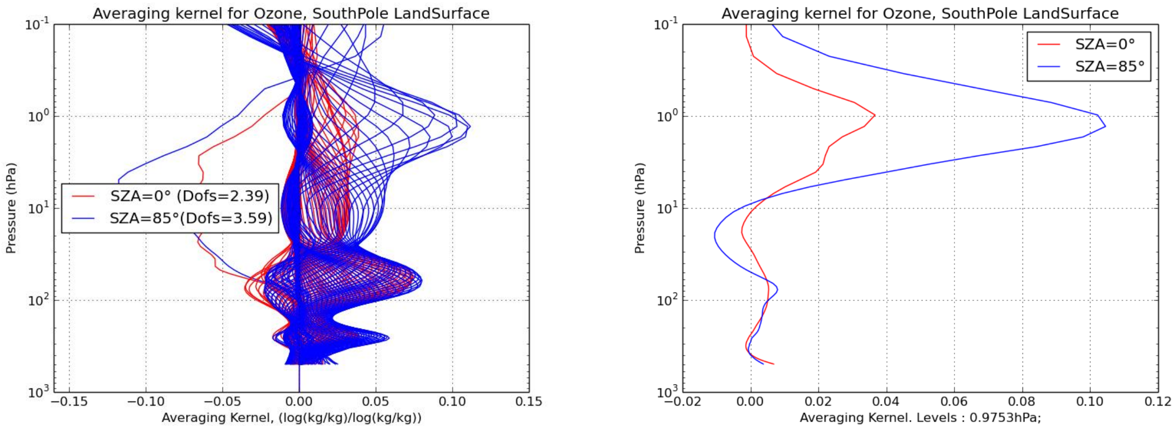

Figure 237: Same as Figure 219 in the South Pole over land.

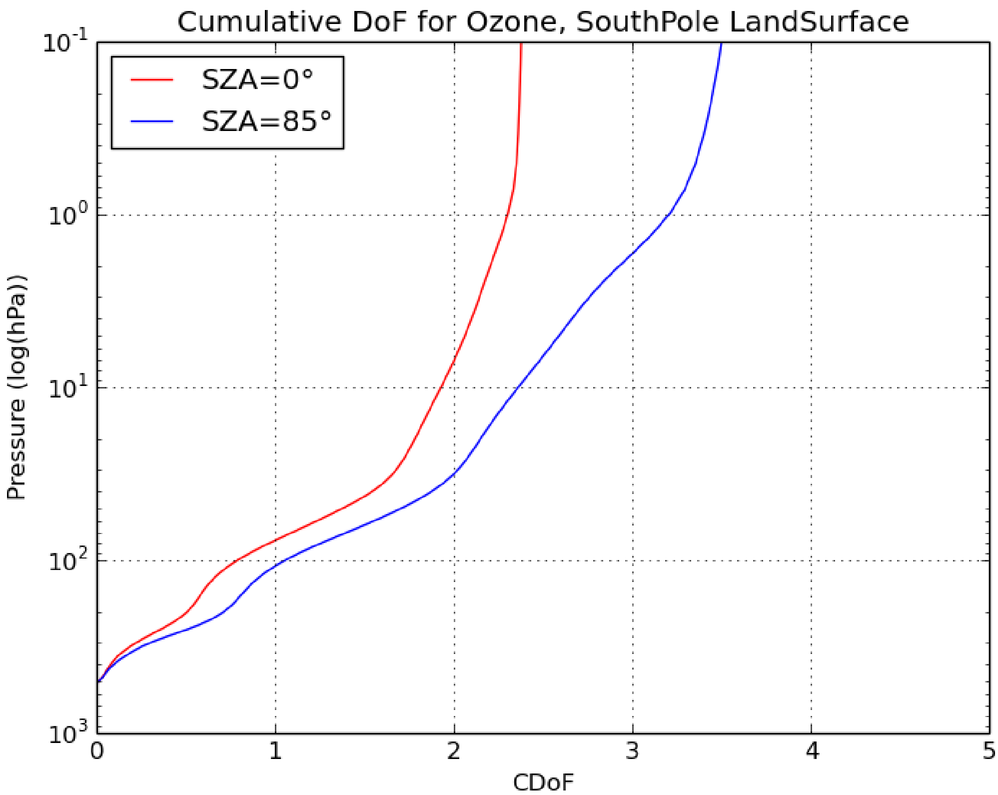

Figure 238: Same as Figure 220 in the South Pole over land.

4 ANNEXE D – ALL FIGURES FOR JACOBIANS W.R.T. SURFACE EMISSIVITY AND SURFACE TEMPERATURE

4.1 VARIATION OF EMISSIVITY JACOBIANS AND VARIATION SATELLITE ZENITH ANGLES

4.1.1 Emissivity Jacobian: Tropics, over sea

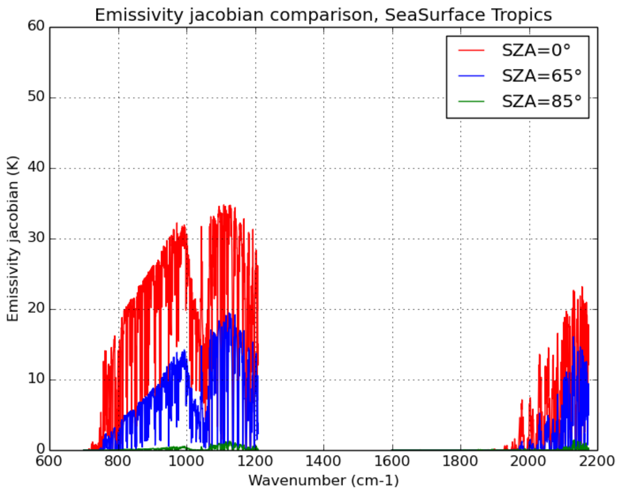

Figure 239 : Emissivity Jacobian comparison w.r.t satellite zenith angle (SatZA) for tropics over sea (in brightness temperature). (Red) SatZA = 0°. (Blue) SatZA = 65°. (Green) SatZA = 85°.

4.1.2 Emissivity Jacobian: Tropics, over land

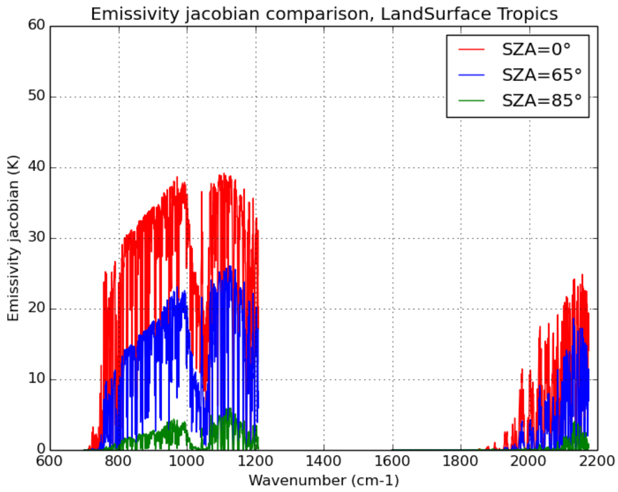

Figure 240 : Emissivity Jacobian comparison w.r.t satellite zenith angle (SatZA) for tropics over land. (Red) SatZA = 0°. (Blue) SatZA = 65°. (Green) SatZA = 85°.

4.1.3 Emissivity Jacobian: Northern mid-latitudes, over sea

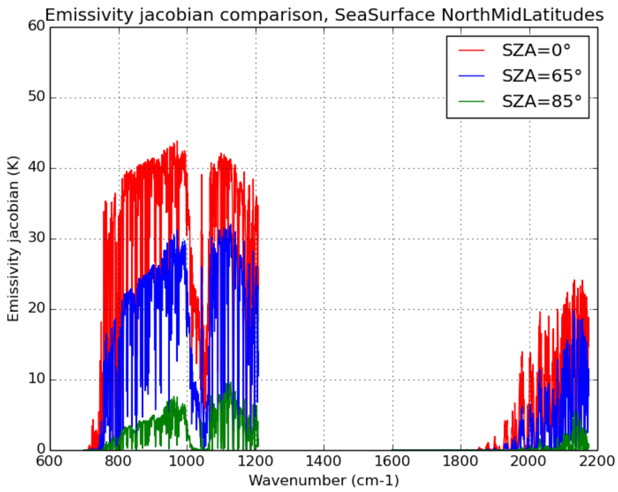

Figure 241 : Emissivity Jacobian comparison w.r.t satellite zenith angle (SatZA) for Nothern mid-latitudes over sea. (Red) SatZA = 0°. (Blue) SatZA = 65°. (Green) SatZA = 85°.

4.1.4 Emissivity Jacobian: Northern mid-latitudes, over land

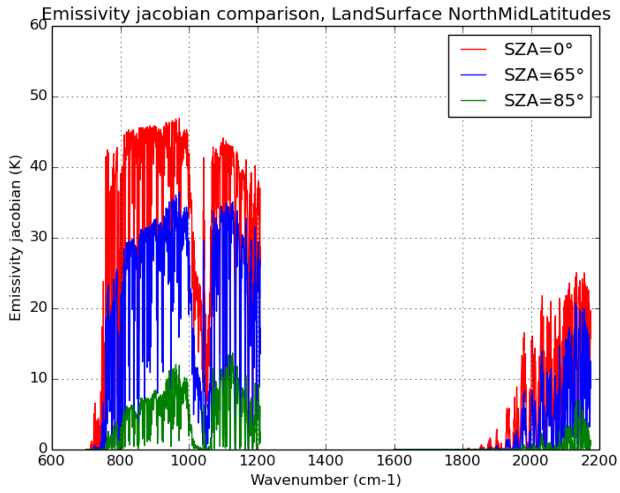

Figure 242 : Emissivity Jacobian comparison w.r.t satellite zenith angle (SatZA) for Nothern mid-latitudes over land. (Red) SatZA = 0°. (Blue) SatZA = 65°. (Green) SatZA = 85°.

4.1.5 Emissivity Jacobian: Southern mid-latitudes, over sea

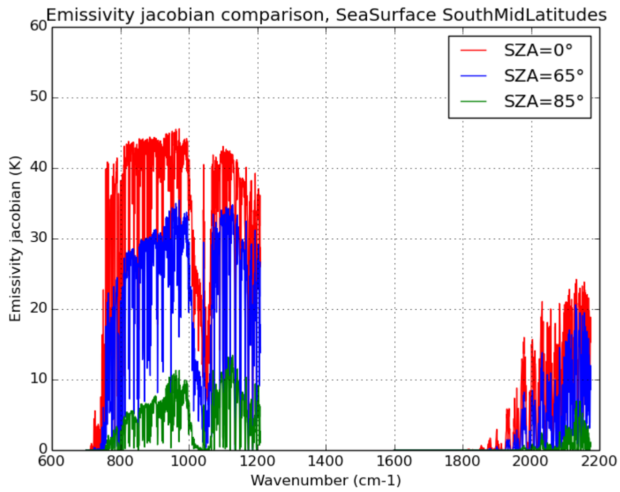

Figure 243 : Emissivity Jacobian comparison w.r.t satellite zenith angle (SatZA) for Southern mid-latitudes over sea. (Red) SatZA = 0°. (Blue) SatZA = 65°. (Green) SatZA = 85°.

4.1.6 Emissivity Jacobian: Southern mid-latitudes, over land

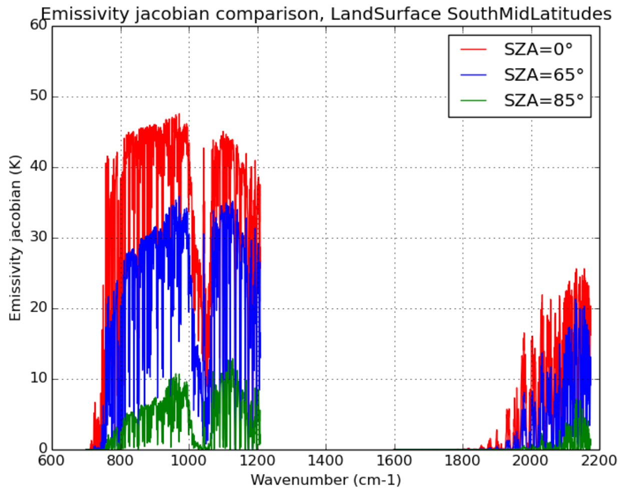

Figure 244 : Emissivity Jacobian comparison w.r.t satellite zenith angle (SatZA) for Southern mid-latitudes over land. (Red) SatZA = 0°. (Blue) SatZA = 65°. (Green) SatZA = 85°.

4.1.7 Emissivity Jacobian: North Pole, over sea

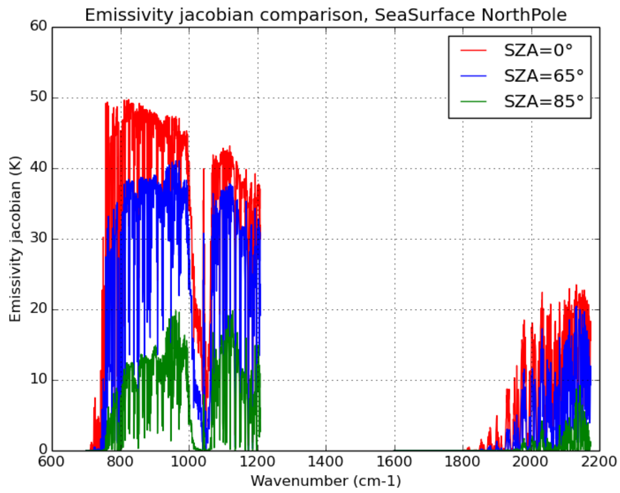

Figure 245 : Emissivity Jacobian comparison w.r.t satellite zenith angle (SatZA) for North Pole over sea. (Red) SatZA = 0°. (Blue) SatZA = 65°. (Green) SatZA = 85°.

4.1.8 Emissivity Jacobian: North Pole, over land

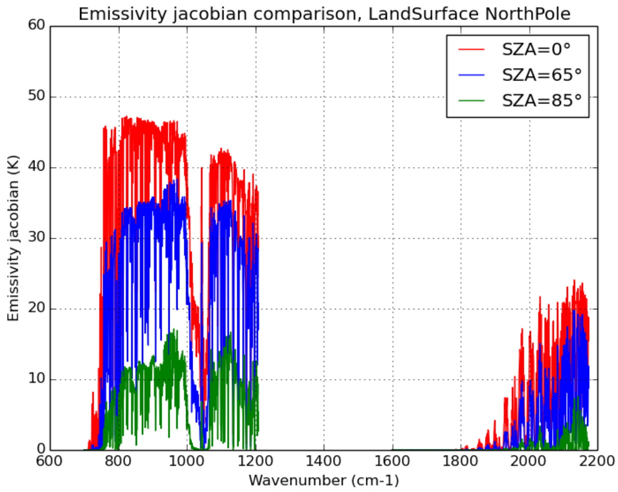

Figure 246 : Emissivity Jacobian comparison w.r.t satellite zenith angle (SatZA) for North Pole over land. (Red) SatZA = 0°. (Blue) SatZA = 65°. (Green) SatZA = 85°.

4.1.9 Emissivity Jacobian: South Pole, over sea

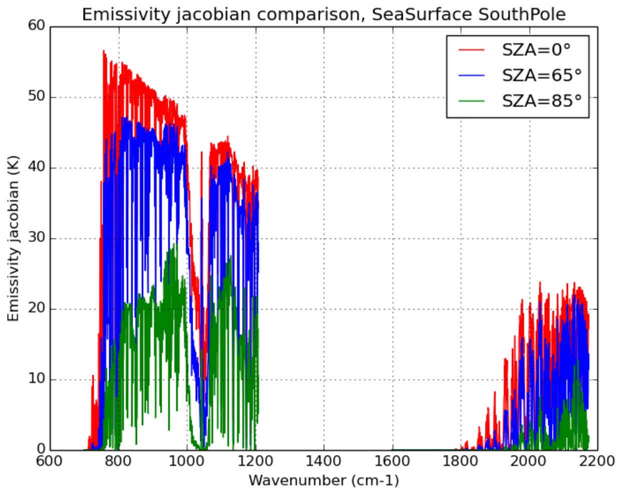

Figure 247 : Emissivity Jacobian comparison w.r.t satellite zenith angle (SatZA) for South Pole over sea. (Red) SatZA = 0°. (Blue) SatZA = 65°. (Green) SatZA = 85°.

4.1.10 Emissivity Jacobian : South Pole, over land

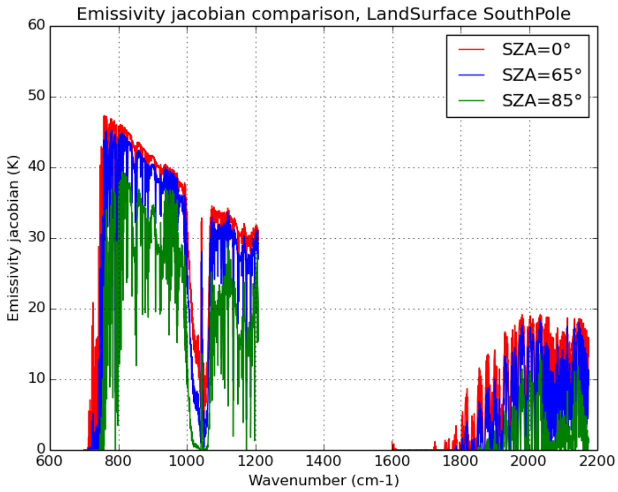

Figure 248 : Emissivity Jacobian comparison w.r.t satellite zenith angle (SatZA) for South Pole over land. (Red) SatZA = 0°. (Blue) SatZA = 65°. (Green) SatZA = 85°.

4.2 VARIATION OF SURFACE TEMPERATURE JACOBIANS WITH SATELLITE ZENITH ANGLES

4.2.1 Surface temperature Jacobian: Tropics, over sea

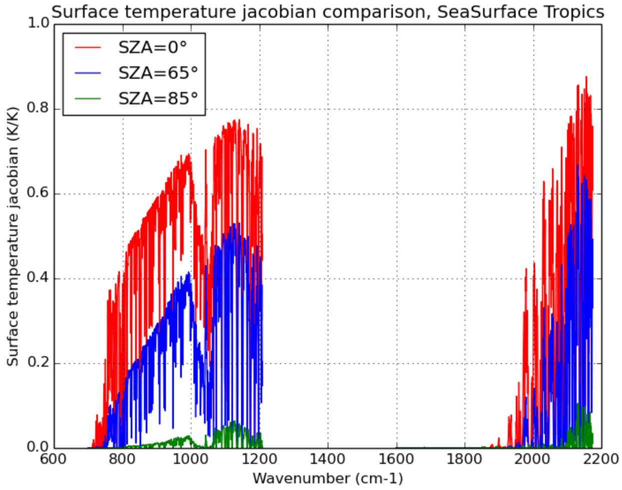

Figure 249 : Surface temperature Jacobian comparison w.r.t satellite zenith angle (SatZA) for tropics over sea. (Red) SatZA = 0°. (Blue) SatZA = 65°. (Green) SatZA = 85°.

4.2.2 Surface temperature Jacobian: Tropics, over land

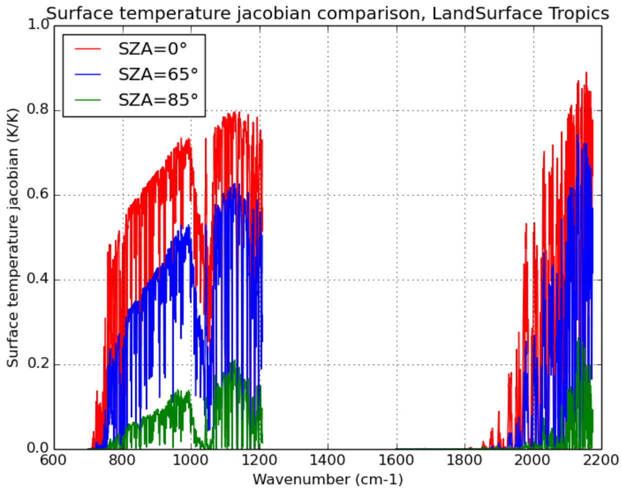

Figure 250 : Surface temperature Jacobian comparison w.r.t satellite zenith angle (SatZA) for tropics over land. (Red) SatZA = 0°. (Blue) SatZA = 65°. (Green) SatZA = 85°.

4.2.3 Surface temperature Jacobian: Nothern mid-latitudes, over sea

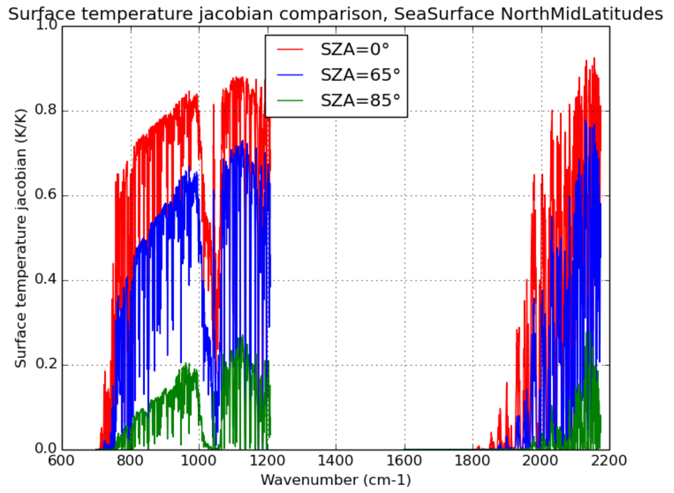

Figure 251 : Surface temperature Jacobian comparison w.r.t satellite zenith angle (SatZA) for Northern mid-latitudes over sea. (Red) SatZA = 0°. (Blue) SatZA = 65°. (Green) SatZA = 85°.

4.2.4 Surface temperature Jacobian: Nothern mid-latitudes, over land

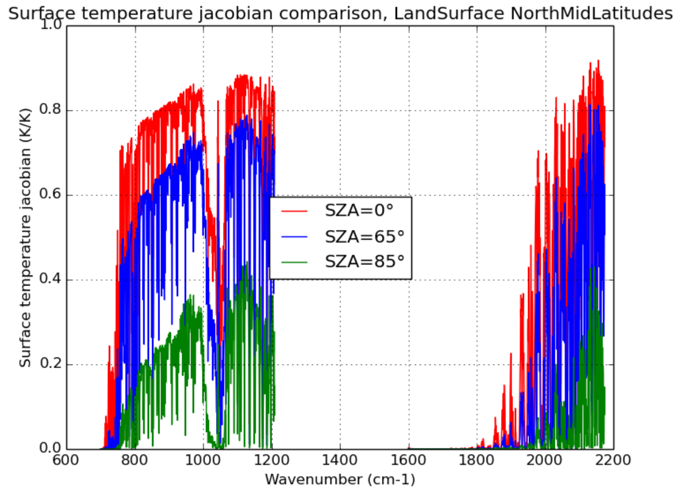

Figure 252 : Surface temperature Jacobian comparison w.r.t satellite zenith angle (SatZA) for Northern mid-latitudes over land. (Red) SatZA = 0°. (Blue) SatZA = 65°. (Green) SatZA = 85°.

4.2.5 Surface temperature Jacobian: Southern mid-latitudes, over sea

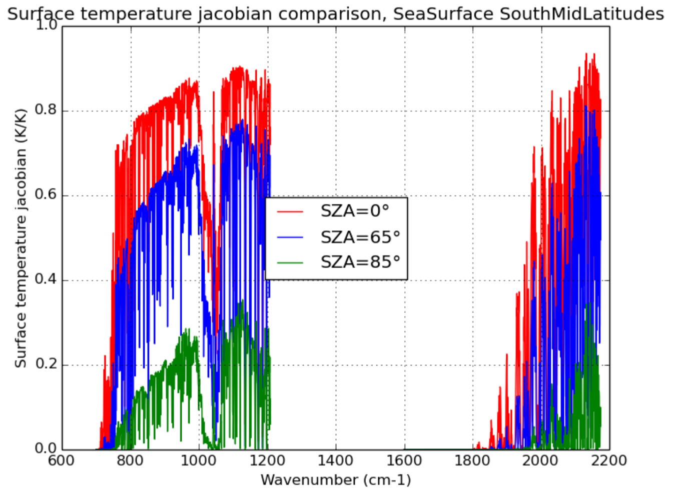

Figure 253 : Surface temperature Jacobian comparison w.r.t satellite zenith angle (SatZA) for Southern mid-latitudes over sea. (Red) SatZA = 0°. (Blue) SatZA = 65°. (Green) SatZA = 85°.

4.2.6 Surface temperature Jacobian: Southern mid-latitudes, over land

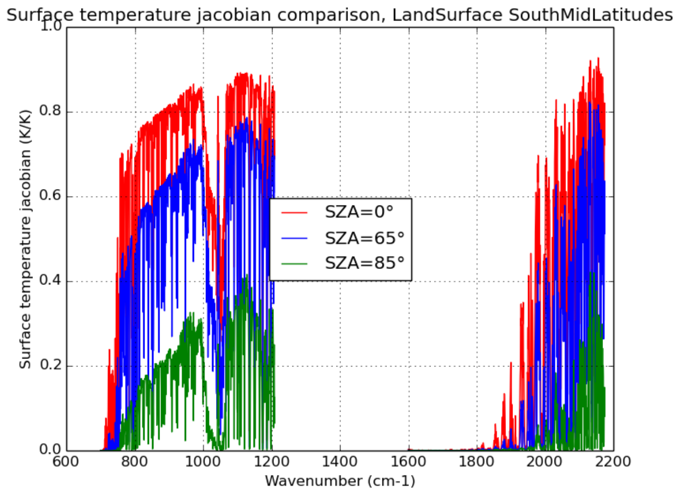

Figure 254 : Surface temperature Jacobian comparison w.r.t satellite zenith angle (SatZA) for Southern mid-latitudes over land. (Red) SatZA = 0°. (Blue) SatZA = 65°. (Green) SatZA = 85°.

4.2.7 Surface temperature Jacobian: North Pole, over sea

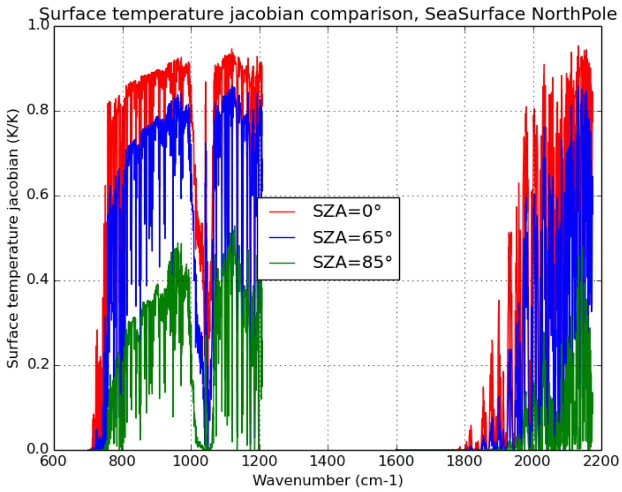

Figure 255 : Surface temperature Jacobian comparison w.r.t satellite zenith angle (SatZA) for North Pole over sea. (Red) SatZA = 0°. (Blue) SatZA = 65°. (Green) SatZA = 85°.

4.2.8 Surface temperature Jacobian: North Pole, over land

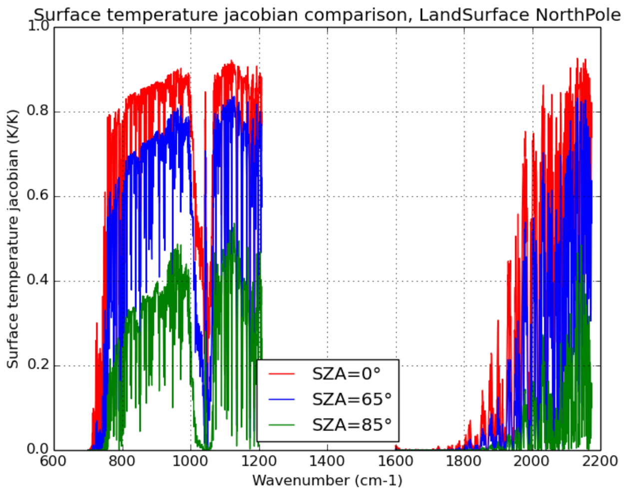

Figure 256 : Surface temperature Jacobian comparison w.r.t satellite zenith angle (SatZA) for North Pole over land. (Red) SatZA = 0°. (Blue) SatZA = 65°. (Green) SatZA = 85°.

4.2.9 Surface temperature Jacobian: South Pole, over sea

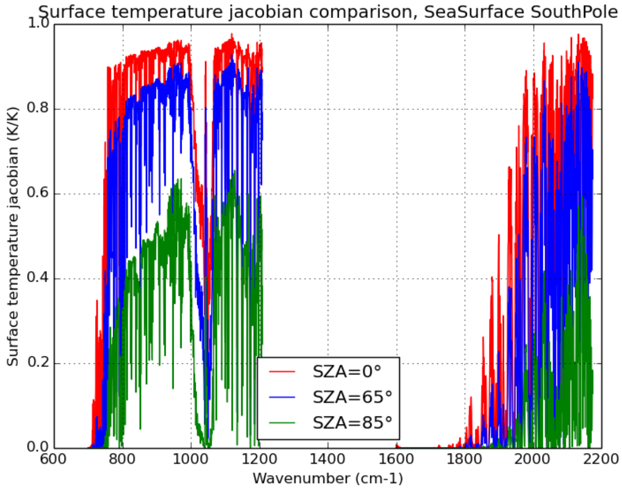

Figure 257 : Surface temperature Jacobian comparison w.r.t satellite zenith angle (SatZA) for South Pole over sea. (Red) SatZA = 0°. (Blue) SatZA = 65°. (Green) SatZA = 85°.

4.2.10 Surface temperature Jacobian: South Pole, over land

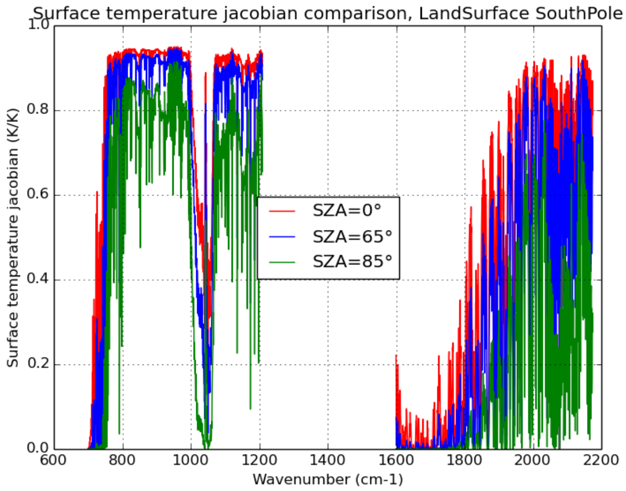

Figure 258 : Surface temperature Jacobian comparison w.r.t satellite zenith angle (SatZA) for South Pole over land. (Red) SatZA = 0°. (Blue) SatZA = 65°. (Green) SatZA = 85°.